No place like home: Hair follicle stem cell's departure from niche environment during aging

by

Chi Zhang

B.A., Sichuan University, 2011

M.A., Sichuan University, 2015

A thesis submitted to the

Faculty of the Graduate School of the

University of Colorado in partial fulfillment

of the requirement for the degree of

Doctor of Philosophy

Department of Molecular, Cellular and Developmental Biology

2022

Committee Members:

Rui Yi

Robin Dowell

Brad Olwin

Lee Niswander

John Rinn

Chi Zhang, (Ph.D., Molecular, Cellular and Developmental Biology)

No place like home: Hair follicle stem cell's departure from niche environment during aging

Thesis directed by Prof. Rui Yi and Prof. Robin Dowell

Stem cell(SC) exhaustion is a hallmark of aging. However, the process of SC depletion during aging has not been observed in live animals and the underlying mechanism contributing to tissue deterioration remains obscure. Combining mouse genetics and intravital live animal imaging, we found that in aged mice, hair follicle stem cells(HF-SCs) escape from the SC compartment and show up in dermis, contributing to SC depletion and hair follicle miniaturization. Single-cell RNA-seq and single-cell ATAC-seq revealed the reduced expression of cell adhesion and extracellular matrix genes in aged HF-SCs, many of which are regulated by transcription factors, *Foxc1* and *Nfatc1*. Deletion of *Foxc1* and *Nfatc1* recapitulated hair follicle miniaturization and caused premature hair loss. Live imaging captured individual HF-SCs migrating away from the SC compartment and hair follicle disintegration. These findings illuminate a hitherto unknown activity of HF-SC escaping from their niche as a mechanism underlying SC reduction and tissue degeneration. Identification of homeless epithelial cells in aged tissues provides a new perspective for understanding aging-associated diseases.

To further understand the physiological aging process in distinct hair follicle lineages, we continued collecting mouse skin samples ranging from early adult to various aging stages. Hair follicles are miniorgans that reside at the surface of mouse skin consisting of multiple well-studied cell types, including HF-SCs, Niche cells, Hair Germs, Dermal Papilla and other differentiated cell types. Mouse hair follicle undergoes cyclic bouts of hair regeneration, degeneration and resting stages, during which multiple cell lineages undergo drastic phenotypical changes including migration and apoptosis. Emerging studies have shown the plasticity of hair follicle lineages upon wound healing, yet the lineage-specific changes of hair follicles during aging have not been systematically studied. By collecting single-cell RNAseq and and single-cell ATACseq at multiple time points in the

mouse lifespan, we found lineage-specific transcriptomic changes during aging, especially the Niche cells and HF-SCs. The Niche cells irreversibly accumulated cellular stress including reactive oxygen species(ROS), hypoxia and DNA damage and activated apopototic signals during the aging process. In contrast, the HF-SCs down-regulated ROS after the intermediate upregulation. Further analysis demonstrated the repopulation of Niche cells during each hair cycle by a newly discovered cell population we here named migratory Niche cells(migNiche). Our study indicates that in addition to the popular idea of stem cell aging, the Niche cells might be another major contributing factor for hair follicle aging.

Single-cell RNAseq makes it possible to study the interaction between immune cells and hair follicle cells in skin. As the first line of defense against pathogens, the skin employs diverse and complicated immune machinery to combat both cellular and environmental attacks. Hair follicles, one of the skin appendages, can escape the attack from surrounding immune cells and thus protect tissue structure from collateral damage caused by the immune response directed against pathogens. The single-cell RNAseq data demonstrated accumulated T cells around *Foxc1* and *Nfatc1* double knockout hair follicles. Consequently, *Foxc1* deletion in hair follicles led to a gradual loss of club hair(old hair shaft), a sign of immune privilege collapse. Gene ontology analysis also showed down-regulated expression of antigen presenting genes in *Foxc1* deleted HF-SCs. The results demonstrate that *Foxc1* can mediate immune privilege regulation by targeting antigen presenting genes in HF-SCs.

Lastly, as an independent project in the Dowell lab, I modeled the global transcription and degradation rate in Down syndrome cells with TimeLapse-seq data during a dynamic process. Mature RNA molecules in a cell are composed of both newly transcribed and older, about to be degraded ones. Both of which are easy to measure in steady-state RNA-seq. However, few studies have been focused on dynamic physiological and pathological process. I set out to model both the transcription and degradation rate using TimeLapse-seq based pulse-chase methods. My preliminary analysis successfully estimated the transcription rate of individual genes.

In conclusion, by applying mouse genetics, large-scale genomics analysis and live animal

imaging, I was able to delineate the complex lineage-specific aging, dynamic HF-SCs behaviors during aging and immune cell interaction in mouse hair follicles. My studies provide a new model of stem cell exhaustion that differs considerably from current knowledge of stem cell aging related to the defects in cell division and self-renewal.

Dedication

I'd like to dedicate my thesis work to my family and friends for their continuous support during my graduate school.

Acknowledgements

The thesis work presented here wouldn't be possible without the help and support of many both in life and science. First and foremost, I would like to thank my advisors and mentors Dr.Rui Yi and Dr.Robin Dowell. Thank you for the guidance throughout my graduate school. Rui's enthusiasm and willingness to explore challenging fields inspire me to pursue my independent scientific career. Robin's passion and critical thinking in bioinformatics really shaped me to be a stringent and consistent explorer in the scientific field. I really appreciate her patience when I slowly accumulated my statistical and computation skills. Thank you to all the members of the Yi and Dowell labs, past and present, for helping with my scientific training and always being there. Specifically, I want to thank Dongmei, Jaimee, Jingjing, Alfonso, Xiyin and Glen for all my wet-lab experiments including mouse genetics, flow cytometry and many other. I want to thank Mary Allen for guiding me through the steep learning stages of bioinformatics. I'd like to thank Jacob for helping me understand the basics of statistical modeling. In addition, I really appreciate other members in the Dowell lab including Ignacio, Joe, Gilson, Rutendo, Jonathan, Taylor, Kendra, Zack and Ariel for all the help.

I'm extremely grateful for my fellow graduate students in the lab, Arpan, Lily, Kevin, Sam, Qin, Jessica, Daniel and Jesse, graduate life wasn't always easy but their supports and friendships made it fun in and out of lab. As an international student, I will never forget the support my cohort offered when I first came to US. Brad, Julie, Ishara, Johnny, Tuium, Willow, Jess and Yao all helped me overcome the culture shock. I cannot thank Yao enough for being there for my laughs and tears.

I'd like to thank my thesis committee, John Rinn, Lee Niswander and Brad Olwin for inspiring me to think critically about both scientific results and career development. Thanks for providing great advice and supporting me during my graduate career.

I'd like to thank the FACS facility, Microscope facility, EM facility, Mouse genetic facility and Sequencing core for providing comprehensive support for my project. Specially, I'd like to thank Dr. Orth for helping establish the two-photon microscopy system just in time for my study and Yumin for performing the flow cytometry experiments. Additionally, I'd like to thank Eileen and Garry for helping me explore the EM related studies. I'd like to thank the administration at MCDB and Biofrontiers especially Karen, Kathy and Sarah for all the help over the years.

This dissertation wouldn't be possible without funding by NIH Individual Predoctoral to Postdoctoral Fellow Transition Award(F99/K00)(1F99CA253738-01). Thanks to the support for international students and I also appreciate the CU grant office especially Kathryn for helping me submitting the application.

Lastly, I want to thank my parents for their unconditional love. It's been tough not being able to visit home amid the pandemic but they always trusted me with my choices and supported me even though they might not understand what I was doing. I'm also grateful for my siblings for taking care of my parents and being there for emotional support.

Contents

Chapter

Figures

Figure

Chapter 1

Introduction

During the last two centuries, the average human life expectancy has been steadily increasing in most developed countries[1], whether there will be a limit to that is still under vigorous debates[2, 3, 4, 5]. However, with increasing life span and declining fertility rates[6], unprecedented challenges are arising worldwide[7], including late-life diseases and other socioeconomic burdens. We likely will not be able to abolish aging, but we can try to mitigate its effects and increase health-span[8]. Stem cell's remarkable capabilities to self-renew and differentiate into lineages specific cell types make it a promising candidate to combat aging. However, without understanding the specific cellular behaviors of tissue stem cell *in vivo*, the effort to develop stem cell-based therapies could be hindered, and in turn the uncertainty caused by the lack of knowledge could bring unanticipated risks.

In this chapter, I will first summarize current understanding of aging and tissue stem cells. To further study the cellular behavior of aging tissue stem cells in physiological context, I will then introduce a powerful model for non-invasive research, hair follicle. Lastly, I will briefly review our current understanding of hair follicle aging.

1.1 Aging and tissue stem cells

Since ancient times, people have been contemplating the unavoidable nature of aging and striving to make their lives longer and healthier. Qin Shi Huang, the first emperor of China, obsessively searched for an elixir of youth and died trying[9]. Aging research has experienced

unprecedented advances over recent years and the modern perception of aging is evolving based on a constantly expanding repertoire of molecular and cellular mechanisms of life and disease.

Aging is now defined as a functional decline of tissues and organisms, and contributes to many human diseases including cancer and neuro-degenerative diseases[10, 11]. Since stem cells(SC) are critical for maintaining somatic cell lineages, its exhaustion could contribute to the decline of tissue regeneration[11]. Indeed, functional decline of tissue stem cells has been found in essentially all adult stem cell compartments, including neural stem cells[12], hematopoietic stem cells[13] and muscle stem cells[14].

Tissue stem cells self-renew to maintain the SC pool and differentiate into lineage-specific cell types. Subsets of tissue stem cells can also persist in quiescent state for prolonged periods of time(Fig 1.1)[15]. Although it is widely recognized that tissue stem cell exhaustion leads to premature aging, the cellular activities of tissue stem cells during aging have been rarely observed in their intact microenvironment in animals[16, 17]. It remains largely unknown how tissue stem cells divide, migrate and perish during aging because the current knowledge of tissue stem cell aging has been acquired through indirect measurement of SC numbers and functions[18, 19, 20, 21, 22, 23]. As a result, our understanding of SC exhaustion is largely limited to the deficiency of cell division and self-renewal, usually caused by DNA damage and cellular senescence[21, 22, 23, 24].

Among the fundamental properties of tissue stem cells, quiescence is known to play an important role in SC maintenance by restricting the number of SC divisions and reducing metabolic stress[25, 26, 27]. Although the loss of quiescence has been shown to cause the lost proliferative potential of SCs[28, 29], SCs activities have not been visualized when they lose quiescence. Furthermore, it is unclear whether the loss of SC quiescence could affect the integrity of SC compartment independently of cell division control. Finally, while SC division rates generally decrease during aging[30], it remains an open question as to how prolonged SC quiescence affects aging.

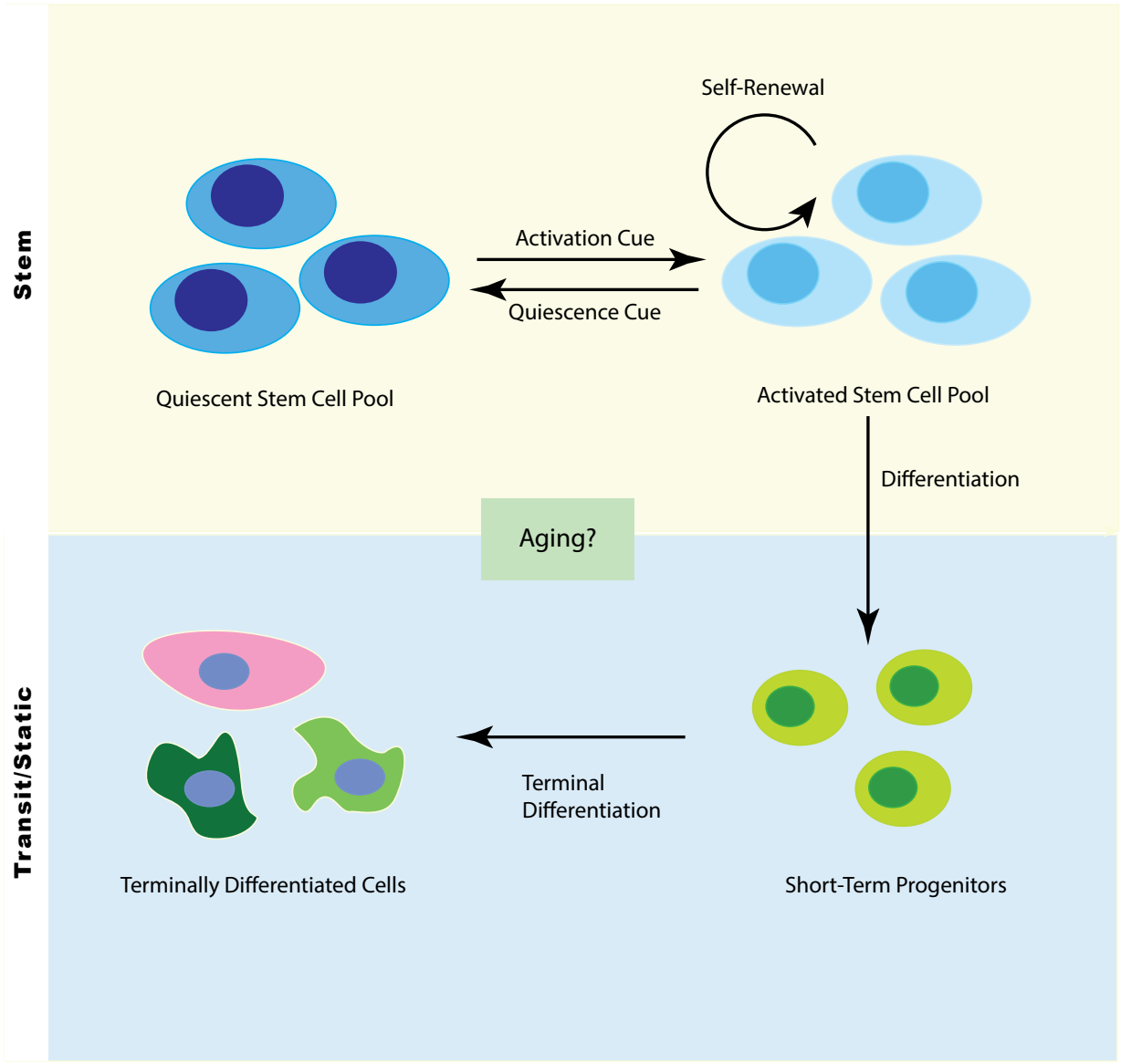

Figure 1.1: **Tissue stem cell properties.** Tissue stem cells can self-renew to maintain the stem cell pool. Subsets of tissue stem cells can also transition into a reversible quiescent state. When activated by extrinsic signals, SCs can self-renew or differentiate to produce committed short-term progenitors that proliferate and terminally differentiate into lineages specific cell types. How different cell lineages behave during aging is still under active investigation. Modified from Keyes, B. E., Fuchs, E. (2018). Journal of Cell Biology, 217(1), 79-92[15].

1.2 Mammalian skin and its appendages

Mammalian skin and its appendages help protect against external assault, retain essential body fluids and regulate body temperature[31]. As the first line of defense, the skin is constantly subjected to physical trauma. Its ability to regenerate and its complex cellular composition make it a great model to study tissue stem cells.

The mouse epidermis is a stratified epithelium consisting of a single layer of basal cells with proliferative potential and several suprabasal layers of terminally differentiated cells(Fig.1.2)[32]. These terminally differentiated suprabasal cells eventually become enucleated and shed as squames (Fig.1.2). Right beneath the epidermis is the dermis composed of collagen, elastic tissue and other extracellular components. The dermis cushions the body from physical and mechanical stress. Separating the epidermis and dermis is a thin layer of a proteinaceous structure called the basement membrane. Both the basal cells and dermal cells produce and secrete proteins involved in extracellular matrix assembly(ECM) and form the basement membrane.

1.2.1 Hair follicle morphogenesis

As an appendage of the skin, hair follicle is a complex mini-organ that serves a wide range of functions including thermoregulation, protection and even social interactions. Originating from embryonic epidermis, hair follicle morphogenesis is regulated by the tight interactions between epithelial cells and underlying dermal cells[33]. After embryonic development, hair follicle continues to communicate with its dermal compartment to coordinate normal hair cycle and hair shaft regeneration throughout the life of an organism.

Murine hair follicle morphogenesis is a well-defined process based on spatiotemporal changes in cellular morphology and dynamic aggregation of cells. In addition, mouse genetic approaches allow for a closer investigation of the molecular events and signaling pathways during each hair follicle morphogenesis stage, such as Wingless/Integrated(*Wnt*), ectodysplasin A/ectodysplasin receptor(*Eda/Edar*), bone morphogenic protein(*Bmp*) and sonic hedgehog(*Shh*) signaling[34, 35,

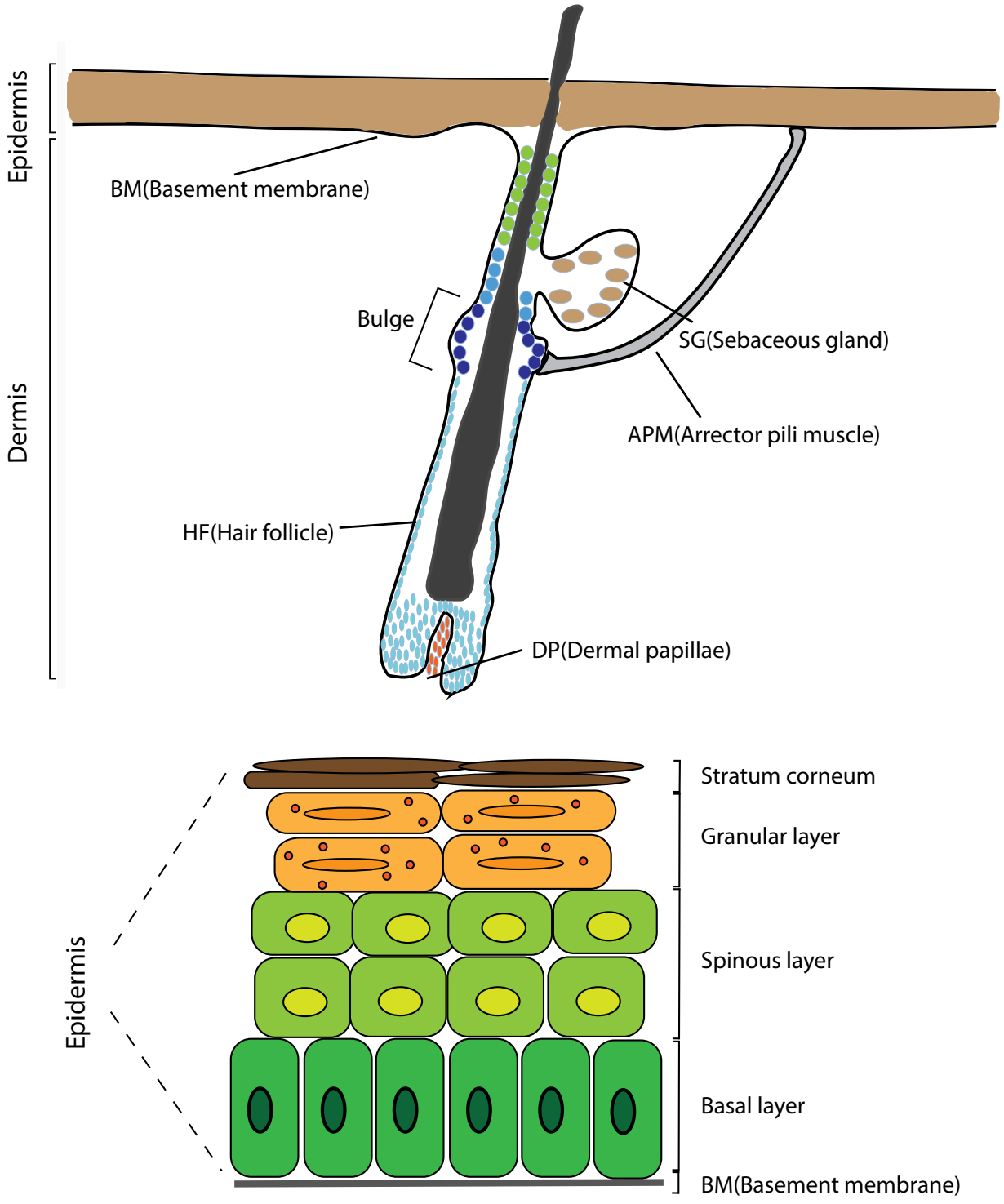

Figure 1.2: **Different layers of mammalian skin.** Mammalian skin comprises epidermis and dermis, separated by the basement membrane. The epidermis consists of multilayered epithelium, hair follicle, sebaceous gland and arrector pili muscle. The basal layer resides on the basement membrane can differentiate into spinous layer, granular layer and stratum corneum.

36, 37]. In recent years, emerging technologies including live animal imaging and single cell genomics have made it possible to examine hair follicle morphogenesis at single cell resolution[38, 39].

Before mouse hair follicle induction begins at around embryonic day 13.5(E13.5), basal epidermal cells are a single uniform layer of cells without distinct morphological signs of hair follicle formation(Fig1.3)[40, 41, 42, 43]. With the activation of *Wnt* signaling in the upper dermis at around E14.5-E17.5, the epidermal cells start to form the hair placode as the future site of hair follicle[40, 42, 43, 44, 45, 46]. The neighboring fibroblast cells in the dermis begin to aggregate into the mesenchymal dermal condensate[43, 45, 46, 47]. At around E16.0, the placode elongates into the hair germ and further invaginates into the dermis. The epithelial cells start to form in a concentric orientation around the axis of the future hair follicle in the following hair peg stage. The *Sox9+* precursor cells are maintained at the posterior of the hair follicle, responsible for future hair follicle stem cells and sebaceous gland[43, 48, 49]. The dermal condensate remains at the leading edge and transitions into mature dermal papillae(DP). The matrix cells in the middle portion begin to form a bulb-like shape and hair follicle lineages start to specify, including inner root sheath(IRS) and hair shaft[43, 50, 51, 52]. The outer root sheath(ORS) contiguous with the basal cells is surrounded by the basement membrane. Maturation continues as a companion layer separates the ORS and IRS and the hair shaft develops further into three concentric layers(cuticle, cortex, medulla)[53]. As the hair follicle continues to grow, it extends to the subcutaneous level downward and the hair shaft penetrates through the epidermis upward[53, 54].

1.2.2 Adult hair cycle and hair follicle structure

Adult mouse hair follicles undergo cyclic bouts of transformation from hair regeneration (anagen), degeneration (catagen) to quiescence (telogen)[44, 45, 53, 55]. This cycling is unique in hair follicles and in each cycle a new hair shaft is generated. The old hair shaft eventually sheds in a process called exogen[53, 56]. For mouse hair follicles, the first two cycles are relatively synchronized in the back skin with minor variations in the timing depending on gender and genetic background. Generally, based on the study of the C57BL mouse strain, the first telogen phase

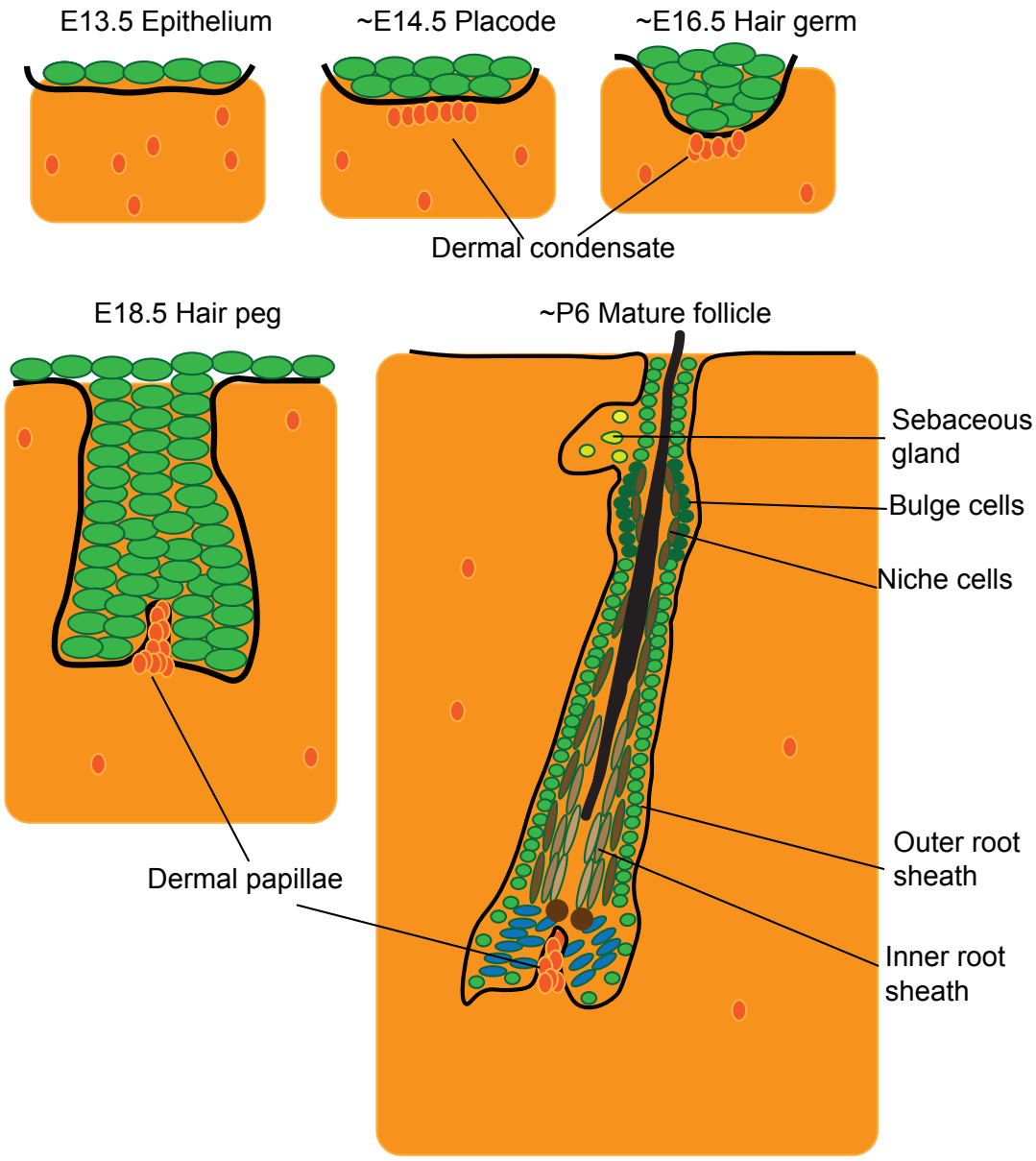

Figure 1.3: **Hair follicle morphogenesis.** Starting around embryonic day 14.5(E14.5), epidermal and dermal cells orchestrate the hair follicle morphogenesis by signal transduction. The dermal cells aggregate to form the dermal condensate and dermal papillae. The epithelial cells invaginate downward and differentiate into mature hair follicles through signaling cross-talk.

starts around postnatal day 19(P19) and lasts only 2-3 days. Immediately following that is the regenerative phase, anagen, from around P22 to P35. During anagen, the hair follicles extend downward in a two-step process[57]. First, the hair germ as the major contributor of hair follicle regeneration starts to proliferate, pushing the dermal papilla downward and reconstituting the hair bulb and matrix(Fig1.4). The transit amplifying matrix cells can then differentiate into IRS and give rise to a new hair shaft. Subsequently, the bulge hair follicle stem cells start to divide at the end of anagen[53, 57]. After the completion of anagen at around P35, the hair follicles enter catagen. The catagen phase is a short transient stage when cells in the lower two-thirds portion of the hair follicle undergo apoptosis and the upper portion remains intact along with the old hair shaft(club hair). Eventually, the lower hair follicle reduces to an epithelial strand, moves upward and brings the dermal papilla close to the bulge. After catagen, the hair follicles enter telogen.

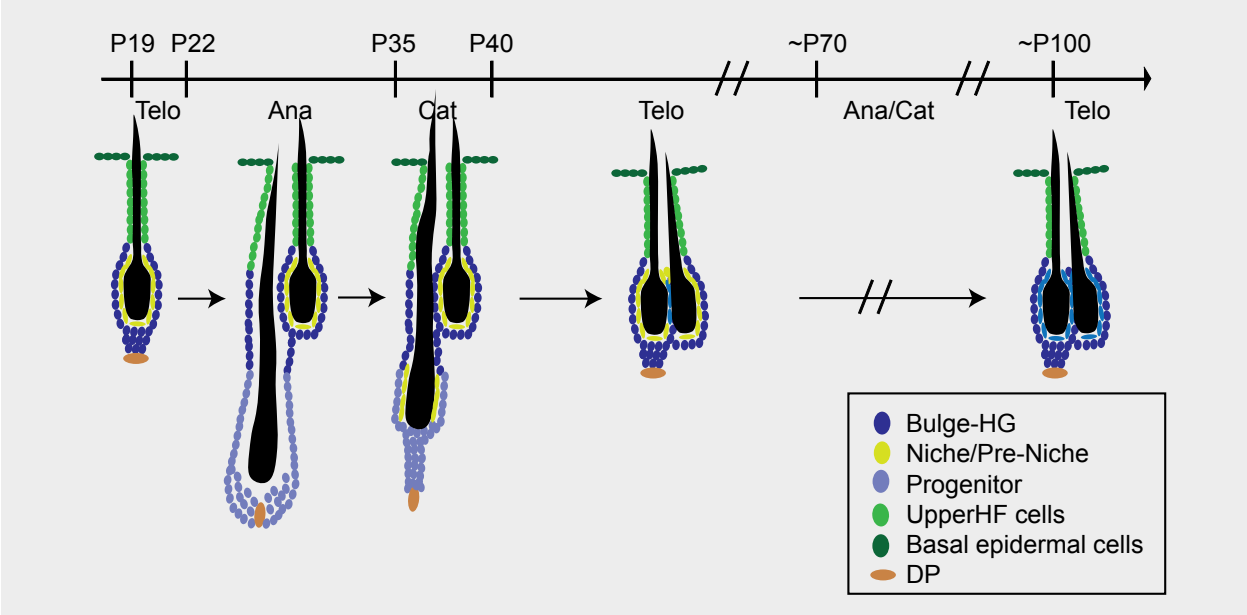

Figure 1.4: **Schematic of the adult mouse hair cycle.** Hair follicle undergoes cycles of telogen (Telo), anagen (Ana), and catagen (Cat) throughout the lifetime of the animal. The hair follicle at each stage has distinct morphology. At the onset of each anagen stage, bulge HF-SCs and HG cells start to proliferate and initiate hair follicle regeneration, followed by the destructive catagen in which the lower portion of hair follicle undergoes apoptosis. The hair follicle then reenters into telogen stage for a long period of time. Figure modified from Lay, K., Kume, T., Fuchs, E. (2016). Proceedings of the National Academy of Sciences, 113(11), E1506-E1515.

The second telogen phase can last for four weeks from around P40 to P70. This periodic hair cycle persists throughout the life of the animal. Although the anagen and catagen lengths are similar irrespective of the hair cycle, the telogen stage becomes significantly longer with age[58]. Hair growth therefore becomes increasingly asynchronous such that aged mice display discrete patches of regenerating, anagen regions and quiescent, telogen regions[59].

1.2.3 Hair follicle stem cell(HF-SC)

In each hair cycle, a new hair follicle will be generated[53, 56, 58]. Like other regenerative tissues, this periodic process is fueled by stem cells. In 1990, nucleotide pulse-chase experiments first revealed the slow-cycling, label-retaining cells in the anatomically distinct bulge region[60]. Around a decade later, researchers used tetracycline-responsive histone H2B-green fluorescent protein(GFP) and further supported the existence of quiescent, slow-cycling hair follicle stem cells(HF-SCs) contributing to the hair follicle regeneration and wound repair[61, 62, 63, 64]. Shortly after the discovery of HF-SC specific cell surface markers CD34 and α6-integrin[63, 65], the isolation of HF-SCs based on fluorescent-activated cell sorting(FACS) led to further molecular characterization. Subsequent transcriptional profiling of HF-SCs showed enriched expression of signature genes, including transcription factors *Foxc1*, *Nfatc1*, *Sox9*, *Lhx2*, *Lgr5*, *Tcf3*[20, 23, 59, 66, 67, 68, 69, 70].

1.2.4 Molecular mechanisms of HF-SC quiescence

In adult mice, HF-SCs can persist in the quiescent stage for long periods of time and only activate during anagen. Temporal analysis of HF-SCs isolated from different stages allows for a closer look at the underlying transcriptomic changes between active and quiescent stages[62, 63]. Indeed, many cell cycle related genes such as *Cyclin D1*, *Top2A*, *CenpE* and components in *Wnt* and *BMP* signaling pathways are highly differentially expressed in active versus quiescent HF-SCs[57, 61, 62, 65, 71, 72]. Further investigations of HF-SCs quiescence/activation regulation mostly focused on signaling pathways and transcription factors. Just like embryonic hair follicle morphogenesis, the adult HF-SC activation is mediated by the interacting signals from the bulge and

dermal papillae(DP). The decision to transition between quiescence and activation appears to result from the antagonistic interplay between *BMP* signaling and *Wnt*/β-catenin signaling(Fig1.5)[51, 72, 73, 74, 75, 76]. *Wnt*/β-catenin signaling is up-regulated at anagen entry mediated by the *Wnt3a* and *10b* ligand expression[77]. Corroborating this, β-catenin translocates into the nucleus just before hair follicle enters anagen[57, 78]. Genetic approaches including expression of constitutively stable β-catenin leads to hyperactive *Wnt*/β-catenin signaling and precocious anagen induction[79, 80]. Conversely, deletion of β-catenin or Wntless genes blocks entry to anagen[75, 76, 81]. On the other hand, accumulating evidence suggests *BMP* play a major role in the regulation of HF-SC quiescence. Postnatal inhibition of *BMP* signaling by ectopic *Noggin* expression and conditional deletion of *Bmpr1a* in HF-SC leads to loss of quiescence[74, 82, 83]. Additional signaling pathways including *Fgf*, *Shh* and *Tgf-*β all collaboratively regulate the activation-quiescence balance in HF-SCs.

Several transcription factors such as *Runx1*, *Foxc1*, *Nfatc1*, *Lhx2* and *Tcf*3/4 are important intrinsic regulators of HF-SC quiescence[20, 23, 59, 66, 68, 70, 84]. Among them, *Runx1* negatively regulates HF-SC quiescence and deletion of which leads to prolonged quiescence. In contrast, *Foxc1*, *Nfatc1*, *Lhx2*, *Tcf*3/4 all functionally maintain HF-SC in the quiescent stage. The transcription factors can target signaling components and cell cycle regulators to control the HF-SC quiescence. For instance, *Nfatc1* has been shown to target *Cdk4* to maintain quiescence and *Foxc1* can activate *BMP* signaling[23, 66]. Understanding the intricate regulation of stem cell quiescence allows me to ask fundamental questions such as whether the quiescence is required for the long-term maintenance of HF-SCs function.

1.3 Hair follicle aging

The mouse hair follicle is an excellent experimental model to examine cellular activities and molecular networks of largely quiescent stem cell populations during aging. Hair follicles loss and graying have been widely recognized as macroscopic signs of aging both scientifically and culturally. At the cellular levels, hair follicle miniaturization associates with hair loss during aging[21]

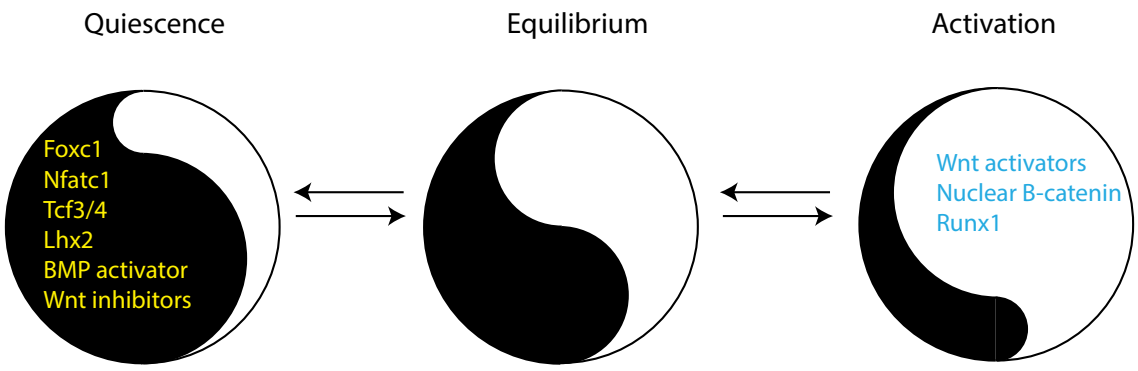

Figure 1.5: **Molecular regulation of HF-SC quiescence.** The balance between *BMP* signaling, *Wnt*/β-catenin and transcriptional regulation mediates the activation and quiescence of HF-SCs.

and alopecia caused by premature hair loss[85, 86]. Although the molecular mechanism of hair follicle aging is not completely understood, recent studies have demonstrated multiple mechanisms including both intrinsic and extrinsic regulations.

1.3.1 Intrinsic mechanism

Accumulation of DNA damage during aging compromises tissue stem cell function. Comparative analysis of transcriptome from aged and young HF-SCs reveals that DNA damage accumulates in HF-SCs during aging. Aging HF-SCs increase γH2A.X foci and DNA strand breaks[21]. This leads to sustained rather than transient DNA damage. The accumulation of DNA damage causes loss of HF-SC signature and the epidermal commitment[21].

Aging reduces chromatin accessibility in HF-SCs, particularly at bivalent lineage-specification genes[87]. In addition, multiple transcription factors play a role in hair follicle aging[15]. *Nfatc1* expression in aging hair follicle stem cells can keep them in quiescent stages for longer times[59]. Conversely, inhibition of *Nfatc1* activity leads to higher colony formation and HF-SC activity in vitro[59]. *Foxc1* ablation in vivo causes repetitive activation and reduces hair regeneration during aging[20]. In addition, when the hair follicles are forced to undergo hair cycle by repeated depilation, the hair coat shows accelerated greying[59]. These lines of evidences all point toward the limited

capacity of HF-SCs and repetitive use could render aging HF-SCs less competent to regeneration.

In aging HF-SCs, miR-31 is upregulated, the deletion of which conversely suppresses physiological hair follicle aging. MiR-31 activates mitogen-activated protein kinases($MAPK$) pathways through a prominent circadian rhythm gene, *Clock* and leads to the trans-epidermal differentiation of HF-SCs. Tantalizing evidence showed that pharmacological inhibition of $MAPK$ can ameliorate the premature hair follicle aging induced by miR-31 overexpression or ionizing radiation. These exciting findings offer new possibilities for treating hair follicle aging[88, 89].

1.3.2 Extrinsic mechanisms, the microenvironment

It has been demonstrated in HF-SCs and muscle satellite cells, changes in the microenvironment also contribute to tissue stem cell aging[19, 59, 90]. Remarkably, engraftment of HF-SCs from old mice along with neonatal dermal cells can generate hair follicles on nude mice recipients. In contrast, even young HF-SCs fail to grow hair when engrafted with old dermis cells[19, 87]. Together, these studies present compelling evidence that the HF-SC microenvironment, especially the dermal environment, could override the limited regeneration capacity of HF-SCs in aging animals.

Growing evidences suggest a role for mechanical stress in HF-SCs aging. Systematic proteome profiling, electron microscopy analysis and atomic force microscopy-based force indentation experiments demonstrate the basement membrane stiffens during aging[87]. The aging induced niche stiffening causes mechanical stress and wide-spread transcription silencing in HF-SCs[87]. The reduction of hair shaft in diameters can prevent the mechanical compression of HF-SCs[91]. The hair shaft miniaturization during aging leads to HF-SC compression and activates mechanosensitive channel *Piezo1*. This can further induce continuous apoptosis of HF-SCs through the influx of calcium[91].

Cell apoptosis as resulted from accumulated DNA damage, mechanical stress or altered signaling pathways is the primary cause of HF-SCs aging[21, 59]. In addition, the microenvironment can limit the regenerative capacity of HF-SCs. The relative contributions of intrinsic versus extrinsic factors on aging in HF-SCs are still unclear, and few studies have systematically and unbiasedly

investigated the gradual changes of hair follicle lineages during aging. In addition, like other tissue SCs, HF-SCs and their activities have not been examined in live animals during aging.

Chapter 2

Escape of hair follicle stem cells causes stem cell exhaustion during aging

All the work in this chapter is published online: Chi Zhang, Dongmei Wang, Jingjing Wang, Li Wang, Wenli Qiu, Tsutomu Kume, Robin Dowell, and Rui Yi. "Escape of hair follicle stem cells causes stem cell exhaustion during aging." Nature Aging 1, no. 10 (2021): 889-903. For this project, C.Z., D.W. and R.Y. designed experiments. C.Z. carried out most experiments and computational analysis with assistance from D.W. J.W. performed two-photon imaging for some control experiments. L.W. helped to analyze scATAC-seq data. W.Q. generated the *Itgb6*-KO mouse and provided samples. T.K. generated *Foxc1* mouse models. R.D. supervised computational analysis. R.Y. and R.D. were co-mentors to C.Z.

2.1 Introduction

Aging is defined as functional decline of tissues and organisms and contributes to many human diseases including cancer and neurodegenerative disease[10, 11]. Although it is widely recognized that stem cell(SC) exhaustion is a hallmark of aging[11], cellular activities of tissue SCs during aging have rarely been observed in their intact microenvironment[16, 17]. It remains largely unknown how tissue SCs divide, migrate and perish during aging. Without a clear picture of these fundamental cellular behaviors, current knowledge of tissue SCs aging has been acquired through indirect measurement of SC numbers and functions[18, 19, 20, 21, 22, 23]. As a result, our understanding of SC exhaustion is largely limited to the deficiency of cell division and self-renewal, usually caused by DNA damage and cellular senescence[21, 24, 92, 93, 87, 91].

Among fundamental properties of tissue SCs, quiescence is known to play an important role in SC maintenance by restricting the number of SC divisions and reducing cellular stress[25, 26, 27, 72]. Although the loss of quiescence was shown to cause the lost proliferative potential of SCs in cell-intrinsic manner[28, 29], SC activities have not been visualized when they lose quiescence. Furthermore, it is unclear whether the loss of SC quiescence affects integrity of the SC compartment independently of cell-division control. Finally, SC division rates generally decrease during aging[30], it remains an open question how prolonged SC quiescence affects aging.

The hair follicle(HF) of mammalian skin is an excellent experimental system to examine cellular activities and molecular networks of largely quiescence SC populations during aging. HF loss and graying have been widely recognized as macroscopic signs of aging both scientifically and culturally. At the cellular level, HF miniaturization was reported to associate with hair loss during aging[21] and alopecia caused by premature hair loss[85, 86]. In these studies, cell apoptosis as a result of accumulated DNA damage or altered signaling pathways, which are critical for hair growth, are identified as underlying mechanisms of SC exhaustion or compromised hair growth, respectively. However, hair follicle stem cells(HF-SCs) and their activities have not been examined in live animals during aging.

In this study, we use noninvasive intravital imaging and single-cell genomic tools to measure multiple modalities of HF-SCs including cellular activities, the transcriptome and open-chromatin landscape in aged HFs. Surprisingly, we observe that numerous epithelial cells, many of them located near the bulge SC compartment, escape to the dermis during aging. We characterize the reduced expression of cell adhesion and extracellualr matrix(ECM) genes as a prominent feature of aged HF-SCs and identify FOXC1 and NFATC1 as key regulators of HF-SC-specific cell adhesion. Deletion of the two corresponding genes recapitulated epithelial cell escape and leads to rapid HF miniaturization and hair loss. Our study reveals SC escape as a new mechanism for SC reduction and tissue degeneration.

2.2 Results

2.2.1 Escaped epithelial cells in aged HFs

To visualize the HF-SC compartment in live animals during aging, we used two-photon intravital imaging to observe histone H2B-green fluorescent protein(H2BGFP)-labeled(*Krt14*-H2BGFP) epithelial cells in HFs[94, 95] in both young(∼6-8-month(mo)-old) and old(>20-mo-old) mice. In young mice, the HF-SC compartment was readily distinguished by the convex morphology of the bulge region, which is located below the morphologically distinct sebaceous gland(SG), and epithelial cells were restricted within the cylinder of HFs regardless of hair cycle stages(Fig2.1a and Fig2.1Sa). By contrast, miniaturized HFs, which are characterized by reduced cellularity, a shrinking bulge compartment and the upward movement of HF-SC compartment toward SGs, were frequently observed in old mice(Fig2.1a). In some of these HFs, individual H2BGFP+ epithelial cells were located outside of the typical HF cylinder but in close proximity to the HF(Fig2.1a and Fig2.1Sb). We also used second-harmonic-generation imaging of dermal collagen fiber and confirmed the localization of these H2BGFP+ epithelial cells in the dermis(Fig2.1b). We therefore refer to these cells as escaped epithelial cells.

We next quantified the size of the HF-SC compartment of telogen HFs in young and old mice. We observed a gradual but significant reduction in the size of the HF-SC compartment in old mice(Fig2.1c). Overall, ∼14.5% of the HF-SC compartment was miniaturized(defined by size smaller than the smallest HF-SC compartment in young mice) in ∼20-mo-old animals(Fig2.1c and Fig2.1Sc). Furthermore, ∼5.8% of aged HFs contained escaped H2BGFP+ epithelial cells near HF-SC compartment(Fig2.1d). HFs with escaped epithelial cells were also significantly smaller than HFs without escaped cells(Fig2.1e). We have also examined apoptotic cells within the HF-SC compartment, which were previously shown to contribute to HF miniaturization[21]. On average, we observed that ∼4.8% aged HFs contained apoptotic HF-SCs marked by activated caspase 3 within the bulge region and ∼4.8% within hair germs(HGs) We also observed ∼3.8% of young HFs contained apoptotic HF-SCs within the bulge and ∼5.8% within HGs(Fig2.1Sd-f). These

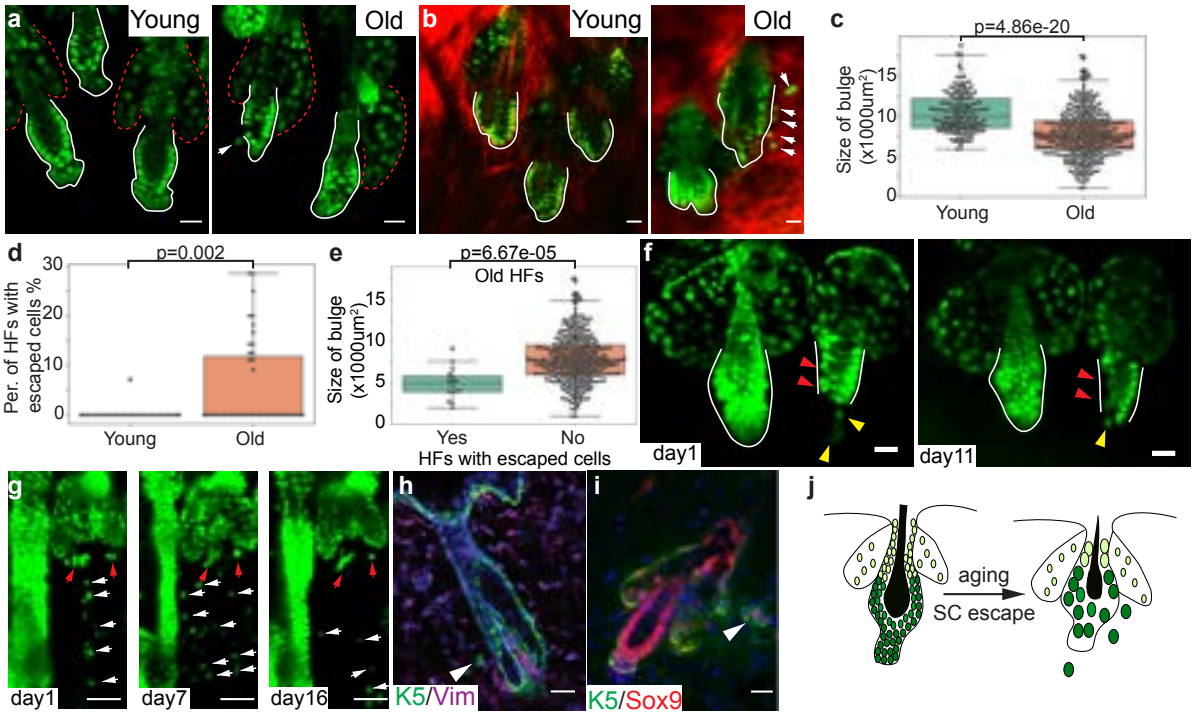

Figure 2.1: **aging HFs are characterized by escaped epithelial cells.** **a-b**, Two-photon intravital imaging of young (P42) and old (20mo) HFs. White arrows point to cells of outside of the HF-SC compartment. Red dashed lines outline the SG. White lines outline the HF-SC compartment. Red signals in (**b**) are second-harmonic-generation from collagen fiber in the dermis. Scale bar, 20μm. **c**, Box plot of the size of HF bulge region, quantified from 3-D scan of live animals. (n=205 HFs from 5 young mice; n=327 HFs from 3 old mice). **d**, Box plot of the percentage of HFs containing escaped epithelial cells, quantified from 3-D scan of live animals. (n=205 HFs from 5 young mice; n=327 HFs from 3 old mice). **e**, Box plot of the size of HF bulge region, classified based on whether HFs containing escaped cells or not. (n=327 HFs from 3 old mice). **f**, Longitudinal tracking of the same HFs in old mice (20mo) over 11 days. Red arrowheads point to epithelial cells in the bulge region, which disappear during the tracking. Yellow arrowheads point to escaped cells outside of HF-SC compartment. White lines outline the bulge region. Scale bar, 20μm. **g**, Longitudinal tracking of a rapidly miniaturized HF in old mice (20mo) over 16 days. White arrows point to escaped epithelial cells in the dermis; red arrows point to the miniaturized HF. Scale bar, 50μm. **h**, Immunofluorescence signals of an old HF (24mo) containing an escaped, KRT5+ epithelial cell near the bulge region. Arrowhead points to a KRT5+(K5) epithelial cell in the dermis. Scale bar, 20μm. **i**, IF signals of an old HF (24mo). The arrowhead points to KRT5+SOX9+ epithelial cells near the bulge region in the dermis. Scale bar, 20μm. **j**, Illustration of HF aging accompanied by escaped cells.

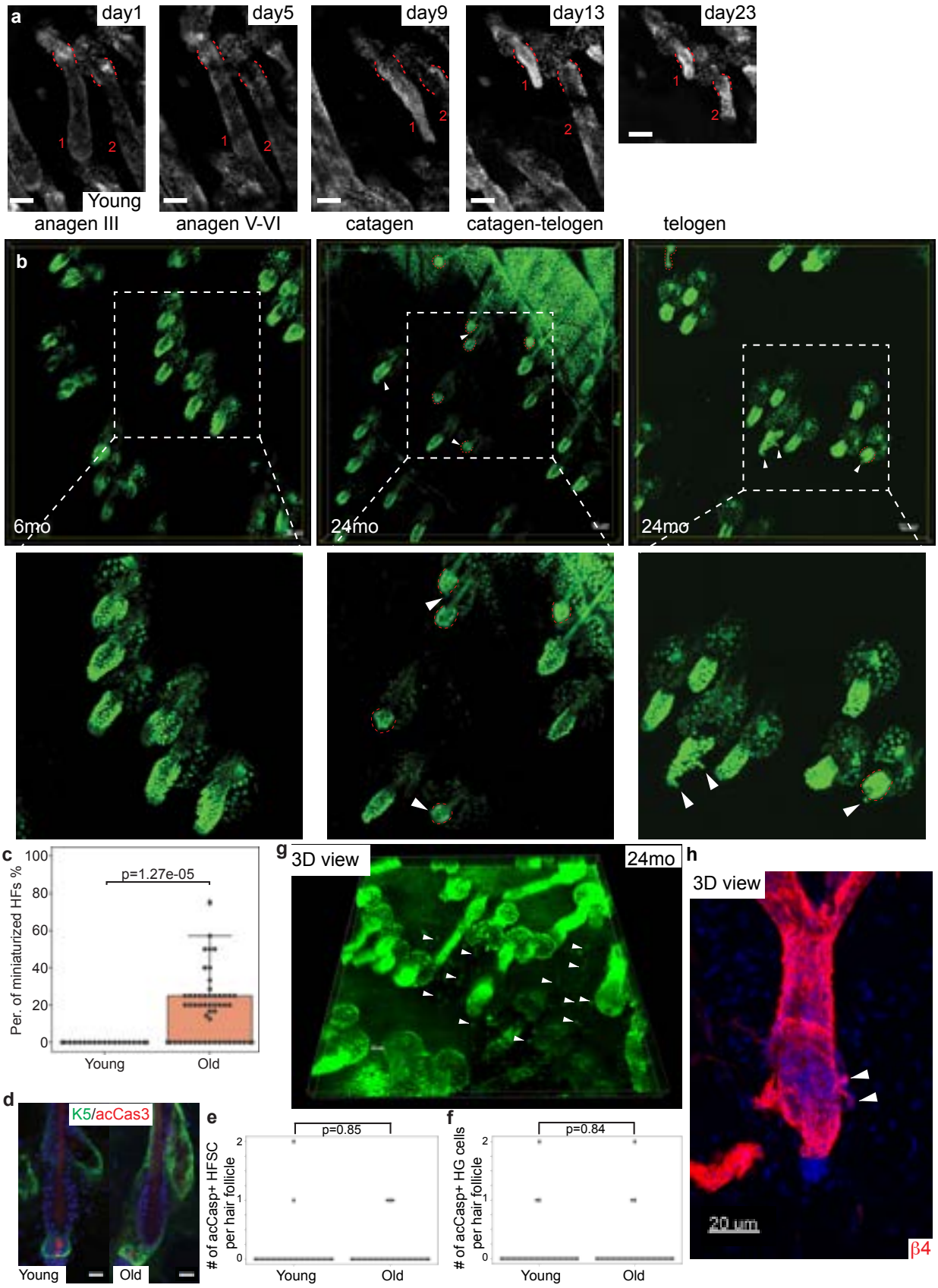
a
day1
day5
day9
day13
day23
Young
anagen III
anagen V-VI
catagen
catagen-telogen
telogen
b
6mo
24mo
24mo
c
Per. of miniaturized HFs %
p=1.27e-05
Young
Old
d
K5/acCas3
Young
Old
e
# of acCasp+ HFSC per hair follicle
p=0.85
Young
Old
f
# of acCasp+ HG cells per hair follicle
p=0.84
Young
Old
g
3D view
24mo
h
3D view
20 um
β4

Figure 2.1S: **Live imaging of escaped cells in aging hair follicles. a**, Two-photon longitudinal tracking of hair follicles in young mice during the anagen to telogen hair cycle. Red numbers designate the same hair follicle in each image. Red dotted lines annotate the bulge region. Scale bar, 50μm. **b**, Two-photon intravital imaging of hair follicles from young (left panel) and old (middle and right panels) mice. White arrowheads point to miniaturized hair follicles and cells located outside of the HF-SC compartments. Red dotted lines outline miniaturized hair follicles. Scale bar, 50μm. **c**, Box plot of the percentage of miniaturized hair follicles, quantified from 3-D scan of live animals. (n=205 HFs from 5 young mice; n=327 HFs from 3 old mice). **d**, Representative images of hair follicles with KRT5 and activated caspase 3(acCas3) signals in young (6$\sim$8mo) and old (20mo) mice. (n=50 hair follicles from young mice; n=62 hair follicles from old mice, 3 pairs of mice). Scale bar, 20μm. **e-f**, Boxplot of number of acCas3+ HF-SCs(e) and HG(f) per hair follicle (n=50 hair follicles from young mice; n=62 hair follicles from old mice, 3 pairs of mice). **g**, 3-D view of hair follicles in 24mo old mice. White arrowheads point to numerous escaped epithelial cells scattering in the dermis. Scale bar, 50μm. **h**, 3-D view of β4 integrin immunofluorescence signals in 24mo old mice. White arrowheads point to HF-SCs with protruding integrin signals in the new bulge side. Scale bar, 20μm.

data suggest that the number of apoptotic cells, as detected by activate caspase 3, does not differ drastically in young and old mice.

To examine the relationship between epithelial cell escape and HF miniaturization, we longitudinally tracked the same HFs, which usually rested in the quiescent telogen phase, in live animals. In most frequently observed cases, we first observed signs of loosely organized epithelial cells in the bulge region in contrast to the stereotypical morphology of tightly packed HF-SC compartment in normal HFs. In $\sim$10 days, these HFs lost some loosely organized epithelial cells and became smaller(Fig2.1Sf). In some rare but more rapidly progressing cases, we observed numerous H2BGFP+ epithelial cells scattering around miniaturizing HFs. Within a few days, these H2BGFP+ cells spread from the HF to neighboring regions or reached deeper regions of the dermis (Fig2.1g and Fig2.1Sg). In about 2 weeks, however, most of these scattered cells were no longer visible, and the miniaturizing HF was rapidly degenerated(Fig2.1g). We further confirmed the epithelial identity of these scattered cells in the dermis as KRT5+/VIM-(vimentin) and KRT5+/SOX9+ cells in aged mice (Fig2.1h-i). Escape of epithelial cells away from the bulge to the dermis suggests compromised basement membrane(BM). Indeed, we observed HF-SCs in the bulge region protruding toward the dermis with immunofluorescence (IF) staining of β4 integrin,

a BM marker, in old mice (Fig2.1Sh). Taken together, these data reveal an unexpected activity of epithelial cells escaping to the dermis in aged HFs, and establish a correlation between epithelial cell escape and HF miniaturization during aging(Fig2.1j).

2.2.2 Reduced cell adhesion in aged HF-SCs

We next applied single-cell RNA-seq(scRNA-seq) to examine cellular states of skin epithelial cells isolated from young and old mice. HFs experience an increasingly long telogen phase and much less frequent anagen growth in old mice, and, by 18-24 mo, most HFs enter extended telogen, often lasting more than 100 days[96]. Therefore, we profiled the telogen phase as the representative hair cycle stage in young mice at postnatal day (P) 53, the middle of second telogen, and in old mice at 24mo, which showed typical signs of aging such as hair thinning and occasionally gray hair. After quality control, we detected 3,524 epithelial cells in the P53 sample and 2,881 epithelial cells in the 24mo sample(Fig2.2Sa). We aggregated both young and old samples together and applied uniform manifold approximation projection(UMAP) for dimension reduction to visualize, detect cell lineages dynamics and changes in the transcriptome[97]. Overall, three well-characterized, spatially distinct epithelial cell lineages, including interfollicular epidermal(IFE) lineages, infundibular and SG lineages, and HF lineages were identified in both samples(Fig2.2a and Fig2.2Sb,c). The projection of each lineage and individual cell clusters from young and old samples largely overlap. To gain deeper insights into different cellular states at a higher resolution, we reclustered IFE and HF cells from young and old samples. Notably, epithelial cells in the HF-SC compartment from young mice were readily resolved into two distinct populations corresponding to outer-bulge HF-SCs and inner-bulge niche cells, marked by Keratin(KRT)24 and fibroblast growth factor(FGF)18, respectively(Fig2.2b,c). In contrast, the demarcation of these two distinct populations was greatly reduced in the old sample(Fig2.2b,c), a trend similar to altered cellular states of fibroblasts during aging[98]. Interestingly, although basal cells of the IFE lineages showed different cellular stages in young and old samples, differentiated suprabasal cells from young and old sample clustered together(Fig2.3Sa-d).

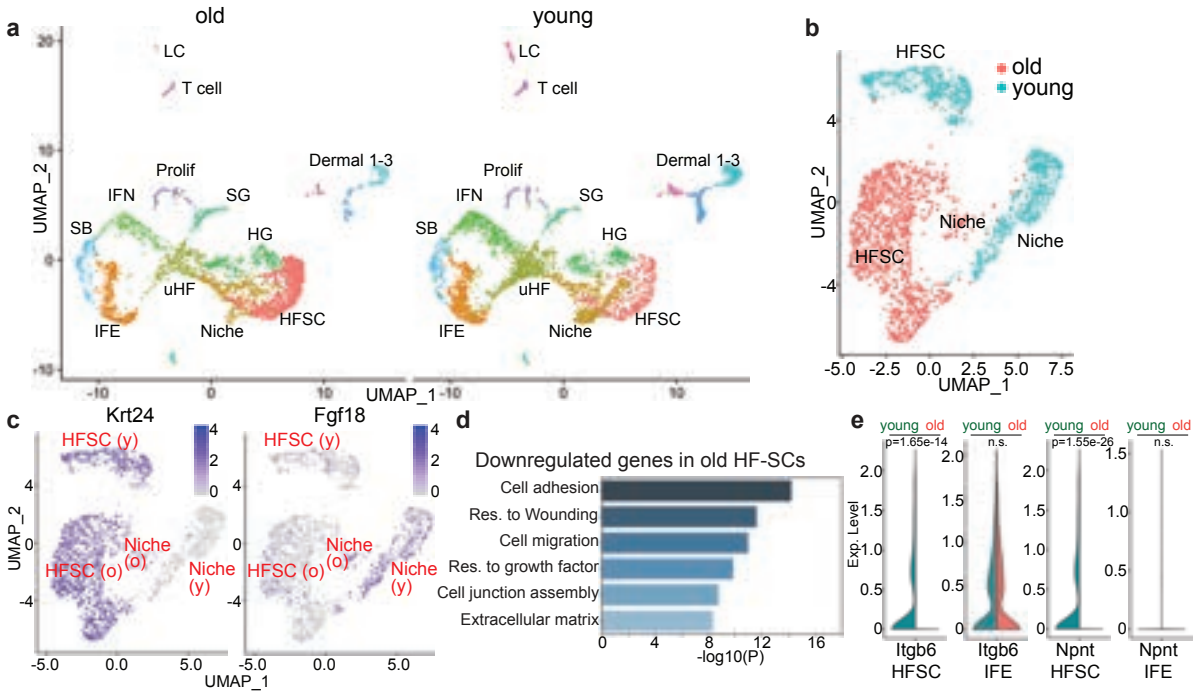

Figure 2.2: **scRNA-seq reveals reduced cell adhesion in aged HF-SCs. a**, UMAP clustering of skin cells from old (left) and young (right) mice. Major cell types are classified using marker genes and color coded with cell identity. uHF, upper HF region; IFN, infundibulum; dermal 1–3, three dermal populations; SB, suprabasal cells; prolif, proliferating cells; LC, Langerhans cells. **b**, UMAP reclustering of HF-SCs and niche cells in old and young mice. **c**, Feature plots of marker genes for HF-SCs (*Krt24*) and inner-bulge niche cells (*Fgf18*) in old (o) and young (y) samples. **d**, Highly enriched GO terms of downregulated genes in old HF-SCs. Res., response. **e**, Violin plots of selected cell adhesion and ECM genes in HF-SCs and IFE cells. Exp., expression; NS, not significant. Nonparametric Wilcoxon rank-sum tests were performed.

a

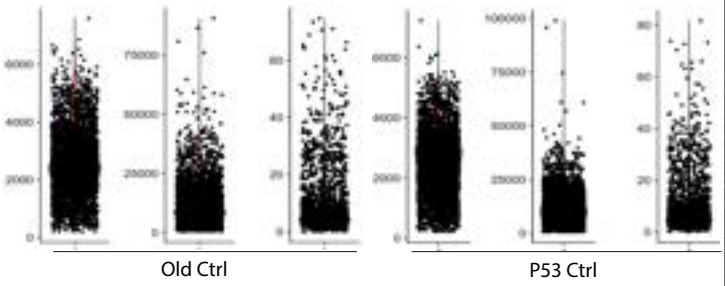

c

	old	% of all cells	young	% of all cells
HFSC	921	31.7	425	11.7
Niche	343	11.8	536	14.8
HG	256	8.8	206	5.7
IFE	396	13.6	492	13.6
Supra	132	4.5	136	3.7
UpperHF	259	8.9	570	15.7
IFN	170	5.8	423	11.7
SG	175	6.0	113	3.1
Prolif	87	3.0	90	2.5
Dermal1	64	2.2	220	6.1
Dermal2	46	1.6	156	4.3
Dermal3	29	1.0	78	2.1
Langer	3	0.1	79	2.2
Tcells	27	0.9	104	2.9
Total	2881	100.0	3524	100.0

b

Figure 2.2S: **Quality control and clustering of single-cell RNA-seq data from young and old mice.** **a**, Quality control and filtering of single cells from old and young samples. Cells were filtered with detected genes numbers (200<nFeature_RNA<5000), transcripts numbers (nCount_RNA) and mitochondrial percentage (percent.mt < 10). **b**, Track plot of marker genes for each cluster. **c**, Table shows cluster names, cell numbers and percentage of cells for each cluster after filtering of old and young scRNAseq data.

We next performed differential gene expression analysis for HF-SCs and IFE basal cells between young and old samples. The most significantly downregulated genes in old HF-SCs were enriched for gene ontology(GO) terms such as regulation of cell adhesion, response to wounding, cell junction assembly and the ECM(Fig2.2d and Table S1). Upregulated genes in old HF-SCs were enriched for the transcription factor(TF) AP1 complex and the apoptotic signaling pathway(Fig2.3Se, Table S2). The most enriched GO categories in downregulated genes from old basal IFE progenitors were the major histocompatibility complex class I peptide-loading complex, response to wounding and negative regulation of cell differentiation(Fig2.3Sf). The specificity of downregulated cell adhesion and ECM genes in old HF-SCs was further supported by examining individual genes. For example, *Actg1* and *Itgb6* are widely expression genes in both HF-SCs and IFE basal cells but were only downregulated in old HF-SCs and not in IFE cells(Fig2.2e and Fig2.3Sg). Npnt(nephronectin), an HF-SC-specific ECM gene[99], was only detectable in HF-SCs and downregulated in old samples(Fig2.2e and Fig2.3Sg). By contrast, Jun and Junb, both encoding AP1 TFs, were upregulated in both HF-SCs and IFE cells from old mice.

We performed pseudotime analysis using Monocle3[100] to examine lineage progression. It recapitulated the differentiation trajectory of distinct HF lineages in both young and old samples (Fig2.3Sh). Interestingly, we observed a differential distribution of young and old HF-SCs along the pseudotime trajectory(Fig2.3Si). Young HF-SCs clustered in a more ground state, which was characterized by elevated gene expression in the adherens junction, tissue morphogenesis and regulation of cell adhesion. By contrast, many more old HF-SCs clustered in a more differentiated state, which was characterized by less cell adhesion (Fig2.3Sj). These data reveal the reduction of cell adhesion and ECM gene expression specifically in aged HF-SCs.

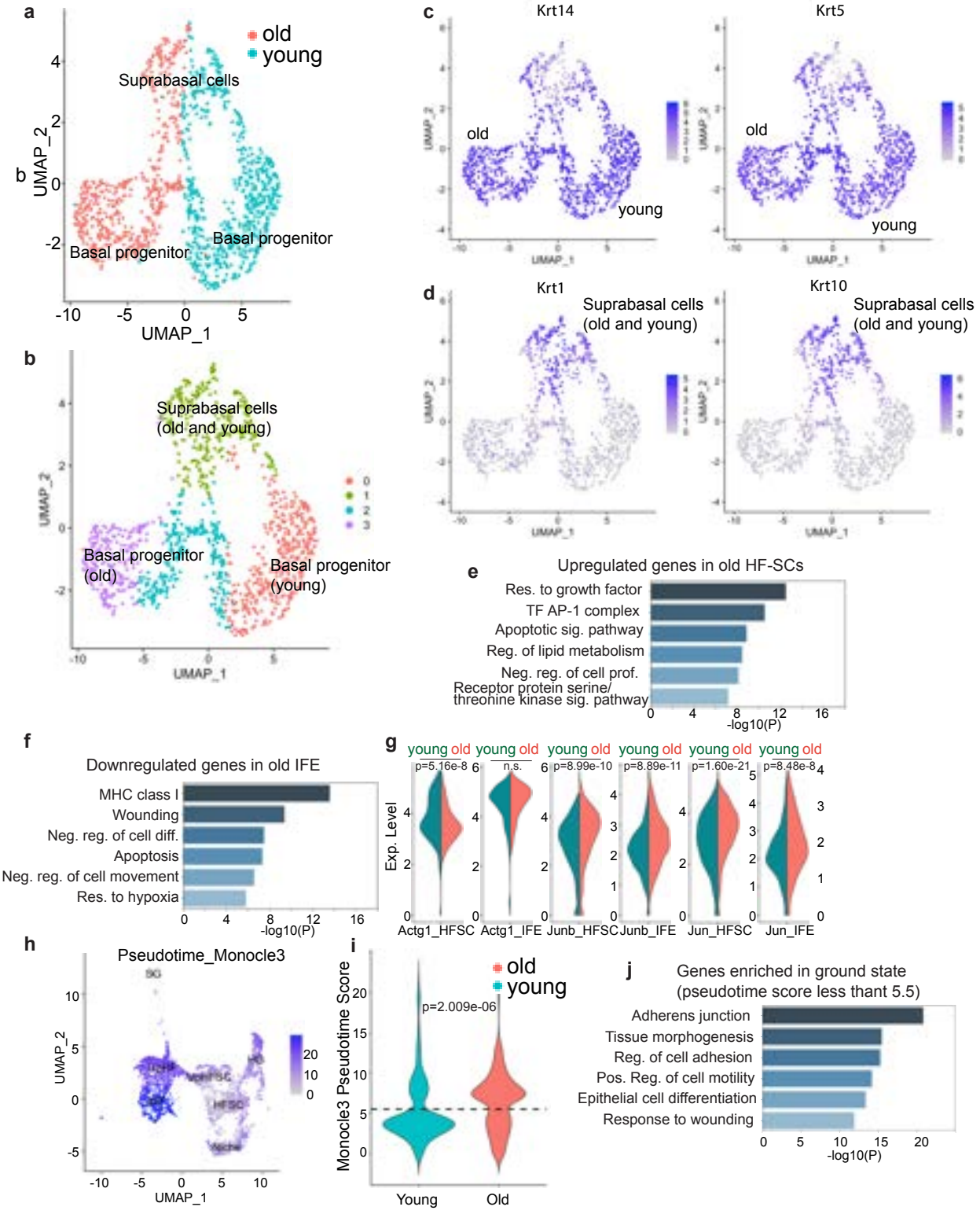
a
old
young
Suprabasal cells
Basal progenitor
Basal progenitor
UMAP_2
UMAP_1
b
Suprabasal cells
(old and young)
Basal progenitor
(old)
Basal progenitor
(young)
UMAP_2
UMAP_1
c
Krt14
Krt5
old
young
old
young
d
Krt1
Suprabasal cells
(old and young)
Krt10
Suprabasal cells
(old and young)
e
Upregulated genes in old HF-SCs
Res. to growth factor
TF AP-1 complex
Apoptotic sig. pathway
Reg. of lipid metabolism
Neg. reg. of cell prof.
Receptor protein serine/
threonine kinase sig. pathway
-log10(P)
f
Downregulated genes in old IFE
MHC class I
Wounding
Neg. reg. of cell diff.
Apoptosis
Neg. reg. of cell movement
Res. to hypoxia
-log10(P)
g
young old
p=5.16e-8
n.s.
p=8.99e-10
p=8.89e-11
p=1.60e-21
p=8.48e-8
Exp. Level
Actg1_HFSC
Actg1_IFE
Junb_HFSC
Junb_IFE
Jun_HFSC
Jun_IFE
h
Pseudotime_Monocle3
UMAP_2
UMAP_1
i
old
young
p=2.009e-06
Monocle3 Pseudotime Score
Young
Old
j
Genes enriched in ground state
(pseudotime score less thant 5.5)
Adherens junction
Tissue morphogenesis
Reg. of cell adhesion
Pos. Reg. of cell motility
Epithelial cell differentiation
Response to wounding
-log10(P)

Figure 2.3S: **Single-cell transcriptomic analysis of old and young skin samples. a-b**, UMAP re-clustering and projection of IFE cells, color coded by sample identity (**a**) and cluster identity (**b**). **c-d**, Feature plots of marker genes for basal progenitor cells (*Krt14*, *Krt5*) and suprabasal cells (*Krt1*, *Krt10*). **e-f**, Highly enriched GO terms for upregulated genes in old HF-SCs (**e**) and downregulated genes in old IFE (**f**). **g**, Violin plots of selected gens in young and old HF-SC and IFE cell clusters. **h**, Feature plot of monocle3 pseudotime score of hair follicle cells from old and young mice. **i**, Violin plot of HF-SCs pseudotime score in young and old samples. **j**, Highly enriched GO terms for HF-SCs in the ground state with lower pseudotime score (<5.5).

2.2.3 Downregulation of *Foxc1* and *Nfatc1* in aged HF-SCs

To probe the transcriptional mechanism that underlies reduced gene expression during aging, we identified several enriched TF motifs in HF-SC-sepcific open chromatin regions, determined by ATAC-seq, that surround downregulated genes in aged HF-SCs(Fig2.3a). Because aged HFs largely rest in extended telogen[96], the enrichment of ETS-RUNX motifs, which are generally associated with activated HF-SCs[101, 84], was consistent with the lack of anagen HF growth. However, it was paradoxical that TFs promoting quiescence, including NFATC1, FOXC1 and TCF7L2[20, 23, 66, 59, 102], were associated with downregulated genes in largely quiescent HF-SCs populations in aged mice. To examine this issue, we monitored the transcriptional activity of the FOXC1 locus by using *Foxc1*-LacZ knock-in middle-aged mice(∼15mo old). In these mice, most HFs rested in telogen, but some HFs were still infrequently cycling and in anagen. We observed an absence of LacZ signals in quiescent HF-SCs located within the telogen bulge but robust LacZ signals in bulge regions of anagen HFs(Fig2.4Sa-c). Furthermore, IF staining and quantification confirmed reduced expression of FOXC1 in aged HF-SCs located within telogen bulge(Fig2.3b). Of note, *Foxc1* expression in the upper HF and SGs, determined by both *Foxc1*-LacZ and IF signals, was not changed(Fig2.3b and Fig2.4S), reflecting HF-SC-specific *Foxc1* downregulation. In addition, NFATC1 expression was also slightly downregulated in aged HF-SCs(Fig2.3c). We previously showed that *Foxc1* is induced in dividing HF-SCs during anagen phase, and FOXC1 promotes the expression of *Nfatc1* and *Bmp2/6*[23]. Thus, the prolonged telogen diminishes expression of *Foxc1* in aged HF-SCs, likely due to lack of anagen activation.

a

Rank	Motif	Best match to known TFs in HFSCs	p-value
1		Nfatc1	1e-57
2		Jun	1e-54
3		Fox	1e-47
4		Tcf7l2 (Tcf4)	1e-43
5		ETS/Runx	1e-41

b

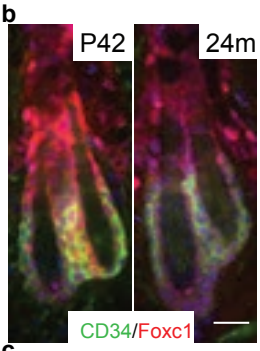

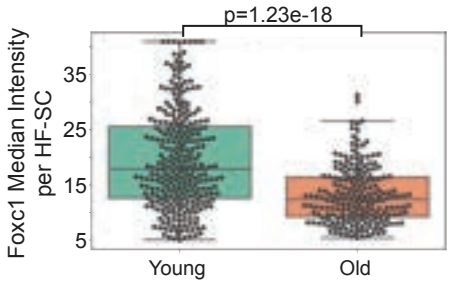

c

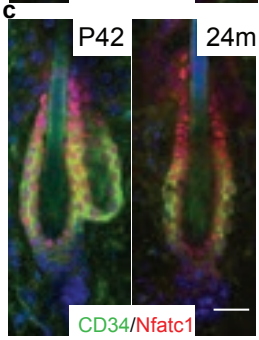

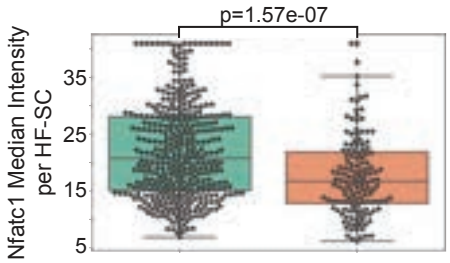

d Downregulated genes in Foxc1 cKO HF-SC

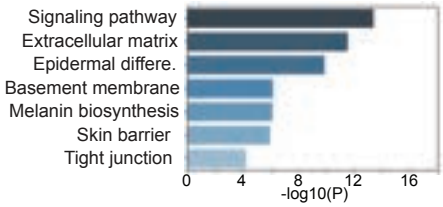

e Downregulated genes in Nfatc1 cKO HF-SC

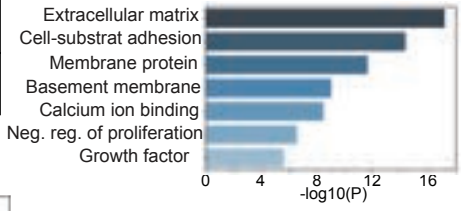

f

Gene	N cKO	F cKO	old
Peg3	-2.74x	-1.41x	-2.62x
Ctgf	-3.51x	n.c.	-1.10x
Itgb6	n.c.	-1.56x	-1.03x
Vwa2	-3.58x	-2.75x	-0.57x
Cd34	-1.52x	n.c.	-0.64x
Fgf18	n.c.	-3.52x	-1.21x
Tle4	n.c.	-1.64x	-0.62x

g

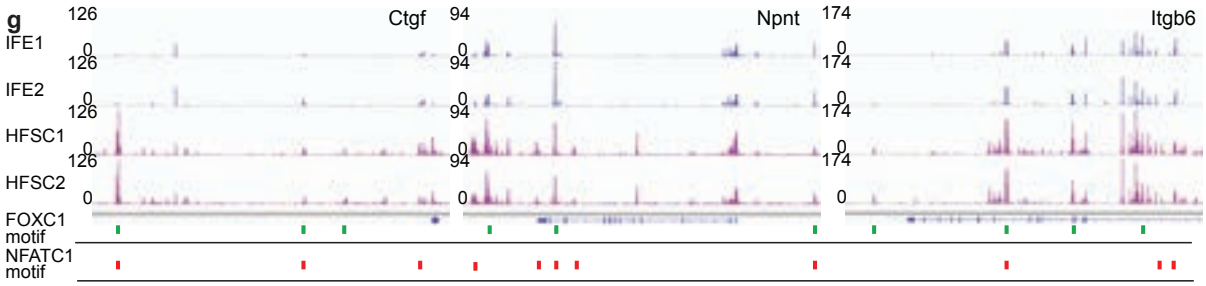

Figure 2.3: **Downregulation of Foxc1 and Nfatc1 in aged HF-SCs.** **a**, Top enriched TF motifs in HF-SC-specific open-chromatin regions surrounding downregulated genes in aged HF-SCs. Hypergeometric tests were performed. **b,c**, IF signals and quantification of FOXC1 and NFATC1 in CD34+ HF-SCs in young (P42) and 24-mo-old (24m) HFs. Scale bar, 20μm. Representative images are from n=5 young mice and n=3 old mice. For FOXC1 signal intensity, means.d.=1,957.39902.23 (young) and 1,312.08512.08 (old). For NFATC1 signal intensity, means.d.=2,198.63845.53 (young) and 1,770.26718.86 (old). Boxes span the first to the third quartile, with the line inside the box representing the median value. Whiskers show minimum and maximum values or values up to 1.5 times the interquartile range below or above the first or third quartile if outliers are present. Data are plotted as individual points and considered outliers beyond whiskers. Two-sided t-tests were performed. **d,e**, Highly enriched GO terms of downregulated genes in *Foxc1*-cKO HF-SCs (**d**) and *Nfatc1*-cKO HF-SCs (**e**). Results from hypergeometric tests with Benjamini–Hochberg P values are shown. Differe., differentiation; neg., negative; reg., regulation. **f**, HF-SC-enriched cell adhesion and ECM genes and their expression change in each cKO strain and old mice. N cKO, *Nfatc1* cKO; F cKO, *Foxc1* cKO; n.c., no change. Wald tests were performed; statistical values are shown in Table S5. **g**, ATAC-seq tracks of *Ccn2*, *Npnt* and *Itgb6* loci in IFE cells and HF-SCs, annotated with FOXC1 (green marks) and NFATC1 (red marks) motifs. ATAC-seq data are normalized and displayed at the same scale across all samples.

We next performed bulk RNA-seq to identify genes downregulated in *Foxc1*-conditional knockout (cKO) (*Krt14-Cre/Foxc1*$^{fl/fl}$) and *Nfatc1*-cKO(*Krt14-Cre/Nfatc1*$^{fl/fl}$) HF-SCs, respectively. Interestingly, cell adhesion, the ECM and BM genes were top enriched GO categories for each cKO, in addition to well-appreciated regulation of signal pathways such as BMP and FGF and the regulation of proliferation(Fig2.3d,e, Table S3 and S4). We further compared these downregulated genes to a published bulk RNA-seq dataset from aged HF-SCs[19] and identified a number of cell adhesion and ECM genes, such as *Ltbp1*, *Ccn2*, *Itgb6* and *Vwa2*, that were commonly downregulated in HF-SCs between aged mice and *Foxc1*- or *Nfatc*-cKOs(Fig2.3f). Interestingly, we also identified genes prominently associated with HF-SC quiescence, such as *Peg3*, *Cd34*, *Fgf18*, *Nog* and *Tle4*[20, 23, 102, 103, 104, 105], that were commonly downregulated in aged and cKO HF-SCs(Table S5). These date lend further support to a link between reduced *Foxc1* and *Nfatc1* expression and the aging of HF-SCs. Our analysis also reveals that extended quiescence of aged HF-SCs diminishes the expression of *Foxc1*.

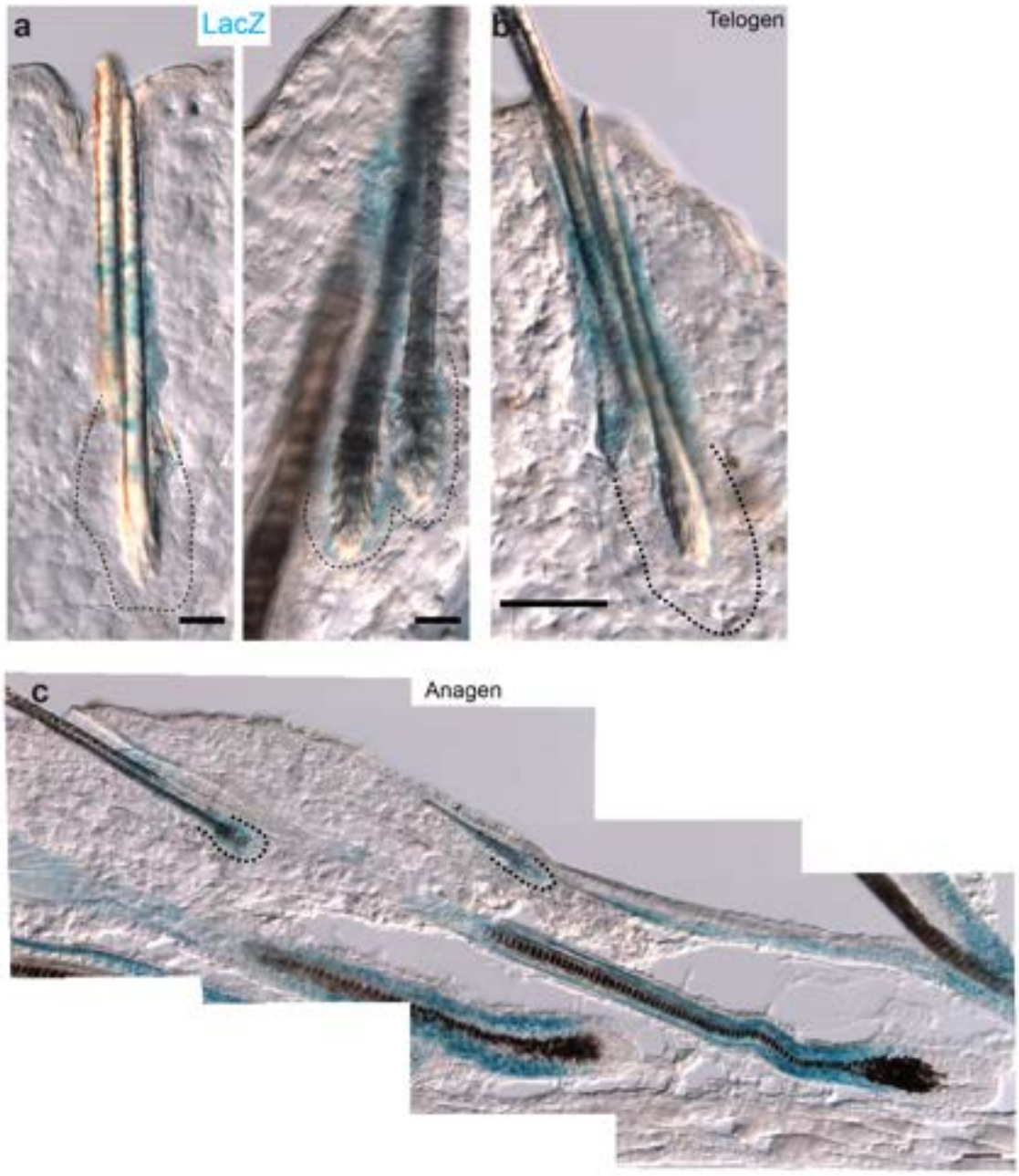
a
LacZ
b
Telogen
c
Anagen

Figure 2.4S: **Transcriptional activity of *Foxc1* locus in 15mo old mouse skin. a**, Transcriptional activity of *Foxc1* locus (*Foxc1*-LacZ knockin) is detected in anagen bulge but not detected in telogen bulge. Scale bar, 20μm. **b**, Transcriptional activity of *Foxc1* locus (*Foxc1*-LacZ knockin) is not detected in telogen bulge. Scale bar, 20μm. **c**, Robust transcriptional activity of *Foxc1* locus (*Foxc1*-LacZ knockin) is detected in both bulge and IRS regions of anagen hair follicles. Scale bar, 20μm.

2.2.4 Loss of *Foxc1* and *Nfatc1* causes premature aging

To test the function of *Foxc1* and *Nfatc1* during aging, we deleted both TFs in the skin using *Krt14-Cre*(*Krt14Cre/Foxc1*$^{fl/fl}$; *Krt14-Cre/Nfatc1*$^{fl/fl}$), hereafter termed double knockout(dKO) mice(Fig2.4a). In young mice, we observed strongly compromised HF-SC quiescence as indicated by widespread Ki67 signals in HF-SCs in anagen I(P22), anagen III(P25) and the second telogen(P42)(Fig2.4b,c and Fig2.5Sa). By contrast, HF-SCs in control animals were only in the active cell cycle transiently, mostly in early to middle anagen(Fig2.5Sa), consistent with the notion that HF-SCs are largely quiescent and infrequently divide for self-renewal[106, 71]. Furthermore, strong Ki67 signals were observed in the HF-SCs of dKO mice but not in those of *Foxc1*- or *Nfatc1*-single cKO mice by late anagen(Fig2.5Sb), indicating a synergistic effect of deleting *Foxc1* and *Nfatc1* in quiescence control. At the tissue scale, young dKO mice rapidly regenerated their hair coat in less than 2 weeks after shaving, in sharp contrast to controls(Fig2.5Sc).

Despite robust hair regeneration in young mice, dKO animals began to show signs of hair loss by $\sim$5mo of age(Fig2.4d). By 12-16 mo, dKO animals largely lost their hair coat, and the remaining hair turned grey, while they were otherwise healthy and had a normal lifespan(Fig2.4e). We first examined whether compromised HF-SC quiescence led to loss of the proliferative potential of HF-SCs in dKO mice, as one may predict. However, we observed numerous Ki67+ proliferative cells in the HF-SC compartment of both growing and resting HFs in 16-mo-old dKO mice when hair loss was widespread(Fig2.4f). We then used intravital imaging to directly monitor dynamics of hair growth and loss in dKO animals. Strikingly, we observed many growing anagen HFs, which reflect robust HF growth, despite widespread hair loss. However, we also observed numerous miniaturized

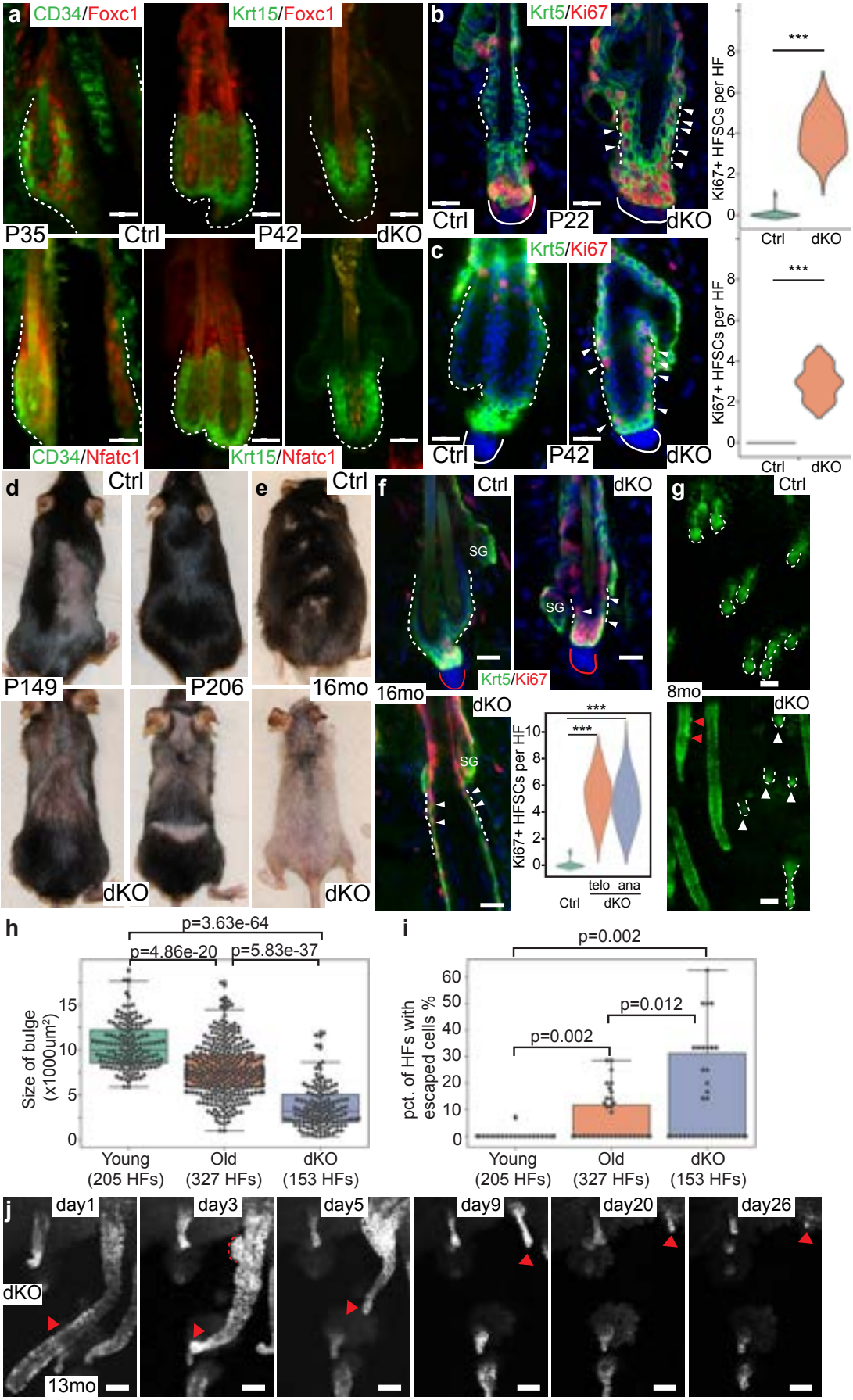
a
CD34/Foxc1
Krt15/Foxc1
P35
Ctrl
P42
dKO
CD34/Nfatc1
Krt15/Nfatc1
b
Krt5/Ki67
Ctrl
P22
dKO
Ki67+ HFSCs per HF
***
c
Krt5/Ki67
Ctrl
P42
dKO
d
Ctrl
P149
P206
dKO
e
Ctrl
16mo
dKO
f
Ctrl
dKO
SG
Krt5/Ki67
16mo
dKO
telo ana
g
Ctrl
8mo
dKO
h
p=3.63e-64
p=4.86e-20
p=5.83e-37
Size of bulge (x1000um²)
Young (205 HFs)
Old (327 HFs)
dKO (153 HFs)
i
p=0.002
p=0.012
p=0.002
pct. of HFs with escaped cells %
Young (205 HFs)
Old (327 HFs)
dKO (153 HFs)
j
day1
day3
day5
day9
day20
day26
dKO
13mo

Figure 2.4: **Genetic deletion of *Foxc1* and *Nfatc1* causes premature hair loss.** **a**, IF signals of FOXC1 and NFATC1 expression in the HF-SC compartment at late anagen (left, marked by CD34) and early telogen (middle, marked by KRT15) and in dKO mice (right, marked by KRT15). Scale bar, 20μm. Ctrl, control. **b,c**, Staining and quantification of Ki67+ cells in the HF-SC compartment in early anagen (**b**) and early telogen (**c**). White arrowheads indicate Ki67+ HF-SCs (n=30 HFs each from three pairs of mice). Scale bar, 20μm. **d,e**, Premature hair loss and graying in dKO mice by 5 mo of age (**d**) and 16 mo of age (**e**) (n5 pairs of mice for each time point). **f**, KRT5 and Ki67 staining in control (telogen, telo) and dKO (telogen and anagen (ana)) HFs in 16-mo-old mice (n=30 HFs each from three pairs of mice). White arrowheads indicate Ki67+ HF-SCs. White dashed lines indicate the bulge region. Red lines indicate dermal papillae. Scale bar, 20μm. **g**, Two-photon intravital imaging of HFs in control and dKO mice (8 mo); white arrowheads denote miniaturized HFs, and red arrowheads mark escaping epithelial cells (n>5 pairs of mice). Scale bar, 70μm. **h**, Box plot of the size of the HF bulge region (means.d.=10,423.622,514.43 (young), 7,736.712,913.99 (old), 3,705.762,420.97 (dKO); n=205 HFs, five young mice; n=327 HFs, three old mice; n=153 HFs, five dKO mice). i, Box plot of the percentage of HFs containing escaped epithelial cells (means.d.=0.251.3 (young), 5.68.9 (old), 12.5717.20 (dKO); n=205 HFs, five young mice; n=327 HFs, three old mice; n=153, five dKO mice). Boxes span the first to the third quartile, with the line inside the box representing the median value. Whiskers show minimum and maximum values or values up to 1.5 times the interquartile range below or above the first or third quartile if outliers are present. Data are plotted as individual points and considered outliers beyond whiskers. **j**, Longitudinal tracking of the same HFs in dKO mice. Red arrowhead points to the same miniaturizing HF. The red dashed line in the image from day 3 marks escaping epithelial cells near the HF-SC compartment. Only three cells are left in the HF at day 26. Scale bar, 70μm. Data in **b**,**c**,**f**,**h**,**i** were assessed with two-sided t-tests.

HFs concurrently in the same dKO animals. Some HFs were reduced to a few remaining cells and progressed toward complete degeneration(Fig2.4g and Fig2.5Se). Unlike control HFs that typically clustered together with 2-4 HFs, which were usually in telogen, dKO HFs had irregular spacing, indicative of widespread but random HF loss as observed at the macroscopic level.

By examining the morphology of miniaturizing HFs, we found that many H2BGFP+ epithelial cells were located in the vicinity of the HF-SC compartment but were clearly outside of the HF cylinder(Fig2.4g), recapitulating escaping epithelial cells as observed in aged HFs(Fig2.1). We next quantified the size of the telogen HF-SC compartment, the percentage of miniaturized HFs and the percentage of HFs containing escaped epithelial cells in dKO mice and compared to these data to those from young and aged mice(Fig2.4h,i and Fig2.5Sf). On average, 12-mo-ld dKO mice had 4.3-fold more (77% versus 14.5%) miniaturized HFs than 20-24-mo-old mice. The percentage of HFs containing escaped epithelial cells was 10.5% in dKO mice and 5.8% in aged mice. These

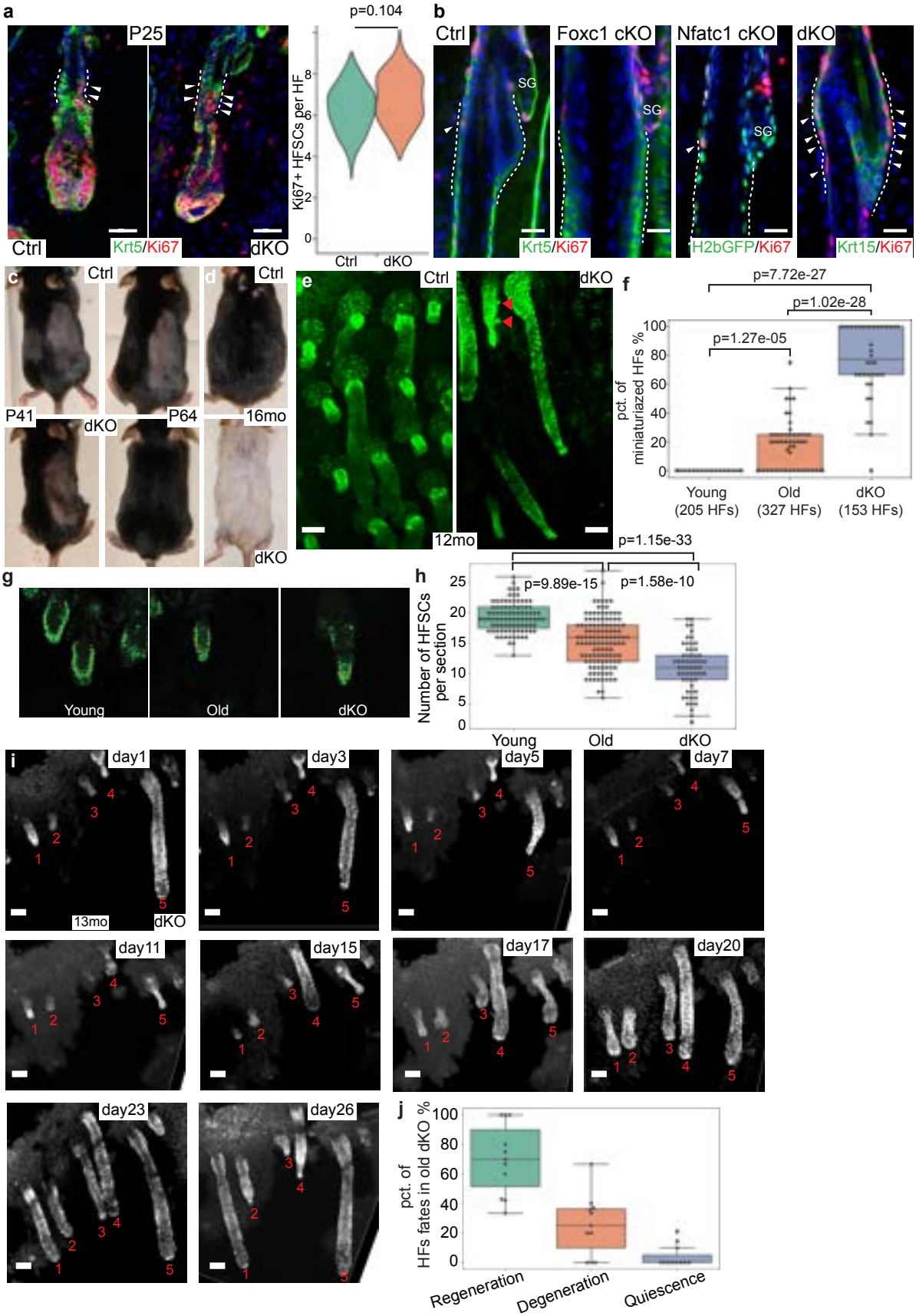
a
P25
Ctrl
Krt5/Ki67
dKO
p=0.104
Ki67+ HFSCs per HF
Ctrl
dKO
b
Ctrl
Foxc1 cKO
Nfatc1 cKO
dKO
SG
Krt5/Ki67
H2bGFP/Ki67
Krt15/Ki67
c
Ctrl
P41
dKO
P64
d
Ctrl
16mo
dKO
e
Ctrl
dKO
12mo
f
p=7.72e-27
p=1.02e-28
p=1.27e-05
pct. of miniaturiazed HFs %
Young (205 HFs)
Old (327 HFs)
dKO (153 HFs)
g
Young
Old
dKO
h
p=1.15e-33
p=9.89e-15
p=1.58e-10
Number of HFSCs per section
Young
Old
dKO
i
day1
day3
day5
day7
13mo
dKO
day11
day15
day17
day20
day23
day26
j
pct. of HFs fates in old dKO %
Regeneration
Degeneration
Quiescence

Figure 2.5S: **Hair follicle miniaturization and loss in dKO mice. a**, *Krt5* and Ki67 staining of hair follicles at early anagen (anagen III, P25) in control and dKO mice, arrowheads indicate Ki67+ HF-SCs, Right panel, quantification of Ki67+ HF-SCs per hair follicle (n=30 hair follicles from 3 pairs of mice). Scale bar, 20μm. **b**, Ki67 staining of hair follicles at late anagen (anagen V-VI) in control, *Foxc1* cKO, *Nfatc1* cKO, and dKO mice, arrowheads indicate Ki67+ HF-SCs. Scale bar, 20μm. **c**, Images of hair coat in the same control and dKO mice on P41 (left panel) and P64 (right panel), the right half of back skin was shaved on P41 and imaged again on P64. **d**, Images of hair coat of control and dKO mice at ∼16mo old. **e**, Two-photon images of hair follicles in control and dKO mice at 12mo old, red arrowheads point to escaped cells outside of hair follicles. Scale bar, 70μm. **f**, Box plot of the percentage of miniaturized hair follicles in young, old and dKO mice. (5 young mice; 3 old mice; 5 dKO mice). **g**, Representative two-Photon images for the quantification of HF-SCs, red asterisks mark HF-SCs. **h**, Box plot of the number of HF-SCs per HF in different samples. **i**, Longitudinal tracking of dKO hair follicles over 26 days. Red numbers indicate the identical hair follicles in each image. Scale bar, 70μm. j, Box plot of the percentage of HFs undergo regeneration, degeneration and quiescence in dKO samples (78 HFs from more than 3 mice were tracked for at least 16 days).

results were consistent with the rapid progression of hair loss and premature HF aging observed in dKO mice.

To monitor the process of HF degeneration in live animals, we longitudinally tracked the same HFs in dKO mice for multiple weeks. We observed that HF miniaturization and degeneration occurred invariably after the catagen-to-telogen transition. Notably, rather than forming the anatomically distinct bulge, miniaturizing HFs in dKO mice first showed signs of abnormal cell egress in the bulge region(day3 in Fig2.4j). These escaping cells were transient and were not observed at day1 or 5 or any time points other than day 3. The HF then regressed to a loosely packed epithelial strand, which lacked convex morphology(day9 in Fig2.4j), mimicking many miniaturized HFs observed in aged skin. In ∼3 weeks, these dKO HFs became further miniaturized until complete degeneration with less than five cells left in the HF(Fig2.4j). To determine the correlation between HF miniaturization and the number of HF-SCs, we quantify the number of HF-SCs in telogen HFs directly in live animals. The number of HF-SCs per HF was significantly reduced in old mice and even more so in dKO mice(Fig2.5Sg,h).

In addition to these rapidly dying HFs, however, we also observed many HFs that went through the hair cycle and continuously regenerated in the same animals(Fig2.5S.i). Notably, these

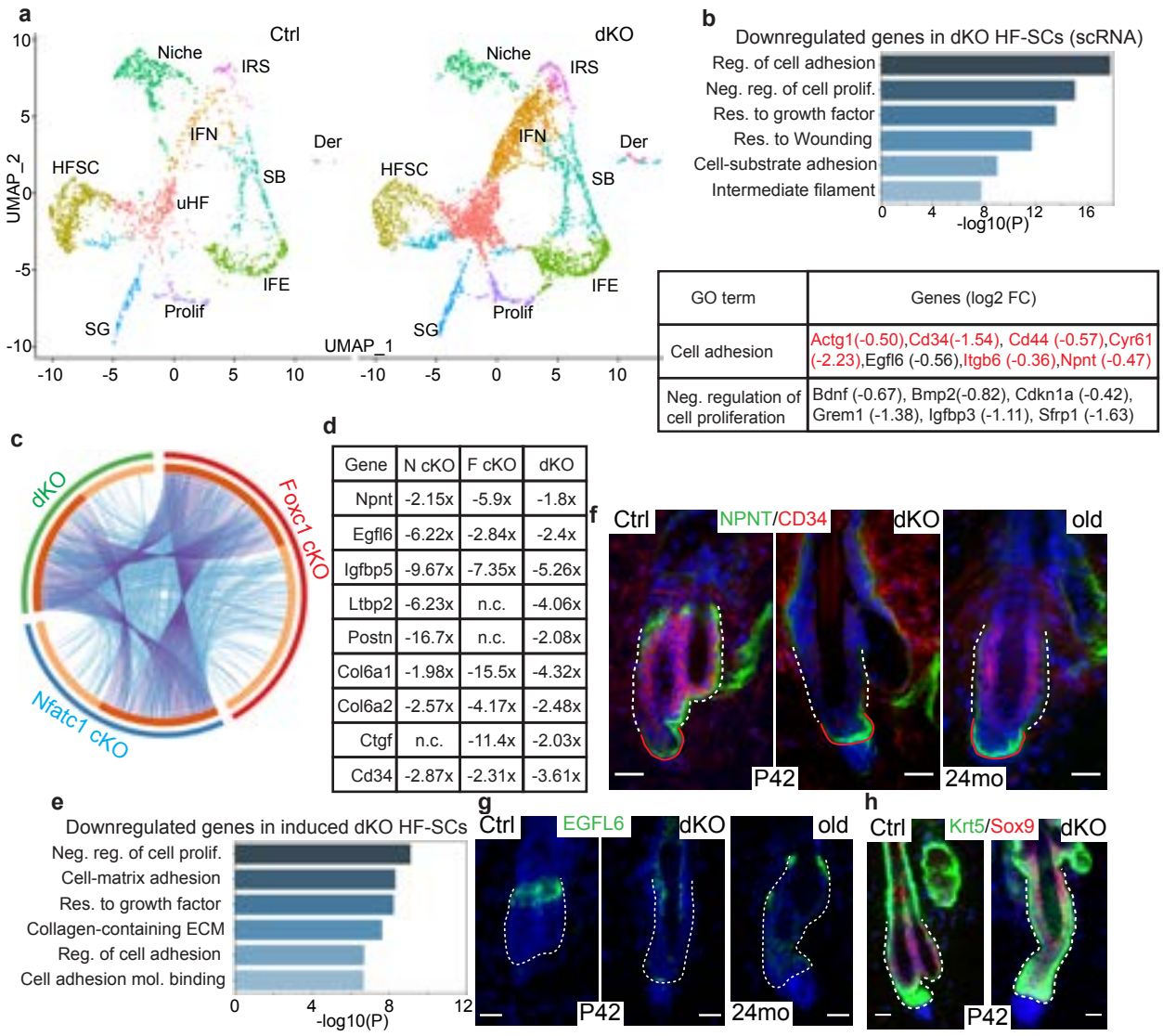

Figure 2.5: **Transcriptomic analysis of dKO HF-SCs.** **a**, UMAP clustering of control (left) and dKO (right) mouse skin samples. Major cell types are characterized using marker genes and color coded with cell identity. Der, dermal. **b**, Highly enriched GO terms in downregulated genes and selected differentially expressed genes in dKO HF-SCs. Red-colored genes are also downregulated in old HF-SCs. **c**, A Circos plot of downregulated genes in *Nfatc1*-cKO, *Foxc1*-cKO and induced dKO HF-SCs. Purple curves link identical genes, colored in dark orange, among all three datasets; blue curves link genes that belong to the same enriched GO term among the datasets. Unique genes from each dataset are colored in light orange. **d**, HF-SC-enriched cell adhesion and ECM genes and their expression change in each cKO and induced dKO strain. **e**, Highly enriched GO terms in downregulated genes in *Krt15-CrePR*-mediated dKO HF-SCs. Mol., molecule. **f,g**, NPNT, CD34 and EGFL6 IF signals in the HF-SC compartment in the second telogen (P42) and in old mice (representative images are from three pairs of mice). **h**, SOX9 IF signals in control and dKO HFs. Dashed lines mark the HF-SC compartment. Scale bar, 20μm in f–h.

HFs did not show signs of epithelial cell escape and continued to cycle within our observation window. Thus, the appearance of escaping epithelial cells from the bulge region distinguished miniaturizing HFs from continuously cycling HFs in dKO mice. Overall, we have tracked 78 individual HFs over the span of at least 16d. We found that 63.8% of HFs underwent regeneration, 26.9% underwent miniaturization and degeneration and 9.0 % remained quiescence(Fig2.5S.j).

These live imaging data reveal the dynamics of HF-SC loss accompanying by HF miniaturization. They suggest that the loss of HF-SCs through cell escape rather than enhanced HF-SC proliferation or compromised proliferative potential is correlated with SC exhaustion in dKO mice.

2.2.5 Reduced expression of cell adhesion and ECM genes

We next performed scRNA-seq to examine changes in gene expression in control and dKO samples at P38, when HFs are in late anagen and HF-SCs return to quiescence[23]. Similar to aged skin, cell clusters of epithelial cell populations did not change drastically, judging by the UMAP projection(Fig2.5a and Fig2.6Sa,c). Notably, genes involved in the regulation of cell adhesion and negative regulation of cell proliferation were among the most enriched among downregulated genes in dKO HF-SCs(Fig2.5b and Table S6). Among those genes, many are commonly downregulated in aged HF-SCs such as *Actg1*, *Cd34*, *Itgb6* and *Npnt*.

To examine the specificity of *Foxc1*- and *Nfatc1*-mediated regulation in HF-SCs, we used *Krt15-CrePR* to delete *Foxc1* and *Nfatc1* only in the HF-SC compartment starting at P22(Fig2.7Sa) and purified dKO HF-SCs for bulk RNA-seq at P30. In support of the notion that these two TFs govern HF-SC gene expression in a cell-intrinsic manner, a large number of genes, which were downregulated in *Foxc1*- and *Nfatc1*-single cKO mice, were also downregulated in induced dKO mice(Fig2.5c,d and Table S7). Because both TFs were only deleted in induced dKO mice shortly before sample collection, nearly all of these genes were more mildly downregulated in induced dKO mice than those in either single cKO strain, in which each TF was deleted at the beginning of skin development with *Krt14-Cre*(Fig2.5d). Consistent with the scRNA-seq data, the most highly enriched gene categories that were downregulated in induced dKO HF-SCs were cell adhesion, neg-

a

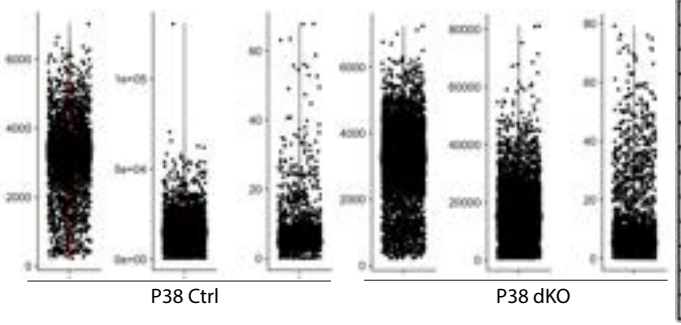

c

	p38ctrl	% of all cells	p38dko	% of all cells
HFSC	508	25.4	427	9.8
HFSC-like	52	2.6	220	5.1
Niche	391	19.6	283	6.5
IRS	39	2.0	150	3.5
IFE	285	14.3	590	13.6
Supra	177	8.9	366	8.4
UpperHF	273	13.7	1016	23.4
IFN	115	5.8	910	21.0
SG	94	4.7	152	3.5
Prolif	62	3.1	176	4.1
Dermal	2	0.1	50	1.2
Total	1998	100.0	4340	100.0

b

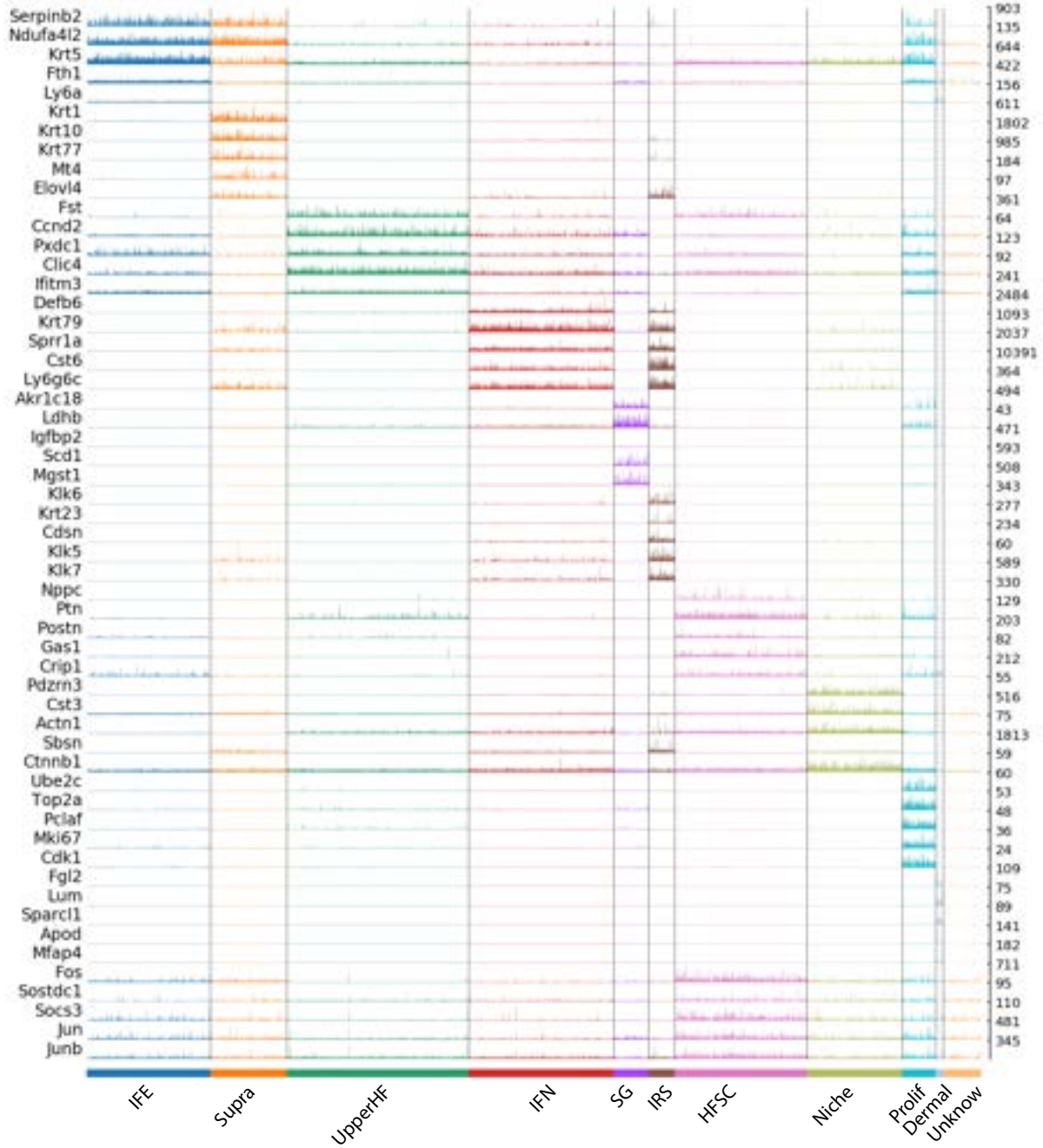

Figure 2.6S: **Quality control and clustering of single-cell RNA-seq data from control and dKO. a**, Quality control and filtering of single cells from both control and dKO samples at P38. Cells were filtered with detected genes numbers (200<nFeatureRNA<5000), transcripts numbers (nCountRNA) and mitochondrial percentage (percent.mt < 10). **b**, Track plot of marker genes for each cluster. **c**, Table shows cluster names, cell numbers and percentage of cells for each cluster after filtering of both control and dKO single-cell RNA-seq data.

ative regulation of cell proliferation and ECM genes(Fig2.5e). Among cell adhesion and ECM genes that were downregulated, *Igfbp5*, *Ccn2*, *Postn*, *Ltbp2*, *Col6a1*, *Npnt* and *Egfl6* are highly enriched in HF-SCs[99]. Among upregulated genes, the strongest elevation of gene expression was associated with mitotic cell cycle and cytokinesis in dKO HF-SCs(Fig2.7Sb).

We next examined the expression of several cell adhesion and ECM genes in cluding *Npnt*, *Cd34* and *Egfl6* in dKO and aged animals. At P42, when dKO HFs were morphologically in the telogen phase, NPNT, CD34 and epidermal growth factor-like domain(EGFL)6 signals were all significantly reduced. In particular, CD34 was not detectable(Fig2.5f). In 24-mo-old samples, NPNT and CD34 signals but not EGFL6 signals were also reduced(Fig2.5f,g). Interestingly, the expression of NPNT, and ECM protein that is localized to the BM of the bulge and HG[99], was lost specifically in bulge HF-SCs but not in HGs of both dKO and old samples(Fig2.5f), further supporting HF-SC specific control of *Npnt* by FOXC1 and NFATC1. We next confirmed the CD34 was absent in *Krt14-Cre/Foxc1*$^{fl/fl}$;*Krt14-Cre/Nfatc1*$^{fl/fl}$ dKO HF-SCs at P30 by using flow cytometry(Fig2.7Sc,d). By comparison, CD34 was expressed at a lower but still detectable level in both *Foxc1-* and *Nfatc1*-single cKO HF-SCs(Fig2.7Se). Furthermore, in *Krt15-CrePR*-induced dKO mice, CD34 levels were also downregulated but not completely lost 8 days after induction of deletion(Fig2.7Sf). These data suggest that *Cd34*, encoding one of the most specific HF-SC surface markers and a cell adhesion gene[62, 61, 63], required the combinatorial control of these two TFs. Despite the complete loss of CD34, however, dKO HF-SCs still maintained their fate as indicated by the robust expression of SOX9, a master TF governing the HF-SC fate[107, 48, 108](Fig2.5h). In addition, dKO HFs continued to grow and cycle when they retained HF-SCs within the bulge(Fig2.5Si). In sum, these analyses reveal that HF-SCs, in the absence

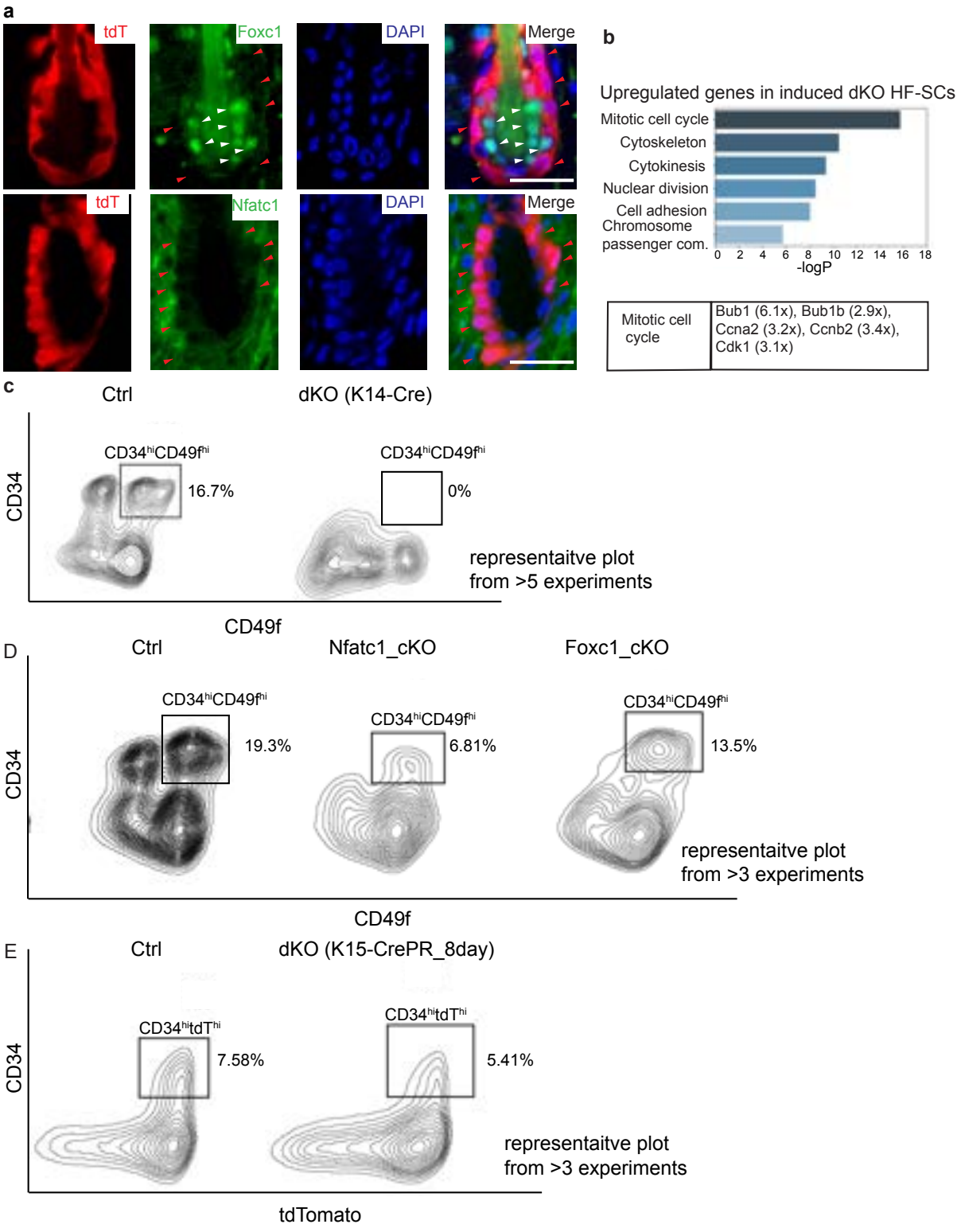
a
tdT
Foxc1
DAPI
Merge
tdT
Nfatc1
DAPI
Merge
b
Upregulated genes in induced dKO HF-SCs
Mitotic cell cycle
Cytoskeleton
Cytokinesis
Nuclear division
Cell adhesion
Chromosome passenger com.
0 2 4 6 8 10 12 14 16 18
-logP
Mitotic cell cycle
Bub1 (6.1x), Bub1b (2.9x), Ccna2 (3.2x), Ccnb2 (3.4x), Cdk1 (3.1x)
c
Ctrl
dKO (K14-Cre)
CD34
CD49f
CD34hiCD49fhi
16.7%
CD34hiCD49fhi
0%
representaitve plot from >5 experiments
D
Ctrl
Nfatc1_cKO
Foxc1_cKO
CD34
CD49f
CD34hiCD49fhi
19.3%
CD34hiCD49fhi
6.81%
CD34hiCD49fhi
13.5%
representaitve plot from >3 experiments
E
Ctrl
dKO (K15-CrePR_8day)
CD34
tdTomato
CD34hitdThi
7.58%
CD34hitdThi
5.41%
representaitve plot from >3 experiments

Figure 2.7S: **Isolation and transcriptomic analysis of *Foxc1* and *Nfatc1* single KO and induced dKO HF-SCs. a**, Immunofluorescence staining of *Foxc1* and *Nfatc1* in *Krt15-CrePR* induced dKO hair follicles. tdT is tdTomato signals from *ROSA26-LSL-tdT* allele, indicating Cre+ dKO HF-SCs. Red arrowheads indicate HF-SCs without *Foxc1* and *Nfatc1* signals, white arrowheads indicate inner bulge region, which is negative for tdT. Scale bar, 20μm. **b**, Highly enriched GO terms of upregulated genes and selected differentially expressed in induced dKO HF-SCs. **c-d**, Flow cytometry analysis and quantification of HF-SCs during the first anagen (P28-P31) in control, *Krt14-Cre*-mediated dKO hair follicles (**c**), *Foxc1* cKO and *Nfatc1* cKO hair follicles (**d**). The rectangle regions are CD34-APC^{hi} and Cd49f-PE^{hi} HF-SC populations. Representative plots for 3$\sim$5 sets of experiments are shown. **e**, Flow cytometry analysis of *Krt15-CrePR*-mediated dKO hair follicles with *ROSA26-LSL-tdT* allele to mark Cre+ dKO cells. The rectangle regions are CD34-APC^{hi} and tdTomato^{hi} populations. Representative plots for 5 sets of experiments are shown.

of *Foxc1* and *Nfatc1*, have severely compromised cell adhesion and ECM gene expression, which resembles the downregulation of these genes during aging.

2.2.6 Enhance-promoter loops mediated by FOXC1 and NFATC1

To investigate how *Foxc1* and *Nfatc1* regualte HF-SC-specific cell adhesion and ECM gene expression, we next performed single-cell ATAC-seq(scATAC-seq) on control and dKO animal at P28. We detected a median of 19,512 fragments per cell in controls and 17,392 fragments per cell in dKO mice. We clustered total epithelial cells using a t-distributed stochastic neighbor embedding(t-SNE) technique based on open-chromatin signatures determined by ATAC-seq[109, 110](Fig2.8Sa). To validate whether scATAC-seq can correctly distinguish IFE and HF-SC lineages, we generated total open-chromatin landscapes of control IFE cells and HF-SCs and compared them with bulk ATAC-seq datasets generated from flow cytometry-purified IFE[111] and HF-SC populations. Indeed, open-chromatin profiles of IFE and HF-SC populations detected in scATAC-seq and bulk ATAC-seq date matched closely(Fig2.6a). We next examined enriched TF motifs in IFE- and HF-SC-specific open chromatin regions. We found that GATA3-GATA6, GRHL2-GRHL3, p63 and KLF motifs were highly enriched in IFE-specific regions, and LHX2, SOX9 and FOXC1 motifs were highly enriched in HF-SC-specific regions(Fig2.6b), consistent with previous studies documenting functions of these TFs in these epithelial lineages[20, 23, 108, 68, 42, 112, 113, 114].

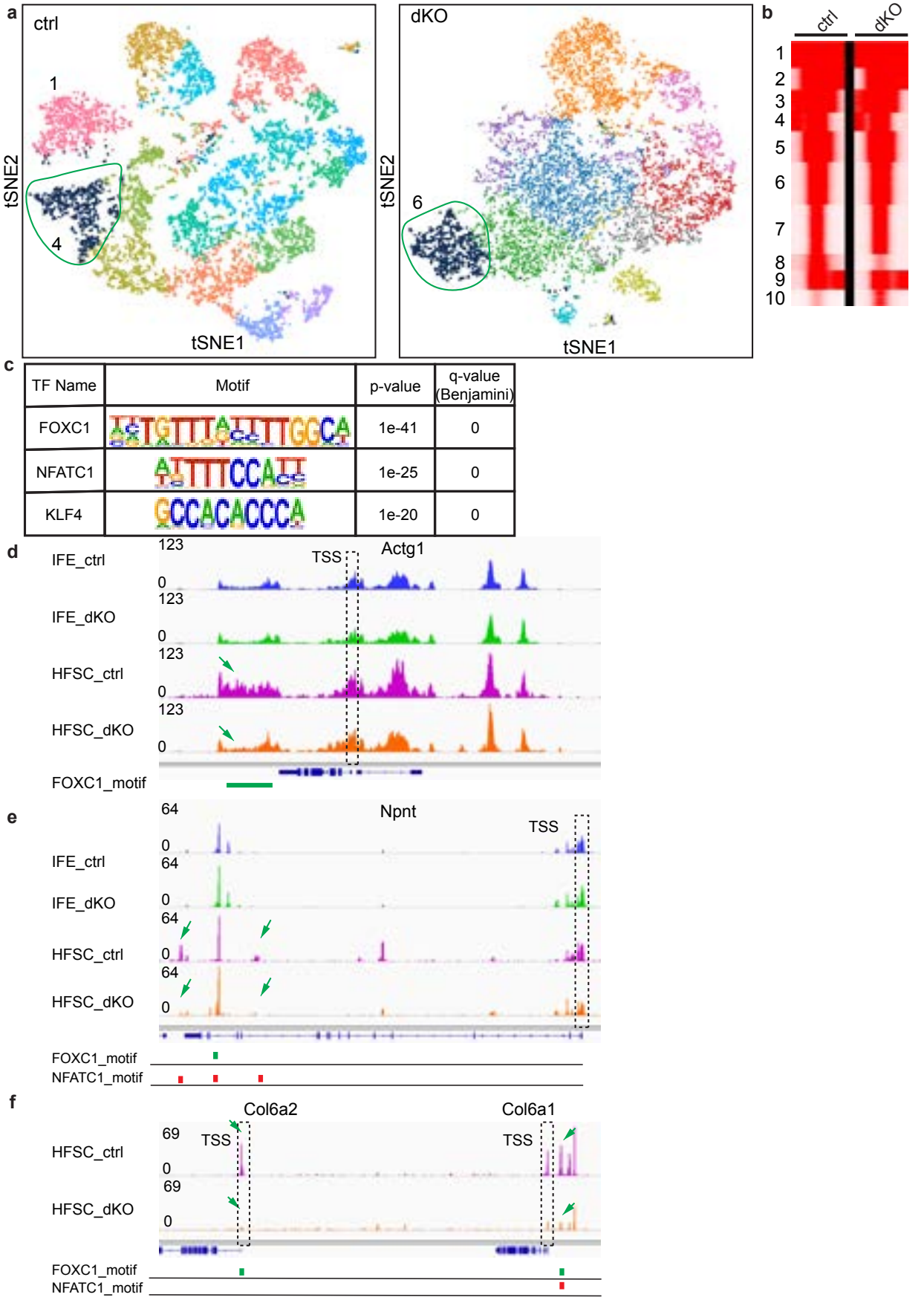
a
ctrl
dKO
tSNE1
tSNE2
1
4
6
b
ctrl
dKO
1
2
3
4
5
6
7
8
9
10
c
TF Name
Motif
p-value
q-value (Benjamini)
FOXC1
1e-41
0
NFATC1
1e-25
0
KLF4
1e-20
0
d
IFE_ctrl
IFE_dKO
HFSC_ctrl
HFSC_dKO
FOXC1_motif
Actg1
TSS
e
Npnt
TSS
NFATC1_motif
f
Col6a2
Col6a1
TSS

Figure 2.8S: **Single-cell ATAC analysis of *Foxc1* and *Nfatc1* controlled open chromatin in HF-SCs. a**, tSNE plots of control and dKO total epithelial cells (*Krt14*-H2bGFP+). The HF-SC populations in each sample are highlighted in blue color and circled. The selected populations show the strongest open chromatin signatures of *Cd34*, the marker for HF-SC, and the weakest signatures of *Gata6*, a differentiation marker. **b**, K-means clustering of control and dKO open chromatin regions from aggregated scATAC-seq data from the HF-SC populations. Cluster 8 is reduced in dKO and cluster 10 is enhanced in dKO. **c**, Top 3 most highly enriched transcription factor motifs in cluster 8. **d-f**, Aggregated scATAC-seq tracks of *Actg1* (d), *Npnt* (e) and *Col6a1/2* (f) loci annotated with FOXC1 and NFATC1 motifs. Location of FOXC1 (green marks) and NFATC1 (red marks) motifs are indicated. Arrows point to HF-SC-specific open chromatin regions that are lost in dKO and the dashed rectangles mark the TSS of *Actg1*, *Npnt* and *Col6a1/2*, respectively.

Next, we examined how the loss of *Foxc1* and *Nfatc1* affected open-chromatin landscape by using aggregated scATAC-seq data. In support of the notion that *Foxc1* and *Nfatc1* are specific to the HF but are not expressed in IFE cells, cellular states determined by open-chromatin signatures revealed largely overlapping and similar populations of control and dKO IFE cells. Notably, cellular states of HF-SCs determined by open-chromatin signatures were different between control and dKO mice(Fig2.6c), in contrast to our scRNA-seq results(Fig2.5a). These data indicate that scATAC-seq is more sensitive to cellular state changes than scRNA-seq, likely due to the much higher number of uniquely identified open-chromatin regions as compared to the number of genes detected in single cells. Indeed, we identified 3,980 open-chromatin regions that were significantly reduced in dKO HF-SCs(Fig2.8Sc). When we searched for enrichment of TF motifs in these regions, we identified FOXC1 and NFATC1 motifs as top two most highly enriched TFs(Fig2.8Sc). Interestingly, we also found that the KLF4 motif was the third most highly enriched motif.

We next examined how FOXC1 and NFATC1 coregulate HF-SC-enriched cell adhesion and ECM genes. CD34 is one of the most specific markers for HF-SCs[62, 61, 63], and its expression was reduced in aged HF-SCs, in each of *Foxc1*- and *Nfatc1*-single cKO strains, and completely abolished in dKO mice(Fig2.5f and Fig2.7Sd-f). Multiple FOXC1- and NFATC1-motif-containing open-chromatin regions were identified at the *Cd34* locus(Fig2.6d). Interestingly, the transcriptional start site(TSS) and several enhancers of *Cd34* were uniquely open in HF-SCs but not in

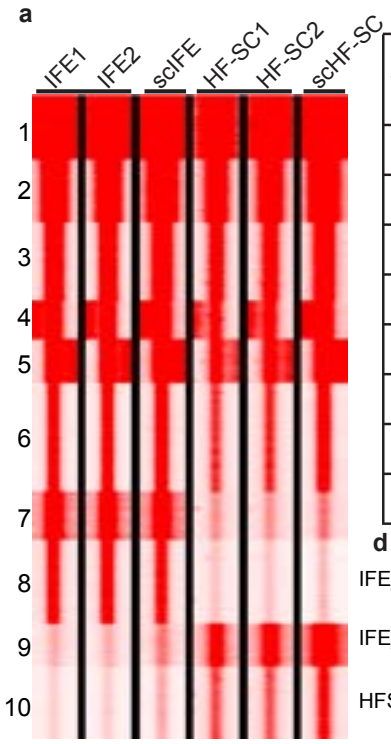

b

TF name	Motif	% of target sequences with Motif/p-value			
		Cluster7	Cluster8	Cluster9	Cluster10
GATA6		18.3%/ 1e-60	19.5%/ 1e-111	N.E.	N.E.
GATA3		26.1%/ 1e-59	27.5%/ 1e-101	N.E.	N.E.
GRHL2/3		11.7%/ 1e-33	12.5%/ 1e-69	N.E.	N.E.
P63		15.6%/ 1e-30	16.2%/ 1e-54	N.E.	N.E.
KLF		25.6%/ 1e-22	24.6%/ 1e-55	N.E.	N.E.
LHX2		N.E.	N.E.	26.8%/ 1e-71	24.7%/ 1e-72
SOX9		N.E.	N.E.	22.7%/ 1e-35	22.0%/ 1e-49
FOXC1		N.E.	N.E.	2.0%/ 1e-12	1.5%/ 1e-8

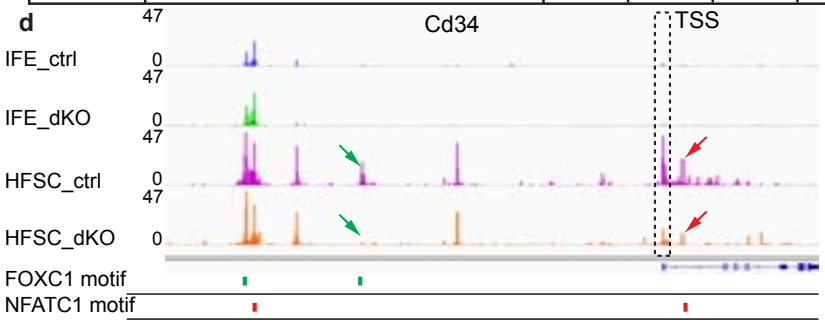

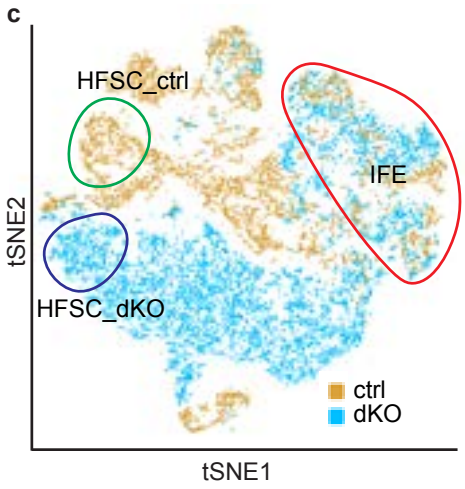

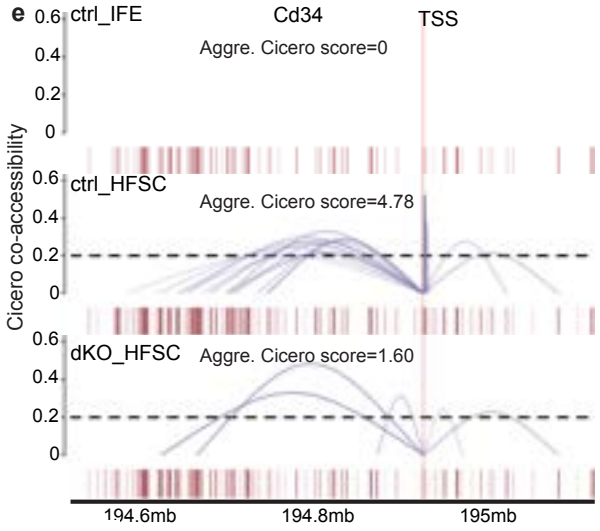

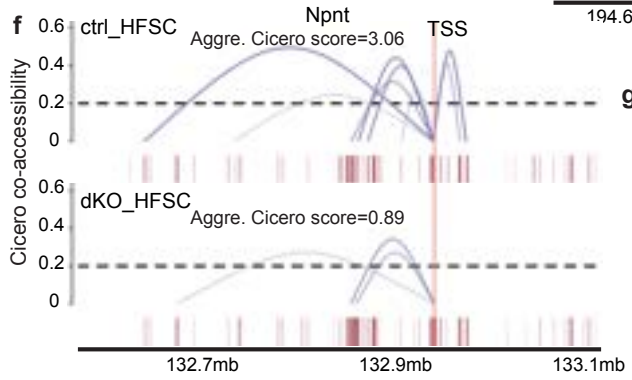

g

Enriched TF motifs in open regions with reduced Cicero scores

TF Name	Motif	p value
KLF4		1e-100
NFATC1		1e-53
FOXC1		1e-31

Figure 2.6: **Single-cell open-chromatin analysis of HF-SCs reveals the role of FOXC1 and NFATC1. a**, k-means clustering comparison of open-chromatin landscapes of purified bulk IFE cells (IFE1, IFE2), aggregated single-cell IFE cells (scIFE), purified bulk HF-SCs (HF-SC1, HF-SC2) and aggregated single-cell HF-SCs (scHF-SC). **b**, Top enriched TF motifs in clusters 7–10 as classified in a. N.E., not enriched. **c**, t-SNE projection of control (light brown) and dKO (blue) epithelial cell lineages based on scATAC-seq data. Circled populations are validated as in a and cell lineage-specific open-chromatin regions. **d**, Aggregated (aggre.) scATAC-seq tracks of the *Cd34* locus annotated with FOXC1 and NFATC1 motifs. Locations of FOXC1 (green marks) and NFATC1 (red marks) motifs are indicated. Arrows point to HF-SC-specific open-chromatin regions that are lost in dKO mice, and the dashed rectangle marks the TSS of *Cd34*. **e,f**, Enhancer–promoter interactions of *Cd34* (**e**) and *Npnt* (**f**) are illustrated in control IFE cells, control HF-SCs and dKO HF-SCs. The aggregated Cicero score is calculated by summing Cicero scores of all enhancer–promoter interactions to the TSS region of each gene. Vertical lines mark the TSS, and the dashed line indicates the Cicero-score cutoff (0.2) used for calculation. **g**, Top enriched TF motifs in open-chromatin regions that have reduced Cicero scores in dKO mice, compared to controls.

IFE cells, mirroring the gene expression pattern in these two lineages. In dKO mice, a FOXC1-motif-containing site lost open-chromatin signals, and the TSS and an NFATC1-motif-containing site also showed strongly reduced open-chromatin signatures(Fig2.6d). Given the complete loss of CD34 expression in HF-SCs, these data suggest that the open state of these FOXC1- and NFATC1-dependent enhancers is required for *Cd34* expression in HF-SCs. Similarly, *Actg1*, *Npnt*, *Col6a1* and *Col6a2* loci also contain FOXC1- and NFATC1-dependent, HF-SC-specific open-chromatin regions(Fig2.8Sd-f). Notably, *Actg1* is widely expressed in both IFE cells and HF-SCs(Fig2.3Sg). However, a FOXC1-motif-containing open-chromatin region was robustly detected in control HF-SCs but not in dKO HF-SCs or IFE samples(Fig2.8Sd). In support of the regulation of *Actg1* by FOXC1, *Actg1* was downregulated in old, *Foxc1*-cKO and dKO HF-SCs but not in *Nfatc1*-cKO or in old IFE cells. These data highlight HF-SC-specific regulation for a widely expressed cell adhesion gene.

Recent studies demonstrated that scATAC-seq can provide insights into enhancer-promoter interactions by computing the co-accessibility of open-chromatin regions in single cells[109, 115]. We next examined the effect of FOXC1 and NFATC1 on local genome organization and enhancer-promoter interactions by computing Cicero co-accessibility[115]. Because cell adhesion and ECM

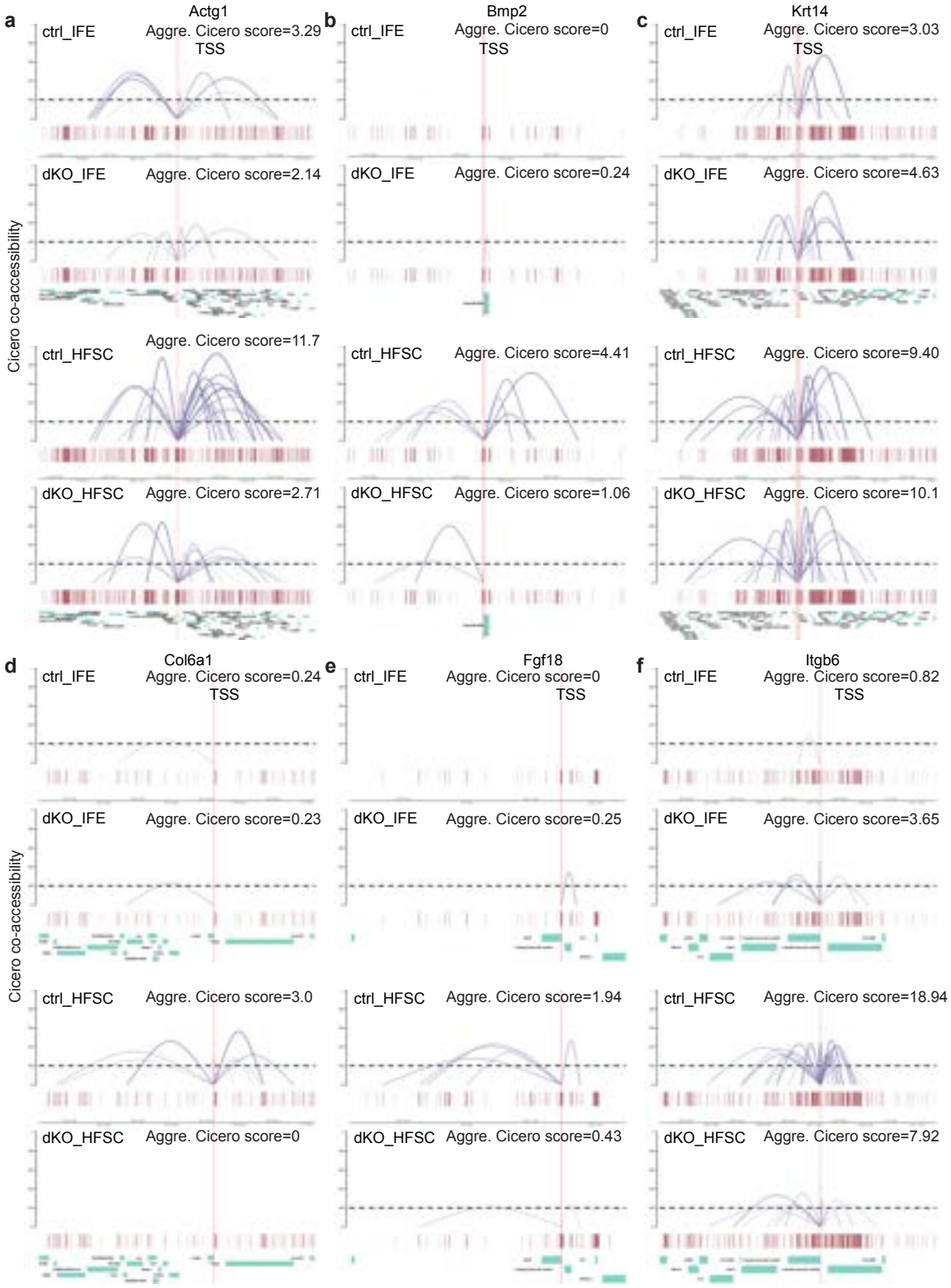
a
Actg1
ctrl_IFE
Aggre. Cicero score=3.29
TSS
dKO_IFE
Aggre. Cicero score=2.14
ctrl_HFSC
Aggre. Cicero score=11.7
dKO_HFSC
Aggre. Cicero score=2.71
b
Bmp2
ctrl_IFE
Aggre. Cicero score=0
TSS
dKO_IFE
Aggre. Cicero score=0.24
ctrl_HFSC
Aggre. Cicero score=4.41
dKO_HFSC
Aggre. Cicero score=1.06
c
Krt14
ctrl_IFE
Aggre. Cicero score=3.03
TSS
dKO_IFE
Aggre. Cicero score=4.63
ctrl_HFSC
Aggre. Cicero score=9.40
dKO_HFSC
Aggre. Cicero score=10.1
Cicero co-accessibility
d
Col6a1
ctrl_IFE
Aggre. Cicero score=0.24
TSS
dKO_IFE
Aggre. Cicero score=0.23
ctrl_HFSC
Aggre. Cicero score=3.0
dKO_HFSC
Aggre. Cicero score=0
e
Fgf18
ctrl_IFE
Aggre. Cicero score=0
TSS
dKO_IFE
Aggre. Cicero score=0.25
ctrl_HFSC
Aggre. Cicero score=1.94
dKO_HFSC
Aggre. Cicero score=0.43
f
Itgb6
ctrl_IFE
Aggre. Cicero score=0.82
TSS
dKO_IFE
Aggre. Cicero score=3.65
ctrl_HFSC
Aggre. Cicero score=18.94
dKO_HFSC
Aggre. Cicero score=7.92
Cicero co-accessibility

Figure 2.9S: **Enhancer-promoter interactions are inferred by using aggregated Cicero scores computed from scATAC-seq. a-f**, Enhancer-promoter interactions of *Actg1* (**a**), *Bmp2* (**b**), *Krt14* (**c**), *Col6a1* (**d**), *Fgf18* (**e**) and *Itgb6* (**f**) are illustrated in ctrl IFE, dKO IFE, ctrl HF-SC and dKO HF-SC. The aggregated Cicero score is calculated by the summation of Cicero scores of all enhancer-promoter interactions to the TSS region of each gene. The vertical lines mark the TSS and the dashed line indicates the cutoff of Cicero score (0.2) used for calculation.

genes such as *Actg1*, *Cd34*, *Col6a1*, *Itgb6* and *Npnt* and signaling genes such as *Bmp2* and *Fgf18* harbored FOXC1- and NFATC1-motif-containing enhancers and were strongly downregulated in dKO and aged HF-SCs, we examined enhancer-promoter interactions in their genomic loci. Enhancer-promoter interactions were generally sparse or absent for these genes in IFE cells, consistent with their HF-SC-specific expression. By contrast, many strong interactions were detected for these genes in control HF-SCs(Fig2.6e,f and Fig2.9S). The majority of these HF-SC-specific interactions, however, were compromised, and aggregated Cicero co-accessibility scores were reduced in dKO HF-SCs, correlating with their reduced gene expression. As a control, aggregated Cicero scores remained unchanged for *Krt14*, a highly expressed gene that is not affected by dKO of *Nfatc1* and *Foxc1*(Fig2.9Sc). However, the score was different for *Krt14* in IFE cells and HF-SCs, perhaps reflecting different transcriptional control of *Krt14* in these cell lineages. To determine TFs underlying reduced enhancer-promoter interactions in dKO mice, we searched open-chromatin regions with reduced Cicero scores. The KLF4 motif was the most highly enriched, followed by NFATC1 and FOXC1 motifs(Fig2.6g). These data reveal that FOXC1 and NFATC1 control cell adhesion, ECM and signaling genes by promoting enhancer-promoter interactions specifically in HF-SCs.

2.2.7 Disintegration of the HF-SC compartment in *Foxc1*;*Nfatc1* dKO mice

To visualize cellular activities underlying HF miniaturization and hair loss, we next examined HF-SCs using time-lapse imaging in dKO animals. In control skin, HFs mostly rested in the telogen phase, and HF-SCs were usually quiescent with minimum cellular activities within the imaging window of 4-6h(Fig2.7a). Less frequently did we observe growing HFs in the anagen

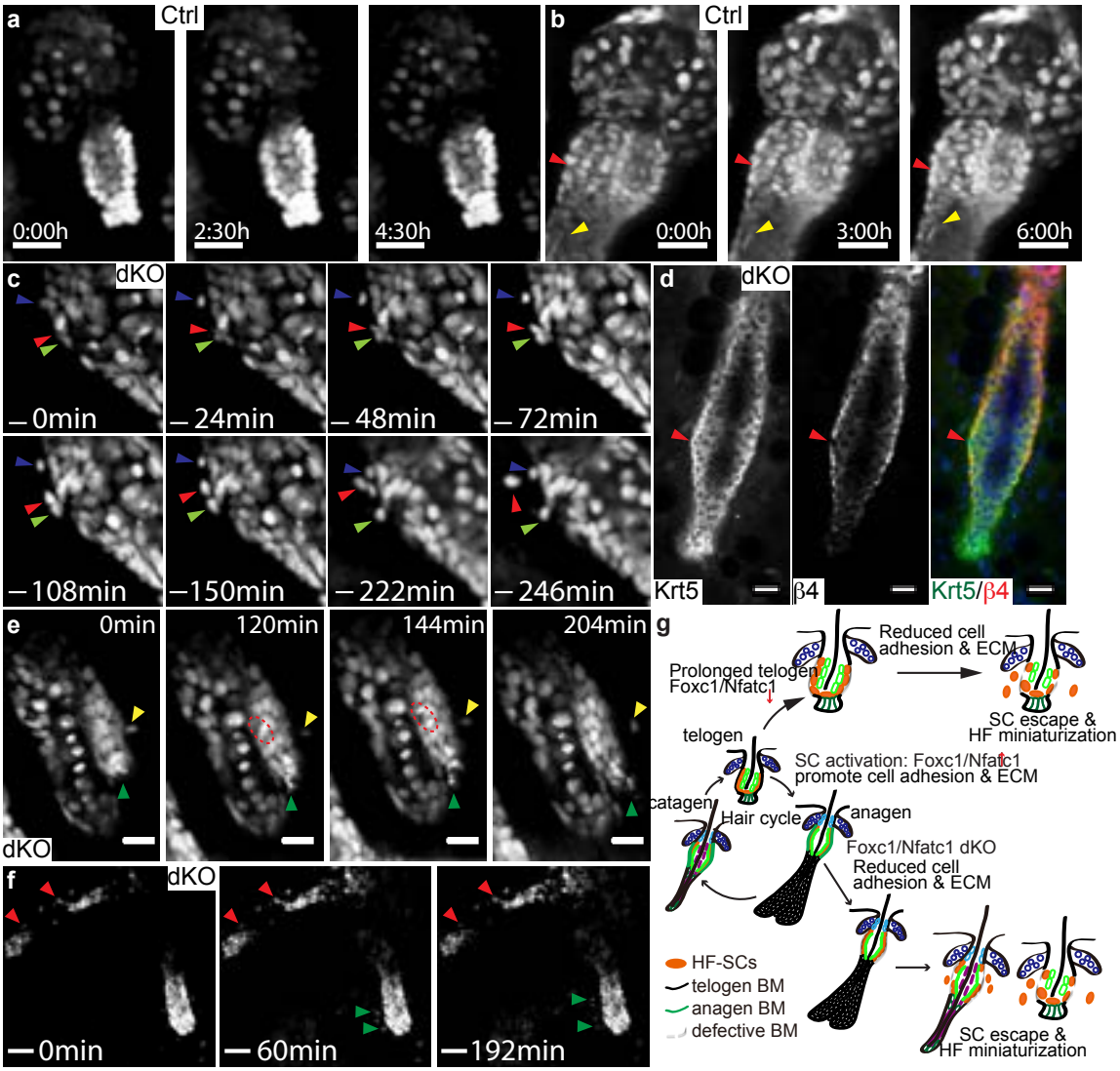
a
Ctrl
0:00h
2:30h
4:30h
b
Ctrl
0:00h
3:00h
6:00h
c
dKO
0min
24min
48min
72min
108min
150min
222min
246min
d
dKO
Krt5
β4
Krt5/β4
e
0min
120min
144min
204min
dKO
f
dKO
0min
60min
192min
g
Reduced cell adhesion & ECM
Prolonged telogen
Foxc1/Nfatc1
SC escape & HF miniaturization
telogen
SC activation: Foxc1/Nfatc1 promote cell adhesion & ECM
catagen
Hair cycle
anagen
Foxc1/Nfatc1 dKO
Reduced cell adhesion & ECM
HF-SCs
telogen BM
anagen BM
defective BM
SC escape & HF miniaturization

Figure 2.7: **Time-lapse imaging captures HF-SCs escaping from the niche in live animals.** **a**, Images from a 5-h movie of telogen HFs in a control reveal no cell division and migration in the HF-SC compartment. Scale bar, 30μm. **b**, Images from a 6-h movie of anagen HFs in a control detect migrating HF-SCs and IRS cells. Red arrowheads indicate a downward-migrating HF-SC, and yellow arrowheads indicate an upward-migrating IRS cell. Scale bar, 30μm. **c**, Images from a 4-h movie of catagen HFs in dKO mice detect HF-SCs escaping from the bulge. Blue arrowheads indicate an HF-SC detaching from the bulge; red and green arrowheads indicate two HF-SCs squeezing through the BM and escaping from the bulge region. Note the changed shape of nuclei during escape. Scale bar, 10μm. **d**, β4 integrin IF signals in dKO HFs. Arrowheads point to disrupted BM with loss of integrin staining. Scale bar, 20μm. **e**, Images from a 3.5-h movie of a miniaturized HF in dKO mice reveal disintegration of HF-SCs, a cell-division event and an escaped cell migrating in the dermis. Green arrowheads indicate two disintegrating cells in the miniaturized HF; red dashed circles indicate a dividing cell; and yellow arrowheads indicate a migrating cell in the dermis. Scale bar, 20μm. **f**, Images from a 3.2-h movie of a dying HF and a miniaturizing HF in dKO mice. Red arrowheads point to escaped epithelial cells with minimum activities in the dermis. Green arrowheads point to rapidly escaping cells from a miniaturizing HF. Scale bar, 50μm. **g**, A model illustrates HF-SC escape and HF miniaturization during aging and in the dKO HF-SC compartment.

phase. In these HFs, we observed limited cell migration, mostly downward movement in the outer root sheath(ORS) compartment and upward movement in the inner root sheat(IRS). HF-SCs were mostly immobile, and we occasionally observed HF-SC migration, but generally no cell division observed within the window of 4-6h(Fig2.7b). In dKO skin, however, we routinely found numerous growing HFs. ORS progenitors in dKO mice rapidly migrated mostly moving along the outer surface of HFs laterally or downward. We also observed strong activities of cells migrating away form the HF-SC compartment. In a 4-h imaging session, we observed an HF-SC that detached from neighboring cells and crawled along the HF. In the same HF, two HF-SCs escaped from the bulge region into the dermis. Strikingly, we observed that these two cells simultaneously changed the shape of their nuclei(24-108min images in Fig2.7c) and squeezed through (likely) a small orifice on the BM before migrating away separately(Fig2.7c). Most notably, one of these two escaping cells 'jumped' more than 16μm away from the HF in less than 30 min after the initial escape, further ruling out the possibility that it remained with the HF(Fig2.7c). These data documented the rapid escape of individual epithelial cells from the HF-SC compartment to the dermis, likely as a result of compromised cell adhesion and defective BM. In support of this, we detected individual dKO

HF-SCs with strongly reduced $\beta 4$ integrin signals by IF staining(Fig2.7d). These time-lapse movies thus provided direct evidence that dKO HF-SCs are a source of H2BGFP+ epithelial cells that have escaped from dKO HFs(Fig2.4g,j and Fig2.7c). Although it appeared to be random when an HF lost cells from the SC compartment into the dermis, their occurrence was generally associated with subsequent HF miniaturization and hair loss as documented in Fig2.4j.

To monitor the degeneration of the HF-SC compartment, we visualized miniaturized HFs before complete HF loss. Although cell migration and division were relatively infrequent, we still observed cell-divison activities in these miniaturized HFs. In a miniaturized HF, we simultaneously observed a cell-division event, three nearby cells disintegrating and being released into the dermis and one escaped cell migrating in the dermis within the span of 2.5h(Fig2.7e). In another miniaturized HF that contained less than 20 cells, one epithelial cell moved downward and was poised to escape from HF. These data suggest that miniaturized HFs are still capable of cell division but continue to lose epithelial cells due to cell escape. Although we were unable to image the fate of these escaped cells due to limitations of the imaging protocol in live animals, they usually scattered around dying HFs, while other HFs continued to shed epithelial cells(Fig2.7f). These cellular activities recapitulated escaped HF-SCs observed from aged HFs, indicating that cell escape is a common mechanism.

To test whether the loss of individual cell adhesion and ECM genes may recapitulate cell escape and premature aging, we genetically deleted *Itgb6*, which is commonly downregulated in both aged and dKO HF-SCs and controlled by FOXC1 and NFATC1. Although genetic deletion of *Itgb6* was reported to result in juvenile baldness[116], *Itgb6*-KO animals largely recovered their normal hair coat as adults(Fig2.10Sa). By 9 months, *Itgb6*-KO animals did not show any defects in hair growth or in the bulge(Fig2.10Sb). Similarly, *Cd34* and *Npnt* have also been individually deleted without affecting the maintenance of HF-SCs or resulting in premature aging phenotypes[99, 117]. Thus, we concluded that genetic deletion of individual cell adhesion and ECM genes may not be sufficient to recapitulate HF aging.

Collectively, our data provide evidence for a new model of SC exhaustion and HF miniatur-

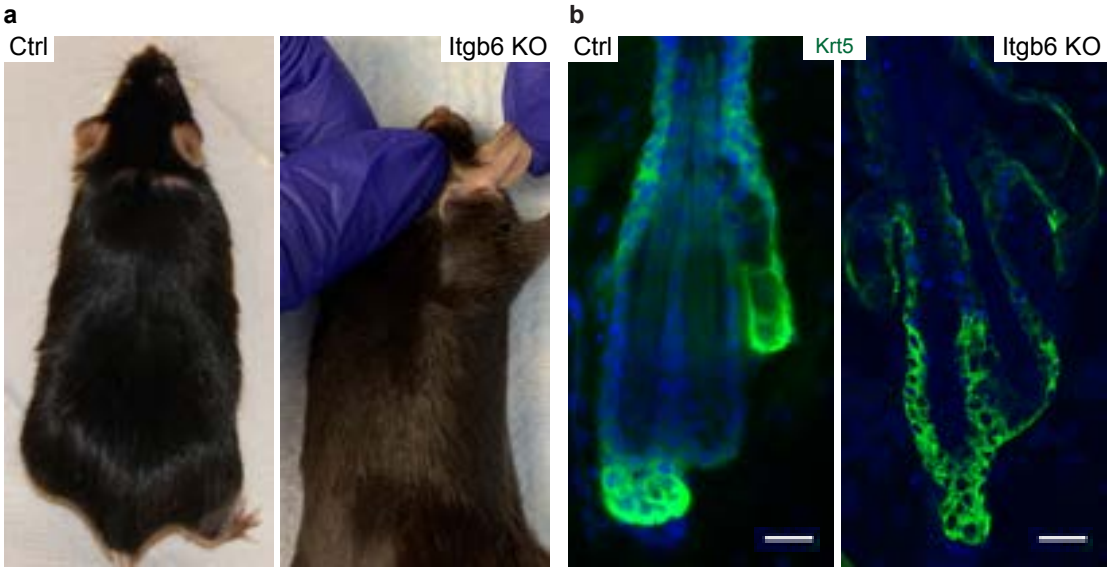

Figure 2.10S: **Deletion of *Itgb6* does not lead to premature hair loss. a**, Hair coat is normal in both control and *Itgb6* KO animals at ∼9-mo old. **b**, HF-SC compartment is normal in both control and *Itgb6* KO animals at ∼9-mo old. Scale bar, 20μm.

ization: dKO and aged HF-SCs fail to maintain expression of many HF-SC-specific cell adhesion and ECM genes, at least in part as a result of reduced *Foxc1* and *Nfatc1* expression. In turn, the compromised niche and reduced cell adhesion allow epithelial cells to escape from the HF-SC compartment into the dermis, resulting in SC exhaustion and eventual degeneration of HFs(Fig2.7g).

2.3 Discussion

2.3.1 SC escape as a mechanism of cell loss and aging

In this study, we imaged HF-SC activities during aging and in a *Foxc1*;*Nfatc1* dKO model in live animals. Leveraging the ability to noninvasively monitor the HF-SC compartment at a time scale ranging from hours to weeks, we observed a hitherto unreported activity of epithelial cells escaping to the dermis. Although many of these escaping cells in both aging and dKO mice are from the bulge region, it is possible that not all escaped cells are SCs. During aging, the process

of cell escape is relatively slow, and we could only monitor cellular activities of single HFs at the resolution of days. We documented the disintegration of HFs accompanies by shedding epithelial cells to the dermis(Fig2.1f,g). In dKO mice, cell adhesion and ECM gene expression was strongly compromised, and this was correlated with more rapid epithelial cell escape and accelerated HF miniaturization. We captured the process of HF-SCs migrating away from the epithelial niche and into the dermis in the time span of a few hours. Although we were unable to label the BM, the most parsimonious explanation for the profound changes of nuclear shape and the distance that these escaping cells traveled during escape is that these epithelial cells squeeze through a small orifice in the defective BM and migrate into dermis. These striking results provide direct evidence that live epithelial cells transverse the BM and reach the dermis. These unexpected observations raise a number of questions for future investigation such as how these epithelial cells remodel cell adhesion and detach from each other, gain motility and change their shape during escape.

We were unable to identify a single cell adhesion or ECM gene, the loss of which recapitulates cell escape or the premature aging phenotype. This is perhaps not surprising because aging and tissue deterioration are generally caused by functional decline of many rather than singular contributing factors[10, 11]. Indeed, the altered HF-SC microenvironment was also shown to drive HF aging[19]. Thus, HF aging is likely controlled by many different regulators. Interestingly, deletion of E-cadherin in the HF-SC compartment causes HF-SC proliferation without triggering HF-SC depletion or premature aging[118]. Furthermore, increased HF-SC proliferation is caused by loss of E-cadherin in the inner-bulge niche layer but not by the defects on the BM of the outer bulge[20, 118]. Thus, the mechanism underlying cell escape and subsequent SC depletion is distinct from the defective adherens junction. Finally, this new mechanism mediated by epithelial cell escape likely functions in parallel with well-studied cell-exhaustion mechanism such as cell death and senescence and adds a new layer of biology to tissue degeneration.

2.3.2 Homeless epithelial cells in aged skin

Using live imaging, we uncovered the presence of escaped, homeless epithelial cells in the dermis of aged and dKO skin. Judging by their *Krt14*-H2BGFP transgene label and their rapid escape through the BM, it is likely that these cells do not undergo profound cell fate changes such as epithelial-to-mesenchymal transition before their escape. These epithelial cells also persist in the dermis rather than immediately initiating programmed cell death such as anoikis upon escape. These observations raise important questions such as whether these escaped cells can self-renew or divide in the dermis, how they interact with foreign environment including dermal fibroblast cells, adipocytes and immune cells and whether those escaped cells play any role in tumorgenesis during aging. These questions warrant future investigation of the fate of escaped cells in normal and pathological conditions.

2.3.3 Mechanisms governing SC quiescence and the niche

Our data suggest that HF-SC quiescence and their niche integrity are coupled through the function of FOXC1 and NFATC1. Our previous study suggests that HF-SC activation promotes the expression of *Foxc1*, and, in turn, FOXC1 reinforces quiescence by inducing *Nfatc1* and *Bmp2/6* expression in activate HF-SCs[23]. Furthermore, *Foxc1*-mediated HF-SC depletion has been linked to defective adherens junctions, although deletion of E-cadherin does not cause HF-SC depletion or premature aging[20, 118]. Now, by examining transcriptomes that are controlled by *Foxc1* and *Nfatc1*, we find that these two TFs coregulate a large number of HF-SC-specific cell adhesion and ECM genes, including *Cd34*, *Npnt* and *Itgb6*. Importantly, we show that the lack of HF-SC division in prolonged telogen during aging also reduces *Foxc1* expression and, to a lesser extent, *Nfatc1* expression. Thus, HF-SC division may serve as a mechanism to rejuvenate cell adhesion of HF-SCs through the upregulation of *Foxc1*.

Our study has further revealed that the loss of SC quiescence per se does not directly cause SC exhaustion. Indeed, increased HF-SC proliferation does not deplete HF-SCs[118]. Furthermore,

we observed numerous rapidly growing HFs when macroscopic hair loss was already widespread. Instead, dKO HF-SCs downregulated cell adhesion and ECM genes and escaped from the defective niche, resulting in excessive cell loss and hair degeneration. In support of this view, we still observe cell-division and escape events concurrently in miniaturized HFs. This model of SC exhaustion provides a new framework for studying SC quiescence and integrity of the SC niche.

2.4 Methods

2.4.1 Mice

All experiments were carried out following IACUC-approved protocols and guidelines at CU Boulder and Northwestern, respectively. Mice were bred and housed according to guidelines of the IACUC at a pathogen-free facility at the University of Colorado ata Boulder and at Northwestern University Feinberg School of Medcine. The following mouse lines were used: *Krt14-Cre*(E.Fuchs, Rockefeller University), *K14*-H2BGFP(E.Fuchs, Rockefeller University), *Foxc1*$^{fl/fl}$, *Foxc1*-LacZ, *Nfatc1*$^{fl/fl}$, *Itgb6*-/-(D.Sheppard, University of California, San Francisco), *K15-CrePR*(Jackson Laboratory, 005249) and *Rosa26-LSL-tdTomato*(Jackson Laboratory, 021876).

K15-CrePR induction was performed by topical application of 4% Ru486(dissolved in ethanol) from P22 to P28 for 2 consecutive days. Samples were collected 2 or 3 days later, at P30 or P31. Sex- and age-matched mice were used for flow cytometry and histology. For quantification, at least 30 HFs from at least three pairs of animals were counted. Male and female mice showed similar phenotypes, and final results were reported by combining all data.

2.4.2 Horizontal whole-mount staining

Back skins were embedded in optimum cutting temperature(OCT, Tissue-Tek) compound. Sections(100μm) were prepared and incubated in PBS to remove the OCT compound. Horizontal whole-mount staining was performed as previously described[119] with minor modifications. Briefly, sections were fixed in 4% PFA for 10 min at room temperature, blocked with a mixture of 0.5%

Triton X-100, 0.25% fish skin gelatin and 0.5% skim milk powder in PBS(blocking solution) for 1h at room temperature and incubated overnight with primary antibodies at 4°C. Antibodies were diluted in blocking solutions. After incubation, sections were washed three times with 1XPBS for 2-3 h. Secondary antibodies were added at a dilution of 1:1000 together with 5μg ml^{-1} Hoechst 33342(Invitrogen) for 1h at room temperature, followed by washing three times with 1XPBS for 30min. Sections were then placed on lsides in VECTASHIELD antifade mounting medium(Vector Laboratories, H-1000) under a dissection microscope to ensure correct orientation and then covered with coverslips for imaging. Confocal imaging of whole-mount staining was performed on a Nikon A1 laser scanning confocal microscope with either a 20X, 0.75-numerical aperture(NA) or a 100X, 1.49-NA objective lens, and images were acquired with NLS Elements(Nikon) software in the light Microscopy Core Facility of the University of Colorado, Boulder.

2.4.3 Cryosectioning and immunostaining

OCT-embedded tissues were sectioned to 20-30mum and fixed with 4% PFA for 10 min at room temperature. Sections were permeabilized for 10 min at room temperature with 0.1% Triton X-100 in 1X PBS. When staining with mouse monoclonal antibodies, we used the mouse-on-mouse basic kit(BMK-2201, Vector Laboratories). Otherwise, blocking was performed with 5% normal serum of the same species that the secondary antibody was raised in. Sections were incubated with primary antibody overnight at 4°C. After incubation with primary antibodies, sections were washed three times in 1XPBS and incubated for 1h at room temperature with Alexa Fluor 594-, Alexa Fluor 488- or Alexa Fluor 747-conjugated secondary antibodies(1:2000, Invitrogen-Molecular Probes). Nuclei were stained with Hoechst 33342(1:5000, Invitrogen).

2.4.4 Flow cytometry cell sorting

Sex- and hair cycle matched mice were euthanized and collected for dissection. We first shaved the hair coat and applied nair hair removal lotion(Amazon, 22339) for around 3 min. After wiping off the lotion and washing away leftover hair shafts, back skin was dissected, and subcutaneous

fat was removed using a blade. As small part of the skin sample was embedded in OCT, and the remaining skin sample was minced and incubated with 0.25% collagenase(Worghington, LS004188) in 4-6 ml 1XHBSS buffer at 37∘C for 2h with rotation. A 5-ml serological pipet was used to further separate the epidermis from the dermis at the 1-h incubation time. After collagenase treatment, we added 10ml cold PBS and centrifuged the sample at 400g for 10min at 4∘C. The pellet was re-suspended with pre-warmed 0.25% trypsin-EDTA(Gibco) for 8min at 37∘C, and the digestion was immediately blocked by adding 10ml cold 1XPBS with 3% chelated PBS. Cells were incubated with appropriate antibodies for 1h on ice. DAPI was used to exclude dead cells. HF-SCs from K14-Cre-based experiments were isolated by enriching for $DAPI^{-}K14-H2BGFP^{hi}SCA1^{lo}\alpha6^{hi}CD34^{hi}$ cells. The following antibodies were used: anti-integrin $\alpha6$ (CD49f, 1:75; eBioscience, PE conjugated, 12-0495; apc conjugated, 17-0495), anti-CD34(1:50; eBioscience, PerCP-Cy5.5 conjugated, 45-5981). Flow cytometry was performed on the MoFlow XDP machine(Beckman Coulter). Flow cytometry data were analyzed with FlowJo.

2.4.5 RNA-seq assay

Total RNA from flow cytometry-sorted cells was isolated using TRIzol(Invitrogen), and RNA quality was assessed with the Agilent 2100 bioanalyzer. RNA with integrity number ¿8 was used to perform RNA-seq assays. Libraries were prepared following the manufacture's protocol(NEBNext Ultra Directional RNA Library Prep kit). cDNA libraries were checked for quality with bioanalyzer before being sent out for sequencing to the Genomics and Microarray Core Facility at the University of Colorado Denver on the Illumina NovaSeq 6000.

2.4.6 Omni-ATAC-seq assay

ATAC-seq was performed as previously described[120] with following modifications: an average of 50,000 flow cytometry-sorted HF-SCs were collected in PBS containing 3% chelated FBS and pelleted by centrifugation for 5min at 500g and 4°C. Cell pellets were resuspended in 50μl lysis buffer containing 10mM Tris-HCl, pH7.4, 10mM NaCl 3mM $MgCl_2$, 0.1% Igepal CA-630, 0.1%

Tween-20 and inverted the tube three times to mix. Nuclei were then pelleted by centrifugation for 15min at 500g and 4°C. The supernatant was carefully discarded, and nuclei were resuspended in 50μl reaction buffer containing 5μl Tn5 transposase and 25μl TD buffer(Nextera DNA Sample Preparation kit, Illumina), 16.5μl PBS, 0.5μl 1% digitonin, 0.5μl 10% Tween-20 and 5μl H_2O. The reaction was incubated at 37°C for 30min with rotation, terminated by adding 10μl clean-up buffer(900mM NaCl, 300mM EDTA) and immediately purified using the MinElute PCR Purification kit(Qiagen). After purification, DNA samples were quantified using NanoDrop, and 50ng DNA was used for library construction. Library amplification was performed for 13 cycles following the manufacture's protocol(Nextera DNA Sample Preparation kit, Illumina) except that we used 2.5μl of each primer and a 2-min extension time in the PCR reaction. Libraries were size selected to enrich for inserts of 150-1000bp in size, checked for quality with bioanalyzer and paired-end sequenced for at least 40 million reads per sample.

2.4.7 Single-cell ATAC-seq assay

Cells from both wild-type and dKO animals were collected from a flow cytometry-sorting machine with cell surface proteins and H2BGFP signals such that epidermal cells and HF cells were at a 1:3 ratio. In total, 10,000 cells were used for preparation of both WT and dKO samples for scATAC-seq. Libraries were prepared using the 10X Chromium Single Cell ATAC Library Gel Bead kit(PN-1000110). In brief, cell nuclei were isolated, and nuclear suspension were incubated in a transposition mix to fragment DNA and add adaptor sequence to the end of DNA fragments. Single-nucleus resolution was achieved using 10X bracoded gel beads, partitioning oil and a master mix on a Chromium Chip E. Libraries were constructed using a 10X sample index plate and double size selected from 150bp to 1000bp.

2.4.8 Intravital live image

Intravital live imaging was performed as previously described[94, 95] with modifications. Mice used for imaging was sedated using 2% oxygena dn ∼1-2% isoflurane. Once the mouse was fully

sedated(∼5min), it was put on a warm pat at 37°C. Oxygen and isoflurane levels were maintained during the course of imaging. Night-time ointment (Genteal, NDC 0078-0473-97) was applied to keep the eyes moisturized. A 30-gauge need and tattoo ink were used to mark the region(it is best to mark the region at least 1d before imaging to allow for healing). A custom-manufactured spatula was used to stretch and flatten the region of interest(near the tatoo ink) and was maintained at an adjustable height. Double-sided tape was used to adhere the lower size of the ear onto the spatula. After applying long-lasting Genteal gel(0078-0429-47) to the region of interest, a second adjustable spatula, glued to a coverglass on one end, was gently pressed down on the ear so that the coverglass was directly on top of the region. A second round of long-lasting Genteal was applied to the coverglass(the Gental gel should cover a region large enough for the objective to move around, and a sufficiently large amount should be used to keep the tip of objective immersed during imaging). We used the Olympus FVMPF-RS mulitphoton imaging system to acquire images. The lasers we used were the InSight X3 with wavelength set to 920nm for GFP signals and the Mai Tai HP with wavelength set to 860nm for second-harmonic-generation signals. Emission wavelengths were 510nm and 430nm respectively. We used 10X and 25X objectives for images. During the imaging session, the light should be turned off, and the stages and scope should be covered with a black curtain to avoid exposure to light. After the imaging session is complete, the mouse was kept in oxygen for around 10min to recover before sending it back to the cage.

2.4.9 Two-photon image processing and quantification

Two-photon images were acquired using FluoView software from Olympus. Images were opened using Fiji(ImageJ) and converted to TIF format using 'Fiji → plugins → bio-formats → bio-formats-exporter'. Time-lapse images were aligned using 'plugins → registration → descriptor-based series registration(2d/3d + t)' before being exported. Exported TIF files were further converted to Imaris files using the Imaris File Converter. Imaris x64 9.2.1 was used to open files for further analysis. Images were adjusted on the x, y or z plane and smoothed with a Gaussian filter for better visualization. Movies were also adjusted and generated with Imaris. For HF quantification,

3D pictures were opened in Imaris, and then the epidermis and upper HF regions were cropped out. Next, 3D rendering was applied to leftover bulge regions to model the surface area. The surface area output was used for quantification and plotting. For HF miniaturization, we used smallest HF in young samples as the cutoff; any HF smaller thant the cutoff was counted as miniaturized. To quantify the number of HF-SCs, we used 3D two-photon images to select one sagittal plane and count all HF-SCs in the outer layer.

To quantify the HF fate, we tracked 78 HFs in total for at least 16 days and monitored HF morphological changes. We defined regeneration as HFs that are cycling with no signs of shrinkage while in telogen, degeneration as noncycling HFs undergoing miniaturization or cycling HFs becoming smaller in telogen and quiescence as noncycling HFs with no significant size change during tracking.

To quantify FOXC1 and NFATC1 immune-staining signals in HF-SCs, we co-stained with CD34 to labe the bulge region and HF-SCs. Images were then converted to Imaris format for further quantification. Briefly, we used the Imaris Surface module to manually select a circle of fixed size in the nucleus of HF-SCs. The mean and/or median intensity of each channel in the selected region was obtained from the statistical tab.

2.4.10 RNA-seq analysis

RNA-seq reads(150nt, paired end) were aligned to the mouse genome(NCBI37/mm10) using HISAT2(version 2.1.0)[121]. The resulting SAM files were converted to BAM files using SAMtools(version 1.3.1)[122]. Expression of each gene was calculated from the resulting BAM alignment file by HTSeq[123]. Differentially expressed genes were determined using DEseq2[124] with an adjusted P-value cutoff of 0.05. GO analysis was performed using Metascape[125]. Selected GO terms were from Metascape results along with the gene list.

2.4.11 Single-cell RNA-seq analysis

The Cell Ranger Single-Cell software Suite was used to perform barcode processing and single-cell 3'gene counting(http://software.10xgenomics.com/single-cell/overview/welcome). Barcodes, features and matrix files were loaded into Seurat 3.0[97] for downstream analysis (https://satijalab.org/seurat/vignettes.html). For each sample, the analysis pipeline followed instruction in the guided tutorial. Cells were filtered using nFeature_RNA(>200 and <5000) and the mitochondrial percentage(<10%). In addition, cell cycle regression was used to regress out additional variation from cell cycle genes. After clustering and UMAP dimension reduction, cluster markers were used to identify distinct cell populations. For comparison between different samples, all samples were integrated to promote identification of common cell types and enable comparative analysis[126]. All differential analyses were based on the nonparametric Wilcoxon rank-sum test. Average log(FC) values were converted to log_2(FC) values for consistency with bulk RNA-seq data. Genes with adjusted P values less than 0.05 were used for GO term analysis.

To recluster specific cell population, we first subset the cells of interest and then re-ran the analysis pipeline with modification for the UMAP resolution.

For differential gene plots, we used both default Seurat options and SCANPY[127]. Note that we used cell cycle regression for initial clustering of total populations; but, for pseudotime analysis, we did not regress out cell cycle genes to capture differential information. After reclustering, we were able to resolve $LGR6^{+}$ HF-SCs, which we thus named the upHF-SC population. Next we kept only HF lineages including HF-SCs, UpHFs, infundibular cells, niche cells, HGs, UpHF-SCs and SCs based on Seurat clustering. Finally, we converted the Seurat object to a single-cell experiment for standard downstream Monocle 3 pseudotime analysis[100]. After obtaining pseudotime scores for each cell, we first filtered out all cells without scores(which are mostly SCs) and then added the information back to the Seurat object for further plotting.

2.4.12 ATAC-seq and motif analysis

ATAC-seq reads (paired end) were aligned to the mouse genome (NCBI37/mm10) using Bowtie 2 (version 2.2.3)[128]. Duplicate reads were removed with Picard tools (http://broadinstitute.github.io/picard/). Mitochondrial reads were removed, and peaks were called on each individual sample by MACS (version 2.0.9)[129]. Peaks from different ATAC-seq samples were merged for downstream analysis. De novo motif discovery was performed using HOMER[130]. Motif scanning was performed with MEME (5.0.3)[131]. BED files were converted to FASTA files by bedtools getfasta[132], and motifs discovered by HOMER were used to scan for instances in open-chromatin regions. HOMER motifs were also converted to MEME format with the R package from GitHub (https://gist.github.com/rtraborn/e395776b965398c54c4d). For IGV visualization[133], we first concatenated all peaks from samples of interest and converted them into a GTF file, counted the number of reads mapped in peaks and then normalized all samples using 'bedtools genomecov -scale' to obtain bedGraph files. Igvtools toTDF was used to obtain TDF files for final visualization.

2.4.13 Single-cell ATAC-seq analysis

FASTQ files were collected from the sequencing facility and concatenated together. We used cellranger-atac (version 3.0.1) counts with the reference downloaded from the 10x Genomics website. Loupe Cell Browser (version 3.1.0) was used to generate a t-SNE plot of wild-type and dKO samples. We used graph-based clustering for P28 control samples and k-means-based clustering for P28 dKO samples for better identification of subpopulations.

IFE and HF-SC populations were first extracted from the BAM file of the cellranger-atac output file. First, we extracted cluster IDs of each population and used suggested methods from 10x Genomics (https://kb.10xgenomics.com/hc/en-us/articles/360022448251) to subset BAM files specific for each population. To predict the cis-regulatory landscape from scATAC-seq data, we used the R package

Cicero[115] to infer enhancer and promoter interactions. The pipeline was performed according to instructions in the tutorial. Cicero connection lists were exported from R and saved for further analysis. For connection scores at TSSs, we first downloaded the mouse gene coordinate GFF file from the UCSC genome browser and then we extracted gene TSS sites based on gene coordinates and strand information. Cicero peaks were imported to Python, and we used pandas to covert to the BED file format. Formatted Cicero BED files were used to intersect with TSS BED files to extract peaks connected to TSS sites and corresponding connection scores. For each individual gene, connection scores were first filtered with 0.2 as the cutoff, and then all connections were summed up as the total score. For global reduced enhancer–promoter interactions, we first used all connection scores greater than and equal to 0.16 to reduce noise and then organized and formatted all peaks from control and dKO samples for comparison. We considered any interactions with greater than or equal to 0.2 as changed interactions and those with less than or equal to 0.1 as background interactions. All peaks with corresponding interactions were pooled, peaks with TSSs were filtered out, and then we used HOMER[130] for de novo motif discovery.

2.4.14 k-means clustering of ATAC peaks

To compare open-chromatin signals across multiple samples, k-means clustering was performed using seqMINER (version 1.3.4)[134]. BAM files were first converted to BED files using bedtools bamtobed. To normalize across samples for depth of sequencing, we downsampled each BED file to 20 million reads for input. Peaks were called by MACS2 from all bulk ATAC-seq data. Next, peaks called from bulk data were concatenated, sorted, merged and then used as genome coordinates. Signals were calculated in a 1.5-kb region (±750bp) surrounding the center of the peak with 50-nt bins.

2.4.15 Statistics and study design

In general, all sequencing experiments (RNA-seq, ATAC-seq) were repeated on at least two pairs of control and cKO or dKO samples per experiment. scATAC-seq was performed with one

pair of control and dKO samples at the same time on the same chip to avoid batch effects. All experiments were designed such that there were always littermate controls. All statistical tests were performed as indicated in figure legends. No statistical methods were used to predetermine sample size. Experiments were not randomized, and investigators were not blinded to allocation during experiments or outcome assessment, except when stated.

2.4.16 Statistics and reproducibility

Results in Fig. 1a,b,f–i were repeated with at least three different animals. Results in Fig. 4a,j were repeated with at least three different animals. Results in Fig. 5h were repeated with at least three different animals. Results in Fig. 7a,b,d–f were repeated with at least three different animals. Results in Fig. 7c were observed in two different animals. Results in Extended Data Figs. 1a,b,d,h, 4a–c, 5b,e,g,i, 7a and 10b were repeated with at least three animals.

2.5 Data availability

All sequencing data were deposited to NCBI–GEO SuperSeries under accession number GSE133648.

Chapter 3

Chromatin and gene-regulatory dynamics of hair follicle aging in single cell resolution

3.1 Introduction

Aging is a natural, continuous process with the gradual accumulation of deleterious damage in cells and tissues[10, 11]. Age-related declines in tissues yield increased vulnerability to chronic disease and mortality[135]. Although excellent studies have provided emerging theories of aging[136, 137], questions about the cell-to-cell variation and gradual cellular state changes during aging remain largely unanswered[138, 139].

As the biggest organ of human body, skin and its appendages offer excellent experimental systems for aging studies[31]. Skin wrinkling, hair greying and hair loss are among the most striking and observable traits of aging. In addition, most hair follicle related changes are benign, which makes it possible to study aging without incurring detrimental damages. Hair follicle miniaturization associates with hair loss during aging[21] and alopecia caused by premature hair loss[85, 86]. These genetic studies identified critical genes and signaling pathways governing hair follicle aging. However, the chronic changes and cell-to-cell variation accumulated during aging in different hair follicle lineages remain unexplored.

Dynamic changes in the transcriptome and cis-regulatory networks, driven by transcription factors, underlie the hair follicle aging[20, 23, 59, 66]. With the development of single cell methods including single cell RNAseq(scRNAseq) for the transcriptome[140, 141] and single cell ATAC-seq(scATACseq) for chromatin accessibility[100, 142], I examined both the cellular heterogeneity

and aging induced chronic changes in hair follicles lineages. By sampling mouse skin at different stages covering the young, middle-age and old stages, I investigated the gradual transcriptomic and epigenetic changes in distinct hair follicle populations during aging. To map the gene regulatory logic of hair follicle aging, I integrated age-matched scRNAseq and scATACseq in mouse skin ranging from postnatal day 28(P28), P53, 6months, 12months to 24months old. In section 3.2, I presented a detailed analysis of these datasets and showed distinct cellular state changes of individual hair follicle populations. This was accomplished by reconstructing a pseudo-aging process that mimics physiological aging. Furthermore, I computationally identified the distinct transcription factor activities that occur during aging.

3.2 Results

3.2.1 Single-Cell Transcriptome of hair follicle aging

To capture the gradual and dynamic changes among the full repertoire of hair follicle cells during aging, I used flow-cytometry to sort for epidermal cells at P38, P53, 6months, 12months and 24months with specific surface proteins and H2B-GFP signals. The scRNAseq libraries were generated using the Chromium platform(10X genomics). Overall, I obtained 14091 single-cell transcriptomes with around 3000 genes per cell and 20000 transcripts per cell after quality control and filtering. To incorporate more data points for analysis, I downloaded published aging single cell data from young and old mouse skin[19]. The published datasets contain low number of transcripts and gene per cell(Fig3.1Sa), thus I excluded them from further analysis. To integrate all the cells from different ages and limit the batch effects, I used unsupervised methods to facilitate the integration and comparison(Fig3.1a)[97]. Next, I applied unsupervised Louvain clustering based on shared nearest neighbor graph[143] to batch corrected samples(Fig3.1b). Based on the differential expression analysis, the top marker genes from each cluster were used to manually annotate cell populations(Fig3.1b). Among the epidermal lineages, I successfully identified the inferfollicular epidermal lineages(*Krt14*+, *Krt5*+), sebaceous gland(SG)(*Scd1*+, *Mgst1*+) lineages and HF

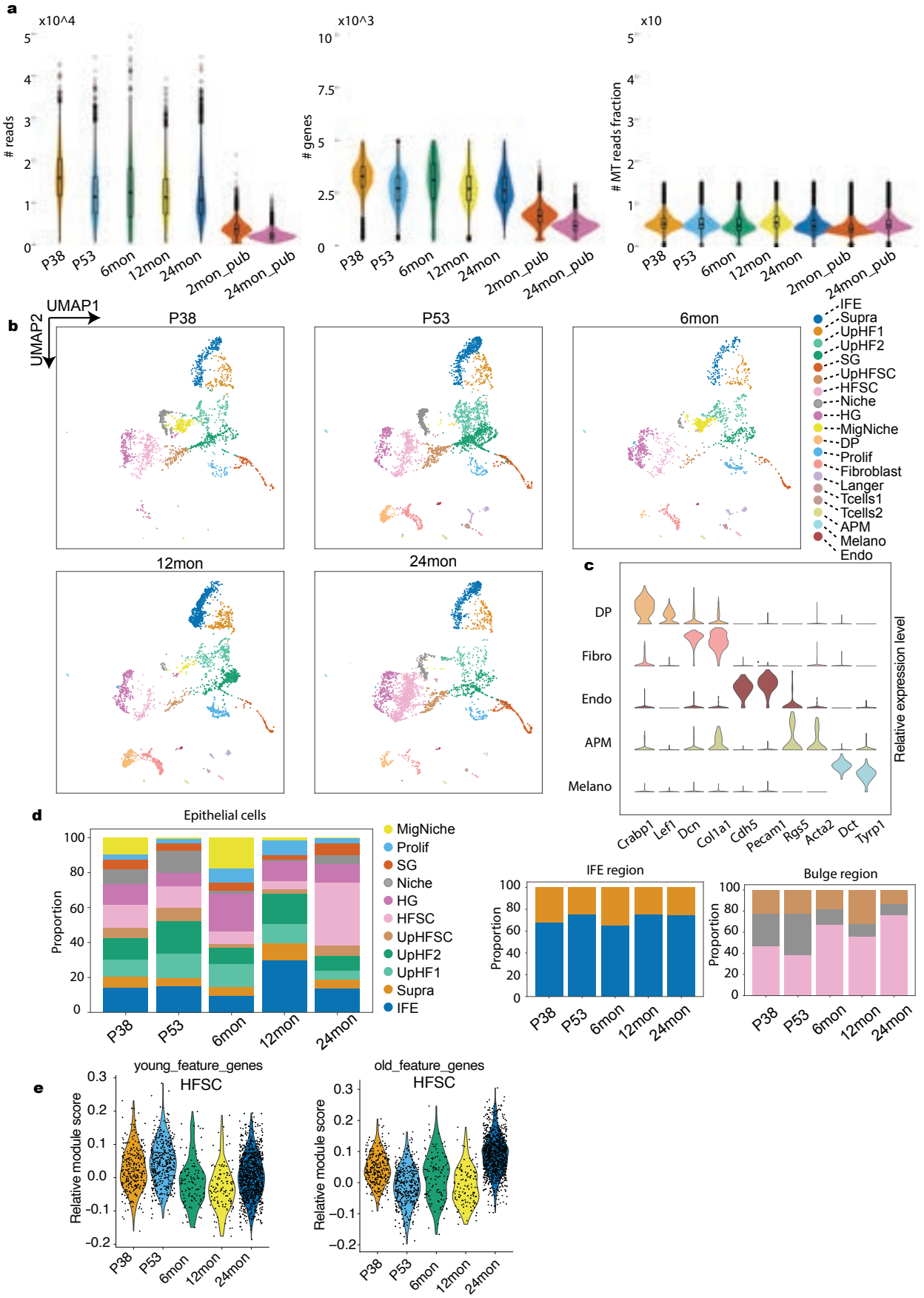
a
x10^4
reads
x10^3
genes
x10
MT reads fraction
P38
P53
6mon
12mon
24mon
2mon_pub
24mon_pub
b
UMAP1
UMAP2
P38
P53
6mon
12mon
24mon
IFE
Supra
UpHF1
UpHF2
SG
UpHFSC
HFSC
Niche
HG
MigNiche
DP
Prolif
Fibroblast
Langer
Tcells1
Tcells2
APM
Melano
Endo
c
DP
Fibro
Endo
APM
Melano
Relative expression level
Crabp1
Lef1
Dcn
Col1a1
Cdh5
Pecam1
Rgs5
Acta2
Dct
Tyrp1
d
Epithelial cells
Proportion
IFE region
Bulge region
e
young_feature_genes
old_feature_genes
HFSC
Relative module score

Figure 3.1S: **Quality control and clustering of scRNAseq data**. **a** Violin plots of number of reads, number of genes and mitochondrial fractions per sample. **b** Umap clustering and population identification of individual sample. Each cell population was color coded and presented in all samples. **c** Marker genes violin plot of DP, Fibro, Endo, APM and Melano cells. **d**. Compositional analysis of cell population proportions. IFE region and bulge region only contain anatomically adjacent populations. **e**. Violin plots of young and old feature genes in HF-SCs. IFE, interfollicular epidermal basal cells; Supra, suprabasal cells; UpHF1/2, differentiated hair follicle cells in the upper portion; SG, sebaceous gland; UpHFSC, Lgr6+ HF-SCs; HF-SC, hair follicle stem cells; Niche, inner layer niche cells; HG, hair germ; MigNiche, migratory niche cells; DP, dermal papillae; Prolif, proliferating cells; Fibroblast, Fibroblast cells; Langer, Langerhan cells; Tcells1/2, T cells; APM, arrector pili muscle; Melano, melanocytes; Endo, endothelial cells.

lineages in all samples(Fig3.1c) as shown in the uniform manifold approximation and projection space(UMAP). The cell populations in the dermis including Fibroblast(*Dcn*+, *Col1a1*+), arrector pili muscle(APM)(*Rgs5*+, *Acta2*+), immune cells(*Cd2*+, *Cd28*+) and endothelial cells(*Cdh5*+, *Pecam1*+) were only captured in some samples(Fig3.1Sc). In the hair follicle bulge region(*Sox9*+), I was able to resolve the hair follicle stem cells(HF-SCs)(*Krt24*+, *Cd34*+), Niche(*Fgf18*+), Upper HF-SC(*Lgr6*+) and hair germ(HG)(*Lgr5+*)(Fig3.1d). In addition, the high resolution data revealed a newly reported migratory cell population[144], I hereafter named migNiche. This distinct cell population displays unique transcriptome with enriched cytoskeletal and migration-associated genes(Fig3.1d).

The majority of hair follicle aging studies rely on hair follicle stem cell specific cell surface markers to quantify the stem cell population[87, 21]. However, with aging it is unclear whether those limited markers can truthfully represent the hair follicle stem cell. The stem cells might fail to express those markers yet still maintained stem cell properties. This begs for the unbiased analysis of cell population changes in hair follicle lineages during aging. Single cell RNAseq allows me to annotate hair follicle lineages based on unsupervised clustering and manually curated annotation. Another issue arises from the sample preparation, the skin samples were scraped to remove dermal cells before digestion and this inevitably led to variation in population proportion(Fig3.1Sd). To overcome this limitation, I decided to only compare anatomically close lineages for compositional analysis. To this end, I first compared interfollicular epidermal basal cells(IFE) and suprabasal cells.

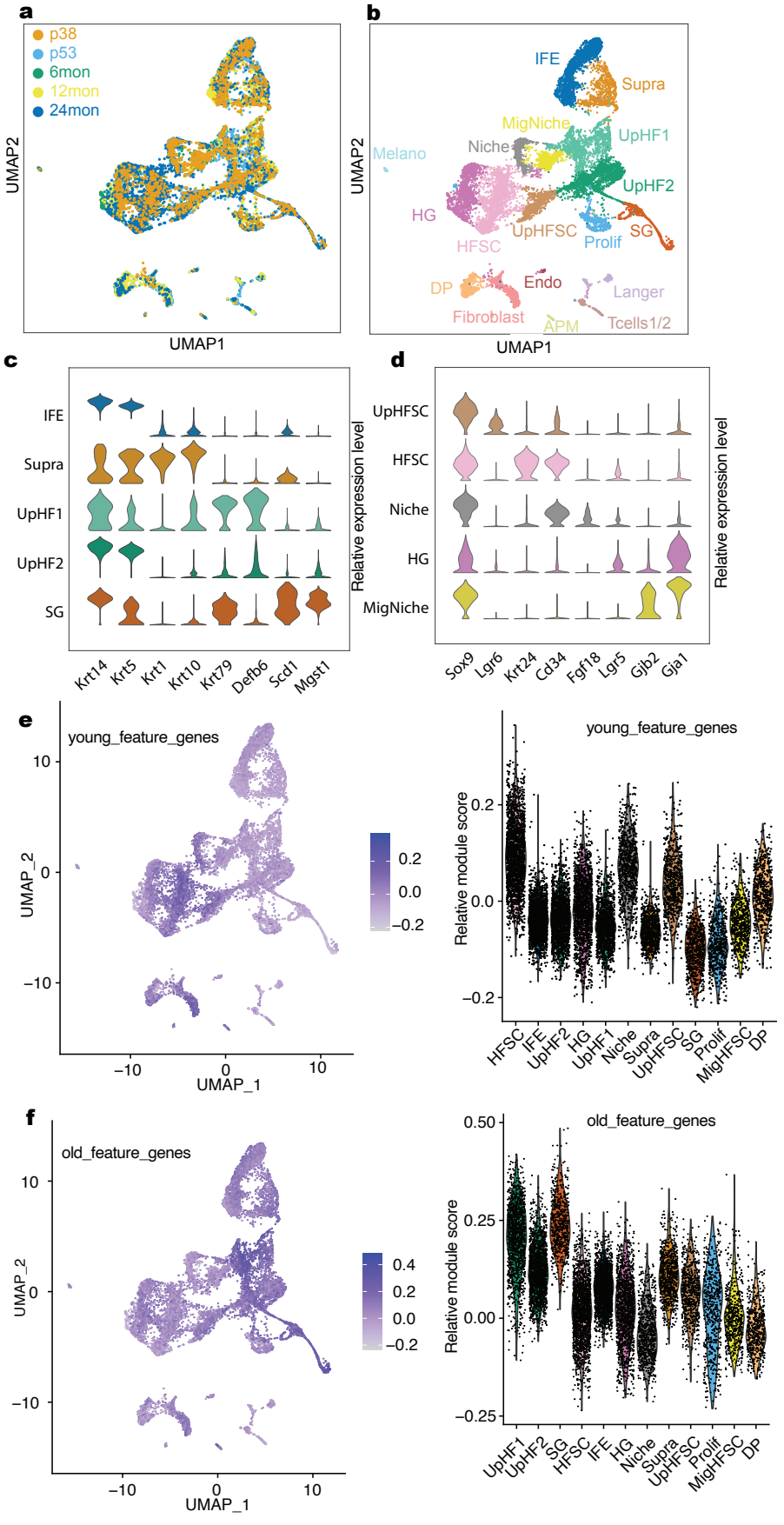
a
p38
p53
6mon
12mon
24mon
UMAP2
UMAP1
b
IFE
Supra
MigNiche
UpHF1
Niche
Melano
UpHF2
HG
UpHFSC
Prolif
SG
HFSC
DP
Endo
Langer
Fibroblast
APM
Tcells1/2
UMAP2
UMAP1
c
IFE
Supra
UpHF1
UpHF2
SG
Relative expression level
Krt14
Krt5
Krt1
Krt10
Krt79
Defb6
Scd1
Mgst1
d
UpHFSC
HFSC
Niche
HG
MigNiche
Relative expression level
Sox9
Lgr6
Krt24
Cd34
Fgf18
Lgr5
Gjb2
Gja1
e
young_feature_genes
UMAP_2
UMAP_1
young_feature_genes
Relative module score
HFSC
IFE
UpHF2
HG
UpHF1
Niche
Supra
UpHFSC
SG
Prolif
MigHFSC
DP
f
old_feature_genes
UMAP_2
UMAP_1
old_feature_genes
Relative module score
UpHF1
UpHF2
SG
HFSC
IFE
HG
Niche
Supra
UpHFSC
Prolif
MigHFSC
DP

Figure 3.1: **Single-Cell transcriptom of aging hair follicles**. **a**. Integration of scRNAseq samples from P38, P53, 6months, 12months and 24months. **b**. UMAP visualization of all epidermal cell lineages. Colored by cell types. IFE, interfollicular epidermal basal cells; Supra, suprabasal cells; UpHF1/2, differentiated hair follicle cells in the upper portion; SG, sebaceous gland; UpHFSC, Lgr6+ HF-SCs; HF-SC, hair follicle stem cells; Niche, inner layer niche cells; HG, hair germ; MigNiche, migratory niche cells; DP, dermal papillae; Prolif, proliferating cells; Fibroblast, Fibroblast cells; Langer, Langerhan cells; Tcells1/2, T cells; APM, arrector pili muscle; Melano, melanocytes; Endo, endothelial cells. **c,d**. Violin plots for marker gene plots of different epithelial cell populations. **e,f**. Feature plot and violin plot of young(**e** and old(**f** feature genes. The feature genes were extracted from differentially expressed bulk RNAseq data

From this comparison, it's evident that the proportion of epidermal cells are relatively consistent during aging(Fig3.1Sd). Secondly, I grouped cells in the hair follicle bulge region including HF-SC, UpHF-SC and Niche cells. I found that the relative proportion of the Niche cells was reduced during aging. This suggests that the miniaturized hair follicle during aging might be caused, at least in part, by the loss of Niche cells(Fig3.1Sd). Furthermore, in my live imaging analysis, I also observed the smaller number of Niche cells in miniaturized HFs[145].

To investigate the transcriptomic changes in HF-SCs, I extracted differentially expressed genes in HF-SCs from published young and aged bulk RNAseq data[19]. When I mapped the genes enriched in HF-SCs from young mice onto the integrated single-cell RNAseq data by calculating module scores[143], the HF-SC population showed the highest expression(Fig3.1e). When further considering only the HF-SCs populations, the old and young genes are enriched in corresponding conditions(Fig3.1Se). Surprisingly, I found the highly expressed genes in HF-SCs from old mice enriched instead in the Upper HF lineages among all samples(Fig3.1f). This data suggests the aging HF-SCs are acquiring the differentiated HF lineages features yet still maintained young HF-SCs signatures. In line with the trans-epidermal differentiation of HF-SCs during aging[21], my analysis further indicates that the HF-SCs are gradually acquiring differentiation genes toward the upper hair follicle lineages.

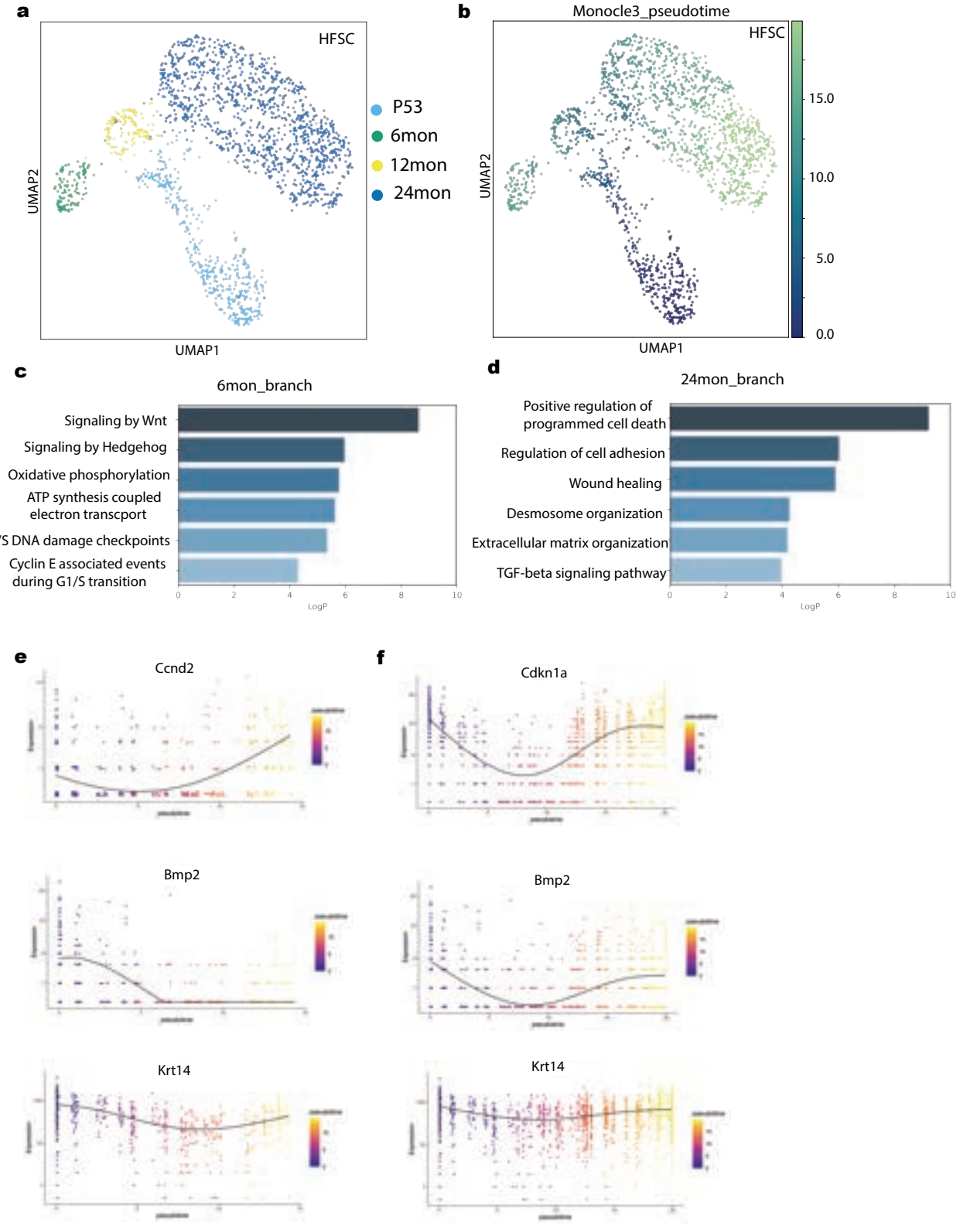
a
HFSC
P53
6mon
12mon
24mon
UMAP2
UMAP1
b
Monocle3_pseudotime
HFSC
15.0
10.0
5.0
0.0
UMAP2
UMAP1
c
6mon_branch
Signaling by Wnt
Signaling by Hedgehog
Oxidative phosphorylation
ATP synthesis coupled electron transcport
1/S DNA damage checkpoints
Cyclin E associated events during G1/S transition
0
2
4
6
8
10
LogP
d
24mon_branch
Positive regulation of programmed cell death
Regulation of cell adhesion
Wound healing
Desmosome organization
Extracellular matrix organization
TGF-beta signaling pathway
0
2
4
6
8
10
LogP
e
Ccnd2
Bmp2
Krt14
f
Cdkn1a
Bmp2
Krt14

Figure 3.2: **Transcriptomic analysis of HF-SCs aging**. **a** UMAP visualization of HF-SCs, color coded by samples. **b**. UMAP visualization of HF-SCs color-coded by pseudotime. **c, d**. Gene ontology(GO) analysis of 6months and 24months branch cells. **e,f**. Example gene expression plot along the pseudotime trajectory.

3.2.2 Pseudo-aging trajectory of hair follicle stem cell

To explore the trajectory of hair follicle stem cell aging, I first extracted the HF-SCs populations from the integrated samples. Since P38 hair follicles are at catagen stage in which cells undergo drastic apoptosis-mediated regression, I also excluded the P38 cells from further analysis. The HF-SCs were subsequently re-clustered and the UMAP projection interestingly reflected a bifurcation trajectory with 6months and 24months cells residing at each branch(Fig3.2a), unlike other permanent upper hair follicle cell lineages which mainly overlap in the clustering(Fig3.2Sa). To further test this phenomenon, partition-based graph abstraction(PAGA)[146] which preserves the global topology was used to initialize forced-directed graph drawing algorithm, Force-Atlas2[147]. The obtained single cell embeddings faithful to global topology showed similar pattern with 6months and 24months samples at the opposite directions(Fig3.2Sb).

The bifurcating trajectory admittedly doesn't reflect the physiological aging. To better understand the transcriptomic dynamics along two different trajectories, I used Monocle3 to order the HF-SCs in pseudo-time with P53 cells at the bottom of UMAP as root[148](Fig3.2b). The inferred pseudo-time progresses along the trajectory from P53 to 12months and then branches outward to 6months and 24months. Next, I separated the cells into two groups based on their branches in the trajectory(Fig3.2Sc,d). To investigate the two different trajectories of HF-SCs, I first directly compared the transcriptome of 6months and 24months samples on each branch. Interestingly, gene ontology(GO) analysis for genes associated with the 6months sample showed enriched signaling pathways including *Wnt*/hedgehog signaling, metabolic pathways including Oxidative phosphorylation and ATP synthesis coupled electron transport and cell cycles G1/S checkpoints(Fig3.2c). These results were consistent with the well-established regulation of HF-SCs activation by Wnt/Hedgehog signaling. Furthermore, the cell cycle gene expression terms indicated that the 6months hair fol-

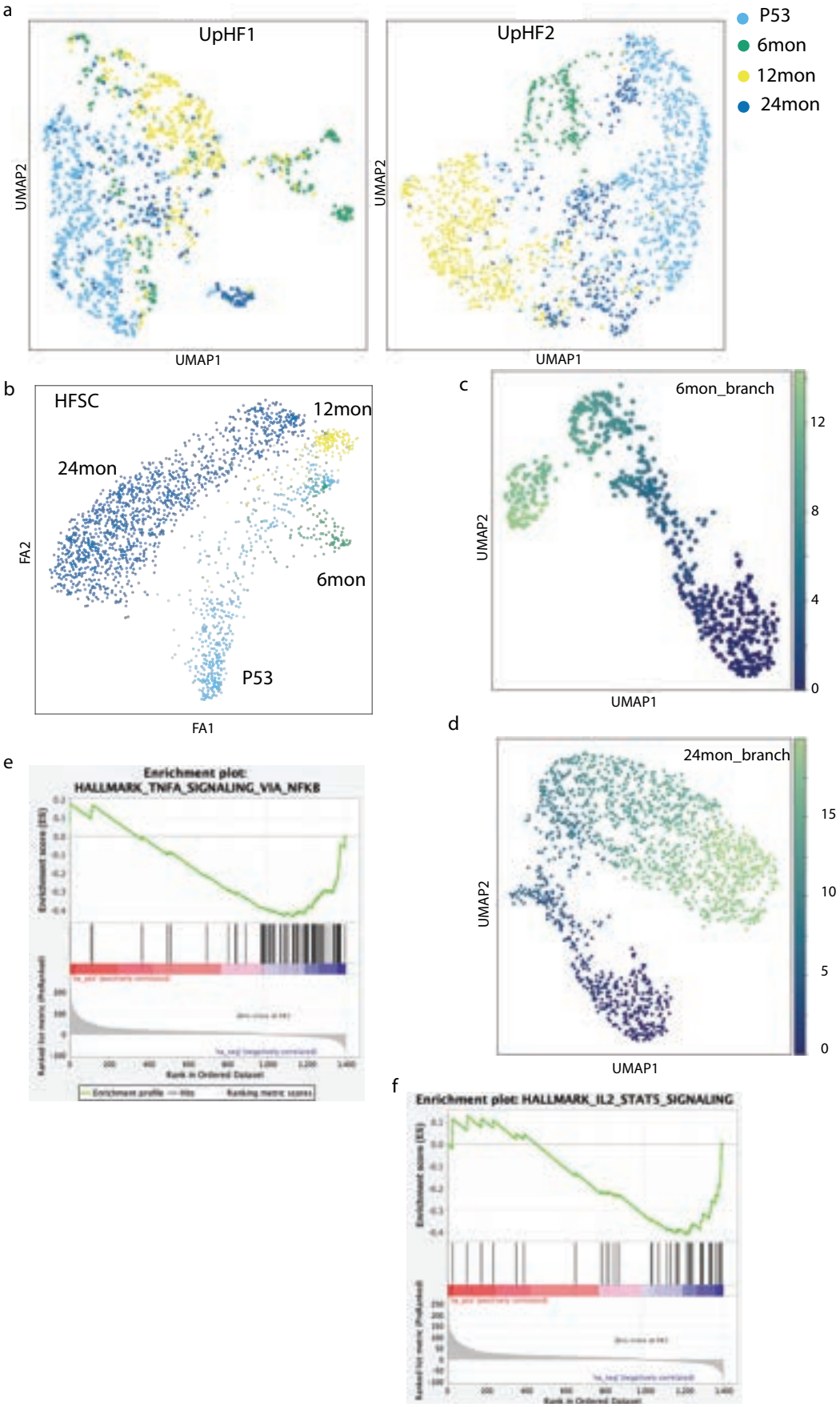
a
UpHF1
UpHF2
UMAP2
UMAP1
P53
6mon
12mon
24mon
b
HFSC
12mon
24mon
6mon
P53
FA2
FA1
c
6mon_branch
UMAP2
UMAP1
12
8
4
0
d
24mon_branch
UMAP2
UMAP1
15
10
5
0
e
Enrichment plot:
HALLMARK_TNFA_SIGNALING_VIA_NFKB
f
Enrichment plot: HALLMARK_IL2_STAT5_SIGNALING

Figure 3.2S: **Lineage specific hair follicle aging**. **a-b** UMAP visualization of differentiated hair follicle lineages UpHF1(left) and UpHF2(right), colored by samples. **b**. Force directed graph visualization of aging HF-SCs, colored by samples. **c,d**. Monocle3 pseudotime plot of 6months branch(**c**) and 24months branch(**d**), colored by pseudotime values. **e,f**. Gene set enrichment analysis(GSEA) of 6months and 24months branch cells.

licles were at anagen stage[75, 149, 150, 151, 152]. On the other hand, the 24months HF-SCs underwent positive regulation of programmed cell death and failed to maintain the extracellular matrix and cell adhesion(Fig3.2d). In addition, TGF-β signal indicated the inhibitory environment of HF-SCs in aging skin(Fig3.2d). The gene set enrichment analysis(GSEA) further showed that the 24months HF-SCs were exposed to pro-inflammatory signals such as TNFα and IL2-Stat5 signaling(Fig3.2Se,f). The activated immune program might be responsible for clearing out the escaped hair follicle cells in aging skin[145].

To understand the gradual transcriptomic changes along the bifurcating trajectory, I manually selected the 24months branch and 6months branch using Monocle3[148](Fig3.2Sc,d). Since every cell is assigned with a pseudo-time value, I can infer the gene dynamics as a function of pseudo-time along specific trajectory. For the 6months branch, cyclin responsible for G1/S transition(*Ccnd2*) was upregulated, conversely cell cycle inhibitor(*Cdkn1a*) showed reduced expression along the trajectory indicative of active hair cycle in 6months HF-SCs(Fig3.2e), as a control Krt14 level remained relatively stable. In addition, *Wnt* signaling components(*Ctnnb1*/β-catenin, *Fzd2*, *Tcf7l2*) gradually increased expression while *Bmp2* signaling was down(Fig3.2e). These evidences further corroborate the previous direct comparison between 6months and 24months samples. To gain further insights on the global gene co-expression patterns, I sought out to dissect the different gene expression patterns along the trajectory. To this end, I used Monocle3 to further group the genes(after UMAP) into different clusters based on Louvain community analysis. It detected two clusters with different patterns(Fig3.3Sa,b) on the 6months branch, which showed aggregated expression of all genes in each cluster. Aggregated cluster1(2614 genes) showed steady increase in expression level, conversely aggregated cluster2(1520) genes showed reduced expression. In addi-

tion to increased *Wnt* signaling and cell cycle genes showed previously by direct comparison among 6months and 24months, I also discovered metabolic stress(Fig3.3Sc), indicating increased replicative stress. The cluster2 genes suggested that defects in cell adhesion and tight junction occur as early as at 6months(Fig3.3Sd).

More strikingly, for the 24months branch, the HF-SCs started to restore the inhibitory signals of quiescent state such as *Bmp2* and *Cdkn1a*(Fig3.2f). Surprisingly, the co-expression pattern showed two distinct but oscillating patterns. Aggregated cluster1(2515) genes started with lower expression, gradually increased and then dropped at the end. On the other hand, aggregated cluster2(1743) genes initially had higher expression then were downregulated before recovering(Fig3.3Se,f). Since cluster1 gene expression levels increased in intermediate stage, the pathways show similar GO terms as cluster1 of 6months branch, *Wnt* signaling and cell cycle checkpoints(Fig3.3Sg). In addition, cluster1 genes showed increased transcriptional regulation by *Runx1* (Fig3.3Sg), which has been reported to promote hair follicle stem cell activation[153, 101]. Interestingly, this analysis also showed strong enrichment for reactive oxygen species(ROS) which was not presented in the direct comparisons, further proving the repair potential of hair follicle stem cells(Fig3.3Sg) and the resolving power of trajectory analysis. The cluster2 genes with reduced expression followed by recovery, showed strong cell adhesion regulation and cell migration(Fig3.3Sh). Previous direct comparison between P53 and 24months samples have also showed cell adhesion and extracellular matrix changes, this oscillating pattern might reflect the HF-SCs' active yet insufficient maintenance of proper ECM environment during aging.

3.2.3 Pseudo-agingqe trajectory of Niche cells

The composition analysis showed that the Niche cell population proportion was reduced during aging. The miniaturizing hair follicles suggests that the niche cells may contribute to this phenomenon. To study the cellular fate change of Niche cells, I first subsetted the Niche population from all cells and re-did the clustering. Interestingly, unlike the bifurcating HF-SCs, the Niche cells showed a linear pattern with P53 cells and 24months cells at the endpoints(Fig3.3a). Similarly, the

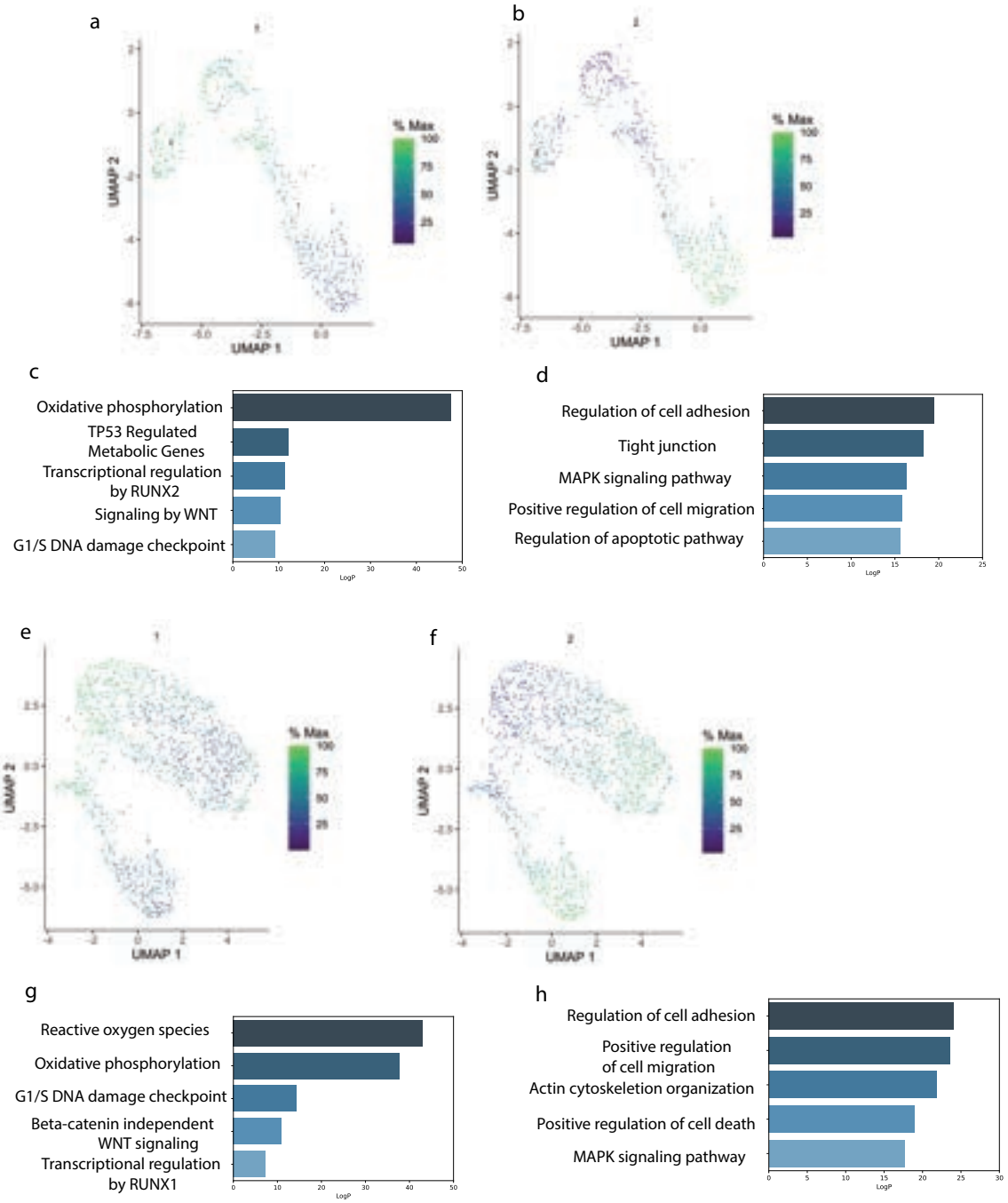
a
b
% Max
100
75
50
25
UMAP 2
UMAP 1
c
Oxidative phosphorylation
TP53 Regulated Metabolic Genes
Transcriptional regulation by RUNX2
Signaling by WNT
G1/S DNA damage checkpoint
LogP
d
Regulation of cell adhesion
Tight junction
MAPK signaling pathway
Positive regulation of cell migration
Regulation of apoptotic pathway
LogP
e
f
g
Reactive oxygen species
Oxidative phosphorylation
G1/S DNA damage checkpoint
Beta-catenin independent WNT signaling
Transcriptional regulation by RUNX1
LogP
h
Regulation of cell adhesion
Positive regulation of cell migration
Actin cytoskeletion organization
Positive regulation of cell death
MAPK signaling pathway
LogP

Figure 3.3S: **Gene co-expression patterns along pseudotime trajectory**. **a,b**. Aggregated expression of all genes in two different co-expression modules along the 6months branch. **c,d**. GO term analysis of gene modules corresponding to **a** and **b**. **e,f** Aggregated expression of all genes in different co-expression modules along the 24months branch. **g,h**. GO term analysis of gene modules corresponding to **e** and **f**

force directed graph also showed linear pattern(Fig3.4Sa).

To understand the dynamics of Niche cell transcriptome, I again adopted Monocle3 to calculate the pseudotime of individual Niche cells. Interestingly, the 24months cells had the highest pseudotime values and 6months/12months cells had intermediate values once I set P53 cells as the root(Fig3.3c). The pseudotime recapitulated the physiological aging in Niche cells, which made it possible to infer the changes along the pseudo-aging process in Niche cells. The gene co-expression clustered into three distinct patterns, with aggregated cluster1(1699 genes) and cluster2(1581 genes) turning on and off later in the trajectory and aggregated cluster3(158 genes) with evenly distributed expression across all stages(Fig3.3c,d and Fig3.4Sb). The cluster1 genes showed increased accumulated reactive oxygen species(ROS)hypoxia and stress response(Fig3.3e). This indicates the Niches cells are accumulating stress unlike the HF-SCs which can recover in later stages in pseudotime(Fig3.3Sc,e). For cluster2, the genes turning off at the later pseudotime points showed regulation of cell death, cell adhesion and regulation of apoptotic signaling pathway(Fig3.3d,f).

The Niche cell analysis indicates that these cells accumulate cell stress including ROS, hypoxia and DNA damage, yet fail to maintain proper cell death regulation during the pseudo-aging process. This is in contrast to the HF-SCs, which are able to restore repair potential, as indicated by the downregulation of ROS after its intermediate upregulation. This suggests a relative fragile fate of Niche cells during aging with increasing cellular stress yet decreasing damage response, which might lead the eventual cell death.

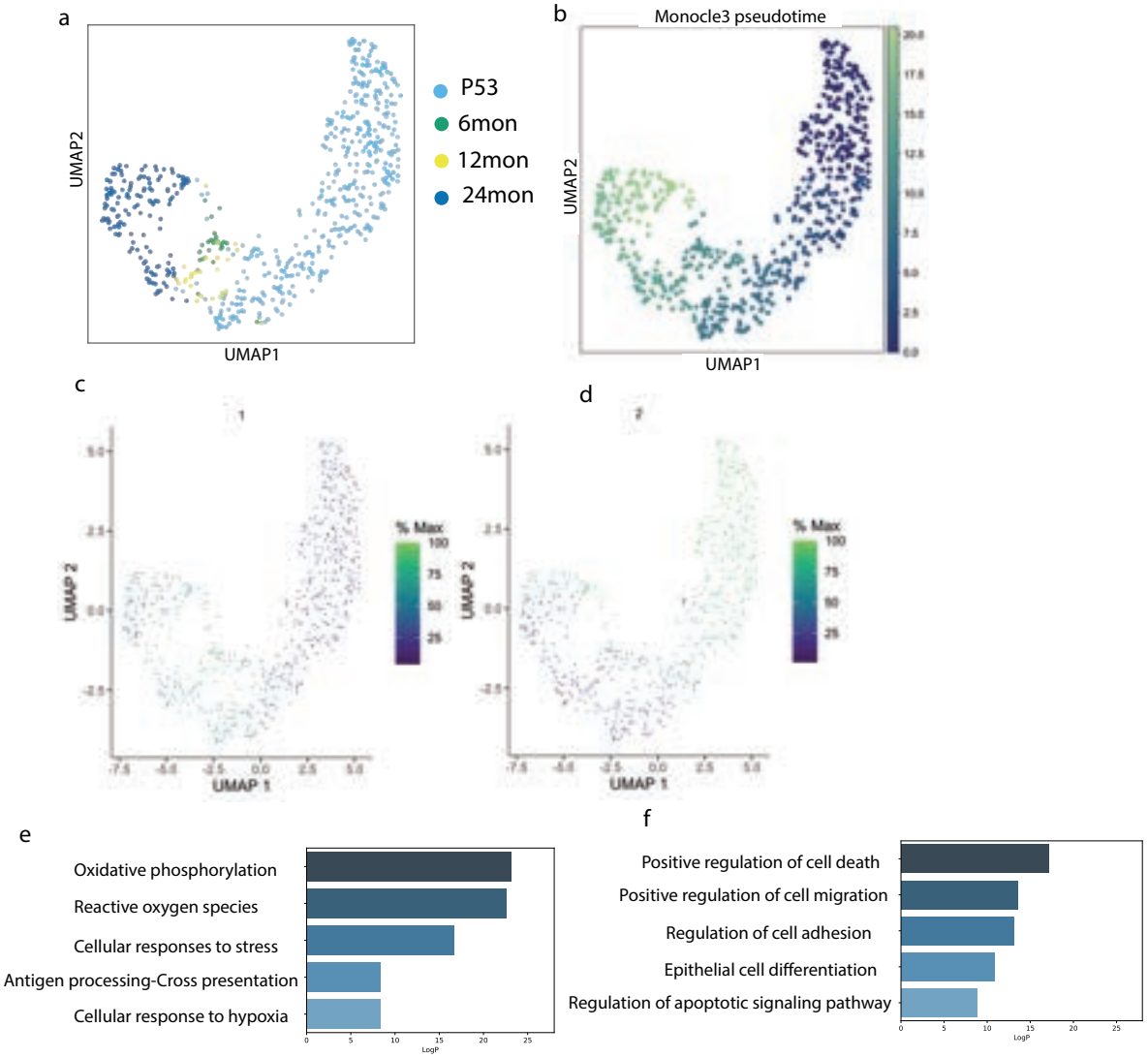
a
UMAP2
UMAP1
P53
6mon
12mon
24mon
b
Monocle3 pseudotime
UMAP2
UMAP1
c
d
% Max
100
75
50
25
UMAP 2
UMAP 1
e
Oxidative phosphorylation
Reactive oxygen species
Cellular responses to stress
Antigen processing-Cross presentation
Cellular response to hypoxia
LogP
f
Positive regulation of cell death
Positive regulation of cell migration
Regulation of cell adhesion
Epithelial cell differentiation
Regulation of apoptotic signaling pathway
LogP

Figure 3.3: **Aging trajectory of Niche cells**. **a**. UMAP visualization of Niche cells during aging, colored by samples. **b**. Monocle3 pseudotime plots of aging Niche cells colored by pseudotime values. **c-e**. Aggregated expression of all genes in different co-expression modules along the aging Niche cells. **f,g**. GO term analysis of gene modules corresponding to **c** and **d**

3.2.4 MigNiche cells are responsible for niche re-population

To explore the maintenance of Niche cell populations during aging, I first sought to determine the cellular lineage origin of Niche cells during each hair cycle. For every hair cycle, a new hair shaft along with associated cell populations are generated. Niche cells located right beneath HF-SCs have very similar transcriptomic profiles compared to HF-SCs, sharing stem cell specific transcriptional factor expression as well as stem cell specific cell surface markers despite relatively lower expression level(Fig3.4a). Previous elegant lineage tracing studies using H2BGFP and BrdU pulse-chase labeling showed that Niche cells are derived from actively cycling lower outer root sheath cells during catagen[154]. Our immunostaining results from P38-P45 also captured newly acquired cell lineages expressing *Sox9*, *Nfatc1*, *Foxc1* but lacking *Cd34* during the catagen to telogen transition(Fig3.4b). To investigate the transcriptomic profile of this cell population and its transcriptional regulation towards the final fate conversion to Niche cells, I profiled the single cell transcriptome of hair follicles at the catagen-telogen transition stage, P38. Interestingly, the clustering analysis confirmed a recently reported cell population with similar profiles as HF-SCs and Niche cells but also unique expression of cytoskeleton reorganization[144]. When integrated with the samples from other stages, this new cell population again showed very few cell number in telogen stages(P53, 12months, 24months) and relatively high cell number in (6months) the active stage. It was previously named as migraBulge[144], but I think it might be appropriate to name it as migNiche since its final destiny is the Niche cells and it was originated from ORS cells by lineage tracing[154].

To further validate the conversion between migNiche cells to Niche cells, I applied PAGA to infer the global topology of cell lineages. Both the force-directed graph and UMAP projection showed close positioning between Niche cells and migNiche cells, indicating similar lineage

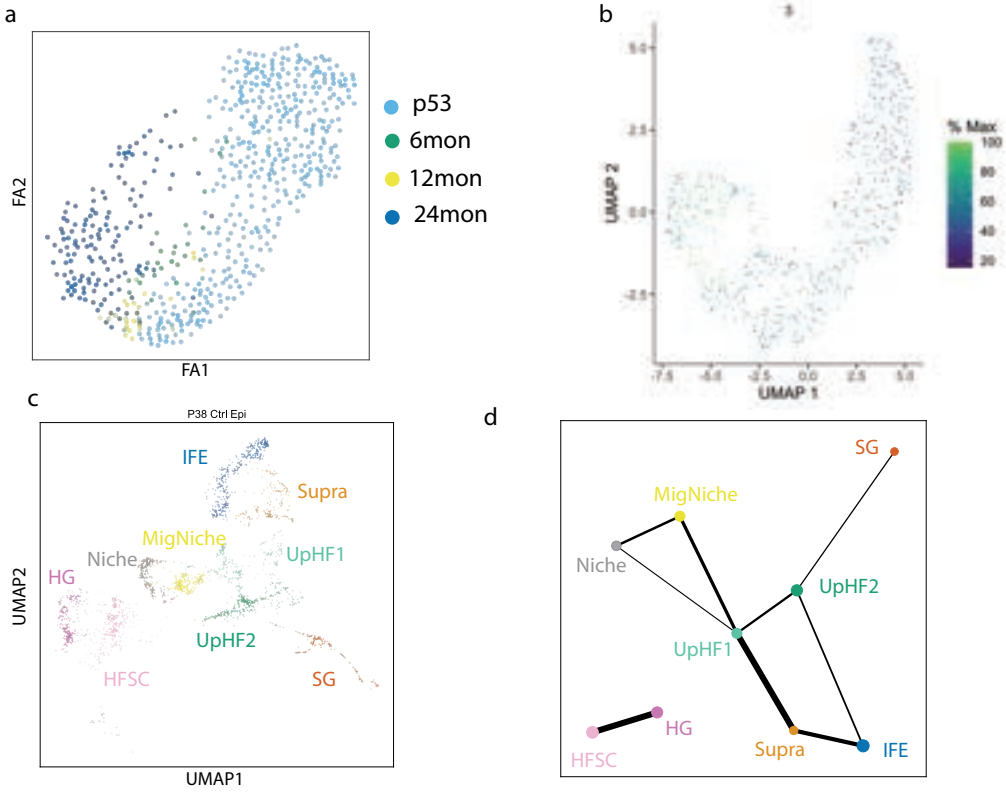
a
FA2
FA1
p53
6mon
12mon
24mon
b
UMAP 2
UMAP 1
% Max
c
P38 Ctrl Epi
IFE
Supra
MigNiche
Niche
UpHF1
HG
UpHF2
HFSC
SG
UMAP2
UMAP1
d
SG
MigNiche
Niche
UpHF2
UpHF1
HG
HFSC
Supra
IFE

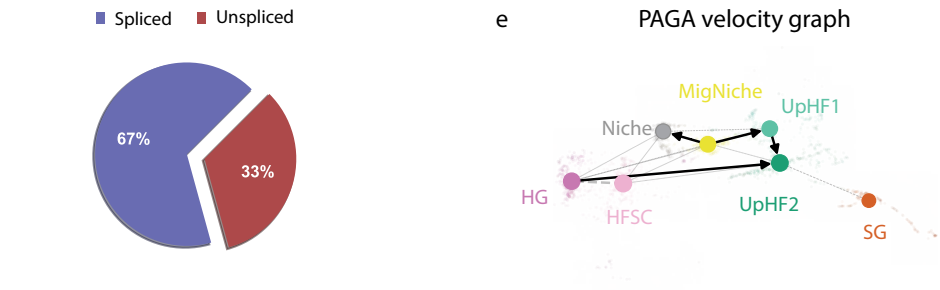
e
Spliced
Unspliced
67%
33%
e
PAGA velocity graph
MigNiche
UpHF1
Niche
HG
HFSC
UpHF2
SG

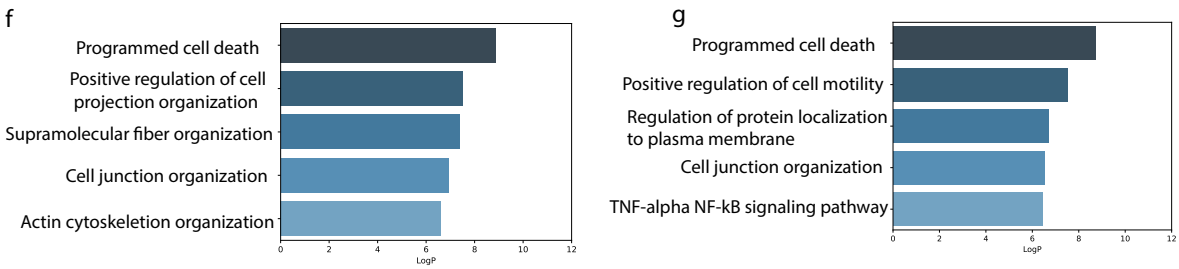
f
Programmed cell death
Positive regulation of cell projection organization
Supramolecular fiber organization
Cell junction organization
Actin cytoskeletion organization
LogP
g
Programmed cell death
Positive regulation of cell motility
Regulation of protein localization to plasma membrane
Cell junction organization
TNF-alpha NF-kB signaling pathway
LogP

Figure 3.4S: **Niche cell dynamics during aging**. **a**. Force directed graph visualization of Niche cells during aging, colored by samples. **b**. Aggregated expression of all genes in cluster3 gene modules along aging Niche cells. **c**. UMAP visualization of P38 control epithelial cells, colored by cell populations. **d**. Partition-based graph abstraction of P38 control epithelial cells, the lines connecting each populations indicating the similarity. **e**. Pie plots of Spliced and Unspliced transcripts of P38 control samples. **f,g**. GO term analysis of differential gene expression among migNiche and Niche cells. IFE, interfollicular epidermal basal cells; Supra, suprabasal cells; UpHF1/UpHF2, differentiated hair follicle lineages in the upper portion of hair follicles; SG, sebaceous gland; MigNiche, migratory niche cells; HG, hair germ; HF-SC, hair follicle stem cell; Niche, inner layer niche cells.

relationships(Fig3.4c and Fig3.4Sc). The PAGA graph also indicated that migNiche cells had stronger lineage similarity to Niche cells compared to other lineages(Fig3.4Sd). To infer the directionality between the migNiche and Niche cells, I used single cell velocity analysis on the hair follicle lineages on P38, an analysis enabled by the fact that P38 sample had more than 30% unspliced transcripts(Fig3.4Se). The velocity graph and stream plot validated the migNiche to Niche transition, in addition to the potential migNiche to UpHF transition(Fig3.4d and Fig3.4Sf).

To study the molecular mechanisms governing the transition between migNiche and Niche cells, I proceeded with differential gene expression analysis. Interestingly, the migNiche cells were enriched with genes related to programmed cell death along with the cell projection organization, cytoskeleton reorganization and cell junction assembly which reflected the migratory function of migNiche cells(Fig3.4Sg). Given the wide-spread apoptosis observed at the catagen stage, the migNiche cells might also have been exposed to the signals. The Niche cells, however, were also enriched for cell junction and the regulation of protein localization to plasma membrane(Fig3.4Sh). To disentangle the different gene sets yet similar GO terms, I further used GSEA to analyze relative changes in expression compared to the random background. Surprisingly, I found that the migNiche cell had higher oxidative phosphorylation compared to Niche cells, indicating the energy consumption of migratory cells(Fig3.4e). Niche cells, on the other hand, strongly enriched for *Myc* target genes, which might suggest the activation of transcription factor *Myc* during the migNiche to Niche transition(Fig3.4f). In addition, the Niche cells also showed upregulation of apical-basal junction genes as showed by *Cdh1* study[118](Fig3.4g), indicating the establishment of Niche cell

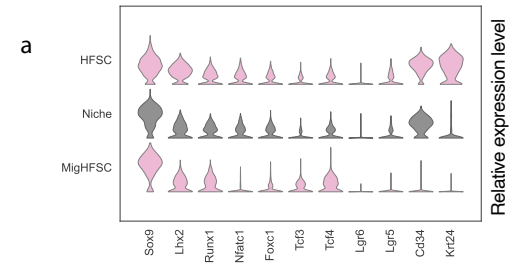
a
HFSC
Niche
MigHFSC
Relative expression level
Sox9
Lhx2
Runx1
Nfatc1
Foxc1
Tcf3
Tcf4
Lgr6
Lgr5
Cd34
Krt24

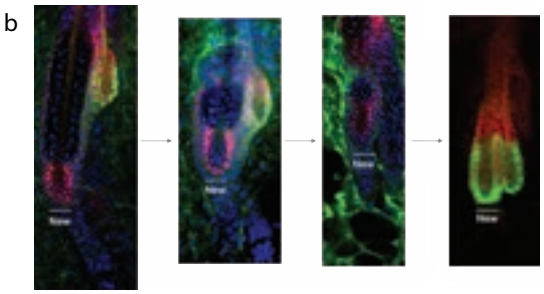
b

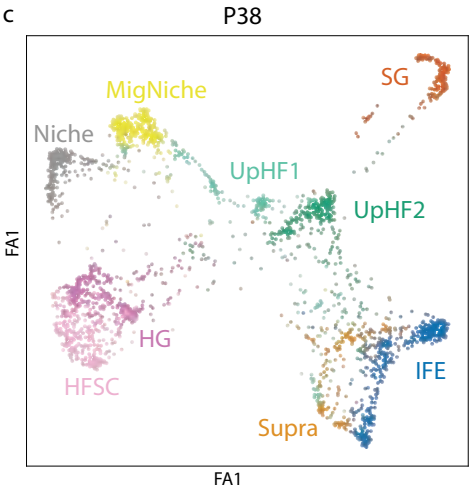
c
P38
MigNiche
SG
Niche
UpHF1
UpHF2
HG
IFE
HFSC
Supra
FA1
FA1

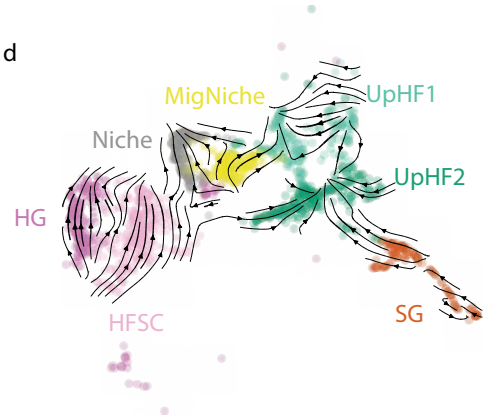
d
MigNiche
UpHF1
Niche
UpHF2
HG
HFSC
SG

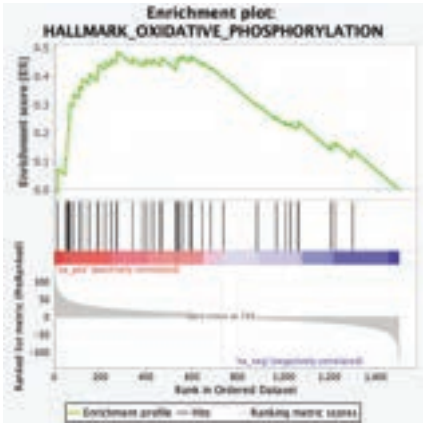
e
Enrichment plot:
HALLMARK_OXIDATIVE_PHOSPHORYLATION

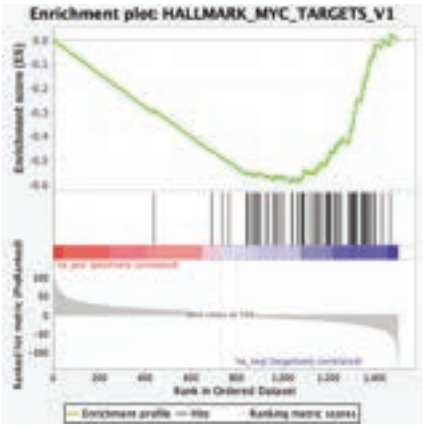
f
Enrichment plot: HALLMARK_MYC_TARGETS_V1

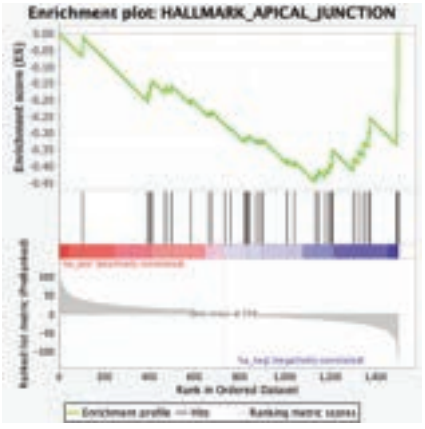
g
Enrichment plot: HALLMARK_APICAL_JUNCTION

Figure 3.4: **Niche cells maintenance during hair cycle**. **a**. Violin plot of HF-SCs related transcription factor and marker genes. **b**. Immunostaining of TFs(red) and Cd34/Krt24(green) during categen to telogen transition. **c**. UMAP visualization of P38 control epithelial cells, colored by cell populations. **d**. Velocity stream plot of hair follicle lineages. **e-g**. GSEA of migNiche and Niche cells. IFE, interfollicular epidermal basal cells; Supra, suprabasal cells; UpHF1/UpHF2, differentiated hair follicle lineages in the upper portion of hair follicles; SG, sebaceous gland; MigNiche, migratory niche cells; HG, hair germ; HF-SC, hair follicle stem cell; Niche, inner layer niche cells

polarity during the transition.

The transition between migNiche cells to Niche cells during each hair cycle serves to repopulate the Niche population. However, during aging, as the terminally differentiated cells, Niche cells irreversibly induce ROS, hypoxia and DNA damage. I think this might lead to both the observed cell loss and miniaturization of aging hair follicles.

3.2.5 Integration of scRNAseq and scATACseq

The scRNAseq has inherent limitation of poor detection rate for low-expression genes including transcription factors. The scATACseq, however, can infer the activity of transcription factors based on the patterns of chromatin accessibility. To understand the multi-modality of hair follicle aging, we next performed single-cell ATACseq on P28, 12months and 24months samples. After preprocessing(Fig3.5Sa,b), I selected cells with number of fragments overlapping peaks between 3000 to 100000, with more than 40% reads in peaks, and blacklist_ratio less than 0.025. Furthermore, I calculated the transcriptional start sites(TSS) enrichment signal and nucleosome signal per cell using signac[155] to filter out low TSS and high nucleosome signal cells. Overall, we sequenced around 20492 cells from all samples(Figs3.5b). With similar sequencing saturation rate(63.6% - 64.1%), the P28 samples had around 20k fragments in peak regions per cell after filtering while 12months and 24months samples had around 10k fragments. This suggested the widespread closing of chromatin accessibility as early as 12months in epithelial cells. To capture high-confidence peaks in all samples, I pooled all the cells from each sample and then called peaks as if bulk data. In total, I detected 178454 peaks in P28, 111246 peaks in 12months and 145689 in 24months sample.

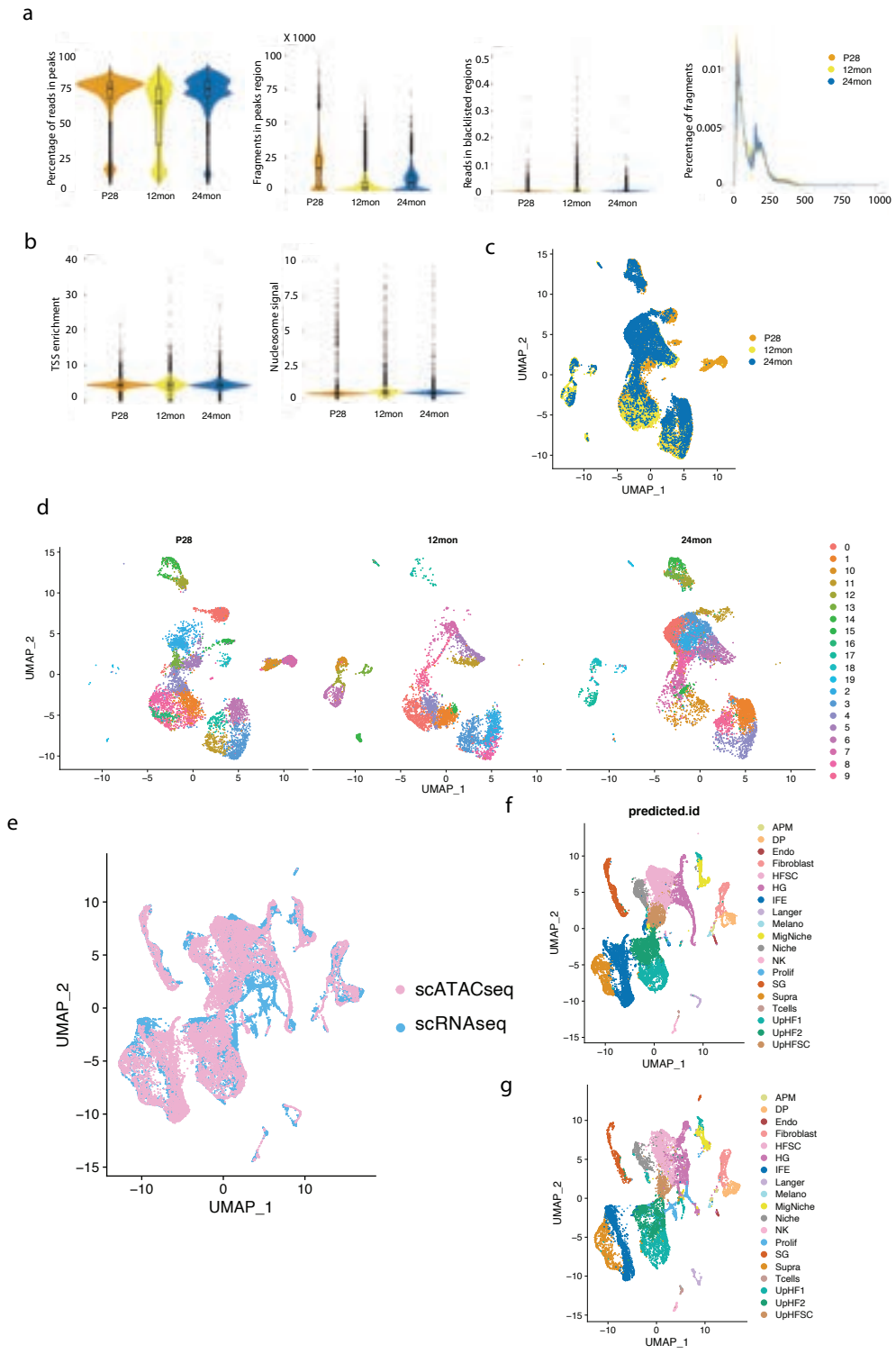
a
Percentage of reads in peaks
Fragments in peaks region
X 1000
Reads in blacklisted regions
Percentage of fragments
P28
12mon
24mon
b
TSS enrichment
Nucleosome signal
c
UMAP_1
UMAP_2
d
P28
12mon
24mon
e
scATACseq
scRNAseq
f
predicted.id
APM
DP
Endo
Fibroblast
HFSC
HG
IFE
Langer
Melano
MigNiche
Niche
NK
Prolif
SG
Supra
Tcells
UpHF1
UpHF2
UpHFSC
g

Figure 3.5S: **Quality control and integration of scATACseq and scRNAseq data**. **a**. Violin plot of percentage of reads in peaks, numbers of fragments in peaks and percentage of reads in blacklisted regions. Distribution of fragment length(right panel). **b**. Violin plots of calcuated TSS enrichemtn score and Nucleosome signals among all samples. **c**. UMAP visualization of integrated scATACseq samples. **d** UMAP plot of individual scATACseq sample. **e**. Integration of scRNAseq and scATACseq samples. **f,g**. UMAP visualization of coembeded scRNAseq and scATACseq samples, colored by cell populations.

To facilitate the integration of all scATACseq data, I combined peaks across all samples. To find integration anchors from all samples, I applied signac[155] to project all samples into a shared low-dimensional space using reciprocal latent semantic indexing(LSI), excluding the first component because it was highly correlated with sequencing depth(Fig3.5Sc,d).

Since all the scRNAseq cells were annotated with specific cell types, I next used scRNAseq as a reference and mapped scATACseq data onto it which facilitated the cell type identification(Fig3.5a,b and Fig3.5Se-g). The full collection of samples at comparable stages allowed me to dissect the gene-expression(scRNAseq), gene activity(counting fragments overlapping the gene body and upstream region based on scATACseq) and motif enrichment(scATACseq). The marker gene expression from scRNAseq and predicted gene activity from scATACseq for each cluster showed strong correlation(Fig3.5c). Interestingly, the open chromatin signatures(dot size) showed widespread shared signals across the epithelial cells yet predicted gene activities(color) were relatively conserved with gene expression unique in each populations(Fig3.5c, right panel). The proliferating cells in scRNAseq data failed to mapped onto the scATACseq space, which has been reported before[156]. This further proves the disparity between open chromatin regions, active transcribing regions and gene expressions.

Next, I calculated the lineages specific TF motifs activity using Chromvar[157]. In line with predicted annotations, the gene expression level, predicted gene activity and motif activity all showed enrichment for lineage specific TFs. For IFE and UpHF populations, *Gata3*, *Gata6*, *Jun* and *Grhl1* all showed high expression level along with high motif activities(Fig3.5d and Fig3.6Sa,b).

For bulge region cells, *Sox9*, *Nfatc1* and *Lhx2* signals were all enriched(Fig3.5d and Fig3.6Sc).

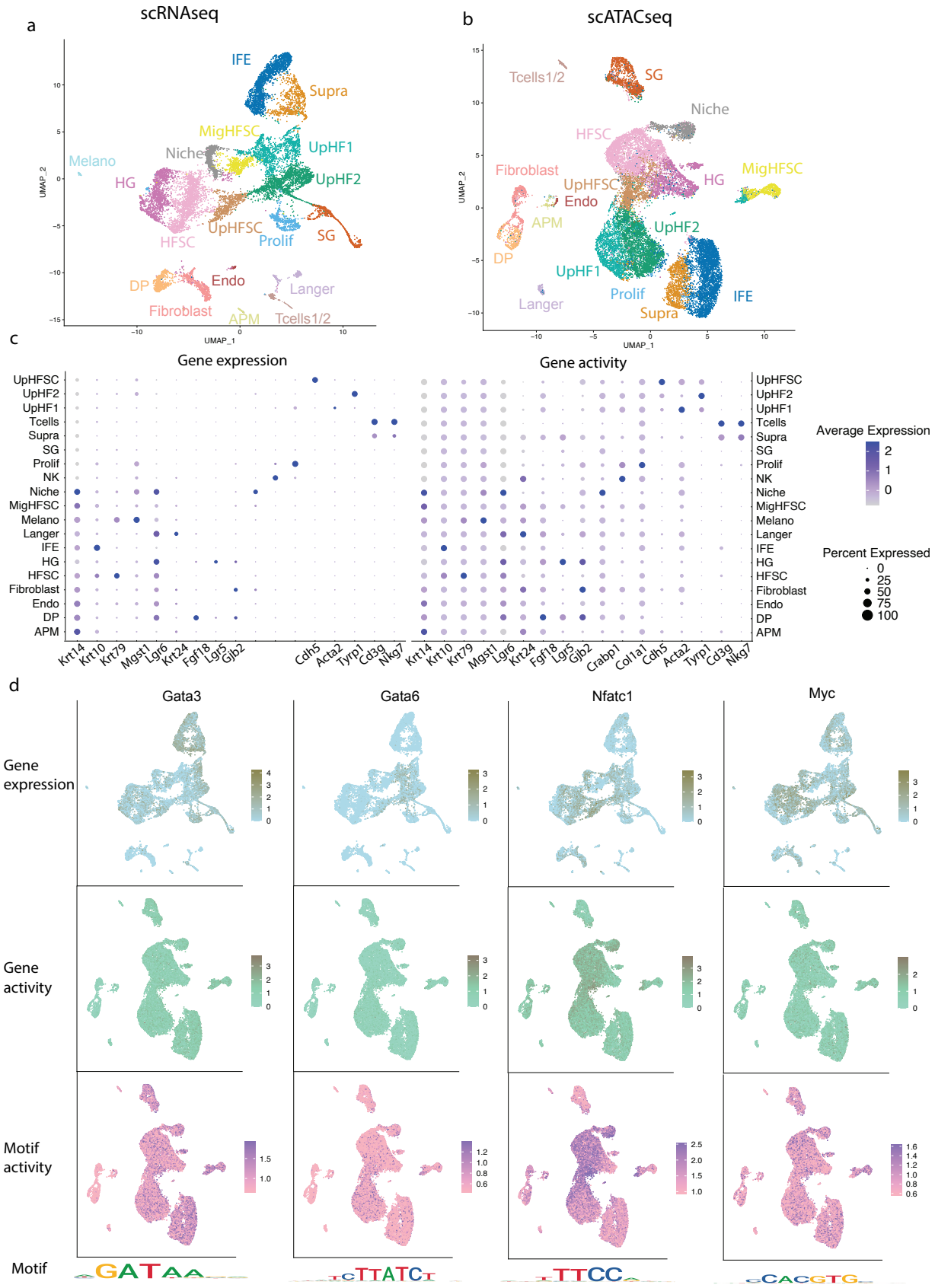
a
scRNAseq
IFE
Supra
MigHFSC
UpHF1
Niche
Melano
HG
UpHF2
UpHFSC
SG
HFSC
Prolif
DP
Endo
Langer
Fibroblast
APM
Tcells1/2
UMAP_1
UMAP_2
b
scATACseq
Tcells1/2
SG
Niche
HFSC
Fibroblast
MigHFSC
UpHFSC
HG
Endo
APM
UpHF2
DP
UpHF1
Prolif
IFE
Langer
Supra
c
Gene expression
Gene activity
UpHFSC
UpHF2
UpHF1
Tcells
Supra
SG
Prolif
NK
Niche
MigHFSC
Melano
Langer
IFE
HG
HFSC
Fibroblast
Endo
DP
APM
Krt14 Krt10 Krt79 Mgst1 Lgr6 Krt24 Fgf18 Lgr5 Gjb2 Cdh5 Acta2 Tyrp1 Cd3g Nkg7
Krt14 Krt10 Krt79 Mgst1 Lgr6 Krt24 Fgf18 Lgr5 Gjb2 Crabp1 Col1a1 Cdh5 Acta2 Tyrp1 Cd3g Nkg7
Average Expression
2
1
0
Percent Expressed
0
25
50
75
100
d
Gata3
Gata6
Nfatc1
Myc
Gene expression
Gene activity
Motif activity
Motif

Figure 3.5: **Integration of scRNAseq and scATACseq data**. **a,b**. UMAP visualization of integrated scRNAseq and scATACseq data, colored by cell populations. **c**. Dotplot of marker genes expression in scRNAseq(left) and inferred gene activities in scATACseq(right). Gene expression levels were indicated by color intensity. Dot size represents the percentage of cells with the inferred activities. **d**. Gene expression, inferred gene activities, motif activities and motif plots of lineage specific transcription factors.

Note that motif activities and gene expression levels were much more specific than predicted gene activity. In addition, even lowly expressed TFs showed strong signals in motif activities(Fig3.6Sd). Interestingly, for the migNiche cells, the *Myc* gene expression was relatively low compared to Niche cells, but the motif activity was relatively comparable(Fig3.5d).

3.2.6 Chromatin accessibility dynamics during hair follicle aging

To study the epigenetic changes during aging, I first downloaded published young and old bulk ATACseq datasets for comparison[87]. The different accessibility regions were then mapped on the scATACseq data. Surprisingly, the accessibility regions open in young HF-SCs were enriched across all epithelial populations(Fig3.6a and Fig3.6Se). The old accessibility regions were, however, only open in HF-SCs, more specifically in HF-SCs from old mice(Fig3.6b and Fig3.6Sf). This suggested that HF-SCs were gradually closing certain chromatin regions universal in epithelial lineages(Fig3.6c). On the other hand, the new chromatin regions in HF-SCs were unique in HF-SCs from old mice(Fig3.6d).

To further understand the transcriptional regulation underlying the chromatin changes, I investigated the motif enrichment of the differential chromatin accessibility regions(Fig3.6e). The regions enriched in HF-SCs from young mice showed *Jun* motifs(Fig3.6g) and regions in old HF-SCs, *Lhx2*(Fig3.6f).

Increased *Lhx2* motif activities along with transcriptional rebound in mRNA level specifically in aging HF-SCs indicate the unique properties of HF-SCs. During aging, HF-SCs initiate transcriptional programs mediated by stem cell specific transcription factors as a way to maintain their functions.

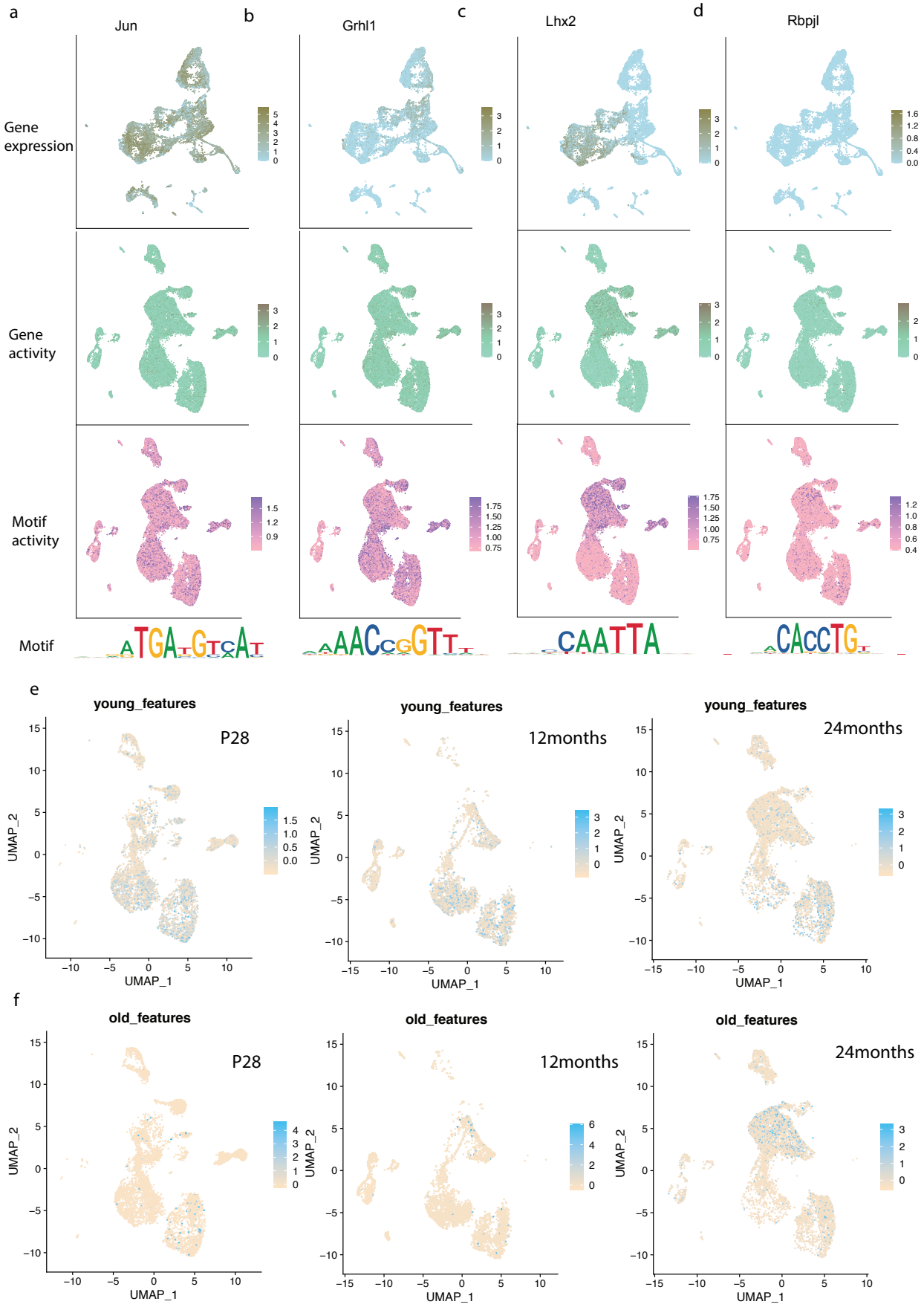
a
Jun
b
Grhl1
c
Lhx2
d
Rbpjl
Gene expression
Gene activity
Motif activity
Motif
e
young_features
P28
12months
24months
UMAP_1
UMAP_2
f
old_features
P28
12months
24months
UMAP_1
UMAP_2

Figure 3.6S: **Open chromatin dynamics of hair follicle lineages and HF-SC aging**. **a-b**. Gene expression, inferred gene activity, motif activities and motifs plot of different transcription factors. **e,f**. Feature plot of young and old open chromatin regions in individual samples.

3.3 Discussion

3.3.1 Lineages specific aging, permanent lineages and dynamic lineages

Our previous understanding of hair follicle aging mostly focused on the stem cell populations demonstrated by stem cell markers based staining or cell surface marker based FACS studies. However, given the lineage similarity between Niche cells and HF-SCs and the gradual cell fate change observed during aging, our data suggests single gene expression characterization may not be accurate to faithfully reflect the stem cell properties. Our comprehensive single cell studies demonstrate the lineage changes of all cell population during aging. We show that the HF-SC and Niche cells are the lineages undergoing drastic changes, and UpHF lineages as the permanent section of hair follicle didn't show aging related trajectories. In addition, we report the repopulation of Niche cells during hair cycle by migNiche populations.

3.3.2 Rethinking hair follicle miniaturization

Unlike in senescence, the hair follicle stem cells are still able to divide in aging[145]. Our longitudinal analysis, which captures the aging stem cells, shows regained stem cell property during aging unlike other cell lineages including Niche cells. The hair follicle stem cell specific transcription factor activities are induced during aging. In addition, the transplantation experiments from independent groups show the regenerative potential of stem cells in young microenvironment[87, 19]. All of those studies indicate that rather than popular ideas of stem cell aging, the irreversible Niche cells and other microenvironment might be the major contributing factors for hair follicle aging. Together, our studies provide new theories of hair follicle miniaturization and stem cell aging.

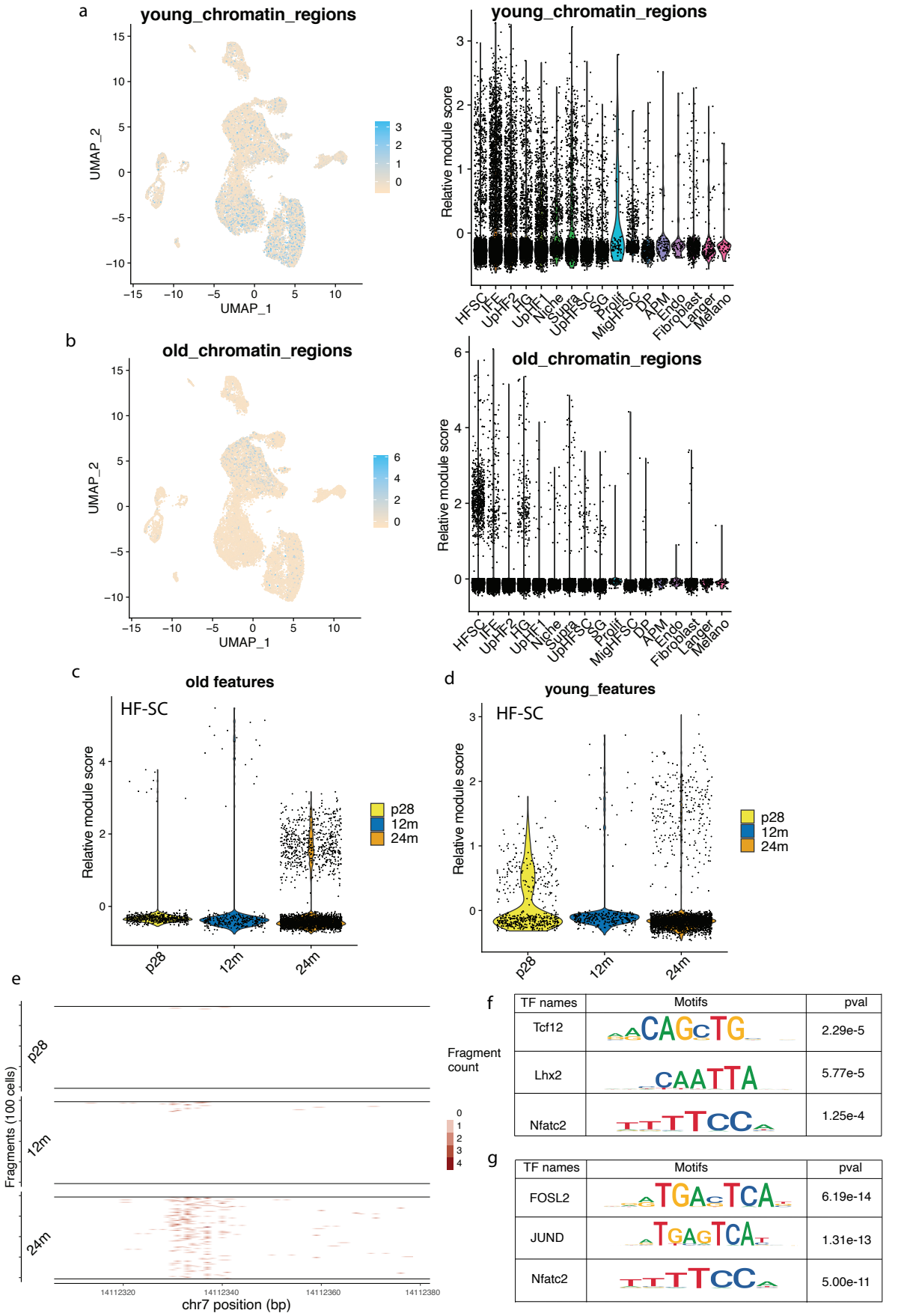

TF names	Motifs	pval
Tcf12	CAGCTG	2.29e-5
Lhx2	CAATTA	5.77e-5
Nfatc2	TTTTCC	1.25e-4

TF names	Motifs	pval
FOSL2	TGACTCA	6.19e-14
JUND	TGAGTCA	1.31e-13
Nfatc2	TTTTCC	5.00e-11

Figure 3.6: **Open chromatin dynamics of hair follicle HF-SC aging**. **a**. Feature plot and violin plot of young open chromatin regions. **b**. Feature plot and violin plot of old open chromatin regions. **c,d**. Violin plot of young and old open chromatin features in HF-SCs of different samples. **e**. Tileplot of chromatin regions gradually open up during aging. **f,g**. Enriched motif in young and old HF-SC open chromatin regions

3.4 Methods

3.4.1 Mice

All experiments were carried out following IACUC-approved protocols and guidelines at CU Boulder and Northwestern University. Mice were housed according to guidelines of the IACUC at a pathogen-free facility at University of Colorado at Boulder and at Northwestern University Feiberg School of Medicine. The K14-H2BGFP(E.Fuchs, Rockefeller University) mouse line was used for sorting epidermal cells. The samples used for sequencing were males except 12months sample.

3.4.2 Cryosectioning and immunostaining

Crysectioning and immunostaining were performed as described[145]. Briefly, OCT-embedded tissues were sectioned to 20-30μm and fixed with 4% PFA for 10 min at room temperature. Sections were permeabilized for 10 min at room temperature with 0.1% Triton X-100 in 1X PBS. When staining with mouse monoclonal antibodies, we used the mouse-on-mouse basic kit(BMK-2201, Vector Laboratories). Otherwise, blocking was performed with 5% normal serum of the same species that the secondary antibody was raised in. Sections were incubated with primary antibody overnight at 4°C. After incubation with primary antibodies, sections were washed three times in 1XPBS and incubated for 1h at room temperature with Alexa Fluor 594-, Alexa Fluor 488- or Alexa Fluor 747-conjugated secondary antibodies(1:2000, Invitrogen-Molecular Probes). Nuclei were stained with Hoechst 33342(1:5000, Invitrogen).

3.4.3 Tissue processing and Fluorescence-activate cell sorting

Mice were euthanized and collected for dissection. We first shaved the hair coat and applied nair hair removal lotion(Amazon, 22339) for around 3 min. After wiping off the lotion and washing away leftover hair shafts, back skin was dissected, and subcutaneous fat was removed using a blade. As small part of the skin sample was embedded in OCT, and the remaining skin sample was minced and incubated with 0.25% collagenase(Worghington, LS004188) in 4-6 ml 1X HBSS buffer at 37°C for 2h with rotation. A 5-ml serological pipet was used to further separate the epidermis from the dermis at the 1-h incubation time. After collagenase treatment, we added 10ml cold PBS and centrifuged the sample at 400g for 10min at 4°C. The pellet was resuspended with pre-warmed 0.25% trypsin-EDTA(Gibco) for 8min at 37°C, and the digestion was immediately blocked by adding 10ml cold 1XPBS with 3% chelated PBS. Cells were incubated with appropriate antibodies for 1h on ice. DAPI was used to exclude dead cells. Cells from K14-Cre-based experiments were isolated by enriching for $DAPI^{-}K14-H2BGFP^{+}$ epidermal cells and $DAPI^{-}K14-H2BGFP^{-}$ dermal cells.

3.4.4 Bulk RNAseq analysis

Bulk RNAseq data from Fuchs group[19](accession number GSE124901) were downloaded using SRA-toolkit(version 2.8.0) fastq-dump. The fastq files were then mapped to mouse genome(mm10) using Hisat2(version 2.1.0) with options -p 32 –rna-strandness RF to generate sam files. The samtools(version 1.3.1) were used to convert samfile to bamfile. The final counts files were generated by htseq(version 0.9.1) with options -t exon -i gene_id –stranded=reverse -f.

3.4.5 scRNAseq library preparation

Single cells from different age groups were collected from a flow cytometry-sorting machine with cell surface proteins and H2BGFP signals such that epidermal cells and hair follicle cells were at a 1:3 ratio. For each sample, around 2000 - 5000 cells were used for scRNAseq libraries. Libraries were prepared using the 10X Chromium Single Cell 3 GEM, Library Gel Bead Kit version

3 chemistry(PN-1000110). In brief, FACS-sorted cell were diluted to suggested concentration. The single cell suspension, single cell 3' gel beads and the reverse transcription mix were then incubated to generate gel beads emulsion and barcode. The resulting cDNA were pooled and amplified followed by library construction. The libraries were then quality-checked using bio-analyzer before sequencing.

3.4.6 Upstream analysis of scRNAseq data

The Cell Ranger Single-Cell Software Suite was used to perform barcode processing and single-cell gene counting on demultiplexed raw sequencing data. The scRNAseq reads were mapped to the mouse(mm10) reference genome and quantified using cellranger count(version 3.0.1). The resulting barcodes, features and matrix files were used for downstream analysis. For the velocity and directionality analysis, velocyto(version 0.17.17)[158] were used to obtain splicing-specific count data. The scRNAseq output files from Fuchs group[19] was downloaded directly through GEO(accession number GSE124901).

3.4.7 Downstream analysis of scRNAseq data

The barcods, features and matrix files were loaded into seurat(version 4.0.5) R(version 4.1.0) package[97] for further analysis. The following criteria were used to filter out low quality cells: nFeature_RNA > 200; nFeature_RNA < 5000; percent.mt < 15. The count data was log-normalized and scaled to 10,000. In addition, cell cycle regression was used to regress out addition variation from cell cycle genes. The PCA analysis was based on top 2000 variable genes. The nearest neighbors were computed based on the euclidean distance in PCA space. To cluster the cells, the Louvain algorithm was implemented. Uniform manifold approximation and projection(UMAP) was used for non-linear dimension reduction. The specific options for each step will be shared on github. To integrate all scRNAseq samples, the FindIntegrationAnchors function from seurat takes all the seurat object and identify anchor by utilize canonical correlation analysis(CCA) as initial dimension reduction. The integrated datasets were then scaled and clustered. To annotate

each clusters, the FindAllMarkers function were used to identify cluster specific marker genes. The integrated datesets were then subsetted based on cell types. For scanpy[127](version 1.7.0) analysis, the seurat object were converted to h5ad file using R packages(SeuratDisk, SeuratData). For PAGA analysis, sc.tl.paga was first used to compute the connectivity of clusters followed by sc.pl.draw_graph to get single-cell embeddings that are faithful to global topology.

For module score analysis, the differential expression gene lists from young and old HF-SC bulk RNAseq were imported in R. The young and old features include gene with basemean value greater than 600 and padj value less than 0.05. The module score were then computed using AddModuleScore function.

For trajectory analysis, the pre-clustered cells from seurate object were the converted to monocle object maintaining the UMAP information with code shared on github. The single-cell trajectory were then constructed by setting P53 samples as root and pseudotime value was calculated by ordering cells along the trajectory. The specific branch of interest was chosen by setting the root cells as P53 and ending nodes as cells on the end of the branch. To find co-regulated genes modules along specific trajectory, the find_module_df function was used with resolution as 0.0001. Aggregated gene expression from different modules were then plotted. Note, the individual genes find in different modules might not reflect the aggregated pattern.

For velocity analysis, the pre-clustered cells from seurat object was converted to scanpy keeping the UMAP information. The loom data containing splice-specific count data from velocyto(version 0.17.17)[158] was also read-in by scvelo(version 0.2.3). Custom code shared on github was used to transfer the seurat pre-analyzed information to loom object. Only the cells pass the quality control in seurat were kept for further analysis. The hair follicle lineages were then subsetted to calculate velocity and PAGA connectivity.

3.4.8 scATACseq library preparation

The single cells solution of skin cells were generated the same as scRNAseq. In total, 10,000 cells from each sample were used for scATAC-seq preparation. Libraries were prepared using the

10X Chromium Single Cell ATAC Library Gel Bead kit(PN-1000110). In brief, cell nuclei were isolated, and nuclear suspension were incubated in a transposition mix to fragment DNA and add adaptor sequence to the end of DNA fragments. Single-nucleus resolution was achieved using 10X bracoded gel beads, partitioning oil and a master mix on a Chromium Chip E. Libraries were constructed using a 10X sample index plate and double size selected from 150bp to 1000bp. The final libraries were quality-checked with bio-analyzer before sequencing.

3.4.9 Upstream analysis of scATACseq data

FASTQ files were collected from the sequencing facility and concatenated together. We used cellranger-atac (version 3.0.1) counts with the reference genome downloaded from the 10x Genomics website. The P28 sample was re-sequenced from the same library previously published and concatenated for this study. The 24months sample was re-analyzed using $cellranger - atacreanalyze$ to filter out low quality cells(scripts on github).

3.4.10 Downstream analysis of scATACseq data

The fragment file, peak file and single-cell metadata were loaded into signac[97] for downstream analysis. The peak file generated from cell-ranger was first used for quality control. The following criteria were used to filter out low quality cells: $3000 <$ peak region fragments < 100000; percentage of reads in peaks > 40; blasklist ratio < 0.025; nucleosome signal < 4; TSS enrichment > 2.

The gene activity matrix was then calculated and added to the seurat object. For integration, we first generate combined peaks containing peaks from all samples. To do this, the R1 and R3 reads file from the single cell sequencing were treated as bulk samples and then mapped to mouse reference genome and called peaks. The peaks files were then merged using bedtools[132]. The combined peaks file were then used on all samples to regenerate the matrix counts file overlapping the genomic regions. The same filtering criteria were used followed by normalization, dimension reduction and clustering. For the UMAP dimention reduction, we excluded dimention 1 suggested by signac[155].

The samples were then first merged followed by standard processing. The integration anchors were then found followed by integration.

For the integration of scRNAseq and scATACseq, the integrated scRNAseq and scATACseq were loaded in seurat. The gene activity matrix calculated from scATAC and the variable genes from scRNAseq were used to find anchors. The cell annotation label from the scRNAseq were then transferred to scATACseq. For visualization, the scRNAseq and scATACseq were co-embedded.

For the differential peaks, the annotated scATACseq data were used to find all markers based on cell types. For motif analysis, the JASPAR2020[159] and TFBSTools[160] were loaded. The motif activities were calculated by chromvar[157]. The differentiall activities were then computed by FindAllMarkers function.

3.4.11 Differential expression analysis

The counts files were calculated from the BAM alignment file by HTSeq[123]. Differentially expressed genes were determined using DEseq2[124] with an adjusted P-value cutoff of 0.05. GO analysis was performed using Metascape[125]. Selected GO terms were from Metascape results along with the gene list. For gene set enrichment analysis[161], the differential expressed genes were ranked by expression value and fold change.

Chapter 4

Transcriptional regulation of hair follicle stem cell immune privilege

4.1 Introduction

An emerging body of data indicates immune privileged sites such as adult stem cells can protect tissue structure from collateral damage caused by immune response directed against pathogens [162, 163, 164, 165].Prominent examples of immune privileged sites include the ocular anterior chamber and fetomaternal placenta [165, 166]. Studies of a wide range of immune privilege mechanisms have unraveled cell autonomous antigen presenting and non-autonomous immune cell activation[167, 168].

As the first line of defense against pathogens, the skin employs diverse and complicated immune machinery to combat both cellular and environmental attacks [169, 170]. Strikingly, hair follicles, one of the skin appendages, can escape the attack from surrounding immune cells. Immune privileged hair follicle stem cells have dynamic expression of major histocompatibility complex(MHC) [171] required for antigen presentation. More specifically, quiescent hair follicle stem cells can downregulate MHC class I and evade immune clearance[171].

However, how immune privileged stem cells regulate the antigen presenting process is largely unknown. My preliminary data indicates that the expression pattern of transcription factor *Foxc1* in hair follicle stem cells strongly correlates with immune privilege. More importantly, I observed a significant increase of immune cells surrounding hair follicle stem cells after *Foxc1* and *Nfatc1* double deletion. Consequently, *Foxc1* deletion in hair follicles also leads to a gradual loss of hair regeneration, a sign of immune privilege collapse.

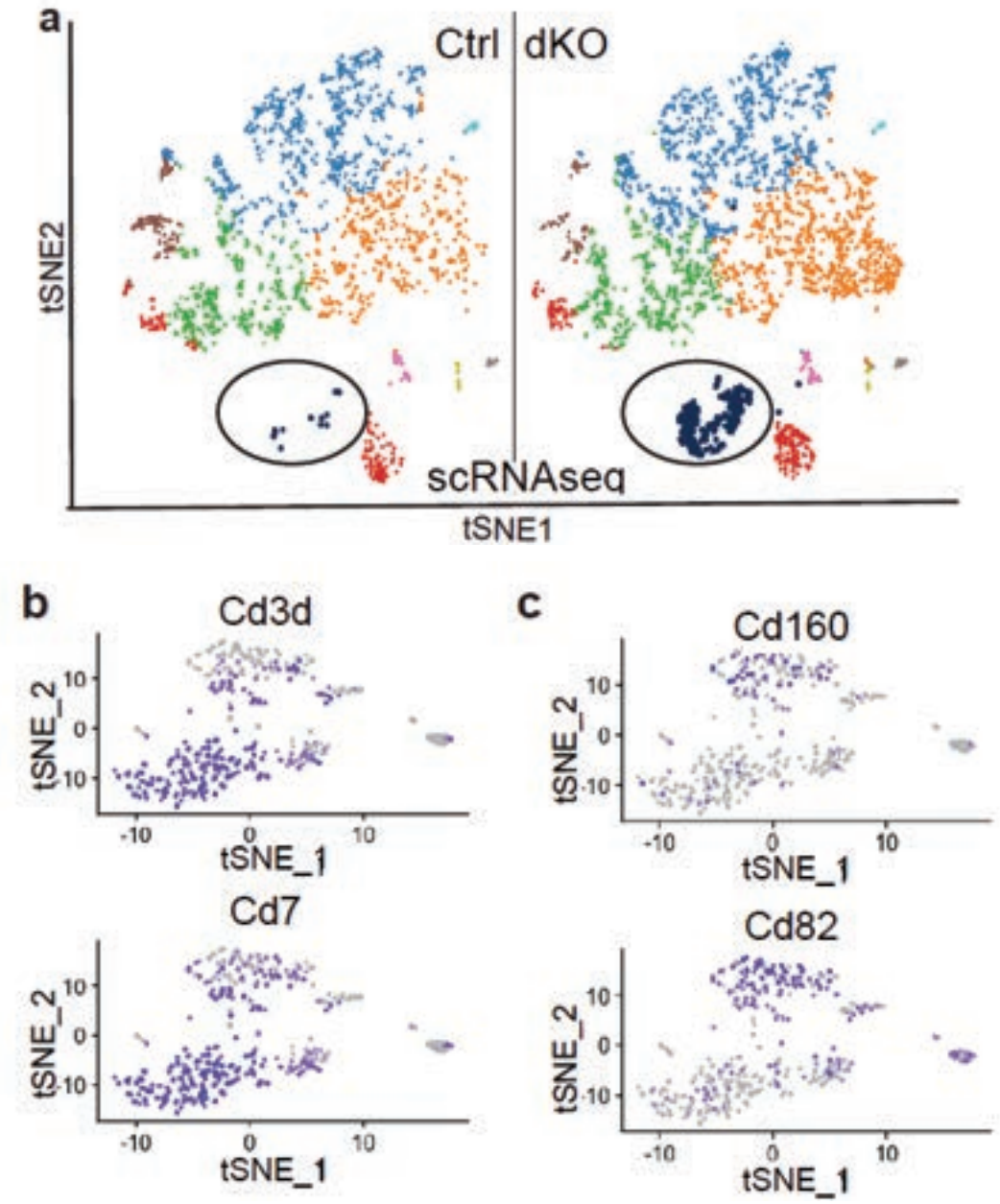

Figure 4.1: **Accumulated immune cells in dKO epidermis.** **a**, tSNE plot of P22 single cell RNAseq, circled cellls are immune cells. **b-c**, Further clustering of immune cells in dKO and marker gene plot of T cells(**b**), natural killer cells(**c**).

4.2 Results

4.2.1 Single cell RNAseq revealed unexpected immune response

Single cell techniques allowed us to the study the cross-talk among different cell populations. The single cell RNA-seq from *Foxc1* and *Nfatc1* double knockout(dKO) skin showed significant increase of immune cells(Fig4.1a). Differential gene analysis indicated that those immune cells were T cells(Fig4.1b) and natural killer cells (Fig4.1c). To further validate the immune response, I checked the localization of immune cells. Surprisingly, I found that immune cells accumulated in the hair follicle compartment. More strikingly, the immune cells can penetrate the hair follicle compartment and reside within the bulge region(Fig4.2a) in dKO.

4.2.2 Transcriptional regulation of hair follicle stem cell immune privilege

To understand the immune privilege property in hair follicle stem cells, I collected the bulk RNA-seq, single cell RNA-seq from both control, conditional knockout and double knockout hair follicle stem cells. Differential analysis indicated the increased expression of antigen presenting machinery, showed by the violin plots of marker genes expression in individual HF-SCs from scRNA-seq(Fig4.2b). To understand the direct regulation of *Foxc1* in immune privilege *in vivo*, I cloned the *Foxc1* overexpression plasmid and generated a doxycycline inducible mouse line. Upon doxycycline treatment (intraperitoneal injection), *Foxc1* can be induced in the epidermis in around 4 hours and I can directly investigate the immune environment of epidermis(Fig4.2c).

4.3 Future directions

To further investigate the direct targets of *Foxc1*, Dr. Dongmei Wang and Dr. Haimin Li from the Yi lab will perform CutRun and ChIP-seq on *Foxc1* in hair follicle stem cells. Along with the bulk ATAC-seq and single cell ATAC-seq, we will identify *Foxc1* bound regions, global chromatin landscapes and functional wiring among promoter and enhancers. They will further confirm whether the putative enhancers functionally drive gene expression in *Foxc1* dependent

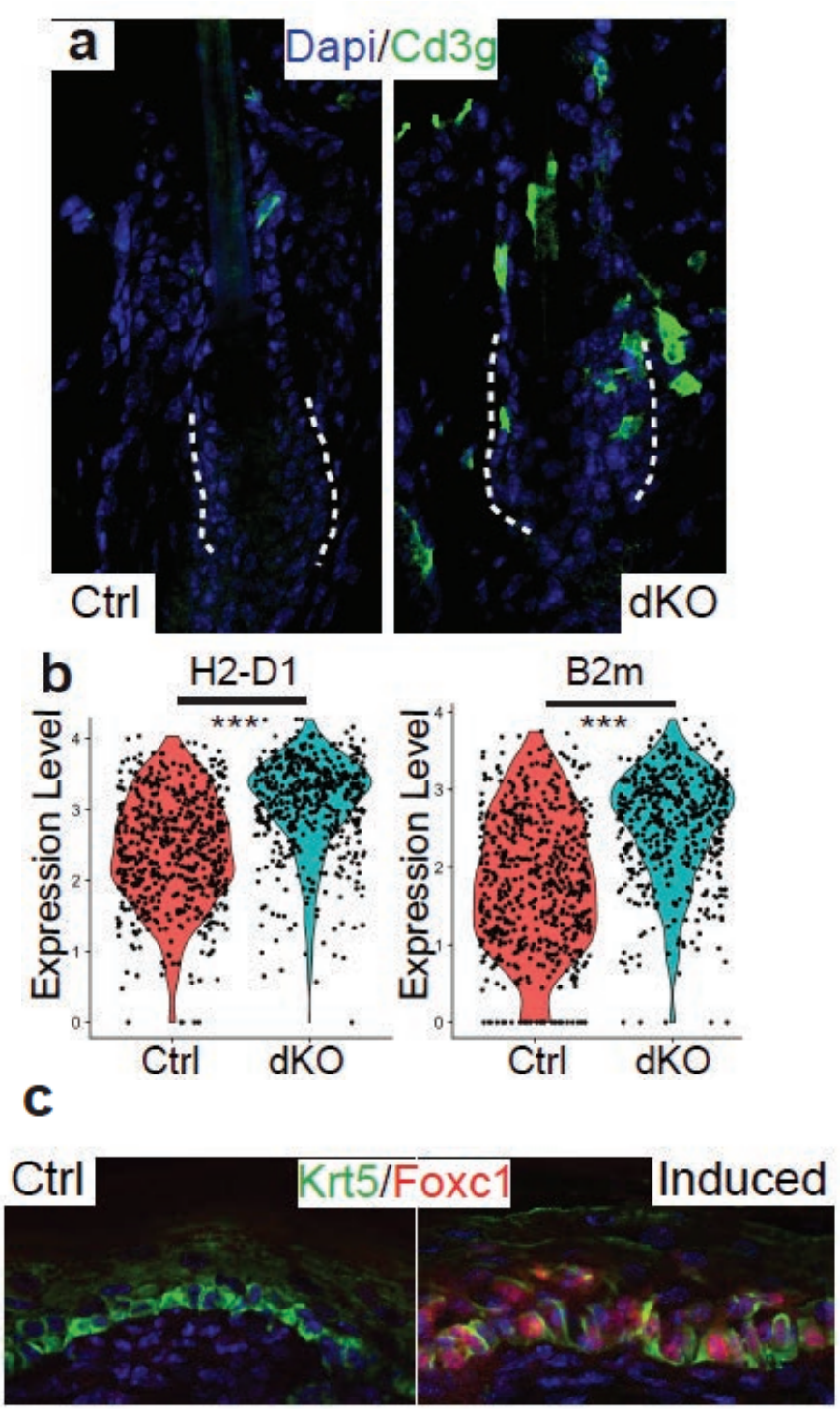

Figure 4.2: **Increased crosstalk between immune cells and HF-SCs**. **a**. Immunostaining of Cd3g positive T cells in HF-SC compartment. The dashed line labels the bulge region. **b**. Violin plot of antigen presenting genes in HF-SCs, *** padj < 0.001. **c**. Immunostaining of *Krt5* and *Foxc1* in 4-hour doxcycline induced control and *Krt14-rtTA-pTRE2-Foxc1* mice epidermis

manner using *in vitro* promoter assay and *in vivo* enhancer deletion by CRISPR-Cas9. These techniques are well-established in the Yi lab. Finally, coculture of immune cells and hair follicle stem cells can help determine whether *Foxc1* expression can affect the survival of hair follicle stem cells against immune cell attack.

In addition, we collaborated with professor Jordan Jacobelli at Department of Immunology and Microbiology at the University of Colorado School of Medicine. Together, we set up the breeding of immune cell RFP reporter line with both the knockout and inducible mouse line. This will allow us confidently validate the functional role of *Foxc1* in hair follicle stem cell immune privilege in vivo by multi-photon imaging.

4.4 Methods

4.4.1 Construction of Foxc1 plasmid

To clone the Foxc1 overexpression plasmid, the mouse tail in lysis buffer was heated at 95°C in PCR machine for 10min to release the genomic DNA. Since Foxc1 gene has no intron, I directly cloned it from the genome. The following primers were used: Foxc1_BamH1_F: agcGGATCCatgcaggcgcgctactcg Foxc1_XbaI_R: acctTCTAGAtcagaatttgctacagtc. The PCR products were digested with BamHI and XbaI enzymes along with the pTRE2 plasmid. The fragments were then ligated before sending out for sequencing.

4.4.2 Transgenic mouse line generation

To generate the pTRE2-Foxc1 transgenic mouse line, the pTRE2-Foxc1 plasmid were digested to generate the full length Foxc1 and Tet operator sequence. The digested fragments were then purified by QIAEX II Gel Extraction Kit and eluded into micro-injection buffer. The following procedures were performed by CU Boulder MCDB transgenic facility. Briefly, the super-ovulated female mice were breed with stud mice to generate donor zygotes. The DNA fragments were then injected into the zygotes before implanted into pseudo-pregnant recipient mice. After the pups were

born, the tails were used for genotyping to maintain founder generations. The primer sequence for genotyping are as follows: F: CGCCTGGAGACGCCATCCACGCT R: AGGTTGTGCCGTATGCTGTTC

Chapter 5

Transcription and degradation dynamics in Down syndrome

For the remaining chapter, I described some preliminary work I conducted in the Dowell lab independent from my previous studies on mouse epidermis.

5.1 Introduction

Down syndrome(DS) is the most common chromosomal condition, approximately 5000 births annually in US[172, 173], caused by an extra copy of Homo sapiens chromosome 21(HSA21). Individuals with DS demonstrate higher rate of numerous health conditions compared to typical population, including dementia, leukemia, Type 1 diabetes and congenital heart disease[174, 175, 176, 177, 178]. The additional chromosome with more than 200 protein coding genes has been the central focus on most research for the understanding of DS[174, 175, 176, 179, 180, 181]. It has been hypothesized that genes on HSA21 are overexpressed approximately 1.5 fold compared to the euploid state[182, 183, 184, 185], however, this is based on the simplest model of gene regulation on pooled RNAs. Indeed, in the case of Down syndrome, many genes on chromosome 21 are expressed at a range of values less than 1.5 folds[174, 175, 178, 186, 187], suggesting more complex patterns of regulatory circuits[174, 176]. For example, trisomy21 leads to constitutive activation of the interferon response, in a number of cell lines, by way of the increased expression of four interferon receptors encoded on HSA21[188]. A dosage-imbalance in even a small number of genes could be amplified to produce large downstream effects, perturbing the transcriptome of every cell[189]. This necessitates the transcriptome-wide study of gene dosage differences between trisomy 21 and disomy

cells. Indeed, there have been a number of different techniques used to probe transcriptome-wide differences including microarrays[179, 181, 186], total RNA sequencing[175, 188, 190, 191, 192, 193], nuclear RNA sequencing[187], and single-cell RNA sequencing[194]. Additionally, there have been more targeted efforts using ChIP for HSA21 proteins[186], qPCR[182], and SLAM-seq[186, 195]. Collectively these efforts have sought to elucidate the underlying molecular basis of the different phenotypes of Down syndrome[178]. Nevertheless, evidence for the gene specific dosage regulation is still missing.

Transcription of DNA into RNA and the subsequent RNA degradation are the two key steps of gene expression that determine the gene dosage in living cells. The equilibrium between transcription and degradation regulates the amount of RNA available for cellular machinery. Thus, the rate of degradation is equally important as transcription[196, 197, 198, 199, 200, 201, 202, 203]. Most of the efforts to date have focused on the transcriptional dynamics which can be directly measured by nascent RNA sequencing assays[204, 205, 206], while ignoring the differences in degradation rate. A number of sequence-based methods for inferring degradation rates are reported, but these methods are only applicable to steady-state cellular conditions[197, 207]. Therefore, they cannot be applied to cellular perturbation with active changes in cellular transcription and degradation.

In this study, we developed a new approach based on two widely applicable experiments PRO-seq and RNAseq to measure the transcription and degradation rates during dynamic cellular processes including interferon response and cellular differentiation process. The techniques will be applied to both euploid and trisomy cells to uncover whether trisomy specific alterations in RNA degradation exist. Thus, this work will provide a more complete picture of the transcriptional dysregulation inherent to Down syndrome. In addition, we used TimeLapse-seq as an independent method to further validate the RNA transcription and degradation rate. Our approach could potentially be extended to any other dynamic biological process.

5.2 Results

5.2.1 Estimation of RNA degradation rate using both RNA-seq and PRO-seq

To investigate the RNA dynamics, we first study the steady-state RNA concentration under equilibrium state. The following discussion follows roughly the model described by Blumberg et. al[197]. The total number of RNA molecules would be the total number of molecules produced minus the number of molecules that have been degraded. Production can be measured by transcription assay (PRO-seq) and the degradation rate should be proportional to the total RNA molecules. Briefly, if X(transcripts/cell) is the total RNA molecules concentration of a given gene, β(transcripts/time*cell) is the transcription rate, and α(1/time) represents the degradation rate, then the following equation models the dynamics of gene specific concentrations(Eq.5.1)[201, 197].

$$\frac{\mathrm{d}X}{\mathrm{d}t} = \beta - \alpha X \tag{5.1}$$

Admittedly, this model assumes the total degradation rate is directly proportional to the RNA concentration and the total production rate is constant. Furthermore, at equilibrium, the changes of RNA concentration should be zero. The degradation rate can then be directly calculated by knowing β and X.

However, in the non-steady state, the assumptions of this model are no longer valid as the production and degradation rate could be changing over time. To circumvent this, Dr. Jacob Stanley, a postdoctoral scholar in the Dowell lab, proposed to take a discrete, linear estimation based approach, using two time points separated by an interval Δt(Eq.5.2).

$$\frac{X_{t+1} - X_t}{\Delta t} = \frac{\beta_{t+1} + \beta_t}{2} - \alpha \frac{X_{t+1} + X_t}{2}$$

(5.2)

In this case, the changes in transcription can be estimated by the nascent sequencing(PRO-seq or uPRO) and changes in total RNA can be estimated by total RNA sequencing(Eq.5.2.1).

$$X \propto R(RNAseq)$$

$$\beta \propto P(PROseq)$$

$$\frac{R_{t+1} - R_t}{\Delta t} \propto \frac{P_{t+1} + P_t}{2} - \alpha \frac{R_{t+1} + R_t}{2}$$

The time-dependent degradation rate can then be estimated as follows 5.3:

$$\alpha(t) \propto \frac{2(R_{t+1} - R_t) - \Delta t(P_{t+1} + P_t)}{\Delta t(R_{t+1} + R_t)} = \frac{\Delta R - \bar{P}(t)\Delta t}{\bar{R}\Delta t} \tag{5.3}$$

Where $\bar{R}$ and $\bar{P}$ are the average RNA-seq and PRO-seq values over the time points Δt, and ΔR is the difference in gene expression values. Note for this to work, we need at least two time points and the Δt needs to be within reasonable gap. This proposed model allows us to monitor both the transcription and degradation rates at the same time during a dynamic cellular process.

5.2.2 Estimate RNA degradation rate using TimeLapse-seq

To further validate the RNA transcription and degradation rates measurements proposed, we sought out to apply TimeLapse-seq to the same time points[207]. We modify the TimeLapse protocol by using a pulse-chase strategy by labeling the cells with 4-Thiouridine(4-SU) for an amount of time before washing it out and collecting samples at specific time points afterwards, tracking the labeled transcripts as they undergo degradation. This allows us a more measurement based approach to estimate the degradation rate under dynamic cellular process.

To examine the dynamics of celluar RNAs, we treated disomy and trisomy cells with 100μM 4-SU to label the nascent mRNAs for 4 hours followed by wash out. The samples were then directly collected or left in fresh medium for additional 1 hour for the chase analysis. The extracted RNAs were then chemically converted before sending out for sequencing. In addition, I also downloaded

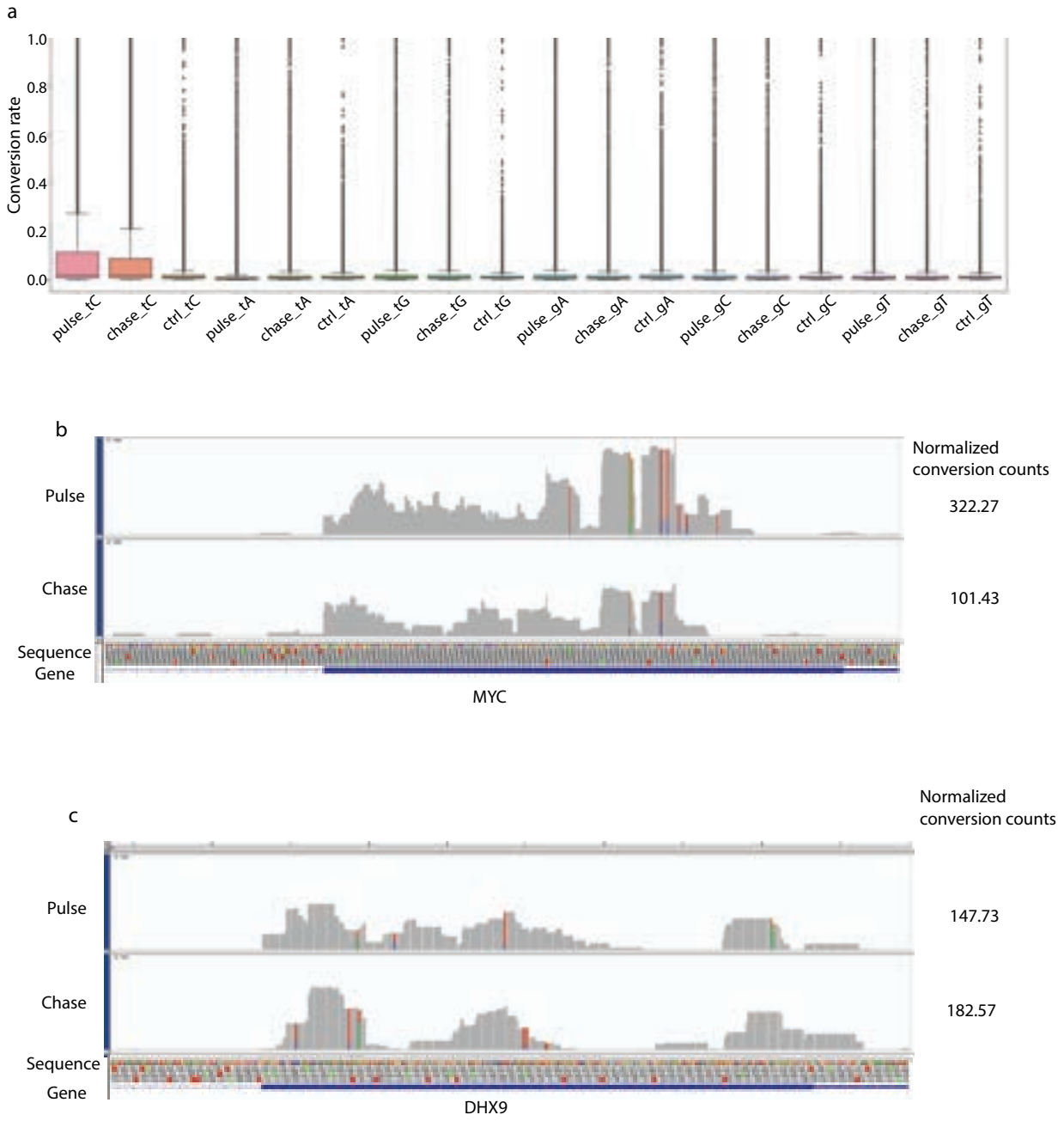

Figure 5.1: **Chemical conversions of TimeLapse libraries**. **a**. The conversion rate of different possible conversions. Lowercase represents original nucleotide, the uppercase represents the converted nucleotide. **b,c**. The representative tracks of MYC and DHX9 genes.

the RNAseq data from the original TimeLapse methods paper for comparison[207]. To validate the chemical labeling and conversion, I first counted the mutations in each aligned read pair on all samples. Indeed, samples with pulse and chase showed specific and reproducible increases in T-to-C conversions(Fig5.1a). Reassuringly, the mapped bam files also showed enriched T-to-C conversions indicated by specific coloring in high turnover genes(Fig5.1b). To compare the number of conversions per gene, I first counted the total number of conversions within the gene body and then normalized by the sequence depth and RNA composition using DESeq2[124]. Indeed, the *MYC* gene is undergoing rapid transcription and degradation indicated by the high conversion at pulse samples and drastically low conversions at chase samples. In contrast, the low turnover gene *DHX9* showed relatively stable conversions between pulse and chase samples(Fig5.1c).

To estimate the gene-specific transcription rate, we modeled the total T-to-C conversion per read as a combination of background mutations and chemically converted mutations[207]. We proposed two different models: Poisson mixture model and a zero-inflated Poisson model. For both models, the number of conversions were calculated on each read and grouped by the genes they mapped onto.

For the Poisson mixture model, the probability mass function of the unmber of conversion per read is as follows 5.4[207]:

$$P(y|\theta_n, \lambda_n, \lambda_o) = \theta_n \text{Poisson}(y; \lambda_n) + (1 - \theta_n)\text{Poisson}(y; \lambda_o) \tag{5.4}$$

where θ_n is the transcription rate(the fraction of new transcripts over all transcripts), λ_n is the rate of conversions in newly labeled transcripts, λ_o is the rate of conversions in non-labeled transcripts(background conversion rate).

For the zero-inflated Poisson model, the probability mass function is

$$P(y|\theta_n, \lambda_n) = (1 - \theta_n)\delta(y) + \theta_n \text{Poisson}(y; \lambda_n)$$

$$\delta(y) = \begin{cases} 1 & \text{if } y = 0 \\ 0 & \text{else.} \end{cases}$$

where θ_n is still the transcription rate, λ_n is the conversion rate of newly labeled transcripts, $\delta(y)$ is the indicator function to describe whether the T-to-C conversion is zero in reads.

To estimate the gene specific parameters, we applied a Bayesian hierarchical modeling approach using PyMC3(version 3.11.4)[208] followed by Monte Carlo sampling to generate the posteriors. For the Poission mixture model, λ_n was given weakly informative priors with half normal distributions. λ_o was an given exponential prior, due to the low background conversion rate. For θ_n, we used a Dirichlet prior for the weights on the two Poisson components. For the zero inflated Poisson, the λ_n is given the same half normal distribution, while the θ_n is given a Beta distribution as a prior.

I firstly tested the model on the high turn-over gene *MYC* and the low turn-over gene *ACTB*. In addition, simulated data and published data were used as a positive control. Note that the distribution of number of conversions per read was relatively lower in our datasets compared to public data(Fig5.2a).

To assess the models, I simulated data with similar distribution and continued with all samples. For the simulated data, only the zero-inflated model successfully predicted the transcription rate(true value 0.35 vs estimated 0.37) along with the associated conversion rate(true value 0.1 vs estimated 0.11)(Fig5.2b). This suggests the zero inflated model better handles the sparse nature of the data. As for the *MYC* and *ACTB* in our dataset, both of the models mentioned above failed to converge. To validate the applicability of the models, I further tested them on the published datasets[207]. Interestingly, both models converged on the high turnover gene and stable genes(Fig5.2c,d). For the high turnover gene *MYC*, both models converged on comparable conversion and transcription rates(Fig5.2c). However, for the low turnover gene *ACTB*, even though both models converged, their estimation differed drastically(Fig5.2d). The discrepancies among the estimated transcription rate will need further validation. Our further analysis indicated the low number of conversions per read obtained in our datasets was problematic and potentially arose due to the shorter read length of sequencing. In this scenario, even the zero inflated model failed

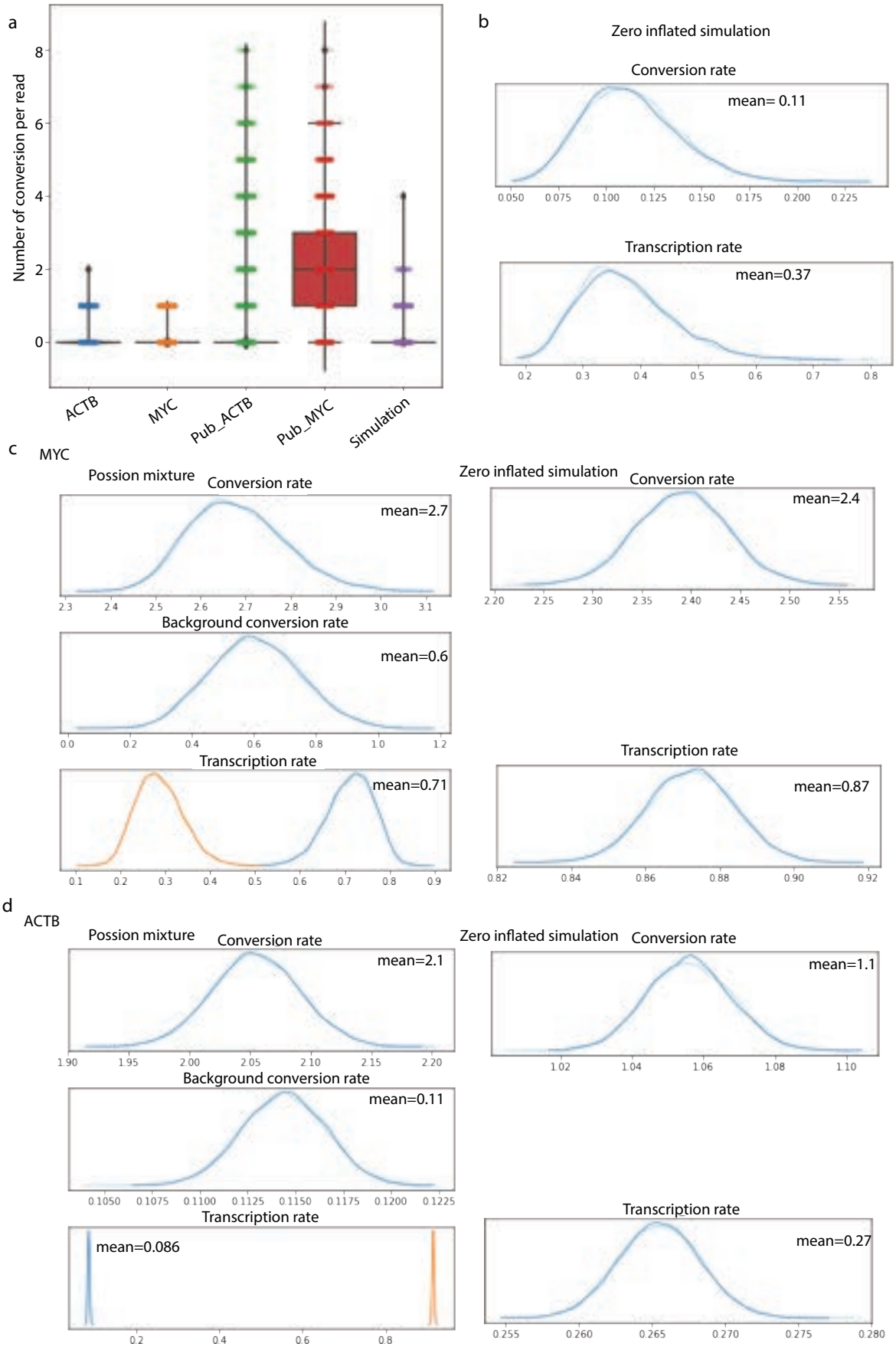
a
Number of conversion per read
ACTB
MYC
Pub_ACTB
Pub_MYC
Simulation
b
Zero inflated simulation
Conversion rate
mean= 0.11
Transcription rate
mean=0.37
c
MYC
Possion mixture
Conversion rate
mean=2.7
Background conversion rate
mean=0.6
Transcription rate
mean=0.71
Zero inflated simulation
Conversion rate
mean=2.4
Transcription rate
mean=0.87
d
ACTB
Possion mixture
Conversion rate
mean=2.1
Background conversion rate
mean=0.11
Transcription rate
mean=0.086
Zero inflated simulation
Conversion rate
mean=1.1
Transcription rate
mean=0.27

Figure 5.2: **Inference of transcription rate**. **a**. Boxplot of number of conversions per read in all samples and simulated data. **b**. The posterior plot of simulated data based on zero inflated possion model. The simulated conversion rate mean is 0.11 versus true value 0.1, the transcription rate mean is 0.37 versus 0.35. **c,d**. Transcription rate and conversion rate inference of MYC(**c** and $ACTB$(**d**) by possion mixture model and zero inflated poisson model

to resolve the chemical induced conversions from the background conversions.

5.3 Future directions

Since our datesets have an inherently low conversion number per read, both our models failed to estimate the transcription rate. This is due to the conversion chemistry used fail to induce a high number of conversions and our read length is shorter compared to that of the published methods[207].Our next immediate goal is to optimize the pulse-chase conditions including the treatment time and concentration. Finally, we will perform the time-series sample preparation after β-interferon perturbation for further degradation rate analysis.

For RNA-seq/PRO-seq sample preparation, Sam Hunter is working on generating both libraries on matched cells after perturbations. Along with Dr. Jacob Stanley, we will work together to estimate the transcription and degradation rate with the newly proposed model.

We are interested in the transcription and degradation dynamics between trisomy and disomy cells under steady state and cellular perturbations. We will be able to dissect out different patterns of degradation and systematically ask whether the transcription rate or transcription elongation could affect the degradation[209]. More importantly, we will identify the dysregulated genes in DS cells under steady state and perturbation, which will give insights in counter-measures in the future.

5.4 Methods

5.4.1 Human samples

The gender and age matched trisomy and disomy cell were immortalized lymphoblastoid cells lines with Epstein-Barr Virus(EBV). Cells were cultured in T12.5 tissue culture flasks with culture medium containing RPMI 1640, 2mM L-glutamine and 20% fetal bovin serum. The cells grow in suspension and split by 1:2 every two days by gentle trituration with pipette.

5.4.2 Proseq and RNAseq

Cells were collected in Falcon tubes and washed three times with ice-cold PBS followed by incubation on ice in 10 mL ice-cold Lysis Buffer (10 mM Tris-HCl pH 7.5, 2 mM MgCl2, 3 mM CaCl2, 0.5% IGEPAL, 10% Glycerol, 2 U/mL SUPERase-IN) for 10 minutes. Cells were then transferred into 50 mL Falcon tubes and centrifuged with a fixed-angle rotor at 1000 x g for 10 minutes at 4°C. The buffers containing the cytoplasmic RNAs were kept for RNA-seq preparation. The cell pellets were resuspend with lysis buffer and washed twice. After the second wash, cells were resuspended with 1 mL Freezing Buffer (50 mM Tris-HCl pH 8.3, 5 mM MgCl2, 40% Glycerol, 0.1 mM EDTA pH 8.0). The resulting nuclei were centrifuged at 1000 x g for 5 minutes at 4°C, and resuspended again with 500 µL Freezing Buffer. For the final step, the nuclei were centrifuged for 2 minutes at 2000 x g, 4°C, and resuspended in 110 µL Freezing Buffer. 10 µL was retained for counting nuclei, while the remaining sample was snap-frozen in liquid nitrogen and stored at -80°C until use.

PRO-seq preparation were adapted from[210]. In brief, isolated nuclei were added to 37°C 100 μL reaction buffer (5 mM Tris-Cl pH 8.0, 2.5 mM MgCl2, 0.5 mM DTT, 150 mM KCl, 10 units of SUPERase In, 0.5% sarkosyl, 125 μM rATP, 125 μM rGTP, 125 μM rUTP, 25 μM biotin11-CTP). The run-on reaction continued for 5 min at 37°C. The RNA was extracted twice with Trizol, washed once with chloroform, and precipitated with 3 volumes of ice-cold ethanol and 1-2 µL GlycoBlue. The final RNA pellet was washed in 75% ethanol before resuspending in 20 µL of DEPC-treated

water. Nascent RNA was extracted and fragmented by base hydrolysis in 0.2 N NaOH on ice for 10–12 min, and neutralized by adding a 1× volume of 1 M Tris-HCl pH 6.8. Fragmented nascent RNA was purified and enriched using streptavidin beads. The resulting RNAs were end-repaired and ligated to adaptors followed by reverse transcription. The resulting cDNA was amplified size selected with 1X AMPure XP beads (Beckman) before being sequenced.

5.4.3 TimeLapse-seq library prep

The TimeLapse-seq protocol was adapted from[207]. In brief, cells were treated with 4-SU at 37°C for 4hrs before collection. Wash the cell pellet in ice-cold 1X PBS and proceeded immediately to RNA isolation following Qiagen RNeasy Mini kit. For each reaction, 2μg of RNAs were diluted in 8.7μL DEPC-treated water and mixed with mastermix containing: 0.84μL 3M sodium acetate, pH 5.2; 12.7 μL DEPC-treated water; 0.2 μL 0.5M EDTA, pH 8 and 1.3 μL TFEA on ice. The freshly made 1.3μL $NaIO_4$(10μM in DEPC water) were then added in the reactions followed by 1hr of incubation at 45°C in a pre-heated PCR machine. After the incubation, the samples were cooled to 4°C followed by RNAClean beads purification. The RNAs were then reduced by mixing with 2μL 10X reducing master mix(10 μL 1 M Tris-HCl, pH 7.4; 10 μL 1 M DTT; 20 μL 5 M NaCl; 2 μL 0.5 M EDTA, pH 8; 58 μL DEPC-treated water). The RNAs were again purified using RNAClean beads and quality-checked with bioanalyzer followed by RNA-seq library preparation using SMARTer Stranded Total RNA-Seq Kit-Pico Input Mammalian.

5.4.4 TimeLapse-seq data analysis

The fastq files were first trimmed by using bbduk(version 38.05). The resulting files were then mapped to the GRCh38/hg38 reference genome using Hisat(version 2.1.0) with parameters '–mp 4,2' to allow for mismatched induced by chemical conversions. The resulting SAM files were converted to BAM files followed by sorting and index by samtools(version 1.3.1).

To identify the position and the number of conversions across the genome, I first found the aligned reads pairs from the BAM files. The genomic positions with mutations containing

12(aC, aG, aT, gA, gC, gT, cA, cG, cT, tC, tA, tG) possible conversions were all recorded and the BAM files were further tagged with corresponding names. After re-indexing the tagged BAM files, the genomic locations of specific conversion were then fetched by the tag information just added. The number of conversions and the read coverage at the specific positions were then counted for conversion rate calculation. The source code for the analysis will be available on Github.

Chapter 6

Discussion

In my graduate work, I studied the dynamics of cellular behaviors and transcriptional regulation of tissue stem cells during physiological aging. Advances in intravital imaging allows me to directly visualize the hair follicle stem cell behavior in live animals[17, 94]. In addition, single cell genomics make it possible to examine not only the transcriptional profile but also the epigenetic landscape of individual cell[211, 212, 213]. Combining those tools, we uncovered new concepts of hair follicle and tissue stem cell aging. For hair follicle stem cells, multiple transcription factors including *Foxc1*, *Nfatc1* and possibly *Klf4* govern the proper maintenance of extracellular matrix and basement membrane. Genetic deletion of *Foxc1* and *Nfatc1* in hair follicle stem cells leads to precocious aging phenotype with progressive hair follicle miniaturization and hair loss. Surprisingly, we found that even the cells within miniaturized hair follicles are not in a senescent state, demonstrated by active cell divisions. More importantly, some epithelial cells, marked by *Krt14* promoter driven H2bGFP, are scattered in the dermis, and their appearance precedes the hair follicle miniaturization. Furthermore, time-lapse movies captured the cell escape in *Foxc1* and *Nfatc1* deletion hair follicles. To the best of my knowledge, this is the first report that directly visualizes the stem cell escape in live animals. Additional epigenetic analysis indicates that transcription factor *Klf4* may also play a role in governing stem cell aging. Indeed, existing genetic deletion and over-expression analysis both demonstrated that *Klf4* can help maintain epidermis barrier function[214, 215]. My study thus revealed unexpected stem cell escape during hair follicle aging, leading to the hair follicle miniaturization. For the remaining hair follicle stem cells, transcrip-

tomic analysis reveals that these aging stem cells down-regulate aging induced metabolic stresses, including reactive oxygen species and oxidative phosphorylation. In addition, by engrafting hair follicle stem cells from old mice to young dermis, other independent studies demonstrated that the exposure to young environment can rejuvenate stem cell functions. Such functional assay provided tantalizing evidence that aging stem cells still maintain stem cell function. When given proper stimulation they can still regenerate hair follicles as robustly as young stem cells. Combining with our analysis, these data suggest that hair follicle stem cells are rather resilient in maintaining its function, but proper extracellular matrix environment is needed to maintain the integrity of the stem cell compartment.

For other epithelial lineages, the permanent sections, including upper hair follicle lineages, do not present aging induced changes at the transcriptomic level. The niche cells, on the other hand, show strong and continuous accumulation of metabolic stress. These stresses may lead to or reflect the reduction of cell numbers and hair follicle miniaturization. Based on the transcriptomic profiling, these Niche cells are a differentiated cell population in hair follicles. Upon the completion of each hair cycle, a new group of niche cells is formed. I identified a spatially and transcriptomically distinct cell lineage, named migNiche, that migrates with the hair shaft, moves upward to the new bulge area and transitions into the Niche cells at the end of catagen during each hair cycle. The transition is accompanied by the expression of transcription factors such as *Myc* and establishment of apical-basal polarity. Because the terminally differentiated Niche cells are repopulated after each hair cycle. This suggests that a new hair cycle is needed to repopulate these Niche cells. However, the increasing number of hair cycles inevitably leads to metabolic stress on stem cells. But if the stem cells can reduce its metabolic stress during aging, we can draw a completely different hypothesis of hair follicle aging. That is, the hair cycle helps keep the hair follicle from miniaturization and therefore aging. Firstly, a new hair cycle can repopulate the Niche cells. Secondly, the hair cycle can induce the expression of *Foxc1* in hair follicle stem cells. Previous study also showed Foxc1 can upregulate *Nfatc1* expression[23]. Thus, the hair cycle mediated upregulation of *Foxc1* and Nfatc1 can help maintain the proper extracellular matrix. With the

robust extracellular matrix and basement membrane, this will keep hair follicle stem cells from escaping the microenvironment. Thus, more frequent activation of hair follicle stem cells has the potential to rejuvenate not only hair follicle stem cells but also their microenvironment. This hair follicle aging theory can potentially provide new perspective to stem cell research and aging. reshape our understanding of stem cell research.

Tissue stem cells are also subject to immune surveillance, and increased immune response in hair follicles could lead to hair follicle miniaturization. Our preliminary study, along with independent reports, indicates that hair follicle stem cells can repress the expression of antigen presenting genes such that immune cells won't be able to recognize them[23, 171]. The *Foxc1* deletion leads to accumulated immune cells within stem cell compartment. Our transgenic mouse model with *Foxc1* induction in epithelial cells could be used to understand the intrinsic regulation network of immune privilege. Recent studies showed cancer stem cells can hide from the immune system and evade immunosurveillance[171]. Understanding the regulation of immune privilege can help modulate immune recognition to target cancer cells or to protect normal stem cells.

These *in vivo* analyses were informative and critical for functional analysis, however, it lacks the resolution for temporal changes. To gain deeper understanding of dynamic transcription and degradation among perturbations, we applied recently developed PROseq/RNAseq/Timelapse-seq approaches to systematically analyze the transcription and degradation rate under perturbation[207, 204, 205, 206]. The time series analysis together with statistical modeling will delineate the gene transcription and degradation changes, which are difficult to infer from traditional bulk RNA-seq methods. This detailed analysis will help to identify early response genes mediated by both transcription and degradation. Successfully implementing this approach will provide an powerful analysis pipeline for transcriptional dysregulation in any biological questions of interests.

Taken together, my PhD studies provide new insights into stem cell biology, cancer biology and aging research. The escaped epithelial cells in the dermis likely do not undergo profound cell fate changes such as epithelial-to-mesenchymal transition judging by the morphology[216]. These epithelial cells also persist in the dermis rather than immediately initiating programmed cell death.

These observations raise important questions such as whether these escaped cells can self-renew or divide in the dermis, how they interact with foreign environment including dermal fibroblast cells, adipocytes and immune cells and whether those escaped cells play any role in tumorgenesis during aging. These questions warrant future investigation of the fate of escaped cells in normal and pathological conditions.

Bibliography

[1] Jim Oeppen and James W Vaupel. Broken limits to life expectancy, 2002.

[2] Xiao Dong, Brandon Milholland, and Jan Vijg. Evidence for a limit to human lifespan. Nature, 538(7624):257–259, 2016.

[3] Maarten P Rozing, Thomas BL Kirkwood, and Rudi GJ Westendorp. Is there evidence for a limit to human lifespan? Nature, 546(7660):E11–E12, 2017.

[4] Nicholas JL Brown, Casper J Albers, and Stuart J Ritchie. Contesting the evidence for limited human lifespan. Nature, 546(7660):E6–E7, 2017.

[5] Adam Lenart and James W Vaupel. Questionable evidence for a limit to human lifespan. Nature, 546(7660):E13–E14, 2017.

[6] Stein Emil Vollset, Emily Goren, Chun-Wei Yuan, Jackie Cao, Amanda E Smith, Thomas Hsiao, Catherine Bisignano, Gulrez S Azhar, Emma Castro, Julian Chalek, et al. Fertility, mortality, migration, and population scenarios for 195 countries and territories from 2017 to 2100: a forecasting analysis for the global burden of disease study. The Lancet, 396(10258):1285–1306, 2020.

[7] Linda Partridge, Joris Deelen, and P Eline Slagboom. Facing up to the global challenges of ageing. Nature, 561(7721):45–56, 2018.

[8] Eileen M Crimmins. Lifespan and healthspan: past, present, and promise. The Gerontologist, 55(6):901–911, 2015.

[9] Shi Huang-Ti. Shi huangdi (qin shi huangdi. Lifelines in World History: The Ancient World, The Medieval World, The Early Modern World, The Modern World, page 93, 2015.

[10] Judith Campisi, Pankaj Kapahi, Gordon J Lithgow, Simon Melov, John C Newman, and Eric Verdin. From discoveries in ageing research to therapeutics for healthy ageing. Nature, 571(7764):183–192, 2019.

[11] Carlos López-Otín, Maria A Blasco, Linda Partridge, Manuel Serrano, and Guido Kroemer. The hallmarks of aging. Cell, 153(6):1194–1217, 2013.

[12] Alexandra M Nicaise, Cory M Willis, Stephen J Crocker, and Stefano Pluchino. Stem cells of the aging brain. Frontiers in Aging Neuroscience, 12, 2020.

[13] Gerald de Haan and Seka Simone Lazare. Aging of hematopoietic stem cells. Blood, The Journal of the American Society of Hematology, 131(5):479–487, 2018.

[14] Ara B Hwang and Andrew S Brack. Muscle stem cells and aging. Current topics in developmental biology, 126:299–322, 2018.

[15] Brice E Keyes and Elaine Fuchs. Stem cells: Aging and transcriptional fingerprints. Journal of Cell Biology, 217(1):79–92, 2018.

[16] Enrico Dall'Ara, Maya Boudiffa, Caroline Taylor, David Schug, Eva Fiegle, Aneurin J Kennerley, C Damianou, Gillian M Tozer, Fabian Kiessling, and Ralph Müller. Longitudinal imaging of the ageing mouse. Mechanisms of ageing and development, 160:93–116, 2016.

[17] Mikael J Pittet and Ralph Weissleder. Intravital imaging. Cell, 147(5):983–991, 2011.

[18] Maria Carolina Florian, Kalpana J Nattamai, Karin Dörr, Gina Marka, Bettina Überle, Virag Vas, Christina Eckl, Immanuel Andrä, Matthias Schiemann, Robert AJ Oostendorp, et al. A canonical to non-canonical wnt signalling switch in haematopoietic stem-cell ageing. Nature, 503(7476):392–396, 2013.

[19] Yejing Ge, Yuxuan Miao, Shiri Gur-Cohen, Nicholas Gomez, Hanseul Yang, Maria Nikolova, Lisa Polak, Yang Hu, Akanksha Verma, Olivier Elemento, et al. The aging skin microenvironment dictates stem cell behavior. Proceedings of the National Academy of Sciences, 117(10):5339–5350, 2020.

[20] Kenneth Lay, Tsutomu Kume, and Elaine Fuchs. Foxc1 maintains the hair follicle stem cell niche and governs stem cell quiescence to preserve long-term tissue-regenerating potential. Proceedings of the National Academy of Sciences, 113(11):E1506–E1515, 2016.

[21] Hiroyuki Matsumura, Yasuaki Mohri, Nguyen Thanh Binh, Hironobu Morinaga, Makoto Fukuda, Mayumi Ito, Sotaro Kurata, Jan Hoeijmakers, and Emi K Nishimura. Hair follicle aging is driven by transepidermal elimination of stem cells via col17a1 proteolysis. Science, 351(6273), 2016.

[22] Manisha Sinha, Young C Jang, Juhyun Oh, Danika Khong, Elizabeth Y Wu, Rohan Manohar, Christine Miller, Samuel G Regalado, Francesco S Loffredo, James R Pancoast, et al. Restoring systemic gdf11 levels reverses age-related dysfunction in mouse skeletal muscle. Science, 344(6184):649–652, 2014.

[23] Li Wang, Julie A Siegenthaler, Robin D Dowell, and Rui Yi. Foxc1 reinforces quiescence in self-renewing hair follicle stem cells. Science, 351(6273):613–617, 2016.

[24] Derrick J Rossi, David Bryder, Jun Seita, Andre Nussenzweig, Jan Hoeijmakers, and Irving L Weissman. Deficiencies in dna damage repair limit the function of haematopoietic stem cells with age. Nature, 447(7145):725–729, 2007.

[25] Tom H Cheung and Thomas A Rando. Molecular regulation of stem cell quiescence. Nature reviews Molecular cell biology, 14(6):329–340, 2013.

[26] Inchul J Cho, Prudence PokWai Lui, Jana Obajdin, Federica Riccio, Wladislaw Stroukov, Thea Louise Willis, Francesca Spagnoli, and Fiona M Watt. Mechanisms, hallmarks, and implications of stem cell quiescence. Stem cell reports, 12(6):1190–1200, 2019.

[27] Ayako Nakamura-Ishizu, Hitoshi Takizawa, and Toshio Suda. The analysis, roles and regulation of quiescence in hematopoietic stem cells. Development, 141(24):4656–4666, 2014.

[28] Tao Cheng, Neil Rodrigues, Hongmei Shen, Yong-guang Yang, David Dombkowski, Megan Sykes, and David T Scadden. Hematopoietic stem cell quiescence maintained by p21cip1/waf1. Science, 287(5459):1804–1808, 2000.

[29] Joe V Chakkalakal, Kieran M Jones, M Albert Basson, and Andrew S Brack. The aged niche disrupts muscle stem cell quiescence. Nature, 490(7420):355–360, 2012.

[30] Cristian Tomasetti and Bert Vogelstein. Variation in cancer risk among tissues can be explained by the number of stem cell divisions. Science, 347(6217):78–81, 2015.

[31] Elaine Fuchs. Epithelial skin biology: three decades of developmental biology, a hundred questions answered and a thousand new ones to address. Current topics in developmental biology, 116:357–374, 2016.

[32] Cédric Blanpain and Elaine Fuchs. Epidermal stem cells of the skin. Annu. Rev. Cell Dev. Biol., 22:339–373, 2006.

[33] Rachel Sennett and Michael Rendl. Mesenchymal–epithelial interactions during hair follicle morphogenesis and cycling. In Seminars in cell & developmental biology, volume 23, pages 917–927. Elsevier, 2012.

[34] Laura Alonso and Elaine Fuchs. Stem cells in the skin: waste not, wnt not. Genes & development, 17(10):1189–1200, 2003.

[35] Marja L Mikkola. The edar subfamily in hair and exocrine gland development. Advances in TNF Family Research, pages 23–33, 2011.

[36] Vladimir A Botchkarev, Natalia V Botchkareva, Wera Roth, Motonobu Nakamura, Ling-Hong Chen, Wiebke Herzog, Gerd Lindner, Jill A McMahon, Christoph Peters, Roland Lauster, et al. Noggin is a mesenchymally derived stimulator of hair-follicle induction. Nature cell biology, 1(3):158–164, 1999.

[37] B St-Jacques, HR Dassule, I Karavanova, VA Botchkarev, J Li, PS Danielian, JA McMahon, PM Lewis, R Paus, and AP McMahon. Sonic hedgehog signaling is essential for hair development. Current Biology, 8(19):1058–1069, 1998.

[38] Ritsuko Morita, Noriko Sanzen, Hiroko Sasaki, Tetsutaro Hayashi, Mana Umeda, Mika Yoshimura, Takaki Yamamoto, Tatsuo Shibata, Takaya Abe, Hiroshi Kiyonari, et al. Tracing the origin of hair follicle stem cells. Nature, pages 1–6, 2021.

[39] Khusali Gupta, Jonathan Levinsohn, George Linderman, Demeng Chen, Thomas Yang Sun, Danni Dong, M Mark Taketo, Marcus Bosenberg, Yuval Kluger, Keith Choate, et al. Single-cell analysis reveals a hair follicle dermal niche molecular differentiation trajectory that begins prior to morphogenesis. Developmental cell, 48(1):17–31, 2019.

[40] Yuhang Zhang, Philip Tomann, Thomas Andl, Natalie M Gallant, Joerg Huelsken, Boris Jerchow, Walter Birchmeier, Ralf Paus, Stefano Piccolo, Marja L Mikkola, et al. Reciprocal requirements for eda/edar/nf-κb and wnt/β-catenin signaling pathways in hair follicle induction. Developmental cell, 17(1):49–61, 2009.

[41] Demeng Chen, Andrew Jarrell, Canting Guo, Richard Lang, and Radhika Atit. Dermal β-catenin activity in response to epidermal wnt ligands is required for fibroblast proliferation and hair follicle initiation. Development, 139(8):1522–1533, 2012.

[42] Xiying Fan, Dongmei Wang, Jeremy Evan Burgmaier, Yudong Teng, Rose-Anne Romano, Satrajit Sinha, and Rui Yi. Single cell and open chromatin analysis reveals molecular origin of epidermal cells of the skin. Developmental cell, 47(1):21–37, 2018.

[43] Nivedita Saxena, Ka-Wai Mok, and Michael Rendl. An updated classification of hair follicle morphogenesis. Experimental dermatology, 28(4):332–344, 2019.

[44] Elaine Fuchs. Scratching the surface of skin development. Nature, 445(7130):834–842, 2007.

[45] Margaret H Hardy. The secret life of the hair follicle. Trends in Genetics, 8(2):55–61, 1992.

[46] Ralf Paus and George Cotsarelis. The biology of hair follicles. New England journal of medicine, 341(7):491–497, 1999.

[47] Ka-Wai Mok, Nivedita Saxena, Nicholas Heitman, Laura Grisanti, Devika Srivastava, Mauro J Muraro, Tina Jacob, Rachel Sennett, Zichen Wang, Yutao Su, et al. Dermal condensate niche fate specification occurs prior to formation and is placode progenitor dependent. Developmental cell, 48(1):32–48, 2019.

[48] Jonathan A Nowak, Lisa Polak, H Amalia Pasolli, and Elaine Fuchs. Hair follicle stem cells are specified and function in early skin morphogenesis. Cell stem cell, 3(1):33–43, 2008.

[49] Daniela Frances and Catherin Niemann. Stem cell dynamics in sebaceous gland morphogenesis in mouse skin. Developmental biology, 363(1):138–146, 2012.

[50] Valerie Horsley, Dónal O'Carroll, Reuben Tooze, Yasuhide Ohinata, Mitinori Saitou, Tetyana Obukhanych, Michel Nussenzweig, Alexander Tarakhovsky, and Elaine Fuchs. Blimp1 defines a progenitor population that governs cellular input to the sebaceous gland. Cell, 126(3):597–609, 2006.

[51] Krzysztof Kobielak, H Amalia Pasolli, Laura Alonso, Lisa Polak, and Elaine Fuchs. Defining bmp functions in the hair follicle by conditional ablation of bmp receptor ia. The Journal of cell biology, 163(3):609–623, 2003.

[52] Charles K Kaufman, Ping Zhou, H Amalia Pasolli, Michael Rendl, Diana Bolotin, Kim-Chew Lim, Xing Dai, Maria-Luisa Alegre, and Elaine Fuchs. Gata-3: an unexpected regulator of cell lineage determination in skin. Genes & development, 17(17):2108–2122, 2003.

[53] Sven Müller-Röver, Kerstin Foitzik, Ralf Paus, Bori Handjiski, Carina van der Veen, Stefan Eichmüller, Ian A McKay, and Kurt S Stenn. A comprehensive guide for the accurate classification of murine hair follicles in distinct hair cycle stages. Journal of investigative dermatology, 117(1):3–15, 2001.

[54] Elaine Fuchs. Skin stem cells: rising to the surface. The Journal of cell biology, 180(2):273–284, 2008.

[55] FW Dry. The coat of the mouse (mus musculus). Journal of Genetics, 16(3):287–340, 1926.

[56] KS Stenn and Ralf Paus. Controls of hair follicle cycling. Physiological reviews, 2001.

[57] Valentina Greco, Ting Chen, Michael Rendl, Markus Schober, H Amalia Pasolli, Nicole Stokes, June dela Cruz-Racelis, and Elaine Fuchs. A two-step mechanism for stem cell activation during hair regeneration. Cell stem cell, 4(2):155–169, 2009.

[58] Herman B Chase and Gordon J Eaton. The growth of hair follicles in waves. Annals of the New York Academy of Sciences, 83(3):365–368, 1959.

[59] Brice E Keyes, Jeremy P Segal, Evan Heller, Wen-Hui Lien, Chiung-Ying Chang, Xingyi Guo, Dan S Oristian, Deyou Zheng, and Elaine Fuchs. Nfatc1 orchestrates aging in hair follicle stem cells. Proceedings of the National Academy of Sciences, 110(51):E4950–E4959, 2013.

[60] George Cotsarelis, Tung-Tien Sun, and Robert M Lavker. Label-retaining cells reside in the bulge area of pilosebaceous unit: implications for follicular stem cells, hair cycle, and skin carcinogenesis. Cell, 61(7):1329–1337, 1990.

[61] Cedric Blanpain, William E Lowry, Andrea Geoghegan, Lisa Polak, and Elaine Fuchs. Self-renewal, multipotency, and the existence of two cell populations within an epithelial stem cell niche. Cell, 118(5):635–648, 2004.

[62] Tudorita Tumbar, Geraldine Guasch, Valentina Greco, Cedric Blanpain, William E Lowry, Michael Rendl, and Elaine Fuchs. Defining the epithelial stem cell niche in skin. Science, 303(5656):359–363, 2004.

[63] Rebecca J Morris, Yaping Liu, Lee Marles, Zaixin Yang, Carol Trempus, Shulan Li, Jamie S Lin, Janet A Sawicki, and George Cotsarelis. Capturing and profiling adult hair follicle stem cells. Nature biotechnology, 22(4):411–417, 2004.

[64] Mayumi Ito, Yaping Liu, Zaixin Yang, Jane Nguyen, Fan Liang, Rebecca J Morris, and George Cotsarelis. Stem cells in the hair follicle bulge contribute to wound repair but not to homeostasis of the epidermis. Nature medicine, 11(12):1351–1354, 2005.

[65] Rebecca J Morris, Carl D Bortner, George Cotsarelis, Jeffrey M Reece, Carol S Trempus, Randall S Faircloth, and Raymond W Tennant. Enrichment for living murine keratinocytes from the hair follicle bulge with the cell surface marker cd34. Journal of Investigative Dermatology, 120(4):501–511, 2003.

[66] Valerie Horsley, Antonios O Aliprantis, Lisa Polak, Laurie H Glimcher, and Elaine Fuchs. Nfatc1 balances quiescence and proliferation of skin stem cells. Cell, 132(2):299–310, 2008.

[67] Angela M Christiano. Hair follicle epithelial stem cells get their sox on. Cell Stem Cell, 3(1):3–4, 2008.

[68] Horace Rhee, Lisa Polak, and Elaine Fuchs. Lhx2 maintains stem cell character in hair follicles. Science, 312(5782):1946–1949, 2006.

[69] Viljar Jaks, Nick Barker, Maria Kasper, Johan H Van Es, Hugo J Snippert, Hans Clevers, and Rune Toftgård. Lgr5 marks cycling, yet long-lived, hair follicle stem cells. Nature genetics, 40(11):1291–1299, 2008.

[70] Hoang Nguyen, Michael Rendl, and Elaine Fuchs. Tcf3 governs stem cell features and represses cell fate determination in skin. Cell, 127(1):171–183, 2006.

[71] Ying V Zhang, Janice Cheong, Nichita Ciapurin, David J McDermitt, and Tudorita Tumbar. Distinct self-renewal and differentiation phases in the niche of infrequently dividing hair follicle stem cells. Cell stem cell, 5(3):267–278, 2009.

[72] Rui Yi. Concise review: mechanisms of quiescent hair follicle stem cell regulation. Stem Cells, 35(12):2323–2330, 2017.

[73] Cédric Blanpain and Elaine Fuchs. Epidermal homeostasis: a balancing act of stem cells in the skin. Nature reviews Molecular cell biology, 10(3):207–217, 2009.

[74] Eve Kandyba, Yvonne Leung, Yi-Bu Chen, Randall Widelitz, Cheng-Ming Chuong, and Krzysztof Kobielak. Competitive balance of intrabulge bmp/wnt signaling reveals a robust gene network ruling stem cell homeostasis and cyclic activation. Proceedings of the National Academy of Sciences, 110(4):1351–1356, 2013.

[75] Yeon Sook Choi, Yuhang Zhang, Mingang Xu, Yongguang Yang, Mayumi Ito, Tien Peng, Zheng Cui, Andras Nagy, Anna-Katerina Hadjantonakis, Richard A Lang, et al. Distinct functions for wnt/β-catenin in hair follicle stem cell proliferation and survival and interfollicular epidermal homeostasis. Cell stem cell, 13(6):720–733, 2013.

[76] Xinhong Lim and Roel Nusse. Wnt signaling in skin development, homeostasis, and disease. Cold Spring Harbor perspectives in biology, 5(2):a008029, 2013.

[77] Seshamma Reddy, Thomas Andl, Alexander Bagasra, Min Min Lu, Douglas J Epstein, Edward E Morrisey, and Sarah E Millar. Characterization of wnt gene expression in developing and postnatal hair follicles and identification of wnt5a as a target of sonic hedgehog in hair follicle morphogenesis. Mechanisms of development, 107(1-2):69–82, 2001.

[78] William E Lowry, Cedric Blanpain, Jonathan A Nowak, Geraldine Guasch, Lisa Lewis, and Elaine Fuchs. Defining the impact of β-catenin/tcf transactivation on epithelial stem cells. Genes & development, 19(13):1596–1611, 2005.

[79] David Van Mater, Frank T Kolligs, Andrzej A Dlugosz, and Eric R Fearon. Transient activation of β-catenin signaling in cutaneous keratinocytes is sufficient to trigger the active growth phase of the hair cycle in mice. Genes & development, 17(10):1219–1224, 2003.

[80] Cristina Lo Celso, David M Prowse, and Fiona M Watt. Transient activation of β-catenin signalling in adult mouse epidermis is sufficient to induce new hair follicles but continuous activation is required to maintain hair follicle tumours. 2004.

[81] Peggy S Myung, Makoto Takeo, Mayumi Ito, and Radhika P Atit. Epithelial wnt ligand secretion is required for adult hair follicle growth and regeneration. Journal of Investigative Dermatology, 133(1):31–41, 2013.

[82] Holger Kulessa, Gail Turk, and Brigid LM Hogan. Inhibition of bmp signaling affects growth and differentiation in the anagen hair follicle. The EMBO journal, 19(24):6664–6674, 2000.

[83] Krzysztof Kobielak, Nicole Stokes, June de la Cruz, Lisa Polak, and Elaine Fuchs. Loss of a quiescent niche but not follicle stem cells in the absence of bone morphogenetic protein signaling. Proceedings of the National Academy of Sciences, 104(24):10063–10068, 2007.

[84] Karen M Osorio, Song Eun Lee, David J McDermitt, Sanjeev K Waghmare, Ying V Zhang, Hyun Nyun Woo, and Tudorita Tumbar. Runx1 modulates developmental, but not injury-driven, hair follicle stem cell activation. 2008.

[85] Luis A Garza, Yaping Liu, Zaixin Yang, Brinda Alagesan, John A Lawson, Scott M Norberg, Dorothy E Loy, Tailun Zhao, Hanz B Blatt, David C Stanton, et al. Prostaglandin d2 inhibits hair growth and is elevated in bald scalp of men with androgenetic alopecia. Science translational medicine, 4(126):126ra34–126ra34, 2012.

[86] Yutaka Shimomura, Dritan Agalliu, Alin Vonica, Victor Luria, Muhammad Wajid, Alessandra Baumer, Serena Belli, Lynn Petukhova, Albert Schinzel, Ali H Brivanlou, et al. Apcdd1 is a novel wnt inhibitor mutated in hereditary hypotrichosis simplex. Nature, 464(7291):1043–1047, 2010.

[87] Janis Koester, Yekaterina A Miroshnikova, Sushmita Ghatak, Carlos Andrés Chacón-Martínez, Jessica Morgner, Xinping Li, Ilian Atanassov, Janine Altmüller, David E Birk, Manuel Koch, et al. Niche stiffening compromises hair follicle stem cell potential during ageing by reducing bivalent promoter accessibility. Nature Cell Biology, 23(7):771–781, 2021.

[88] Chi Zhang and Rui Yi. Inhibition of microrna turns back the clock of hair follicle aging. Nature Aging, 1(9):753–754, 2021.

[89] Yao Yu, Xia Zhang, Fengzhen Liu, Peiying Zhu, Liping Zhang, You Peng, Xinyu Yan, Yin Li, Peng Hua, Caiyue Liu, et al. A stress-induced mir-31–clock–erk pathway is a key driver and therapeutic target for skin aging. Nature Aging, 1(9):795–809, 2021.

[90] Irina M Conboy, Michael J Conboy, Amy J Wagers, Eric R Girma, Irving L Weissman, and Thomas A Rando. Rejuvenation of aged progenitor cells by exposure to a young systemic environment. Nature, 433(7027):760–764, 2005.

[91] Yuhua Xie, Daoming Chen, Kaiju Jiang, Lifang Song, Nannan Qian, Yingxue Du, Yong Yang, Fengchao Wang, and Ting Chen. Hair shaft miniaturization causes stem cell depletion through mechanosensory signals mediated by a piezo1-calcium-tnf-α axis. Cell Stem Cell, 2021.

[92] Viktor Janzen, Randolf Forkert, Heather E Fleming, Yoriko Saito, Michael T Waring, David M Dombkowski, Tao Cheng, Ronald A DePinho, Norman E Sharpless, and David T Scadden. Stem-cell ageing modified by the cyclin-dependent kinase inhibitor p16 ink4a. Nature, 443(7110):421–426, 2006.

[93] Norman E Sharpless and Ronald A DePinho. How stem cells age and why this makes us grow old. Nature reviews Molecular cell biology, 8(9):703–713, 2007.

[94] Cristiana M Pineda, Sangbum Park, Kailin R Mesa, Markus Wolfel, David G Gonzalez, Ann M Haberman, Panteleimon Rompolas, and Valentina Greco. Intravital imaging of hair follicle regeneration in the mouse. Nature protocols, 10(7):1116–1130, 2015.

[95] Panteleimon Rompolas, Elizabeth R Deschene, Giovanni Zito, David G Gonzalez, Ichiko Saotome, Ann M Haberman, and Valentina Greco. Live imaging of stem cell and progeny behaviour in physiological hair-follicle regeneration. Nature, 487(7408):496–499, 2012.

[96] Chih-Chiang Chen, Philip J Murray, Ting Xin Jiang, Maksim V Plikus, Yun-Ting Chang, Oscar K Lee, Randall B Widelitz, and Cheng-Ming Chuong. Regenerative hair waves in aging mice and extra-follicular modulators follistatin, dkk1, and sfrp4. Journal of Investigative Dermatology, 134(8):2086–2096, 2014.

[97] Tim Stuart, Andrew Butler, Paul Hoffman, Christoph Hafemeister, Efthymia Papalexi, William M Mauck III, Yuhan Hao, Marlon Stoeckius, Peter Smibert, and Rahul Satija. Comprehensive integration of single-cell data. Cell, 177(7):1888–1902, 2019.

[98] Marion Claudia Salzer, Atefeh Lafzi, Antoni Berenguer-Llergo, Catrin Youssif, Andrés Castellanos, Guiomar Solanas, Francisca Oliveira Peixoto, Camille Stephan-Otto Attolini, Neus Prats, Monica Aguilera, et al. Identity noise and adipogenic traits characterize dermal fibroblast aging. Cell, 175(6):1575–1590, 2018.

[99] Hironobu Fujiwara, Manuela Ferreira, Giacomo Donati, Denise K Marciano, James M Linton, Yuya Sato, Andrea Hartner, Kiyotoshi Sekiguchi, Louis F Reichardt, and Fiona M Watt. The basement membrane of hair follicle stem cells is a muscle cell niche. Cell, 144(4):577–589, 2011.

[100] Junyue Cao, Malte Spielmann, Xiaojie Qiu, Xingfan Huang, Daniel M Ibrahim, Andrew J Hill, Fan Zhang, Stefan Mundlos, Lena Christiansen, Frank J Steemers, et al. The single-cell transcriptional landscape of mammalian organogenesis. Nature, 566(7745):496–502, 2019.

[101] Jayhun Lee, Charlene SL Hoi, Karin C Lilja, Brian S White, Song Eun Lee, David Shalloway, and Tudorita Tumbar. Runx1 and p21 synergistically limit the extent of hair follicle stem cell quiescence in vivo. Proceedings of the National Academy of Sciences, 110(12):4634–4639, 2013.

[102] Wen-Hui Lien, Lisa Polak, Mingyan Lin, Kenneth Lay, Deyou Zheng, and Elaine Fuchs. In vivo transcriptional governance of hair follicle stem cells by canonical wnt regulators. Nature cell biology, 16(2):179–190, 2014.

[103] Vanessa Besson, Piera Smeriglio, Amélie Wegener, Frédéric Relaix, Brahim Nait Oumesmar, David A Sassoon, and Giovanna Marazzi. Pw1 gene/paternally expressed gene 3 (pw1/peg3) identifies multiple adult stem and progenitor cell populations. Proceedings of the National Academy of Sciences, 108(28):11470–11475, 2011.

[104] Miho Kimura-Ueki, Yuko Oda, Junko Oki, Akiko Komi-Kuramochi, Emi Honda, Masahiro Asada, Masashi Suzuki, and Toru Imamura. Hair cycle resting phase is regulated by cyclic epithelial fgf18 signaling. Journal of Investigative Dermatology, 132(5):1338–1345, 2012.

[105] Maksim V Plikus, Julie Ann Mayer, Damon de La Cruz, Ruth E Baker, Philip K Maini, Robert Maxson, and Cheng-Ming Chuong. Cyclic dermal bmp signalling regulates stem cell activation during hair regeneration. Nature, 451(7176):340–344, 2008.

[106] Ya-Chieh Hsu, Lishi Li, and Elaine Fuchs. Transit-amplifying cells orchestrate stem cell activity and tissue regeneration. Cell, 157(4):935–949, 2014.

[107] Rene C Adam, Hanseul Yang, Shira Rockowitz, Samantha B Larsen, Maria Nikolova, Daniel S Oristian, Lisa Polak, Meelis Kadaja, Amma Asare, Deyou Zheng, et al. Pioneer factors govern super-enhancer dynamics in stem cell plasticity and lineage choice. Nature, 521(7552):366–370, 2015.

[108] Valerie PI Vidal, Marie-Christine Chaboissier, Susanne Lützkendorf, George Cotsarelis, Pleasantine Mill, Chi-Chung Hui, Nicolas Ortonne, Jean-Paul Ortonne, and Andreas Schedl. Sox9 is essential for outer root sheath differentiation and the formation of the hair stem cell compartment. Current Biology, 15(15):1340–1351, 2005.

[109] Jason D Buenrostro, Beijing Wu, Ulrike M Litzenburger, Dave Ruff, Michael L Gonzales, Michael P Snyder, Howard Y Chang, and William J Greenleaf. Single-cell chromatin accessibility reveals principles of regulatory variation. Nature, 523(7561):486–490, 2015.

[110] Jason D Buenrostro, Paul G Giresi, Lisa C Zaba, Howard Y Chang, and William J Greenleaf. Transposition of native chromatin for fast and sensitive epigenomic profiling of open chromatin, dna-binding proteins and nucleosome position. Nature methods, 10(12):1213–1218, 2013.

[111] Shruti Naik, Samantha B Larsen, Nicholas C Gomez, Kirill Alaverdyan, Ataman Sendoel, Shaopeng Yuan, Lisa Polak, Anita Kulukian, Sophia Chai, and Elaine Fuchs. Inflammatory memory sensitizes skin epithelial stem cells to tissue damage. Nature, 550(7677):475–480, 2017.

[112] Meelis Kadaja, Brice E Keyes, Mingyan Lin, H Amalia Pasolli, Maria Genander, Lisa Polak, Nicole Stokes, Deyou Zheng, and Elaine Fuchs. Sox9: a stem cell transcriptional regulator of secreted niche signaling factors. Genes & development, 28(4):328–341, 2014.

[113] Rachel Herndon Klein, Ziguang Lin, Amelia Soto Hopkin, William Gordon, Lam C Tsoi, Yun Liang, Johann E Gudjonsson, and Bogi Andersen. Grhl3 binding and enhancers rearrange as epidermal keratinocytes transition between functional states. PLoS genetics, 13(4):e1006745, 2017.

[114] Cristina de Guzman Strong, Philip W Wertz, Chenwei Wang, Fan Yang, Paul S Meltzer, Thomas Andl, Sarah E Millar, I Ho, Sung-Yun Pai, Julia A Segre, et al. Lipid defect underlies selective skin barrier impairment of an epidermal-specific deletion of gata-3. Journal of Cell Biology, 175(4):661–670, 2006.

[115] Hannah A Pliner, Jonathan S Packer, José L McFaline-Figueroa, Darren A Cusanovich, Riza M Daza, Delasa Aghamirzaie, Sanjay Srivatsan, Xiaojie Qiu, Dana Jackson, Anna Minkina, et al. Cicero predicts cis-regulatory dna interactions from single-cell chromatin accessibility data. Molecular cell, 71(5):858–871, 2018.

[116] Xiao-Zhu Huang, Jian Feng Wu, Darrell Cass, David J Erle, David Corry, Stephen G Young, Robert V Farese, and Dean Sheppard. Inactivation of the integrin beta 6 subunit gene reveals a role of epithelial integrins in regulating inflammation in the lung and skin. The Journal of cell biology, 133(4):921–928, 1996.

[117] Carol S Trempus, Rebecca J Morris, Matthew Ehinger, Amy Elmore, Carl D Bortner, Mayumi Ito, George Cotsarelis, Joanne GW Nijhof, John Peckham, Norris Flagler, et al. Cd34 expression by hair follicle stem cells is required for skin tumor development in mice. Cancer research, 67(9):4173–4181, 2007.

[118] Kenneth Lay, Shaopeng Yuan, Shiri Gur-Cohen, Yuxuan Miao, Tianxiao Han, Shruti Naik, H Amalia Pasolli, Samantha B Larsen, and Elaine Fuchs. Stem cells repurpose proliferation to contain a breach in their niche barrier. Elife, 7:e41661, 2018.

[119] Ryan R Driskell, Beate M Lichtenberger, Esther Hoste, Kai Kretzschmar, Ben D Simons, Marika Charalambous, Sacri R Ferron, Yann Herault, Guillaume Pavlovic, Anne C Ferguson-Smith, et al. Distinct fibroblast lineages determine dermal architecture in skin development and repair. Nature, 504(7479):277–281, 2013.

[120] M Ryan Corces, Alexandro E Trevino, Emily G Hamilton, Peyton G Greenside, Nicholas A Sinnott-Armstrong, Sam Vesuna, Ansuman T Satpathy, Adam J Rubin, Kathleen S Montine, Beijing Wu, et al. An improved atac-seq protocol reduces background and enables interrogation of frozen tissues. Nature methods, 14(10):959–962, 2017.

[121] Daehwan Kim, Ben Langmead, and Steven L Salzberg. Hisat: a fast spliced aligner with low memory requirements. Nature methods, 12(4):357–360, 2015.

[122] Heng Li, Bob Handsaker, Alec Wysoker, Tim Fennell, Jue Ruan, Nils Homer, Gabor Marth, Goncalo Abecasis, and Richard Durbin. The sequence alignment/map format and samtools. Bioinformatics, 25(16):2078–2079, 2009.

[123] Simon Anders, Paul Theodor Pyl, and Wolfgang Huber. Htseq—a python framework to work with high-throughput sequencing data. bioinformatics, 31(2):166–169, 2015.

[124] Michael I Love, Wolfgang Huber, and Simon Anders. Moderated estimation of fold change and dispersion for rna-seq data with deseq2. Genome biology, 15(12):1–21, 2014.

[125] Yingyao Zhou, Bin Zhou, Lars Pache, Max Chang, Alireza Hadj Khodabakhshi, Olga Tanaseichuk, Christopher Benner, and Sumit K Chanda. Metascape provides a biologist-oriented resource for the analysis of systems-level datasets. Nature communications, 10(1):1–10, 2019.

[126] Andrew Butler, Paul Hoffman, Peter Smibert, Efthymia Papalexi, and Rahul Satija. Integrating single-cell transcriptomic data across different conditions, technologies, and species. Nature biotechnology, 36(5):411–420, 2018.

[127] F Alexander Wolf, Philipp Angerer, and Fabian J Theis. Scanpy: large-scale single-cell gene expression data analysis. Genome biology, 19(1):1–5, 2018.

[128] Ben Langmead and Steven L Salzberg. Fast gapped-read alignment with bowtie 2. Nature methods, 9(4):357–359, 2012.

[129] Yong Zhang, Tao Liu, Clifford A Meyer, Jérôme Eeckhoute, David S Johnson, Bradley E Bernstein, Chad Nusbaum, Richard M Myers, Myles Brown, Wei Li, et al. Model-based analysis of chip-seq (macs). Genome biology, 9(9):1–9, 2008.

[130] Sven Heinz, Christopher Benner, Nathanael Spann, Eric Bertolino, Yin C Lin, Peter Laslo, Jason X Cheng, Cornelis Murre, Harinder Singh, and Christopher K Glass. Simple combinations of lineage-determining transcription factors prime cis-regulatory elements required for macrophage and b cell identities. Molecular cell, 38(4):576–589, 2010.

[131] Timothy L Bailey, James Johnson, Charles E Grant, and William S Noble. The meme suite. Nucleic acids research, 43(W1):W39–W49, 2015.

[132] Aaron R Quinlan and Ira M Hall. Bedtools: a flexible suite of utilities for comparing genomic features. Bioinformatics, 26(6):841–842, 2010.

[133] JT Robinson, H Thorvaldsdóttir, W Winckler, M Guttman, and ES Lander. Getz g1, et al. Integrative genomics viewer. Nat Biotechnol, 29:24–26, 2011.

[134] Tao Ye, Arnaud R Krebs, Mohamed-Amin Choukrallah, Celine Keime, Frederic Plewniak, Irwin Davidson, and Laszlo Tora. seqminer: an integrated chip-seq data interpretation platform. Nucleic acids research, 39(6):e35–e35, 2011.

[135] Robin Holliday. Understanding ageing. Number 30. Cambridge University Press, 1995.

[136] Jan M Van Deursen. The role of senescent cells in ageing. Nature, 509(7501):439–446, 2014.

[137] Miren Revuelta and Ander Matheu. Autophagy in stem cell aging. Aging cell, 16(5):912–915, 2017.

[138] Michael E Todhunter, Rosalyn W Sayaman, Masaru Miyano, and Mark A LaBarge. Tissue aging: the integration of collective and variant responses of cells to entropic forces over time. Current opinion in cell biology, 54:121–129, 2018.

[139] Celia Pilar Martinez-Jimenez, Nils Eling, Hung-Chang Chen, Catalina A Vallejos, Aleksandra A Kolodziejczyk, Frances Connor, Lovorka Stojic, Timothy F Rayner, Michael JT Stubbington, Sarah A Teichmann, et al. Aging increases cell-to-cell transcriptional variability upon immune stimulation. Science, 355(6332):1433–1436, 2017.

[140] Valentine Svensson, Roser Vento-Tormo, and Sarah A Teichmann. Exponential scaling of single-cell rna-seq in the past decade. Nature protocols, 13(4):599–604, 2018.

[141] Amos Tanay and Aviv Regev. Scaling single-cell genomics from phenomenology to mechanism. Nature, 541(7637):331–338, 2017.

[142] Sebastian Preissl, Rongxin Fang, Hui Huang, Yuan Zhao, Ramya Raviram, David U Gorkin, Yanxiao Zhang, Brandon C Sos, Veena Afzal, Diane E Dickel, et al. Single-nucleus analysis of accessible chromatin in developing mouse forebrain reveals cell-type-specific transcriptional regulation. Nature neuroscience, 21(3):432–439, 2018.

[143] Yuhan Hao, Stephanie Hao, Erica Andersen-Nissen, William M Mauck III, Shiwei Zheng, Andrew Butler, Maddie J Lee, Aaron J Wilk, Charlotte Darby, Michael Zager, et al. Integrated analysis of multimodal single-cell data. Cell, 2021.

[144] Gopal Chovatiya, Sangeeta Ghuwalewala, Lauren D Walter, Benjamin D Cosgrove, and Tudorita Tumbar. High-resolution single-cell transcriptomics reveals heterogeneity of self-renewing hair follicle stem cells. Experimental dermatology, 30(4):457–471, 2021.

[145] Chi Zhang, Dongmei Wang, Jingjing Wang, Li Wang, Wenli Qiu, Tsutomu Kume, Robin Dowell, and Rui Yi. Escape of hair follicle stem cells causes stem cell exhaustion during aging. Nature Aging, 1(10):889–903, 2021.

[146] F Alexander Wolf, Fiona K Hamey, Mireya Plass, Jordi Solana, Joakim S Dahlin, Berthold Göttgens, Nikolaus Rajewsky, Lukas Simon, and Fabian J Theis. Paga: graph abstraction reconciles clustering with trajectory inference through a topology preserving map of single cells. Genome biology, 20(1):1–9, 2019.

[147] Mathieu Jacomy, Tommaso Venturini, Sebastien Heymann, and Mathieu Bastian. Forceatlas2, a continuous graph layout algorithm for handy network visualization designed for the gephi software. PloS one, 9(6):e98679, 2014.

[148] Cole Trapnell, Davide Cacchiarelli, Jonna Grimsby, Prapti Pokharel, Shuqiang Li, Michael Morse, Niall J Lennon, Kenneth J Livak, Tarjei S Mikkelsen, and John L Rinn. The dynamics and regulators of cell fate decisions are revealed by pseudotemporal ordering of single cells. Nature biotechnology, 32(4):381–386, 2014.

[149] Xiaoyan Sun, Alexandra Are, Karl Annusver, Unnikrishnan Sivan, Tina Jacob, Tim Dalessandri, Simon Joost, Anja Füllgrabe, Marco Gerling, and Maria Kasper. Coordinated hedgehog signaling induces new hair follicles in adult skin. Elife, 9:e46756, 2020.

[150] Hans Clevers, Kyle M Loh, and Roel Nusse. An integral program for tissue renewal and regeneration: Wnt signaling and stem cell control. science, 346(6205), 2014.

[151] Yulia Shwartz, Meryem Gonzalez-Celeiro, Chih-Lung Chen, H Amalia Pasolli, Shu-Hsien Sheu, Sabrina Mai-Yi Fan, Farnaz Shamsi, Steven Assaad, Edrick Tai-Yu Lin, Bing Zhang, et al. Cell types promoting goosebumps form a niche to regulate hair follicle stem cells. Cell, 182(3):578–593, 2020.

[152] Mingxing Lei, Haiying Guo, Weiming Qiu, Xiangdong Lai, Tian Yang, Randall B Widelitz, Cheng-Ming Chuong, Xiaohua Lian, and Li Yang. Modulating hair follicle size with w nt10b/dkk 1 during hair regeneration. Experimental dermatology, 23(6):407–413, 2014.

[153] Charlene SL Hoi, Song Eun Lee, Shu-Yang Lu, David J McDermitt, Karen M Osorio, Caroline M Piskun, Rachel M Peters, Ralf Paus, and Tudorita Tumbar. Runx1 directly promotes proliferation of hair follicle stem cells and epithelial tumor formation in mouse skin. Molecular and cellular biology, 30(10):2518–2536, 2010.

[154] Ya-Chieh Hsu, H Amalia Pasolli, and Elaine Fuchs. Dynamics between stem cells, niche, and progeny in the hair follicle. Cell, 144(1):92–105, 2011.

[155] Tim Stuart, Avi Srivastava, Shaista Madad, Caleb A Lareau, and Rahul Satija. Single-cell chromatin state analysis with signac. Nature methods, 18(11):1333–1341, 2021.

[156] Alexandro E Trevino, Fabian Müller, Jimena Andersen, Laksshman Sundaram, Arwa Kathiria, Anna Shcherbina, Kyle Farh, Howard Y Chang, Anca M Pașca, Anshul Kundaje, et al. Chromatin and gene-regulatory dynamics of the developing human cerebral cortex at single-cell resolution. Cell, 184(19):5053–5069, 2021.

[157] Alicia N Schep, Beijing Wu, Jason D Buenrostro, and William J Greenleaf. chromvar: inferring transcription-factor-associated accessibility from single-cell epigenomic data. Nature methods, 14(10):975–978, 2017.

[158] Gioele La Manno, Ruslan Soldatov, Amit Zeisel, Emelie Braun, Hannah Hochgerner, Viktor Petukhov, Katja Lidschreiber, Maria E Kastriti, Peter Lönnerberg, Alessandro Furlan, et al. Rna velocity of single cells. Nature, 560(7719):494–498, 2018.

[159] Oriol Fornes, Jaime A Castro-Mondragon, Aziz Khan, Robin Van der Lee, Xi Zhang, Phillip A Richmond, Bhavi P Modi, Solenne Correard, Marius Gheorghe, Damir Baranašić, et al.

Jaspar 2020: update of the open-access database of transcription factor binding profiles. Nucleic acids research, 48(D1):D87–D92, 2020.

[160] Ge Tan and Boris Lenhard. Tfbstools: an r/bioconductor package for transcription factor binding site analysis. Bioinformatics, 32(10):1555–1556, 2016.

[161] Aravind Subramanian, Pablo Tamayo, Vamsi K Mootha, Sayan Mukherjee, Benjamin L Ebert, Michael A Gillette, Amanda Paulovich, Scott L Pomeroy, Todd R Golub, Eric S Lander, et al. Gene set enrichment analysis: a knowledge-based approach for interpreting genome-wide expression profiles. Proceedings of the National Academy of Sciences, 102(43):15545–15550, 2005.

[162] Ann P Chidgey and Richard L Boyd. Immune privilege for stem cells: not as simple as it looked. Cell stem cell, 3(4):357–358, 2008.

[163] Alma J Nauta and Willem E Fibbe. Immunomodulatory properties of mesenchymal stromal cells. Blood, The Journal of the American Society of Hematology, 110(10):3499–3506, 2007.

[164] Paolo Fiorina, Mollie Jurewicz, Andrea Augello, Andrea Vergani, Shirine Dada, Stefano La Rosa, Martin Selig, Jonathan Godwin, Kenneth Law, Claudia Placidi, et al. Immunomodulatory function of bone marrow-derived mesenchymal stem cells in experimental autoimmune type 1 diabetes. The Journal of Immunology, 183(2):993–1004, 2009.

[165] Jerry Y Niederkorn. See no evil, hear no evil, do no evil: the lessons of immune privilege. Nature immunology, 7(4):354–359, 2006.

[166] Colette Kanellopoulos-Langevin, Stéphane M Caucheteux, Philippe Verbeke, and David M Ojcius. Tolerance of the fetus by the maternal immune system: role of inflammatory mediators at the feto-maternal interface. Reproductive Biology and Endocrinology, 1(1):1–6, 2003.

[167] David Abi-Hanna, Denis Wakefield, and Stanley Watkins. Hla antigens in ocular tissues. i. in vivo expression in human eyes. Transplantation, 45(3):610–613, 1988.

[168] Lois A Lampson and Cheryl A Fisher. Weak hla and beta 2-microglobulin expression of neuronal cell lines can be modulated by interferon. Proceedings of the National Academy of Sciences, 81(20):6476–6480, 1984.

[169] Vassili Soumelis, Pedro A Reche, Holger Kanzler, Wei Yuan, Gina Edward, Bernhart Homey, Michel Gilliet, Steve Ho, Svetlana Antonenko, Annti Lauerma, et al. Human epithelial cells trigger dendritic cell–mediated allergic inflammation by producing tslp. Nature immunology, 3(7):673–680, 2002.

[170] AL Lima, I Karl, T Giner, H Poppe, M Schmidt, D Presser, M Goebeler, and B Bauer. Keratinocytes and neutrophils are important sources of proinflammatory molecules in hidradenitis suppurativa. British Journal of Dermatology, 174(3):514–521, 2016.

[171] Judith Agudo, Eun Sook Park, Samuel A Rose, Eziwoma Alibo, Robert Sweeney, Maxime Dhainaut, Koichi S Kobayashi, Ravi Sachidanandam, Alessia Baccarini, Miriam Merad, et al. Quiescent tissue stem cells evade immune surveillance. Immunity, 48(2):271–285, 2018.

[172] Gert De Graaf, Frank Buckley, and Brian G Skotko. Estimates of the live births, natural losses, and elective terminations with down syndrome in the united states. American Journal of Medical Genetics Part A, 167(4):756–767, 2015.

[173] Cara T Mai, Jennifer L Isenburg, Mark A Canfield, Robert E Meyer, Adolfo Correa, Clinton J Alverson, Philip J Lupo, Tiffany Riehle-Colarusso, Sook Ja Cho, Deepa Aggarwal, et al. National population-based estimates for major birth defects, 2010–2014. Birth defects research, 111(18):1420–1435, 2019.

[174] Helena Ahlfors, Nneka Anyanwu, Edvinas Pakanavicius, Natalia Dinischiotu, Eva Lana-Elola, Sheona Watson-Scales, Justin Tosh, Frances Wiseman, James Briscoe, Karen Page, et al. Gene expression dysregulation domains are not a specific feature of down syndrome. Nature communications, 10(1):1–12, 2019.

[175] Patrick K Gonzales, Christine M Roberts, Virginia Fonte, Connor Jacobsen, Gretchen H Stein, and Christopher D Link. Transcriptome analysis of genetically matched human induced pluripotent stem cells disomic or trisomic for chromosome 21. PloS one, 13(3):e0194581, 2018.

[176] Stylianos E Antonarakis. Down syndrome and the complexity of genome dosage imbalance. Nature Reviews Genetics, 18(3):147–163, 2017.

[177] Jonathan Witton, Ragunathan Padmashri, Larissa E Zinyuk, Victor I Popov, Igor Kraev, Samantha J Line, Thomas P Jensen, Angelo Tedoldi, Damian M Cummings, Victor LJ Tybulewicz, et al. Hippocampal circuit dysfunction in the tc1 mouse model of down syndrome. Nature Neuroscience, 18(9):1291–1298, 2015.

[178] Stylianos E Antonarakis, Robert Lyle, Emmanouil T Dermitzakis, Alexandre Reymond, and Samuel Deutsch. Chromosome 21 and down syndrome: from genomics to pathophysiology. Nature reviews genetics, 5(10):725–738, 2004.

[179] Faycal Guedj, Jeroen LA Pennings, Millie A Ferres, Leah C Graham, Heather C Wick, Klaus A Miczek, Donna K Slonim, and Diana W Bianchi. The fetal brain transcriptome and neonatal behavioral phenotype in the ts1cje mouse model of down syndrome. American journal of medical genetics Part A, 167(9):1993–2008, 2015.

[180] Eva Lana-Elola, Sheona D Watson-Scales, Elizabeth MC Fisher, and Victor LJ Tybulewicz. Down syndrome: searching for the genetic culprits. Disease models & mechanisms, 4(5):586–595, 2011.

[181] Min Chen, Jiayan Wang, Yingjun Luo, Kailing Huang, Xiaoshun Shi, Yanhui Liu, Jin Li, Zhengfei Lai, Shuya Xue, Haimei Gao, et al. Identify down syndrome transcriptome associations using integrative analysis of microarray database and correlation-interaction network. Human genomics, 12(1):1–12, 2018.

[182] Robert Lyle, Corinne Gehrig, Charlotte Neergaard-Henrichsen, Samuel Deutsch, and Stylianos E Antonarakis. Gene expression from the aneuploid chromosome in a trisomy mouse model of down syndrome. Genome research, 14(7):1268–1274, 2004.

[183] Pascal Kahlem, Marc Sultan, Ralf Herwig, Matthias Steinfath, Daniela Balzereit, Barbara Eppens, Nidhi G Saran, Mathew T Pletcher, Sarah T South, Gail Stetten, et al. Transcript level alterations reflect gene dosage effects across multiple tissues in a mouse model of down syndrome. Genome research, 14(7):1258–1267, 2004.

[184] L Dauphinot, Robert Lyle, I Rivals, M Tran Dang, RX Moldrich, G Golfier, L Ettwiller, K Toyama, J Rossier, L Personnaz, et al. The cerebellar transcriptome during postnatal development of the ts1cje mouse, a segmental trisomy model for down syndrome. Human molecular genetics, 14(3):373–384, 2005.

[185] Rong Mao, Xiaowen Wang, Edward L Spitznagel, Laurence P Frelin, Jason C Ting, Huashi Ding, Jung-whan Kim, Ingo Ruczinski, Thomas J Downey, and Jonathan Pevsner. Primary and secondary transcriptional effects in the developing human down syndrome brain and heart. Genome biology, 6(13):1–20, 2005.

[186] Cody T Mowery, Jaime M Reyes, Lucia Cabal-Hierro, Kelly J Higby, Kristen L Karlin, Jarey H Wang, Robert J Kimmerling, Paloma Cejas, Klothilda Lim, Hubo Li, et al. Trisomy of a down syndrome critical region globally amplifies transcription via hmgn1 overexpression. Cell reports, 25(7):1898–1911, 2018.

[187] Valerio Costa, Claudia Angelini, Luciana D'Apice, Margherita Mutarelli, Amelia Casamassimi, Linda Sommese, Maria Assunta Gallo, Marianna Aprile, Roberta Esposito, Luigi Leone, et al. Massive-scale rna-seq analysis of non ribosomal transcriptome in human trisomy 21. PloS one, 6(4):e18493, 2011.

[188] Kelly D Sullivan, Hannah C Lewis, Amanda A Hill, Ahwan Pandey, Leisa P Jackson, Joseph M Cabral, Keith P Smith, L Alexander Liggett, Eliana B Gomez, Matthew D Galbraith, et al. Trisomy 21 consistently activates the interferon response. Elife, 5:e16220, 2016.

[189] Nidhi G Saran, Mathew T Pletcher, JoAnne E Natale, Ying Cheng, and Roger H Reeves. Global disruption of the cerebellar transcriptome in a down syndrome mouse model. Human molecular genetics, 12(16):2013–2019, 2003.

[190] Maria Sobol, Joakim Klar, Loora Laan, Mansoureh Shahsavani, Jens Schuster, Göran Annerén, Anne Konzer, Jia Mi, Jonas Bergquist, Jessica Nordlund, et al. Transcriptome and proteome profiling of neural induced pluripotent stem cells from individuals with down syndrome disclose dynamic dysregulations of key pathways and cellular functions. Molecular neurobiology, 56(10):7113–7127, 2019.

[191] Konstantin Popadin, Stephan Peischl, Marco Garieri, M Reza Sailani, Audrey Letourneau, Federico Santoni, Samuel W Lukowski, Georgii A Bazykin, Sergey Nikolaev, Diogo Meyer, et al. Slightly deleterious genomic variants and transcriptome perturbations in down syndrome embryonic selection. Genome research, 28(1):1–10, 2018.

[192] King-Hwa Ling, Chelsee A Hewitt, Kai-Leng Tan, Pike-See Cheah, Sharmili Vidyadaran, Mei-I Lai, Han-Chung Lee, Ken Simpson, Lavinia Hyde, Melanie A Pritchard, et al. Functional transcriptome analysis of the postnatal brain of the ts1cje mouse model for down syndrome reveals global disruption of interferon-related molecular networks. BMC genomics, 15(1):1–19, 2014.

[193] Audrey Letourneau, Federico A Santoni, Ximena Bonilla, M Reza Sailani, David Gonzalez, Jop Kind, Claire Chevalier, Robert Thurman, Richard S Sandstrom, Youssef Hibaoui, et al. Domains of genome-wide gene expression dysregulation in down's syndrome. Nature, 508(7496):345–350, 2014.

[194] Georgios Stamoulis, Marco Garieri, Periklis Makrythanasis, Audrey Letourneau, Michel Guipponi, Nikolaos Panousis, Frédérique Sloan-Béna, Emilie Falconnet, Pascale Ribaux, Christelle Borel, et al. Single cell transcriptome in aneuploidies reveals mechanisms of gene dosage imbalance. Nature communications, 10(1):1–11, 2019.

[195] Veronika A Herzog, Brian Reichholf, Tobias Neumann, Philipp Rescheneder, Pooja Bhat, Thomas R Burkard, Wiebke Wlotzka, Arndt von Haeseler, Johannes Zuber, and Stefan L Ameres. Thiol-linked alkylation of rna to assess expression dynamics. Nature methods, 14(12):1198–1204, 2017.

[196] Michal Rabani, Raktima Raychowdhury, Marko Jovanovic, Michael Rooney, Deborah J Stumpo, Andrea Pauli, Nir Hacohen, Alexander F Schier, Perry J Blackshear, Nir Friedman, et al. High-resolution sequencing and modeling identifies distinct dynamic rna regulatory strategies. Cell, 159(7):1698–1710, 2014.

[197] Amit Blumberg, Yixin Zhao, Yi-Fei Huang, Noah Dukler, Edward J Rice, Alexandra G Chivu, Katie Krumholz, Charles G Danko, and Adam Siepel. Characterizing rna stability genome-wide through combined analysis of pro-seq and rna-seq data. BMC biology, 19(1):1–17, 2021.

[198] Edward Yang, Erik van Nimwegen, Mihaela Zavolan, Nikolaus Rajewsky, Mark Schroeder, Marcelo Magnasco, and James E Darnell. Decay rates of human mrnas: correlation with functional characteristics and sequence attributes. Genome research, 13(8):1863–1872, 2003.

[199] Lioudmila V Sharova, Alexei A Sharov, Timur Nedorezov, Yulan Piao, Nabeebi Shaik, and Minoru SH Ko. Database for mrna half-life of 19 977 genes obtained by dna microarray analysis of pluripotent and differentiating mouse embryonic stem cells. DNA research, 16(1):45–58, 2009.

[200] Shengli Hao and David Baltimore. The stability of mrna influences the temporal order of the induction of genes encoding inflammatory molecules. Nature immunology, 10(3):281–288, 2009.

[201] Michal Rabani, Joshua Z Levin, Lin Fan, Xian Adiconis, Raktima Raychowdhury, Manuel Garber, Andreas Gnirke, Chad Nusbaum, Nir Hacohen, Nir Friedman, et al. Metabolic labeling of rna uncovers principles of rna production and degradation dynamics in mammalian cells. Nature biotechnology, 29(5):436–442, 2011.

[202] Björn Schwanhäusser, Dorothea Busse, Na Li, Gunnar Dittmar, Johannes Schuchhardt, Jana Wolf, Wei Chen, and Matthias Selbach. Global quantification of mammalian gene expression control. Nature, 473(7347):337–342, 2011.

[203] Hidenori Tani and Nobuyoshi Akimitsu. Genome-wide technology for determining rna stability in mammalian cells: historical perspective and recent advantages based on modified nucleotide labeling. RNA biology, 9(10):1233–1238, 2012.

[204] Leighton J Core, Joshua J Waterfall, and John T Lis. Nascent rna sequencing reveals widespread pausing and divergent initiation at human promoters. Science, 322(5909):1845–1848, 2008.

[205] Hojoong Kwak, Nicholas J Fuda, Leighton J Core, and John T Lis. Precise maps of rna polymerase reveal how promoters direct initiation and pausing. Science, 339(6122):950–953, 2013.

[206] L Stirling Churchman and Jonathan S Weissman. Nascent transcript sequencing visualizes transcription at nucleotide resolution. Nature, 469(7330):368–373, 2011.

[207] Jeremy A Schofield, Erin E Duffy, Lea Kiefer, Meaghan C Sullivan, and Matthew D Simon. Timelapse-seq: adding a temporal dimension to rna sequencing through nucleoside recoding. Nature methods, 15(3):221–225, 2018.

[208] John Salvatier, Thomas V Wiecki, and Christopher Fonnesbeck. Probabilistic programming in python using pymc3. PeerJ Computer Science, 2:e55, 2016.

[209] Boris Slobodin, Anat Bahat, Urmila Sehrawat, Shirly Becker-Herman, Binyamin Zuckerman, Amanda N Weiss, Ruiqi Han, Ran Elkon, Reuven Agami, Igor Ulitsky, et al. Transcription dynamics regulate poly (a) tails and expression of the rna degradation machinery to balance mrna levels. Molecular cell, 78(3):434–444, 2020.

[210] Dig Bijay Mahat, Hojoong Kwak, Gregory T Booth, Iris H Jonkers, Charles G Danko, Ravi K Patel, Colin T Waters, Katie Munson, Leighton J Core, and John T Lis. Base-pair-resolution genome-wide mapping of active rna polymerases using precision nuclear run-on (pro-seq). Nature protocols, 11(8):1455–1476, 2016.

[211] Ehud Shapiro, Tamir Biezuner, and Sten Linnarsson. Single-cell sequencing-based technologies will revolutionize whole-organism science. Nature Reviews Genetics, 14(9):618–630, 2013.

[212] Fuchou Tang, Catalin Barbacioru, Yangzhou Wang, Ellen Nordman, Clarence Lee, Nanlan Xu, Xiaohui Wang, John Bodeau, Brian B Tuch, Asim Siddiqui, et al. mrna-seq whole-transcriptome analysis of a single cell. Nature methods, 6(5):377–382, 2009.

[213] Darren A Cusanovich, Riza Daza, Andrew Adey, Hannah A Pliner, Lena Christiansen, Kevin L Gunderson, Frank J Steemers, Cole Trapnell, and Jay Shendure. Multiplex single-cell profiling of chromatin accessibility by combinatorial cellular indexing. Science, 348(6237):910–914, 2015.

[214] Julia A Segre, Christoph Bauer, and Elaine Fuchs. Klf4 is a transcription factor required for establishing the barrier function of the skin. Nature genetics, 22(4):356–360, 1999.

[215] Satyakam Patel, Zong Fang Xi, Eun Young Seo, David McGaughey, and Julia A Segre. Klf4 and corticosteroids activate an overlapping set of transcriptional targets to accelerate in utero epidermal barrier acquisition. Proceedings of the National Academy of Sciences, 103(49):18668–18673, 2006.

[216] Elizabeth D Hay. An overview of epithelio-mesenchymal transformation. Cells Tissues Organs, 154(1):8–20, 1995.

[217] Linheng Li and Hans Clevers. Coexistence of quiescent and active adult stem cells in mammals. science, 327(5965):542–545, 2010.

[218] Tony Wyss-Coray. Ageing, neurodegeneration and brain rejuvenation. Nature, 539(7628):180–186, 2016.

[219] Basel Abu-Jamous and Steven Kelly. Clust: automatic extraction of optimal co-expressed gene clusters from gene expression data. Genome biology, 19(1):1–11, 2018.

[220] Ilya Korsunsky, Nghia Millard, Jean Fan, Kamil Slowikowski, Fan Zhang, Kevin Wei, Yuriy Baglaenko, Michael Brenner, Po-ru Loh, and Soumya Raychaudhuri. Fast, sensitive and accurate integration of single-cell data with harmony. Nature methods, 16(12):1289–1296, 2019.

[221] Seokmann Hong and Luc Van Kaer. Immune privilege: keeping an eye on natural killer t cells. The Journal of experimental medicine, 190(9):1197–1200, 1999.

[222] Elaine Fuchs and Srikala Raghavan. Getting under the skin of epidermal morphogenesis. Nature Reviews Genetics, 3(3):199–209, 2002.

Appendix

Description: What follows is the supplementary tables for the main text of *Escape of hair follicle stem cells causes stem cell exhaustion during aging.*

Supplementary Table 1. Downregulated genes in old vs young HF-SCs (scRNA-seq)

	p_val	log2_FC	pct.1	pct.2
Gm8797	1.27E-205	-3.037948	0.955	0.192
Gm12840	9.48E-141	-3.771101	0.656	0.04
Ybx3	1.31E-102	-1.212135	0.948	0.655
Uba52	6.77E-92	-1.092016	0.958	0.81
Rps27rt	5.60E-58	-0.838787	0.929	0.78
Cst6	1.74E-57	-0.850664	0.602	0.183
mt-Nd4	2.25E-52	-0.469726	0.998	1
Tnc	1.67E-51	-0.637974	0.325	0.031
Adrb2	1.22E-50	-0.945749	0.334	0.04
Flrt3	4.94E-49	-1.446259	0.402	0.081
Xist	1.73E-48	-0.754103	0.991	0.886
Rpl10-ps3	8.59E-48	-0.751779	0.765	0.438
S100a11	2.88E-44	-0.94473	0.976	0.899
Serpinb5	4.76E-44	-1.067052	0.96	0.938
Sostdc1	1.38E-43	-1.180566	0.701	0.344
Adgrg1	1.56E-43	-0.695701	0.48	0.137
Gja1	5.96E-40	-1.175083	0.346	0.071
mt-Cytb	1.48E-39	-0.399337	1	1
Prdx1	3.30E-38	-0.699622	0.965	0.925
Nme2	5.48E-37	-0.448042	0.395	0.104
Rab21	8.58E-37	-0.755503	0.689	0.381
Uap1	8.89E-37	-1.362164	0.739	0.491
Actb	2.95E-35	-0.880963	1	0.998
Sowahc	7.59E-35	-0.804986	0.539	0.226
Anxa2	1.52E-34	-0.584954	0.995	0.99
Sbsn	3.63E-34	-0.959148	0.974	0.929
Suco	4.46E-34	-0.797596	0.591	0.304
Samd5	1.17E-33	-0.489301	0.294	0.056
Anxa1	1.88E-33	-1.126039	0.861	0.676
Dmkn	3.34E-33	-0.711319	0.998	0.993
Cebpb	6.69E-33	-1.137853	0.873	0.67
Cdk2ap1	8.35E-33	-0.629405	0.694	0.396
Trib1	9.16E-33	-0.897765	0.609	0.305
mt-Nd3	1.98E-32	-0.478147	0.995	0.979
Eif1a	1.64E-30	-0.763851	0.706	0.464
Dlc1	3.53E-30	-0.517873	0.285	0.061
Peg3	4.98E-30	-0.45636	0.198	0.021
Lgals3	1.21E-28	-0.577207	0.984	0.974
Pi15	2.93E-28	-0.548245	0.226	0.036
Wfdc3	6.72E-28	-0.623103	0.598	0.301
AY036118	2.04E-27	-1.218176	0.584	0.346
Ddx5	9.46E-27	-0.461627	0.993	0.997
Sgms2	1.15E-26	-0.79166	0.506	0.252

Npnt	1.55E-26	-0.548778	0.438	0.174
Hexb	7.90E-26	-0.6579	0.527	0.27
Gm11808	1.67E-25	-0.459622	0.948	0.86
Rnaset2a	8.60E-25	-0.429967	0.515	0.253
Gm2000	1.60E-24	-0.493498	0.616	0.362
mt-Nd4l	2.28E-24	-0.57778	0.882	0.72
Them5	3.27E-24	-0.474589	0.273	0.069
Zfp655	3.49E-24	-0.498311	0.609	0.334
Tiparp	5.61E-24	-0.812558	0.788	0.603
Ism1	7.47E-24	-0.499578	0.355	0.131
Pdlim3	1.40E-23	-0.544143	0.28	0.077
Wdr89	1.55E-23	-0.514002	0.72	0.501
Tuba1c	2.77E-23	-0.74675	0.845	0.721
Tjp2	2.50E-22	-0.717139	0.468	0.236
S100a10	2.78E-22	-0.505758	0.995	0.988
Setbp1	3.30E-22	-0.490049	0.511	0.261
Mbd2	5.48E-22	-0.399863	0.485	0.233
Top1	8.52E-22	-0.697493	0.934	0.878
Mast4	1.24E-21	-0.828686	0.762	0.628
Bach1	1.34E-21	-0.681836	0.664	0.45
Tax1bp1	1.03E-20	-0.452398	0.962	0.919
Ube2j1	2.16E-20	-0.577357	0.534	0.319
Fosl1	5.56E-20	-0.883279	0.72	0.553
Ryk	7.61E-20	-0.476674	0.631	0.388
Srsf5	1.08E-19	-0.505286	0.835	0.734
Gjb4	1.21E-19	-0.636649	0.275	0.094
Cd44	1.37E-19	-0.718297	0.786	0.643
Tsc22d2	1.42E-19	-0.890527	0.767	0.64
Robo2	1.93E-19	-0.400407	0.148	0.022
Jmjd1c	4.06E-19	-0.573957	0.501	0.27
Tpm1	4.07E-19	-1.001409	0.765	0.591
S100a6	4.61E-19	-0.415982	1	0.999
Ppp1r14b	6.23E-19	-0.416889	0.92	0.843
Tppp3	9.29E-19	-0.393593	0.205	0.05
Tpm3	1.99E-18	-0.508638	0.76	0.598
Hspa5	2.20E-18	-0.570599	0.941	0.924
Sdcbp	2.33E-18	-0.461334	0.753	0.587
Sbno2	4.00E-18	-0.568117	0.567	0.353
Eif5	4.24E-18	-0.559961	0.896	0.851
Epha4	1.95E-17	-0.514624	0.449	0.239
Kdm6b	2.73E-17	-0.729708	0.729	0.571
Mat2a	4.39E-17	-0.88058	0.821	0.727
Osmr	4.94E-17	-0.432881	0.515	0.295
Noct	8.23E-17	-0.518656	0.466	0.264
Stim1	8.50E-17	-0.457017	0.776	0.625

Arhgef28	8.99E-17	-0.437479	0.485	0.276
Nop58	1.34E-16	-0.542952	0.652	0.464
Ccnd2	1.73E-16	-0.537682	0.384	0.179
Has2	2.06E-16	-0.989629	0.379	0.185
Calm1	2.65E-16	-0.415324	0.929	0.878
Abi1	3.69E-16	-0.453208	0.546	0.362
Ints6	5.00E-16	-0.468744	0.499	0.288
Txnrd1	1.25E-15	-0.396806	0.275	0.107
Dapl1	1.68E-15	-0.377553	0.179	0.047
Eif2s2	2.22E-15	-0.450099	0.887	0.848
Ssfa2	2.48E-15	-0.475511	0.788	0.641
Dusp7	2.99E-15	-0.648498	0.744	0.603
Actr3	3.36E-15	-0.450628	0.845	0.738
Golim4	5.02E-15	-0.425282	0.911	0.862
Rock2	8.29E-15	-0.503423	0.715	0.555
Bcl10	1.22E-14	-0.462186	0.694	0.542
Ckap4	1.39E-14	-0.529151	0.572	0.403
Itgb6	1.65E-14	-0.414097	0.296	0.131
Ube2n	2.01E-14	-0.570565	0.765	0.662
Pum2	2.16E-14	-0.470076	0.753	0.596
Sub1	2.29E-14	-0.429521	0.845	0.749
Gng12	2.53E-14	-0.391172	0.494	0.295
Gm42418	2.76E-14	-1.160189	0.972	0.976
Wnt4	2.87E-14	-0.420025	0.473	0.287
Pof1b	3.97E-14	-0.376498	0.494	0.287
Ccdc3	6.68E-14	-0.386978	0.287	0.123
Rap1b	8.54E-14	-0.456428	0.76	0.664
Erc1	1.39E-13	-0.414204	0.513	0.332
Ptprf	1.48E-13	-0.362597	0.882	0.759
Eif4a1	2.02E-13	-0.4322	0.965	0.954
Clic4	2.05E-13	-0.603979	0.845	0.822
Map4k4	2.34E-13	-0.400283	0.76	0.591
Nedd9	2.35E-13	-0.669513	0.647	0.494
Stat3	3.22E-13	-0.406799	0.802	0.675
Cd24a	3.38E-13	-0.475408	0.621	0.409
Zfp593	3.71E-13	-0.402349	0.569	0.389
Krt6a	5.22E-13	-1.011197	0.856	0.861
Zyx	5.28E-13	-0.450323	0.645	0.481
Nedd4l	6.62E-13	-0.517576	0.513	0.34
Cnksr3	6.80E-13	-0.453969	0.264	0.116
Eif3j1	6.80E-13	-0.432653	0.668	0.535
Eif6	9.54E-13	-0.425688	0.8	0.706
Lypd3	9.76E-13	-1.007273	0.744	0.668
Lmo7	1.38E-12	-0.417932	0.428	0.251
Hnrnpa0	1.76E-12	-0.37359	0.616	0.443

Urah	2.12E-12	-0.715692	0.887	0.86
Nfkb1	3.96E-12	-0.460033	0.689	0.55
Tgfb2	4.23E-12	-0.440541	0.122	0.028
Tle4	5.79E-12	-0.417579	0.619	0.441
Vmp1	6.08E-12	-0.569967	0.402	0.246
Gclc	6.11E-12	-0.852318	0.351	0.199
Ppp4r2	6.26E-12	-0.431915	0.624	0.456
Arid4b	7.50E-12	-0.394437	0.696	0.541
Map2k3	1.90E-11	-0.54476	0.541	0.396
Pim1	2.22E-11	-0.624775	0.675	0.567
Trim13	2.77E-11	-0.443883	0.464	0.3
Rtn4	2.99E-11	-0.409894	0.925	0.896
Ptpn12	3.56E-11	-0.435897	0.471	0.314
Eif1ax	4.87E-11	-0.406942	0.732	0.588
Homer1	5.59E-11	-0.443072	0.344	0.192
Trabd2b	5.81E-11	-0.376359	0.56	0.383
Skp1a	1.52E-10	-0.37001	0.821	0.722
Jak1	2.53E-10	-0.417721	0.652	0.501
Rap2b	2.75E-10	-0.370438	0.344	0.19
Lama3	3.54E-10	-0.49659	0.548	0.39
Avpi1	4.74E-10	-0.583255	0.751	0.697
Creb5	6.96E-10	-0.362903	0.551	0.387
Arl13b	8.34E-10	-0.374593	0.551	0.382
Clec2d	1.58E-09	-0.458102	0.473	0.311
Calml3	2.26E-09	-0.398428	0.941	0.902
Arl5b	2.73E-09	-0.383714	0.675	0.55
Ifrd1	2.80E-09	-0.739719	0.868	0.882
Cldn1	3.54E-09	-0.674219	0.551	0.441
Sprr1a	4.64E-09	-1.140801	0.294	0.165
Rnf217	5.43E-09	-0.366147	0.579	0.434
Cdcp1	8.08E-09	-0.3808	0.384	0.248
Pqlc1	8.99E-09	-0.464657	0.609	0.506
Nfkbiz	1.69E-08	-0.43097	0.645	0.501
Utp14b	1.99E-08	-0.373512	0.442	0.302
Cebpd	2.41E-08	-0.437391	0.682	0.573
S100a14	4.94E-08	-0.406032	0.932	0.897
Actg1	5.16E-08	-0.471434	0.986	1
Cxcl16	6.03E-08	-0.497381	0.694	0.61
H2-Q6	7.37E-08	-0.48436	0.209	0.107
Crip1	8.53E-08	-0.533123	0.842	0.793
Cstb	9.88E-08	-0.421583	0.795	0.686
9130008F2	2.35E-07	-0.410274	0.435	0.317
Dusp6	2.45E-07	-0.432217	0.555	0.41
Acpp	1.08E-06	-0.621164	0.781	0.752
Tnfrsf12a	1.70E-06	-0.390903	0.805	0.801

Lamc2	1.96E-06	-0.513119	0.614	0.539
Serpinb8	2.02E-06	-0.39539	0.678	0.599
Zfp703	2.67E-06	-0.548434	0.576	0.486
Tacstd2	2.34E-05	-0.586276	0.398	0.301
Arid5b	2.72E-05	-0.403422	0.833	0.84
Aspn	4.65E-05	-0.629793	0.16	0.092
Irf6	6.38E-05	-0.382096	0.758	0.732
F3	0.000106	-0.54377	0.242	0.16
Serpinb2	0.000218	-0.888525	0.544	0.722
Ppif	0.000237	-0.361968	0.209	0.137
Krt16	0.000242	-1.724544	0.334	0.258
Klf5	0.000522	-0.421491	0.511	0.447
Klf3	0.002484	-0.374874	0.628	0.59
Icam1	0.002553	-0.425791	0.268	0.204
Pthlh	0.002727	-0.773867	0.278	0.216
Jag1	0.003287	-0.367112	0.6	0.559
Phlda1	0.003947	-1.07384	0.718	0.758
Bmp2	0.004155	-0.391813	0.456	0.388
Fst	0.006867	-0.839456	0.779	0.819
Cyr61	0.01268	-0.522897	0.831	0.86
Plet1	0.043098	-0.663682	0.64	0.65
Adamts1	0.044784	-0.369338	0.315	0.267

Supplementary Table 2. Upregulated genes in old vs young HF-SCs (scRNA-seq)

	p_val	log2_FC	pct.1	pct.2
Postn	4.04E-109	1.475625405	0.805	1
Gm13305	1.15E-76	1.214463973	0.078	0.629
Cck	5.82E-68	2.273416056	0.12	0.625
Grik1	1.26E-67	1.055672749	0.085	0.597
Cxcl12	1.41E-62	1.362814516	0.252	0.723
Sncg	2.22E-61	1.319252936	0.195	0.673
Gm10260	8.14E-56	0.718126047	0	0.429
Cox7b	8.66E-52	1.042952272	0.715	0.865
Serpinb11	6.90E-50	1.401469959	0.339	0.754
Slc39a8	2.48E-44	0.97836482	0.395	0.754
Eef1a1	1.97E-43	0.385056976	1	1
Rpl7	2.50E-42	0.434227308	0.995	0.999
Rpl13a	6.02E-41	0.60885726	0.925	0.962
Rpl6	1.42E-39	0.460579129	0.991	1
Emb	3.56E-39	0.774709171	0.713	0.912
Hes1	2.12E-38	1.502437945	0.351	0.67
Rpl27-ps3	1.17E-37	0.581805723	0.059	0.403
Timp3	1.49E-37	0.894800386	0.548	0.835
Adra2a	1.84E-37	0.862732468	0.002	0.314
Rpl38	2.61E-37	0.422229371	0.993	0.993
Mgst1	2.09E-36	0.673189089	0.047	0.382
Lmo1	5.35E-35	0.779419257	0.527	0.802
Rps4x	8.80E-33	0.380597545	0.998	0.998
Marcksl1	1.08E-31	0.932737563	0.391	0.675
Phyhipl	5.01E-31	0.60284092	0.038	0.322
Ccl27a	1.52E-30	0.814121592	0.689	0.895
Nbl1	1.60E-30	0.620339537	0.694	0.864
Id1	1.94E-30	1.161381805	0.824	0.915
Hspa1a	1.62E-29	0.584306777	0.732	0.907
Gm26825	6.00E-29	0.892972412	0.012	0.266
Gm11361	6.48E-29	0.472244255	0.045	0.322
Rpl29	8.27E-29	0.447609296	0.969	0.975
Bdnf	5.52E-28	0.807731955	0.221	0.555
Eef2	6.16E-28	0.401980083	0.991	0.998
G0s2	7.11E-28	1.021575843	0.007	0.252
Col12a1	7.78E-28	0.780645174	0.226	0.507
Rps28	3.62E-27	0.362138716	0.986	0.997
Rpl12	5.06E-27	0.362446309	0.991	0.991
Klf10	1.01E-26	0.982695511	0.56	0.737
Slc38a2	2.54E-25	0.658890532	0.993	1
Fam129a	1.08E-24	0.486612312	0.075	0.344
Id3	1.52E-24	0.883078817	0.962	0.976
Nxn	2.37E-24	0.537259553	0.652	0.799

Tekt2	2.57E-24	0.486941871	0.073	0.327
AC160336.	5.05E-24	0.925390789	0.096	0.352
Hspa1b	5.18E-24	0.374584754	0.824	0.959
Laptm4a	6.61E-24	0.438913014	0.906	0.939
Nr4a1	1.23E-23	0.913650743	0.824	0.897
Serpina3g	3.44E-23	0.581934664	0.094	0.355
Cap1	1.73E-22	0.515423635	0.376	0.624
Fgfr1	1.25E-21	0.546360414	0.732	0.86
Jund	1.60E-21	0.554912733	0.988	0.993
Egr1	2.04E-21	0.742035754	0.868	0.95
Fzd2	1.18E-20	0.551478575	0.696	0.839
Camk4	4.57E-20	0.461820531	0.129	0.371
Dapk2	6.15E-20	0.507546032	0.511	0.737
Ltbp2	2.13E-19	0.480100838	0.195	0.45
Socs2	2.50E-19	0.457944421	0.071	0.289
Fam213a	2.78E-19	0.507310088	0.388	0.619
Ddit4	5.83E-19	0.607234907	0.059	0.269
Gas1	7.19E-19	0.501407725	0.701	0.878
Igfbp3	4.00E-18	1.182343311	0.445	0.651
Ier3	1.33E-17	0.778597831	0.922	0.962
H2-D1	1.46E-17	0.443669291	0.936	0.978
Ly6e	2.10E-17	0.386152049	0.028	0.205
Elavl2	2.16E-17	0.414583963	0.002	0.157
Cyb5r3	2.54E-17	0.457262162	0.833	0.9
Mfge8	2.66E-17	0.566729668	0.261	0.488
Hoxb9	4.74E-17	0.515402851	0.148	0.37
Selenof	1.30E-16	0.416583643	0.779	0.861
Fgfbp1	1.90E-16	0.416821947	0.304	0.547
Sik1	2.05E-16	0.553915235	0.553	0.72
Tbx1	3.27E-16	0.447752767	0.553	0.757
S100a4	3.97E-16	0.643228519	0.765	0.881
Fxyd6	4.34E-16	0.587461602	0.416	0.603
Ifitm3	6.75E-16	0.430879475	0.647	0.792
Ier2	9.55E-16	0.781413392	0.873	0.9
Stard4	1.43E-15	0.383434127	0.085	0.27
Sertad4	2.25E-15	0.373634445	0.165	0.383
Cdh13	2.44E-15	0.452306173	0.574	0.738
Tspo	3.50E-15	0.382686555	0.864	0.897
Bhlhe40	4.16E-15	0.797827784	0.325	0.528
Pik3r1	4.98E-15	0.457476162	0.449	0.654
Acot1	1.39E-14	0.502765766	0.344	0.546
Igfbp6	1.67E-14	0.450872014	0.278	0.491
Btg2	1.74E-14	0.808110067	0.92	0.937
Tob1	2.12E-14	0.64814062	0.849	0.897
Eif4b	2.39E-14	0.38238921	0.689	0.813

Ctsl	8.45E-14	0.591616493	0.671	0.813
Cited2	2.45E-13	0.912337556	0.678	0.809
Krt24	5.22E-13	0.459404063	0.661	0.881
Ldlr	5.41E-13	0.48920599	0.348	0.555
Cryab	7.60E-13	0.528787311	0.336	0.531
Crabp1	9.05E-13	0.378703815	0.016	0.144
Ephx1	9.75E-13	0.365798514	0.584	0.725
Irx3	1.60E-12	0.428485263	0.339	0.519
Fos	6.39E-12	0.495551122	0.899	0.963
Dusp1	6.61E-12	0.667202251	0.833	0.924
Auts2	1.08E-11	0.424950694	0.362	0.535
Jun	1.41E-11	0.487873161	0.969	0.979
Insig1	1.73E-11	0.553690183	0.228	0.4
Cd47	1.91E-11	0.391251757	0.755	0.844
Ch25h	2.20E-11	0.58927455	0.042	0.173
Plpp3	6.97E-11	0.402873543	0.433	0.615
Dnaja4	7.11E-11	0.535294997	0.504	0.664
Tgfb1	8.91E-11	0.374689769	0.231	0.4
Igfbp7	9.06E-11	0.422935816	0.56	0.71
Hoxb6	9.10E-11	0.370107295	0.186	0.353
Sorl1	2.07E-10	0.366658931	0.332	0.499
Scx	2.31E-10	0.47497942	0.336	0.504
Fcgbp	5.42E-10	0.380861958	0.546	0.707
Junb	8.99E-10	0.559306647	0.934	0.953
Zfp36l1	1.24E-09	0.489357628	0.934	0.957
Bbc3	2.00E-09	0.396001844	0.224	0.376
Trim59	2.32E-09	0.426584252	0.296	0.448
Ptges	5.18E-09	0.452498663	0.169	0.312
Gem	6.81E-09	0.660796976	0.438	0.585
Nfil3	7.98E-09	0.370838168	0.518	0.637
Slc6a6	8.78E-09	0.604678637	0.849	0.925
Pdzrn4	1.61E-08	0.440527915	0.475	0.605
Iffo2	4.11E-08	0.670250142	0.786	0.839
Vdr	5.62E-08	0.375398492	0.586	0.663
Irx5	1.54E-07	0.387432605	0.532	0.645
Maff	2.96E-07	0.673509612	0.612	0.673
Txnip	6.04E-07	0.397096388	0.513	0.631
Nog	7.35E-07	0.400755816	0.402	0.511
Plk3	1.48E-06	0.373132738	0.322	0.443
Ovol1	9.16E-06	0.637055141	0.299	0.403
Serpinh1	2.11E-05	0.414556353	0.765	0.788
Atf3	3.00E-05	0.427220319	0.904	0.906
Ncoa4	0.000409	0.496344464	0.445	0.514
Nr4a2	0.000879	0.479655932	0.334	0.425
Nr4a3	0.001392	0.456803587	0.372	0.429

Hmgcs1	0.002849	0.434324802	0.593	0.626

Supplementary Table 3. Differentially Expressed Genes in Foxc1 cKO HF-SCs.

	baseMean	log2FoldCh	lfcSE	stat	pvalue	padj
Eif2s3y	429.075	-25.38751	4.784867	-5.305793	1.12E-07	1.98E-05
Foxc1	1419.97	-8.35886	0.649777	-12.86419	7.16E-38	9.71E-34
Chst13	24.70943	-7.954108	1.80735	-4.400979	1.08E-05	0.000974
Ccnb1ip1	22.18383	-7.799268	1.777003	-4.389001	1.14E-05	0.001009
Sphkap	179.2693	-7.411228	1.091067	-6.792645	1.10E-11	6.79E-09
Atp2a3	737.1937	-7.010119	1.342322	-5.222381	1.77E-07	2.82E-05
Kcnd3	12.24304	-6.941632	1.935243	-3.586956	0.000335	0.014586
Grik1	34.09759	-5.870123	1.551543	-3.783409	0.000155	0.008161
Tgm5	3734.793	-5.296973	0.512009	-10.34547	4.39E-25	2.97E-21
Adcy1	1350.288	-5.252348	0.657432	-7.989188	1.36E-15	1.53E-12
Opcml	49.5987	-5.17924	1.216664	-4.256919	2.07E-05	0.001683
Krt24	7601.544	-4.895181	0.553038	-8.851436	8.64E-19	1.46E-15
Slc13a4	20.35729	-4.620413	1.329466	-3.47539	0.00051	0.020048
Ednra	361.4581	-4.553555	0.733124	-6.211168	5.26E-10	1.93E-07
Scn5a	49.21572	-4.527534	0.87353	-5.183031	2.18E-07	3.40E-05
Gfra1	3366.322	-4.483301	0.525311	-8.534565	1.41E-17	1.73E-14
Chat	336.2668	-4.421112	0.585472	-7.55137	4.31E-14	3.65E-11
Nptx1	503.3179	-4.341945	0.720567	-6.025733	1.68E-09	5.19E-07
Hid1	93.67629	-4.33107	0.728753	-5.943127	2.80E-09	8.24E-07
Ngef	150.5315	-4.259039	0.550144	-7.741673	9.81E-15	1.02E-11
Trpm3	55.0574	-4.245226	0.8978	-4.728475	2.26E-06	0.000251
Camk4	1260.042	-4.22138	1.206094	-3.500042	0.000465	0.018885
Dhrs2	120.4289	-4.166433	0.63616	-6.549348	5.78E-11	2.45E-08
Mir7014	21.93144	-4.160767	1.24129	-3.35197	0.000802	0.028259
Myoc	245.5352	-4.027177	0.605942	-6.646137	3.01E-11	1.43E-08
8430436N(	23.23306	-3.98784	1.156313	-3.448754	0.000563	0.021694
Wdfy4	65.18455	-3.987481	1.076164	-3.705273	0.000211	0.010536
Col6a1	3728.138	-3.946752	0.443137	-8.906384	5.27E-19	1.02E-15
Fam171b	188.9935	-3.923609	0.62734	-6.254356	3.99E-10	1.50E-07
Mme	129.2645	-3.893945	0.715615	-5.441393	5.29E-08	1.05E-05
Smad9	58.9013	-3.845155	0.935957	-4.108262	3.99E-05	0.002848
Galnt15	32.61854	-3.844523	0.931262	-4.128292	3.65E-05	0.002693
Ccdc88c	568.4375	-3.824062	0.440249	-8.686131	3.75E-18	5.65E-15
Sncg	58.95061	-3.717855	0.941466	-3.949008	7.85E-05	0.004926
Hhip	187.5331	-3.708738	0.670854	-5.528383	3.23E-08	6.96E-06
Col4a3	100.0191	-3.665954	0.74846	-4.897997	9.68E-07	0.000129
Pcsk6	2145.841	-3.648753	0.408984	-8.921514	4.60E-19	1.02E-15
Syt9	47.34569	-3.595026	1.09425	-3.285379	0.001018	0.034784
Serpinb3b	114.435	-3.592423	0.646487	-5.556837	2.75E-08	6.21E-06
Me3	32.01877	-3.557895	0.921504	-3.860965	0.000113	0.006601
Rnf112	35.62492	-3.549317	0.98572	-3.600735	0.000317	0.014153

Fgf18	93.40289	-3.5203	0.719854	-4.890298	1.01E-06	0.000132
Ptger1	32.30482	-3.47704	0.889181	-3.910386	9.21E-05	0.005617
Col4a4	174.176	-3.436445	0.602519	-5.703459	1.17E-08	2.89E-06
Abhd12b	106.9221	-3.414494	0.606819	-5.626874	1.84E-08	4.37E-06
Spink2	32.9517	-3.367747	0.904296	-3.724164	0.000196	0.009952
Lrat	848.4434	-3.361214	0.468125	-7.180157	6.96E-13	5.55E-10
Atoh8	174.0231	-3.349125	0.505557	-6.624628	3.48E-11	1.57E-08
Nog	259.2369	-3.34419	0.580365	-5.762221	8.30E-09	2.18E-06
Grem1	528.5941	-3.340674	0.556808	-5.999688	1.98E-09	5.96E-07
Fam46c	1475.369	-3.326885	0.512261	-6.494517	8.33E-11	3.32E-08
Fam19a5	65.94332	-3.320368	0.955149	-3.476281	0.000508	0.020048
Crlf1	752.1876	-3.300451	0.363912	-9.069367	1.20E-19	3.25E-16
Nt5e	4535.262	-3.283584	0.502544	-6.533922	6.41E-11	2.63E-08
Bdnf	476.2332	-3.266538	0.593134	-5.507254	3.64E-08	7.72E-06
Ramp3	310.5794	-3.246275	0.596578	-5.441493	5.28E-08	1.05E-05
Msrb2	49.99276	-3.183593	0.893166	-3.564391	0.000365	0.015599
Eml1	144.3364	-3.164357	0.636572	-4.970934	6.66E-07	9.23E-05
Wfdc21	41.27382	-3.158637	0.849469	-3.718367	0.000201	0.01011
Klk13	68.67818	-3.15168	0.771316	-4.086108	4.39E-05	0.003056
Pappa2	39.29997	-3.141149	0.913472	-3.43869	0.000585	0.022016
Cacna1c	349.5071	-3.115332	0.548237	-5.68246	1.33E-08	3.21E-06
Cacna2d2	165.6016	-3.043578	0.458146	-6.643249	3.07E-11	1.43E-08
Guca2a	119.9167	-3.037451	0.609105	-4.986745	6.14E-07	8.67E-05
Pvt1	82.26476	-3.035727	0.808987	-3.752504	0.000175	0.009095
Stfa3	795.9677	-3.017976	0.538554	-5.603851	2.10E-08	4.90E-06
Mitf	462.0016	-3.013835	0.598308	-5.037262	4.72E-07	6.81E-05
Ache	56.15276	-3.007503	0.778037	-3.865498	0.000111	0.006507
Slc38a3	328.4952	-3.004231	0.480154	-6.256802	3.93E-10	1.50E-07
Pcolce2	129.0677	-2.987253	0.738088	-4.047286	5.18E-05	0.003513
Slc39a8	725.0885	-2.981908	0.554352	-5.379089	7.49E-08	1.39E-05
Alox8	119.7417	-2.953695	0.601171	-4.913236	8.96E-07	0.00012
Serpinb11	1318.421	-2.935843	0.512077	-5.733207	9.85E-09	2.47E-06
Atp6v0e2	113.0263	-2.92665	0.675823	-4.330499	1.49E-05	0.001285
Krt83	64.74443	-2.910898	0.904578	-3.217961	0.001291	0.040996
Tnfrsf11b	999.9396	-2.898838	0.594481	-4.876253	1.08E-06	0.000136
Igfbp5	3041.045	-2.878134	0.412792	-6.972358	3.12E-12	2.11E-09
Fam25c	897.1871	-2.875645	0.554138	-5.189397	2.11E-07	3.33E-05
Ano1	240.7863	-2.863779	0.640121	-4.473811	7.68E-06	0.00076
Lepr	41.46189	-2.861442	0.867721	-3.297653	0.000975	0.033638
Mrgprf	497.9876	-2.857074	0.423968	-6.738894	1.60E-11	9.41E-09
Ptges	1318.233	-2.839621	0.526799	-5.390332	7.03E-08	1.32E-05
Cpa4	1404.054	-2.838357	0.399063	-7.112557	1.14E-12	8.58E-10
Ogdhl	121.5313	-2.831525	0.694025	-4.079863	4.51E-05	0.003102

Tspan2	327.1922	-2.818347	0.742677	-3.794847	0.000148	0.007997
Npas2	165.0548	-2.813373	0.583044	-4.82532	1.40E-06	0.000166
Prkcz	61.82769	-2.806275	0.701817	-3.998583	6.37E-05	0.004114
Krt80	2144.848	-2.802398	0.504583	-5.553883	2.79E-08	6.21E-06
Lrrn3	146.7244	-2.796787	0.797257	-3.508012	0.000451	0.018606
Ereg	212.6154	-2.79217	0.529078	-5.277424	1.31E-07	2.22E-05
Vwa2	2200.293	-2.754962	0.36049	-7.64227	2.13E-14	2.07E-11
Cystm1	236.5787	-2.741139	0.572989	-4.783926	1.72E-06	0.000201
Aff3	320.7229	-2.737527	0.515804	-5.307305	1.11E-07	1.98E-05
Gm7694	183.4865	-2.701782	0.488322	-5.532786	3.15E-08	6.89E-06
Clic3	532.1396	-2.630401	0.540901	-4.862996	1.16E-06	0.000144
Adamts17	195.188	-2.603582	0.717343	-3.629479	0.000284	0.013076
Selenbp1	136.5128	-2.597931	0.535227	-4.853889	1.21E-06	0.000147
Ccdc27	79.34269	-2.592186	0.60283	-4.300032	1.71E-05	0.001429
Ngf	5636.483	-2.590651	0.537004	-4.82427	1.41E-06	0.000166
Tmem108	59.09001	-2.589449	0.629768	-4.111751	3.93E-05	0.002847
Zbtb16	389.2769	-2.575171	0.678751	-3.793986	0.000148	0.007997
Mt4	161.7986	-2.571538	0.624172	-4.119919	3.79E-05	0.002778
Tslp	205.8015	-2.566597	0.502518	-5.107471	3.26E-07	4.86E-05
Paqr5	312.4196	-2.563222	0.560144	-4.576004	4.74E-06	0.000506
Npnt	8487.749	-2.561414	0.516435	-4.959797	7.06E-07	9.66E-05
Sh3gl2	54.81095	-2.549055	0.805201	-3.165738	0.001547	0.04724
Esyt3	696.0739	-2.516587	0.361864	-6.954503	3.54E-12	2.28E-09
Phospho1	571.4245	-2.501935	0.512093	-4.885702	1.03E-06	0.000133
Anpep	1414.509	-2.498431	0.628293	-3.976541	6.99E-05	0.004435
Slc45a2	36.28835	-2.496485	0.77003	-3.242062	0.001187	0.038959
Flg2	354.0145	-2.492913	0.371554	-6.709427	1.95E-11	1.09E-08
Sms	101.8078	-2.485565	0.562032	-4.422461	9.76E-06	0.0009
Nos1ap	41.72225	-2.448653	0.762477	-3.211446	0.001321	0.041762
Antxr1	2177.364	-2.412249	0.485291	-4.970727	6.67E-07	9.23E-05
Kcnc4	161.8465	-2.377533	0.592162	-4.015005	5.94E-05	0.003943
Hddc3	246.3839	-2.367163	0.564412	-4.194032	2.74E-05	0.002111
Ankrd35	301.4353	-2.365683	0.579186	-4.084498	4.42E-05	0.003056
Tgm7	96.47531	-2.350621	0.576628	-4.076495	4.57E-05	0.003131
Syngr1	103.9968	-2.343647	0.642202	-3.649393	0.000263	0.012419
Serpina12	59.47027	-2.328002	0.633723	-3.67353	0.000239	0.011543
Krt36	105.5657	-2.323564	0.566412	-4.102252	4.09E-05	0.002889
Ptpre	289.2722	-2.313472	0.38316	-6.037878	1.56E-09	5.04E-07
Nrep	4210.18	-2.302441	0.511142	-4.504499	6.65E-06	0.000673
Trpm1	211.4134	-2.295149	0.484514	-4.737018	2.17E-06	0.000243
Tyr	81.61735	-2.286319	0.582401	-3.92568	8.65E-05	0.005379
Lgr6	337.954	-2.25961	0.465268	-4.856575	1.19E-06	0.000147
Sgcd	93.60546	-2.257976	0.656902	-3.437308	0.000588	0.022067

Tjp3	144.7082	-2.254536	0.654745	-3.443379	0.000574	0.021767
Igf2bp3	48.83914	-2.251949	0.69598	-3.235653	0.001214	0.039463
Bmp2	1044.307	-2.240725	0.341719	-6.557224	5.48E-11	2.40E-08
Aqp3	33806.8	-2.222184	0.332368	-6.685925	2.29E-11	1.15E-08
Nkd1	153.7003	-2.211544	0.530994	-4.164911	3.11E-05	0.002386
Ramp1	271.8273	-2.193136	0.619604	-3.539575	0.000401	0.016981
Dmkn	28552.94	-2.175717	0.372604	-5.839223	5.24E-09	1.45E-06
Klk10	507.5091	-2.17232	0.454763	-4.776819	1.78E-06	0.000205
Camkk1	720.9271	-2.163947	0.443858	-4.875318	1.09E-06	0.000136
Mira	421.5973	-2.161592	0.620102	-3.485865	0.000491	0.019505
Gal3st1	230.0781	-2.159757	0.560201	-3.855322	0.000116	0.006697
Duox1	724.9357	-2.157875	0.32184	-6.704812	2.02E-11	1.09E-08
Mlana	91.40174	-2.153418	0.653701	-3.294193	0.000987	0.033882
Arhgap44	987.7042	-2.153003	0.366011	-5.882346	4.04E-09	1.17E-06
S100a4	4792.152	-2.145554	0.34836	-6.159012	7.32E-10	2.61E-07
Dap	1635.247	-2.144048	0.480946	-4.457979	8.27E-06	0.00079
Cadm1	2940.067	-2.141544	0.415908	-5.149083	2.62E-07	3.94E-05
Avpr1a	111.4936	-2.131426	0.650682	-3.275678	0.001054	0.035498
Krt75	1418.521	-2.130759	0.547348	-3.892878	9.91E-05	0.005917
Dapl1	2014.949	-2.123707	0.530295	-4.004766	6.21E-05	0.004047
Krt15	163201.1	-2.116619	0.44265	-4.7817	1.74E-06	0.000201
Psors1c2	65.72389	-2.115498	0.626603	-3.376136	0.000735	0.026369
Enpp2	157.2814	-2.111445	0.566404	-3.727806	0.000193	0.009846
Skint3	109.1144	-2.109576	0.493398	-4.275608	1.91E-05	0.001566
Dkkl1	130.3577	-2.109348	0.583256	-3.616504	0.000299	0.013451
Adamtsl4	1723.912	-2.102389	0.383745	-5.478602	4.29E-08	8.94E-06
Col8a2	681.7383	-2.100417	0.614119	-3.420212	0.000626	0.023061
Robo2	516.5297	-2.09442	0.521201	-4.018445	5.86E-05	0.003913
Ltbp1	1228.301	-2.092745	0.477932	-4.378752	1.19E-05	0.001051
Tekt2	1062.818	-2.092205	0.502813	-4.161001	3.17E-05	0.002399
Hspb8	9075.489	-2.090484	0.437917	-4.773702	1.81E-06	0.000206
Ptn	5698.688	-2.089704	0.359399	-5.814443	6.08E-09	1.65E-06
Trim2	799.8507	-2.085058	0.422792	-4.931643	8.15E-07	0.000111
Cnksr3	5702.874	-2.073001	0.296147	-6.999907	2.56E-12	1.83E-09
Moxd1	7585.187	-2.07202	0.426923	-4.853383	1.21E-06	0.000147
Sh3rf2	388.6429	-2.067664	0.463004	-4.465762	7.98E-06	0.000767
Papln	837.0912	-2.065334	0.35851	-5.76088	8.37E-09	2.18E-06
Scel	3092.701	-2.060535	0.441733	-4.664659	3.09E-06	0.000335
Col6a2	1189.893	-2.055071	0.376847	-5.453331	4.94E-08	1.02E-05
Calml3	10096.82	-2.049383	0.457681	-4.477753	7.54E-06	0.000752
Asap2	674.3501	-2.044289	0.418098	-4.889501	1.01E-06	0.000132
Mfap3l	1173.419	-2.044142	0.458892	-4.454522	8.41E-06	0.000792
Cadm4	118.5052	-2.041079	0.59759	-3.415519	0.000637	0.023266

Unc13b	242.1811	-2.037707	0.506551	-4.022709	5.75E-05	0.003874
Ank	6244.985	-2.037105	0.500396	-4.070984	4.68E-05	0.00319
Kif26a	257.2406	-2.032133	0.472076	-4.304669	1.67E-05	0.001408
Gdpd2	187.3624	-2.030944	0.620584	-3.272631	0.001066	0.035761
Lce1m	141.3733	-2.024839	0.526749	-3.844027	0.000121	0.006809
Anxa8	22107.38	-2.019219	0.466666	-4.326903	1.51E-05	0.001298
Inpp4b	511.8687	-2.019148	0.48539	-4.159844	3.18E-05	0.002399
Rarres1	119.2976	-2.016452	0.580027	-3.476477	0.000508	0.020048
Myh14	5205.58	-2.010942	0.300378	-6.694702	2.16E-11	1.13E-08
Zfhx3	129.7236	-2.007726	0.485583	-4.134669	3.55E-05	0.002648
Prkaa2	278.5826	-2.006246	0.572507	-3.504319	0.000458	0.018733
Rnf208	804.1477	-1.982454	0.369167	-5.370079	7.87E-08	1.44E-05
Fmn1	336.2565	-1.969491	0.56735	-3.471388	0.000518	0.02029
Cdc42ep1	1538.265	-1.969242	0.354395	-5.556635	2.75E-08	6.21E-06
Fgf1	279.1826	-1.963171	0.54935	-3.573623	0.000352	0.015203
Sema3d	150.6889	-1.956626	0.615195	-3.180498	0.00147	0.045703
Klk8	277.6079	-1.955458	0.437324	-4.471419	7.77E-06	0.000762
Tns1	5496.281	-1.953151	0.321447	-6.076118	1.23E-09	4.17E-07
Serpinb10	708.736	-1.951635	0.451638	-4.321239	1.55E-05	0.001315
Them5	3930.609	-1.947062	0.601319	-3.237986	0.001204	0.03933
Nt5dc2	976.1523	-1.94247	0.439525	-4.419479	9.89E-06	0.000906
Sgms2	5020.92	-1.938171	0.523154	-3.704779	0.000212	0.010536
Crispld1	356.659	-1.930732	0.494018	-3.908223	9.30E-05	0.005617
S100a3	409.9425	-1.91593	0.407634	-4.700127	2.60E-06	0.000287
Ptgds	211.6247	-1.911651	0.524096	-3.64752	0.000265	0.012466
Pdlim3	1008.514	-1.897137	0.522894	-3.628148	0.000285	0.013076
Nrtn	246.3703	-1.892761	0.473532	-3.997116	6.41E-05	0.00412
Lypd6	244.0401	-1.890557	0.59839	-3.159407	0.001581	0.048041
Gpt	740.3211	-1.889081	0.520436	-3.629809	0.000284	0.013076
Tmem45a	1704.616	-1.887027	0.415309	-4.543675	5.53E-06	0.000572
Marveld3	372.5234	-1.886763	0.433296	-4.354446	1.33E-05	0.001167
Dct	1205.044	-1.878347	0.411491	-4.564739	5.00E-06	0.000522
Cdon	1347.762	-1.872752	0.347002	-5.396949	6.78E-08	1.29E-05
Trim16	1342.545	-1.870411	0.346349	-5.40036	6.65E-08	1.29E-05
Dnph1	215.2314	-1.854533	0.537733	-3.448797	0.000563	0.021694
Lor	1739.876	-1.852537	0.379425	-4.88249	1.05E-06	0.000134
Ankrd29	281.4562	-1.84398	0.449345	-4.103705	4.07E-05	0.002886
Tyrp1	429.7793	-1.836527	0.412121	-4.456283	8.34E-06	0.000791
Hoxa7	206.7001	-1.834217	0.574387	-3.193346	0.001406	0.044038
Aloxe3	572.545	-1.819673	0.504137	-3.609477	0.000307	0.013775
Sostdc1	4296.333	-1.818462	0.360782	-5.040335	4.65E-07	6.78E-05
Wif1	398.2032	-1.817576	0.44497	-4.08472	4.41E-05	0.003056
Fam213a	388.2367	-1.812836	0.481905	-3.761812	0.000169	0.008831

Skint4	521.8824	-1.802885	0.518736	-3.475533	0.00051	0.020048
Gjb4	4294.886	-1.80234	0.471648	-3.821368	0.000133	0.007316
Neu2	890.0133	-1.799925	0.572056	-3.146414	0.001653	0.049692
Hrnr	140.4803	-1.792886	0.537464	-3.335826	0.00085	0.02972
Cdh13	362.2246	-1.782157	0.470163	-3.790508	0.00015	0.007997
Aldh3a1	228.9741	-1.774366	0.455961	-3.891483	9.96E-05	0.005925
Ecm1	8482.581	-1.771561	0.302668	-5.853144	4.82E-09	1.36E-06
Cyp4b1	643.5928	-1.765539	0.502397	-3.514232	0.000441	0.018343
Gsdma3	342.3704	-1.760869	0.517865	-3.40025	0.000673	0.024531
Pmel	732.7648	-1.757509	0.340094	-5.16772	2.37E-07	3.65E-05
Dpp4	135.3906	-1.742432	0.51254	-3.399603	0.000675	0.024531
Hopx	3306.906	-1.738239	0.45488	-3.821316	0.000133	0.007316
Bok	5408.138	-1.734407	0.394241	-4.39936	1.09E-05	0.000975
Slc16a2	600.3099	-1.714093	0.417258	-4.107996	3.99E-05	0.002848
Adrb2	3851.206	-1.711134	0.463502	-3.691755	0.000223	0.010941
Vit	193.1115	-1.698876	0.484869	-3.503783	0.000459	0.018733
Sulf2	1912.006	-1.696617	0.361176	-4.697482	2.63E-06	0.000288
Gpc6	785.6695	-1.693159	0.462763	-3.658805	0.000253	0.012098
Kprp	298.896	-1.682175	0.443799	-3.790399	0.00015	0.007997
Cysrt1	236.6806	-1.68088	0.475461	-3.535261	0.000407	0.017207
Rcan1	10433.07	-1.649818	0.398646	-4.138549	3.50E-05	0.002618
Tns4	27849.08	-1.645822	0.400633	-4.108055	3.99E-05	0.002848
Extl1	148.9703	-1.643195	0.51785	-3.173108	0.001508	0.046581
Sbsn	27128.34	-1.641249	0.37205	-4.41137	1.03E-05	0.000935
Tle4	2853.824	-1.639364	0.449923	-3.643656	0.000269	0.012611
Crct1	391.9135	-1.636883	0.363697	-4.500678	6.77E-06	0.00068
Krt35	1278.081	-1.61363	0.43643	-3.697341	0.000218	0.010781
Mfsd2a	465.2575	-1.609504	0.383761	-4.194025	2.74E-05	0.002111
Cry1	1237.523	-1.587307	0.369721	-4.293253	1.76E-05	0.001463
Spns2	137.9794	-1.556684	0.451241	-3.44978	0.000561	0.021694
Itgb6	3748.79	-1.556664	0.455352	-3.418597	0.000629	0.023129
Klk7	2965.542	-1.542287	0.292687	-5.269409	1.37E-07	2.29E-05
Prelp	597.8121	-1.53578	0.427307	-3.594088	0.000326	0.014284
Klk11	209.2073	-1.535117	0.410782	-3.737058	0.000186	0.009526
Efnb2	4748.157	-1.521643	0.401138	-3.793313	0.000149	0.007997
Egfl6	1435.33	-1.506759	0.465984	-3.2335	0.001223	0.039571
Nrcam	250.0435	-1.506247	0.423127	-3.559802	0.000371	0.015825
Net1	7055.002	-1.503368	0.351751	-4.273953	1.92E-05	0.001569
Emp1	55937.42	-1.493781	0.35363	-4.224137	2.40E-05	0.001902
Slc16a10	190.0606	-1.486819	0.439202	-3.385275	0.000711	0.02571
Tmem40	410.8895	-1.479126	0.386227	-3.829683	0.000128	0.007159
Pgm2l1	166.8875	-1.465018	0.462672	-3.166429	0.001543	0.047236
Ablim1	902.7079	-1.464912	0.374698	-3.909585	9.25E-05	0.005617

Gpnmb	526.1945	-1.449928	0.335258	-4.32481	1.53E-05	0.001302
Alox12b	169.2083	-1.449028	0.43069	-3.364431	0.000767	0.027297
Cgnl1	752.1862	-1.446906	0.362411	-3.992443	6.54E-05	0.004183
Arsb	229.4331	-1.445963	0.451991	-3.199099	0.001379	0.043269
Ttc39b	1022.5	-1.433913	0.417391	-3.435423	0.000592	0.022088
Ndrg4	409.4797	-1.433544	0.425281	-3.37082	0.000749	0.026741
Sdk2	436.9496	-1.429648	0.45226	-3.161117	0.001572	0.047888
Smarca2	4659.387	-1.426545	0.404581	-3.52598	0.000422	0.017766
Prnp	5583.699	-1.421305	0.336946	-4.218194	2.46E-05	0.001941
Nrip3	359.5317	-1.416888	0.384035	-3.689476	0.000225	0.011
Prlr	2020.842	-1.415832	0.386034	-3.667638	0.000245	0.01177
Peg3	479.7542	-1.413246	0.367408	-3.846527	0.00012	0.006809
Gmds	493.7995	-1.405198	0.341705	-4.112312	3.92E-05	0.002847
Adamtsl5	1322.621	-1.385238	0.35971	-3.850987	0.000118	0.006759
Klk5	226.9441	-1.378059	0.438082	-3.145666	0.001657	0.049709
Pard6b	1460.885	-1.374129	0.303167	-4.532582	5.83E-06	0.000599
Hmcn1	5899.925	-1.371063	0.340896	-4.021942	5.77E-05	0.003874
Krt25	805.7709	-1.358023	0.413853	-3.281413	0.001033	0.035078
Ppap2a	577.652	-1.354043	0.346512	-3.907631	9.32E-05	0.005617
Dedd2	1956.278	-1.347746	0.359704	-3.746818	0.000179	0.009233
Nppb	386.8461	-1.345894	0.353223	-3.810324	0.000139	0.007619
Pim2	178.1646	-1.345544	0.42319	-3.179526	0.001475	0.045703
Pacsin3	1479.412	-1.345489	0.391614	-3.435751	0.000591	0.022088
Hk2	6713.523	-1.338519	0.32399	-4.131358	3.61E-05	0.002672
Ak3	1520.42	-1.333363	0.355056	-3.755361	0.000173	0.009027
Wnt7b	711.1641	-1.329642	0.332393	-4.000209	6.33E-05	0.004106
Sema3e	2631.452	-1.323913	0.386416	-3.426134	0.000612	0.022681
Epb4.1l1	400.1938	-1.316033	0.374019	-3.518625	0.000434	0.018098
Ccdc3	1756.015	-1.312156	0.397817	-3.29839	0.000972	0.033635
Kank1	5827.399	-1.308316	0.286414	-4.567926	4.93E-06	0.000518
Cers5	1865.994	-1.307502	0.3592	-3.640042	0.000273	0.012745
Klrg2	374.3784	-1.307229	0.374673	-3.488989	0.000485	0.019393
1500015A0	522.2486	-1.303171	0.409398	-3.183141	0.001457	0.045515
Gphn	906.9396	-1.29699	0.378333	-3.42817	0.000608	0.022574
Pcdh7	2190.719	-1.29379	0.35658	-3.628328	0.000285	0.013076
Dhx32	785.7913	-1.291016	0.372837	-3.462682	0.000535	0.020838
Rufy4	375.0389	-1.282288	0.365291	-3.51032	0.000448	0.018552
Lamb3	11079.23	-1.27615	0.293538	-4.347485	1.38E-05	0.001197
Evpl	2851.577	-1.275763	0.290236	-4.39561	1.10E-05	0.000985
Hmox1	15136.16	-1.257403	0.348959	-3.6033	0.000314	0.01406
Unc5b	834.5773	-1.256649	0.326537	-3.848407	0.000119	0.006802
Fgd4	263.5129	-1.256457	0.384687	-3.266178	0.00109	0.036495
Rhbdl3	1172.727	-1.255099	0.341595	-3.674235	0.000239	0.011543

AI661453	2247.14	-1.246186	0.310747	-4.010287	6.06E-05	0.003972
Arhgap23	2622.802	-1.23964	0.321897	-3.851049	0.000118	0.006759
Rora	1730.973	-1.23674	0.340048	-3.636958	0.000276	0.01281
Calm4	1467.825	-1.229755	0.359816	-3.417735	0.000631	0.02314
Mdga1	2110.758	-1.220046	0.304095	-4.012058	6.02E-05	0.003962
Nfatc1	4767.913	-1.219701	0.36445	-3.346688	0.000818	0.028728
Ppif	8228.866	-1.213294	0.344789	-3.518943	0.000433	0.018098
E130012A1	1322.635	-1.195948	0.355885	-3.360486	0.000778	0.027617
Chd3os	416.8286	-1.194954	0.349388	-3.420136	0.000626	0.023061
Ttll7	324.2461	-1.194623	0.367233	-3.25304	0.001142	0.037939
Gm973	735.4196	-1.190092	0.333422	-3.569328	0.000358	0.015357
Igfbp6	904.7594	-1.182281	0.348855	-3.389033	0.000701	0.025428
Thrb	339.5216	-1.164137	0.362951	-3.207425	0.001339	0.042231
Kazn	960.4101	-1.151406	0.354465	-3.248292	0.001161	0.038395
Actb	80647.49	-1.146131	0.29461	-3.890338	0.0001	0.005927
Ankrd10	4232.118	-1.14309	0.318553	-3.588378	0.000333	0.014554
Zmynd19	519.3451	-1.140782	0.349526	-3.263799	0.001099	0.036713
Mafk	8383.896	-1.139769	0.313199	-3.639116	0.000274	0.012747
Enox1	1279.164	-1.139017	0.346936	-3.283072	0.001027	0.034982
Cldn4	3582.656	-1.130821	0.334828	-3.37732	0.000732	0.026325
Hsp90aa1	13414.7	-1.1235	0.326079	-3.44549	0.00057	0.021767
Ppp2r3a	3228.726	-1.113597	0.300204	-3.70947	0.000208	0.01043
Asprv1	2147.061	-1.085587	0.293979	-3.692731	0.000222	0.010939
Pcbp3	530.5666	-1.078886	0.334831	-3.222181	0.001272	0.040492
Txnrd3	1242.593	-1.076216	0.340695	-3.158881	0.001584	0.048041
Igfbp3	21526.2	-1.055214	0.325998	-3.236874	0.001208	0.039389
Actg1	40054.05	-1.026743	0.283547	-3.621065	0.000293	0.013305
Vps37b	8294.859	-1.012565	0.289634	-3.496022	0.000472	0.019057
Peli2	2189.095	-1.01166	0.320486	-3.156647	0.001596	0.048302
Tuba4a	8778.568	-0.917533	0.283685	-3.234335	0.001219	0.03955
Mbd1	1146.52	1.044323	0.315342	3.311719	0.000927	0.032155
Ucp2	109396.8	1.079314	0.34252	3.151103	0.001627	0.049119
Bcl2l11	1708.952	1.095272	0.338029	3.240173	0.001195	0.039124
Insig2	7446.583	1.110219	0.308722	3.596182	0.000323	0.014262
Scd2	2534.355	1.110987	0.334741	3.318943	0.000904	0.031415
Nlrp10	693.3173	1.120417	0.319244	3.509597	0.000449	0.018552
Igsf8	7484.494	1.126088	0.342415	3.28867	0.001007	0.034467
Slc35f6	1101.989	1.133321	0.328784	3.447008	0.000567	0.021711
Dnase2a	2005.917	1.137119	0.313531	3.626813	0.000287	0.0131
Acp5	2559.528	1.14416	0.332616	3.439878	0.000582	0.021981
Alg10b	666.8361	1.157404	0.32418	3.570254	0.000357	0.015351
Fam49a	1118.443	1.164836	0.325153	3.582423	0.00034	0.014747
Rasgef1b	1054.362	1.171017	0.36312	3.224875	0.00126	0.040302

Lrrc4	603.058	1.17531	0.340198	3.454779	0.000551	0.021397
Cd200	3855.651	1.195563	0.370571	3.226272	0.001254	0.040265
Bhlhe41	1096.712	1.222128	0.334115	3.657804	0.000254	0.012103
Dhrs3	2173.934	1.262265	0.383018	3.295579	0.000982	0.033801
D8Ertd82e	1282.471	1.266303	0.359268	3.524678	0.000424	0.017799
Irx4	3946.53	1.274096	0.338409	3.764956	0.000167	0.008754
Cpt2	333.6593	1.286805	0.371433	3.464434	0.000531	0.020762
Lacc1	486.93	1.316291	0.346	3.804312	0.000142	0.007743
Fads3	1274.803	1.32678	0.413159	3.211304	0.001321	0.041762
Hoxc13	3549.524	1.338059	0.412434	3.244298	0.001177	0.038749
Cd276	570.5913	1.347965	0.351659	3.833157	0.000127	0.007088
Eif4e3	608.4346	1.353501	0.347111	3.899327	9.65E-05	0.005787
Lgals9	1537.426	1.368317	0.417057	3.280887	0.001035	0.035078
Ddit4	5360.694	1.373425	0.43308	3.171297	0.001518	0.046766
Pmaip1	3587.82	1.375546	0.383676	3.585174	0.000337	0.014639
Mfge8	11470.82	1.385551	0.326449	4.244308	2.19E-05	0.001749
3632451O(	255.8435	1.395685	0.379087	3.681696	0.000232	0.01126
Sepp1	8274.716	1.396883	0.388583	3.594816	0.000325	0.014284
Stat1	1633.431	1.41319	0.357498	3.952998	7.72E-05	0.004867
Aknad1	175.9543	1.414258	0.431745	3.275679	0.001054	0.035498
Hilpda	4439.101	1.417018	0.425843	3.327559	0.000876	0.030538
Stard5	3972.592	1.443603	0.428222	3.371158	0.000749	0.026741
Rin2	2839.129	1.481435	0.455492	3.252384	0.001144	0.037939
Cxcl10	872.4623	1.50381	0.459121	3.275413	0.001055	0.035498
Gem	10535.74	1.572739	0.451065	3.48672	0.000489	0.0195
Casp4	126.8929	1.596763	0.489863	3.259611	0.001116	0.037167
Snn	1274.667	1.609545	0.347417	4.632887	3.61E-06	0.000388
Eid2	175.0569	1.615702	0.513101	3.148896	0.001639	0.049381
Lurap1l	364.5788	1.624475	0.396677	4.095205	4.22E-05	0.002963
Serpine2	798.2895	1.647759	0.31425	5.243468	1.58E-07	2.57E-05
Cmah	9884.321	1.664831	0.52516	3.170139	0.001524	0.046846
Mettl20	145.3667	1.666761	0.463022	3.599749	0.000319	0.01416
Nuak1	2492.094	1.669714	0.484288	3.447772	0.000565	0.021711
Wipi1	936.1793	1.704557	0.381387	4.469361	7.85E-06	0.000762
Ggact	344.052	1.706004	0.486702	3.505232	0.000456	0.018733
Afap1l1	271.5097	1.710447	0.43473	3.934503	8.34E-05	0.005209
Ncald	283.3014	1.713897	0.462702	3.704106	0.000212	0.010536
Ctsc	1945.289	1.72922	0.402878	4.292164	1.77E-05	0.001463
Tubb2b	1031.287	1.742728	0.519153	3.356864	0.000788	0.027835
Timp3	39646.03	1.745194	0.519785	3.357535	0.000786	0.027835
Ivl	3020.804	1.751499	0.517633	3.38367	0.000715	0.025792
Prr5l	222.6298	1.75474	0.509614	3.443275	0.000575	0.021767
Scrg1	2274.127	1.805789	0.50212	3.596328	0.000323	0.014262

Arrdc3	4175.37	1.825384	0.361517	5.049235	4.44E-07	6.54E-05
Gfra3	103.5438	1.869834	0.493668	3.787636	0.000152	0.008055
Tmem95	171.2313	1.88531	0.548884	3.434809	0.000593	0.022088
Mab21l3	408.1396	1.90296	0.490674	3.878254	0.000105	0.006202
Casp1	1792.169	1.918778	0.499074	3.844673	0.000121	0.006809
Prss12	422.227	1.923637	0.397386	4.840726	1.29E-06	0.000155
Meox1	130.1864	1.939163	0.555413	3.491392	0.000481	0.019276
AW011738	243.786	1.951539	0.46459	4.200566	2.66E-05	0.002075
Hist1h2bc	2189.635	1.985247	0.560808	3.539978	0.0004	0.016981
Has1	2820.62	1.997433	0.551466	3.622039	0.000292	0.013299
Ehd3	600.3051	2.030322	0.550496	3.688167	0.000226	0.011017
Prickle1	2205.748	2.034119	0.529024	3.845043	0.000121	0.006809
Mkx	59.38152	2.03783	0.627688	3.246566	0.001168	0.038535
1810011O1	3477.664	2.047921	0.339756	6.027629	1.66E-09	5.19E-07
Slc16a6	644.2481	2.084355	0.396156	5.261453	1.43E-07	2.36E-05
Dusp4	1076.076	2.088495	0.462497	4.515696	6.31E-06	0.000643
Ptpru	609.1837	2.125037	0.607459	3.498237	0.000468	0.018956
Lcn2	306.6298	2.178691	0.402746	5.409587	6.32E-08	1.24E-05
AU018091	203.5994	2.195922	0.600926	3.654234	0.000258	0.012229
Lrrn1	99.85966	2.236727	0.579626	3.858913	0.000114	0.006628
Adcy7	826.307	2.245615	0.528743	4.247086	2.17E-05	0.001738
Slc39a4	102.6454	2.265765	0.678655	3.33861	0.000842	0.0295
Actn3	45.21925	2.279258	0.70573	3.229647	0.001239	0.040013
Dclk1	359.8375	2.283822	0.454228	5.027922	4.96E-07	7.08E-05
Adamts15	60.8996	2.334983	0.737421	3.166417	0.001543	0.047236
Adamts4	335.3282	2.33661	0.667466	3.500715	0.000464	0.018885
Dnmt3l	76.57002	2.342093	0.58901	3.976322	7E-05	0.004435
Hist1h1c	3522.658	2.344813	0.598587	3.917245	8.96E-05	0.005495
Astn2	87.62213	2.352389	0.632654	3.718288	0.000201	0.01011
Car12	13570.57	2.385195	0.388244	6.143549	8.07E-10	2.81E-07
Cdkn2b	306.8094	2.386846	0.522161	4.57109	4.85E-06	0.000514
Ppp1r3b	1961.131	2.3911	0.445469	5.367596	7.98E-08	1.44E-05
Cd14	497.4416	2.440982	0.467266	5.223968	1.75E-07	2.82E-05
Gstp2	51.47349	2.45613	0.655944	3.744419	0.000181	0.009286
Olfml3	253.2299	2.467998	0.658354	3.748741	0.000178	0.009198
Trf	6407.388	2.485521	0.432527	5.746513	9.11E-09	2.33E-06
Thap6	611.948	2.491525	0.63499	3.923725	8.72E-05	0.005398
Lyz2	228.7426	2.504626	0.63867	3.921629	8.8E-05	0.005421
Pld4	107.859	2.534856	0.668661	3.790943	0.00015	0.007997
Htra1	3184.817	2.574478	0.486522	5.291602	1.21E-07	2.08E-05
Ucp3	45.67352	2.600755	0.806231	3.225818	0.001256	0.040265
Gprin3	49.87638	2.619088	0.723654	3.619255	0.000295	0.013353
Lilrb4a	44.15011	2.639905	0.830344	3.179291	0.001476	0.045703

Gsr	2239.445	2.650139	0.437791	6.053429	1.42E-09	4.69E-07
Serpinf1	741.4509	2.76712	0.623768	4.436138	9.16E-06	0.000851
Tll1	271.3066	2.837385	0.550008	5.158808	2.49E-07	3.79E-05
Itga8	86.48385	2.87117	0.683264	4.202137	2.64E-05	0.002072
Hist1h4i	93.14613	2.890954	0.827361	3.494188	0.000476	0.019132
Syn3	340.3864	2.904358	0.610076	4.760651	1.93E-06	0.000218
Batf3	48.02232	2.943704	0.733304	4.014303	5.96E-05	0.003943
Mmp12	68.49214	2.961236	0.711478	4.16209	3.15E-05	0.002399
Sstr1	92.19713	2.973929	0.863641	3.443478	0.000574	0.021767
Alpl	317.4526	3.030107	0.678079	4.468665	7.87E-06	0.000762
Cntn2	1108.247	3.170894	0.328388	9.655927	4.64E-22	2.1E-18
Lmo2	31.39435	3.238824	0.851243	3.804816	0.000142	0.007743
Lyz1	31.13521	3.497946	1.083705	3.227764	0.001248	0.040182
Cyp26a1	58.1838	3.576193	0.804025	4.447865	8.67E-06	0.000811
Serpina3i	116.2732	3.584544	0.937263	3.82448	0.000131	0.007282
Dscam	25.21678	3.621742	1.131171	3.201765	0.001366	0.04297
Aldh1a2	496.3459	3.62947	0.420401	8.633354	5.96E-18	8.08E-15
Tmem151b	109.9201	3.656666	0.998742	3.661272	0.000251	0.012024
Amer2	30.35051	3.996443	1.240007	3.222919	0.001269	0.040483
Gm20744	44.55565	4.088475	0.962319	4.248568	2.15E-05	0.001736
Pcp4	290.0879	4.135414	0.547504	7.553219	4.25E-14	3.65E-11
Cybb	22.48278	4.20452	1.322446	3.179352	0.001476	0.045703
Slc4a4	383.6727	5.039851	0.524174	9.614842	6.92E-22	2.35E-18
Srd5a2	64.66566	6.698083	1.264254	5.298051	1.17E-07	2.03E-05

Supplementary Table 4. Differentially Expressed Genes in Nfatc1 cKO HF-SCs.

	baseMean	log2FoldCha	lfcSE	stat	pvalue	padj
Slc22a3	181.0191	-10.808898	1.68718	-6.406488	1.49E-10	6.46E-08
Kcnk10	84.72062	-9.7136261	1.894064	-5.128458	2.92E-07	4.68E-05
Kcnd3	72.10404	-9.4807626	1.860046	-5.097058	3.45E-07	5.24E-05
Rab17	71.00791	-9.4584018	1.86654	-5.067345	4.03E-07	6.01E-05
Grik1	70.42835	-9.4468698	2.774538	-3.404844	0.00066	0.02719
Xlr4b	58.91092	-9.1891794	1.936135	-4.746146	2.07E-06	0.00024
Kirrel2	50.20144	-8.958719	2.154448	-4.158242	3.21E-05	0.00257
Dhrs2	128.1004	-8.8480865	1.649601	-5.363774	8.15E-08	1.65E-05
Glrb	122.4943	-8.829794	1.750376	-5.044514	4.55E-07	6.57E-05
Lrrc18	44.94199	-8.7990488	2.184358	-4.028208	5.62E-05	0.00391
Trpm3	206.3426	-8.5594283	1.411786	-6.062835	1.34E-09	4.29E-07
Spock1	37.71451	-8.5461491	2.442995	-3.498226	0.00047	0.02179
Itga4	36.77751	-8.5097616	2.249121	-3.783595	0.00015	0.00904
Cdh4	36.40689	-8.4949958	2.202899	-3.856279	0.00012	0.00716
Grin3a	35.51157	-8.4583246	2.559496	-3.304683	0.00095	0.03574
Lancl3	33.15055	-8.3597955	2.257668	-3.702845	0.00021	0.01191
Mmp28	32.83077	-8.345997	2.323272	-3.592346	0.00033	0.01638
A330035P11Rik	32.80432	-8.3442381	2.25979	-3.692483	0.00022	0.01226
Col27a1	32.73112	-8.3415758	2.307234	-3.6154	0.0003	0.0153
D030025P21Rik	32.19272	-8.3175256	2.282185	-3.644545	0.00027	0.01421
D330023K18Rik	31.0249	-8.2635853	2.344686	-3.524389	0.00042	0.02019
Kcnh2	30.93594	-8.2599519	2.291661	-3.604351	0.00031	0.0158
Snhg11	30.2384	-8.2266608	2.326204	-3.536517	0.00041	0.01947
Nav3	29.93946	-8.21218	2.37932	-3.451482	0.00056	0.02463
Klk14	71.66648	-8.0564555	1.817882	-4.431781	9.35E-06	0.00092
Odf3l1	25.74817	-7.9950511	2.41969	-3.304163	0.00095	0.03574
Pcdhb3	24.30786	-7.9118021	2.471346	-3.201414	0.00137	0.04711
St8sia2	55.30856	-7.6878061	1.981818	-3.879169	0.0001	0.0066
Acyp2	49.64841	-7.4512291	1.905289	-3.910813	9.20E-05	0.00595
Ptger1	97.57333	-7.3849912	1.434574	-5.147865	2.63E-07	4.32E-05
Tmem59l	32.37237	-6.9138318	2.111239	-3.274775	0.00106	0.03928
Pcolce2	226.8705	-6.5121986	0.984412	-6.615321	3.71E-11	1.76E-08
Krt24	11236.74	-6.3870586	1.150122	-5.553373	2.80E-08	6.56E-06
Klhl32	59.10906	-5.9967241	1.570762	-3.817718	0.00013	0.00814
Ramp3	865.5594	-5.9528474	1.812375	-3.284555	0.00102	0.03803
Hhip	427.8914	-5.7134824	0.726195	-7.867701	3.61E-15	2.80E-12
Chat	1440.556	-5.5427278	0.655944	-8.450001	2.91E-17	3.07E-14
Lmcd1	310.7768	-5.442594	1.035902	-5.253966	1.49E-07	2.74E-05
Serpinb11	3100.752	-5.3824446	0.373058	-14.42792	3.45E-47	5.09E-43
Cnksr2	74.13002	-5.2352158	1.498419	-3.493827	0.00048	0.02201
1700019D03Rik	65.51077	-5.0768466	1.560011	-3.254366	0.00114	0.04127

Slit1	97.64575	-5.0583244	1.311059	-3.858196	0.00011	0.00714
Galnt15	445.6574	-5.044099	0.601484	-8.386093	5.03E-17	4.63E-14
Egflam	160.9817	-5.0226482	1.419004	-3.539558	0.0004	0.01931
Strip2	376.1831	-4.9391267	0.537401	-9.190769	3.90E-20	5.75E-17
Pcdh20	118.4075	-4.9199871	1.326701	-3.708436	0.00021	0.0117
Ptprd	59.4071	-4.9085263	1.536109	-3.195428	0.0014	0.04799
Dab2	1004.978	-4.8210794	0.757993	-6.360324	2.01E-10	8.25E-08
Vit	519.8352	-4.7121396	0.674869	-6.982305	2.90E-12	1.65E-09
Col4a4	365.9708	-4.6070166	0.856668	-5.377832	7.54E-08	1.54E-05
Mrgprf	1856.242	-4.5036715	0.384091	-11.72554	9.43E-32	4.63E-28
Sphkap	153.7391	-4.4635789	0.990011	-4.508615	6.53E-06	0.00068
Kcnma1	233.4435	-4.3459836	1.299317	-3.344822	0.00082	0.03178
Bdnf	1468.294	-4.3077269	0.431325	-9.987193	1.73E-23	5.11E-20
Postn	58246.07	-4.056342	1.245885	-3.255792	0.00113	0.04117
Grem1	5318.975	-3.9967035	1.088559	-3.671556	0.00024	0.01317
Atp2a3	2841.636	-3.8672456	0.294429	-13.13473	2.08E-39	1.54E-35
Pcdh7	3777.946	-3.8367798	0.573043	-6.695442	2.15E-11	1.06E-08
H2-Q4	5377.397	-3.6715919	0.602377	-6.095177	1.09E-09	3.84E-07
Vwa2	8258.789	-3.575422	0.386504	-9.250683	2.23E-20	3.65E-17
Aspn	262.6753	-3.5611871	1.035382	-3.439492	0.00058	0.02511
Calml3	28101.48	-3.5321691	0.414315	-8.525318	1.52E-17	1.73E-14
Ctgf	10735.45	-3.505159	0.392659	-8.926731	4.39E-19	5.88E-16
Adamts7	192.2608	-3.4509149	0.707231	-4.87947	1.06E-06	0.00013
Cdh13	1676.989	-3.3754705	0.500456	-6.744791	1.53E-11	7.79E-09
Igfbp5	14708.02	-3.2731467	0.514964	-6.356071	2.07E-10	8.25E-08
Ntf3	233.6997	-3.23807	0.8865	-3.652644	0.00026	0.01392
Ano1	1816.713	-3.1982194	0.371149	-8.61708	6.87E-18	8.44E-15
Tsga10	132.8085	-3.1292563	0.76798	-4.074659	4.61E-05	0.00338
Wdfy4	615.1064	-3.0371871	0.491509	-6.179316	6.44E-10	2.37E-07
Sorbs2	1637.752	-3.0226938	0.318833	-9.480503	2.53E-21	5.33E-18
Olfm1	282.0632	-3.0165251	0.714031	-4.22464	2.39E-05	0.00204
Sgcd	233.2609	-3.0141755	0.86273	-3.493764	0.00048	0.02201
Col8a2	4449.939	-3.0060891	0.304679	-9.866407	5.82E-23	1.43E-19
Crispld1	690.0161	-2.9794166	0.552935	-5.388367	7.11E-08	1.48E-05
Slc2a12	200.619	-2.9487904	0.659637	-4.470325	7.81E-06	0.00079
Crlf1	2186.15	-2.8780647	0.371753	-7.741874	9.80E-15	6.88E-12
Klk8	415.3138	-2.8623079	0.834122	-3.431522	0.0006	0.02558
Wfdc3	599.4157	-2.7775124	0.698529	-3.97623	7.00E-05	0.00465
Robo2	1748.398	-2.7594204	0.683357	-4.038039	5.39E-05	0.0038
Peg3	3618.187	-2.7431766	0.326873	-8.392173	4.77E-17	4.63E-14
Osbp2	106.5987	-2.7351475	0.842647	-3.245901	0.00117	0.04215
Ccdc109b	176.0161	-2.6783137	0.752045	-3.561375	0.00037	0.01813
Pla2g2f	4869.616	-2.6778883	0.345169	-7.7582	8.61E-15	6.35E-12

Dpysl3	415.1972	-2.6548956	0.789211	-3.363985	0.00077	0.03053
Fstl1	6169.152	-2.6534744	0.562245	-4.719431	2.37E-06	0.00027
Ltbp2	9302.801	-2.6385093	0.319426	-8.260151	1.45E-16	1.19E-13
Egfl6	2819.842	-2.6356726	0.4593	-5.738458	9.55E-09	2.65E-06
Gm8801	178.4508	-2.6278879	0.749021	-3.508432	0.00045	0.02114
Fbln1	2690.789	-2.6103538	0.456232	-5.721552	1.06E-08	2.78E-06
Tfcp2l1	167.9461	-2.5793438	0.708295	-3.641621	0.00027	0.01432
Lgi4	214.3697	-2.526753	0.62461	-4.045328	5.23E-05	0.0037
Il31ra	6483.22	-2.3468287	0.448084	-5.237478	1.63E-07	2.89E-05
Ppap2a	1585.486	-2.3238688	0.426202	-5.452501	4.97E-08	1.09E-05
Rcan1	19955.5	-2.29188	0.276947	-8.275527	1.28E-16	1.11E-13
Serpinb3b	449.3891	-2.2690869	0.672587	-3.373671	0.00074	0.02964
Tmem200b	250.9468	-2.249672	0.61506	-3.657649	0.00025	0.0137
Crebl2	298.628	-2.2405502	0.689977	-3.247284	0.00117	0.04215
S1pr5	628.76	-2.229897	0.45126	-4.941488	7.75E-07	0.0001
Ank	25411.97	-2.2247073	0.295911	-7.518151	5.56E-14	3.41E-11
Nkd1	1100.762	-2.1527197	0.38917	-5.53156	3.17E-08	7.09E-06
Hs3st3b1	372.4476	-2.1488513	0.658355	-3.263969	0.0011	0.04025
Nos1ap	387.9215	-2.1394396	0.547745	-3.905907	9.39E-05	0.00602
Nt5e	15443.54	-2.1186388	0.338685	-6.255493	3.96E-10	1.50E-07
Rps6ka2	583.5336	-2.1076889	0.607328	-3.470427	0.00052	0.02329
Pdlim3	3590.015	-2.1018269	0.3575	-5.879231	4.12E-09	1.17E-06
Tekt2	2188.234	-2.0775231	0.510292	-4.071243	4.68E-05	0.00341
Sema3e	5943.027	-2.0772979	0.486058	-4.273761	1.92E-05	0.00173
Sgms2	11725.35	-2.0356285	0.357643	-5.691782	1.26E-08	3.20E-06
Gdpd2	505.0254	-2.0249365	0.593138	-3.41394	0.00064	0.02661
Tns1	24294.37	-1.9680521	0.259105	-7.595577	3.06E-14	2.05E-11
Cacna1c	4198.851	-1.9605904	0.354106	-5.536729	3.08E-08	7.09E-06
Igfbp7	2098.851	-1.9573754	0.367207	-5.330446	9.80E-08	1.93E-05
Ltbp1	1804.503	-1.9172458	0.456706	-4.197984	2.69E-05	0.00227
Antxr1	3554.264	-1.9156913	0.39245	-4.881358	1.05E-06	0.00013
Wnt7b	2493.992	-1.8731469	0.381838	-4.90561	9.31E-07	0.00012
Ngef	297.4893	-1.8476021	0.55111	-3.35251	0.0008	0.0314
Adarb1	5237.02	-1.8392564	0.360274	-5.105161	3.31E-07	5.13E-05
Ablim1	2930.388	-1.8388713	0.302379	-6.081356	1.19E-09	3.95E-07
Vwa1	2874.034	-1.8352078	0.506844	-3.620855	0.00029	0.01503
Fbxo2	682.0167	-1.7965974	0.438666	-4.09559	4.21E-05	0.00317
Tuba8	619.804	-1.7483301	0.396312	-4.411495	1.03E-05	0.00101
Gjb4	8873.519	-1.7347632	0.334253	-5.189975	2.10E-07	3.56E-05
Lgr6	1591.472	-1.7086465	0.496856	-3.438915	0.00058	0.02511
Gsdma3	1341.743	-1.699864	0.406415	-4.182584	2.88E-05	0.0024
S100a4	9430.424	-1.6964712	0.351302	-4.829096	1.37E-06	0.00017
Prlr	9970.575	-1.6958014	0.238704	-7.10421	1.21E-12	7.14E-10

Cyp26b1	2274.927	-1.6930624	0.392458	-4.314002	1.60E-05	0.00151
Megf6	8730.288	-1.6764844	0.341133	-4.914467	8.90E-07	0.00012
Gjb5	1282.672	-1.6555054	0.380952	-4.345709	1.39E-05	0.00133
Pi15	42866.65	-1.6426989	0.50782	-3.234804	0.00122	0.04324
Arrb1	2153.204	-1.6376247	0.302442	-5.414678	6.14E-08	1.33E-05
Krt80	10607.79	-1.598348	0.300482	-5.319285	1.04E-07	2.02E-05
Rnf150	1852.704	-1.5725119	0.28294	-5.557749	2.73E-08	6.50E-06
Fmn1	2291.196	-1.5548151	0.298543	-5.208014	1.91E-07	3.27E-05
Syne3	920.6451	-1.5393239	0.401095	-3.837802	0.00012	0.00756
Atp6v0e2	1203.361	-1.5255938	0.479054	-3.1846	0.00145	0.04948
Cd34	44996.69	-1.5241067	0.290411	-5.248096	1.54E-07	2.76E-05
Gm7694	784.3175	-1.500198	0.444428	-3.375571	0.00074	0.02954
Nudt4	12992.47	-1.4792652	0.259915	-5.691337	1.26E-08	3.20E-06
Gjb3	2405.409	-1.4790958	0.279871	-5.284917	1.26E-07	2.35E-05
Tcta	574.3245	-1.46249	0.424259	-3.447167	0.00057	0.02479
Grip1	1979.584	-1.4454105	0.362045	-3.992356	6.54E-05	0.00438
Tnfrsf11b	5611.909	-1.4445252	0.272848	-5.294249	1.20E-07	2.26E-05
Tnfrsf21	1457.654	-1.4354688	0.305314	-4.70162	2.58E-06	0.00029
Ppap2b	3269.309	-1.4218938	0.341656	-4.161769	3.16E-05	0.00254
Hpcal1	2251.316	-1.4116223	0.315871	-4.468981	7.86E-06	0.00079
Dkk3	16203.72	-1.3943091	0.252037	-5.53217	3.16E-08	7.09E-06
Ergic1	3374.064	-1.3808006	0.364878	-3.784276	0.00015	0.00904
Gm53	1147.756	-1.3710348	0.321145	-4.269202	1.96E-05	0.00174
Abhd1	1304.325	-1.3705274	0.373657	-3.667879	0.00024	0.01331
Adamtsl4	9511.009	-1.3629544	0.285504	-4.773849	1.81E-06	0.00021
Igdcc4	4645.589	-1.362902	0.291062	-4.682507	2.83E-06	0.00031
Phospho1	3178.546	-1.3606661	0.399338	-3.407302	0.00066	0.02702
Col6a2	4928.957	-1.3581674	0.264413	-5.13654	2.80E-07	4.53E-05
Ccdc3	6609.883	-1.3579883	0.263792	-5.147952	2.63E-07	4.32E-05
Inpp4b	1839.716	-1.3351708	0.325137	-4.106486	4.02E-05	0.00304
Ptges	2897.374	-1.3277706	0.275941	-4.811797	1.50E-06	0.00018
Pard3b	702.515	-1.3271899	0.395843	-3.352817	0.0008	0.0314
Bcl2	2728.324	-1.3211441	0.265087	-4.983809	6.23E-07	8.75E-05
Anxa8	44395.17	-1.3185845	0.272954	-4.830797	1.36E-06	0.00017
Spon2	3017.207	-1.3140239	0.321111	-4.092118	4.27E-05	0.0032
Vsig10	1149.385	-1.3014325	0.388735	-3.347862	0.00081	0.0316
Ngf	5084.636	-1.30029	0.29522	-4.404473	1.06E-05	0.00104
Man1a	1287.551	-1.2993794	0.391916	-3.315455	0.00091	0.0345
Ecm1	30886.37	-1.2967313	0.324639	-3.994374	6.49E-05	0.00437
Duox1	3548.409	-1.2954262	0.305356	-4.242344	2.21E-05	0.00194
Mfap3l	5135.817	-1.2863852	0.292289	-4.401075	1.08E-05	0.00104
Sdk2	6134.787	-1.2716778	0.252771	-5.030957	4.88E-07	6.99E-05
Mras	874.198	-1.2691586	0.349532	-3.631025	0.00028	0.01471

Ptn	21867.61	-1.2593948	0.315225	-3.995227	6.46E-05	0.00437
Camkk1	2627.335	-1.2332018	0.312968	-3.94035	8.14E-05	0.00536
Esyt3	5486.969	-1.2271587	0.337592	-3.635034	0.00028	0.01458
Hoxb9	2552.796	-1.2265902	0.295458	-4.151483	3.30E-05	0.00262
Camk4	4592.786	-1.2234644	0.358393	-3.413754	0.00064	0.02661
Tns4	62658.39	-1.2232777	0.255432	-4.789045	1.68E-06	0.0002
Gpr3	835.4099	-1.2153454	0.382011	-3.181441	0.00147	0.04979
Caskin2	4247.846	-1.2151047	0.363885	-3.339256	0.00084	0.03221
Tgm5	12397.09	-1.213703	0.351664	-3.451315	0.00056	0.02463
Phyhip	7257.62	-1.20435	0.355245	-3.390193	0.0007	0.02832
Tcaf2	1336.659	-1.1881985	0.33445	-3.552691	0.00038	0.01856
Hoxc8	4120.769	-1.1723841	0.348925	-3.35999	0.00078	0.03073
Garem	1107.093	-1.1634693	0.325007	-3.579825	0.00034	0.01707
Cacnb1	1873.233	-1.1597111	0.305663	-3.794084	0.00015	0.00881
Serpinb8	9629.602	-1.1560017	0.283554	-4.076836	4.57E-05	0.00337
Npnt	29940.27	-1.1045088	0.308075	-3.585194	0.00034	0.01678
Kazn	1285.863	-1.0864913	0.338126	-3.213272	0.00131	0.04575
Rab8b	7852.059	-1.0754625	0.289279	-3.717728	0.0002	0.0114
Cgnl1	4150.353	-1.0658699	0.255753	-4.167573	3.08E-05	0.00249
Ppp2r3a	13236.31	-1.0649592	0.290935	-3.660471	0.00025	0.0136
Fry	4224.933	-1.0617655	0.329613	-3.221249	0.00128	0.04481
Slc35e4	4774.459	-1.0573997	0.249921	-4.230927	2.33E-05	0.00201
Foxn2	5274.796	-1.0447929	0.244581	-4.271773	1.94E-05	0.00173
Pmp22	3378.115	-1.0355042	0.285686	-3.624628	0.00029	0.01502
Pogk	6960.913	-1.0183408	0.298657	-3.409728	0.00065	0.02686
Rab11fip5	8430.057	-1.0158067	0.315978	-3.214802	0.00131	0.04572
Tnk1	7090.496	-1.0126333	0.300006	-3.375374	0.00074	0.02954
Tob1	15557.01	-0.9862173	0.272992	-3.612627	0.0003	0.01541
Col6a1	20375.31	-0.9839774	0.235435	-4.179409	2.92E-05	0.00241
Adgrg6	12383.45	-0.9539493	0.23158	-4.119309	3.80E-05	0.00293
Frem2	9342.37	-0.950429	0.267205	-3.556934	0.00038	0.01832
Hspb8	34822.54	-0.9468634	0.27519	-3.440767	0.00058	0.02511
Slc39a13	4866.098	-0.943396	0.27503	-3.430154	0.0006	0.02563
Sbsn	83957.48	-0.9311828	0.207142	-4.495388	6.94E-06	0.00072
Tpst1	3250.076	-0.916616	0.28805	-3.182144	0.00146	0.04978
Rnf208	3015.707	-0.9126427	0.261605	-3.488626	0.00049	0.02223
Cd109	15414.8	-0.8994313	0.225168	-3.994486	6.48E-05	0.00437
Hagh	5726.641	-0.8938982	0.263375	-3.39401	0.00069	0.02806
Dusp14	3803.348	-0.887535	0.261164	-3.398375	0.00068	0.02769
Aqp3	129286.5	-0.8821536	0.242913	-3.631568	0.00028	0.01471
Kif21a	13299.71	-0.8808482	0.251236	-3.506063	0.00045	0.02122
Ankrd10	11701.52	-0.8754149	0.263676	-3.320045	0.0009	0.03403
Sptbn1	32584.71	-0.871137	0.211446	-4.1199	3.79E-05	0.00293

Arhgap44	6267.131	-0.8683561	0.252992	-3.432344	0.0006	0.02557
Csrp1	71003.06	-0.8649085	0.236	-3.664871	0.00025	0.01341
Ube2q2	5750.959	-0.854767	0.263292	-3.246457	0.00117	0.04215
Avpi1	17695.42	-0.8443312	0.260828	-3.237124	0.00121	0.043
S100a6	95438.68	-0.8158424	0.243643	-3.348512	0.00081	0.0316
Crebrf	3949.98	-0.8105749	0.247978	-3.268735	0.00108	0.03972
Cd44	69685.74	-0.7856264	0.228213	-3.442508	0.00058	0.02511
Tmbim1	24460.65	-0.7510359	0.225294	-3.333577	0.00086	0.03258
Evpl	12553.05	-0.73825	0.225809	-3.269349	0.00108	0.03972
Macf1	80893.46	-0.6887717	0.212966	-3.234192	0.00122	0.04324
Rhob	35501.26	0.6958273	0.214502	3.243921	0.00118	0.0423
H3f3b	167007	0.731348	0.225568	3.24225	0.00119	0.04234
Cald1	10537.84	0.8595407	0.227472	3.778673	0.00016	0.00919
Gstm1	8401.35	0.8679606	0.243628	3.56264	0.00037	0.01811
Plk2	19652.43	0.8690886	0.26061	3.334828	0.00085	0.03252
Ppp1r10	3201.591	0.8866871	0.274911	3.225362	0.00126	0.04438
Irx1	6449.629	0.8995277	0.258009	3.486426	0.00049	0.02232
B4galnt1	4421.135	0.9156631	0.266168	3.440175	0.00058	0.02511
Atp1b3	32989.36	0.9469578	0.213207	4.441503	8.9E-06	0.0009
Slc39a6	14297.9	0.9538802	0.242838	3.928049	8.6E-05	0.00561
Oplah	22166.87	1.0017345	0.256737	3.901797	9.5E-05	0.00604
Ermp1	2153.993	1.0100653	0.310084	3.257396	0.00112	0.04104
Rpl7a	53997.33	1.0147637	0.228905	4.43313	9.3E-06	0.00092
Insig2	12413.58	1.0171197	0.298871	3.403207	0.00067	0.02728
Hes1	3586.944	1.0313095	0.262672	3.926231	8.6E-05	0.00561
Cers4	5419.742	1.0403209	0.257809	4.035234	5.5E-05	0.00383
Dlx2	1857.811	1.068766	0.287148	3.722009	0.0002	0.01125
Igsf8	12119.29	1.0799814	0.336651	3.208017	0.00134	0.04615
Rassf5	1795.691	1.0805051	0.323002	3.345195	0.00082	0.03178
Hmga2-ps1	1375.934	1.0862371	0.324195	3.350571	0.00081	0.03146
Smoc1	2011.162	1.0867241	0.338609	3.209379	0.00133	0.04604
Nrarp	1167.966	1.0937359	0.327642	3.338208	0.00084	0.03221
St3gal4	2556.366	1.1380203	0.31429	3.620921	0.00029	0.01503
Dusp10	14263.42	1.1407586	0.259667	4.393153	1.1E-05	0.00108
Alad	3530.019	1.1481309	0.298274	3.849251	0.00012	0.00734
Tppp3	17530.76	1.1629334	0.364877	3.187194	0.00144	0.04915
Ttyh3	5928.186	1.1710286	0.286849	4.08239	4.5E-05	0.00332
Ggct	2123.355	1.1743202	0.365615	3.211904	0.00132	0.04575
Eif4e3	1729.702	1.1781489	0.292821	4.023438	5.7E-05	0.00396
Fam83a	2131.783	1.1828171	0.340437	3.474405	0.00051	0.02302
Sepp1	11650.05	1.2006505	0.347817	3.451958	0.00056	0.02463
Hist1h2bc	5026.717	1.2410009	0.301471	4.116484	3.8E-05	0.00295
Epas1	3836.368	1.2480215	0.292953	4.260143	2E-05	0.0018

Creb3l1	931.7638	1.2557997	0.368214	3.410515	0.00065	0.02686
Ect2	1116.631	1.261011	0.388526	3.245632	0.00117	0.04215
1190002N15Rik	6257.169	1.2677049	0.339656	3.73232	0.00019	0.01084
Dbn1	3597.749	1.2720797	0.352828	3.605378	0.00031	0.01579
Gstm5	6224.411	1.2859712	0.392926	3.272804	0.00106	0.03945
Syde2	1406.224	1.2969403	0.378575	3.425852	0.00061	0.02582
Il33	1188.623	1.3081877	0.348827	3.750248	0.00018	0.01018
Decr1	2474.641	1.3084246	0.37094	3.527319	0.00042	0.0201
Ucp2	117964.8	1.3248743	0.277093	4.781342	1.7E-06	0.00021
Tapbpl	907.0765	1.3276884	0.38818	3.420293	0.00063	0.0262
Hoxc13	2434.199	1.3417553	0.309439	4.336095	1.5E-05	0.00138
Mki67	3304.493	1.3460474	0.322548	4.173166	3E-05	0.00246
Hist1h1c	11958.2	1.3486817	0.31413	4.293386	1.8E-05	0.00162
D17H6S56E-5	944.7133	1.376767	0.413938	3.326026	0.00088	0.03339
Mtap	1661.467	1.3830502	0.413873	3.341729	0.00083	0.03205
Cbs	4134.911	1.3864992	0.382871	3.62132	0.00029	0.01503
Plbd1	799.3047	1.3937923	0.40661	3.427837	0.00061	0.02578
Pmaip1	3207.58	1.4006232	0.326896	4.284615	1.8E-05	0.00167
Nuak1	3797.133	1.4031501	0.429936	3.263629	0.0011	0.04025
Ppp1r3b	2286.937	1.404287	0.417753	3.361527	0.00078	0.03072
Stard5	6006.103	1.4224699	0.350348	4.060157	4.9E-05	0.00352
Adamts9	831.4506	1.4237345	0.367464	3.874486	0.00011	0.0067
Pm20d1	3602.742	1.4289095	0.252145	5.667024	1.5E-08	3.6E-06
Slc1a4	3735.121	1.4859934	0.266355	5.579004	2.4E-08	5.8E-06
Rrm2	2075.527	1.5260219	0.361167	4.225247	2.4E-05	0.00204
Gpc4	11615.45	1.5398875	0.403325	3.817982	0.00013	0.00814
Rab27b	1294.682	1.5455506	0.478003	3.233347	0.00122	0.04326
Eif4ebp1	1963.024	1.5516971	0.451362	3.437813	0.00059	0.02514
Erdr1	3062.706	1.5746519	0.44676	3.524602	0.00042	0.02019
Icam1	16645.57	1.5766448	0.378222	4.168565	3.1E-05	0.00249
Ldlrad4	770.7509	1.5969874	0.455256	3.507886	0.00045	0.02114
Plagl1	11525.31	1.6005223	0.396742	4.034167	5.5E-05	0.00383
Ptprv	3799.53	1.6032904	0.247778	6.470665	9.8E-11	4.4E-08
Hmgcs2	2047.725	1.6092558	0.353747	4.549177	5.4E-06	0.00057
Mal2	1990.87	1.6346584	0.470448	3.474685	0.00051	0.02302
Sema6a	665.3864	1.6573937	0.515923	3.212482	0.00132	0.04575
Glul	3058.061	1.6933422	0.373178	4.537632	5.7E-06	0.0006
Tsc22d1	12478.61	1.7169955	0.323437	5.308601	1.1E-07	2.1E-05
Plekhh2	1187.524	1.7433133	0.472235	3.691625	0.00022	0.01226
1810011O10Rik	3413.376	1.7497961	0.313138	5.587942	2.3E-08	5.6E-06
Gnmt	1979.372	1.7542519	0.293592	5.975134	2.3E-09	6.9E-07
Col16a1	26507.07	1.7677758	0.412384	4.286726	1.8E-05	0.00166
Cntfr	1100.174	1.7787132	0.481482	3.694245	0.00022	0.01223

Sox4	8776.496	1.7791826	0.329295	5.403	6.6E-08	1.4E-05
Etv4	420.0964	1.7898304	0.529467	3.380439	0.00072	0.02916
Smox	3578.599	1.7934105	0.433899	4.133243	3.6E-05	0.00279
Inhbb	3527.647	1.7942129	0.299895	5.982807	2.2E-09	6.7E-07
Fam101a	627.4218	1.7953884	0.504363	3.559711	0.00037	0.01819
Slc16a7	3288.128	1.8062112	0.426248	4.237461	2.3E-05	0.00196
Cd248	365.5096	1.8280447	0.496871	3.679114	0.00023	0.01283
Bpifc	739.1497	1.8354658	0.530928	3.457093	0.00055	0.02432
Pappa	4056.095	1.8479329	0.530115	3.48591	0.00049	0.02232
Glrx	995.5362	1.8501936	0.530198	3.489627	0.00048	0.02222
Pla2g7	517.9125	1.8569382	0.53372	3.479239	0.0005	0.02274
Car12	13185.86	1.8602976	0.488992	3.804353	0.00014	0.00852
Nrip1	12720.99	1.8688604	0.541636	3.4504	0.00056	0.02464
Krt79	6221.127	1.8788436	0.315696	5.951442	2.7E-09	7.8E-07
Fas	506.7558	1.8837231	0.560534	3.360586	0.00078	0.03073
Gja1	155156.3	1.8857223	0.367833	5.126566	3E-07	4.7E-05
Sdr16c5	856.0009	1.9079264	0.443386	4.303084	1.7E-05	0.00156
Arrdc3	5288.837	1.9171019	0.371694	5.157737	2.5E-07	4.2E-05
Pdpn	540.354	1.9445956	0.42743	4.549503	5.4E-06	0.00057
Lacc1	830.66	1.9462039	0.46266	4.206555	2.6E-05	0.0022
Mill1	4585.768	1.9599024	0.553544	3.540647	0.0004	0.0193
Flrt3	22304.59	1.9755297	0.410438	4.813227	1.5E-06	0.00018
Lrrc8c	968.9204	1.9813543	0.403204	4.914024	8.9E-07	0.00012
Pde4d	393.5606	1.9869691	0.571006	3.479771	0.0005	0.02274
Srpx	359.6712	1.9898734	0.495969	4.012089	6E-05	0.00411
Rgs2	11034.25	1.9974598	0.580796	3.439176	0.00058	0.02511
Tril	1135.094	2.0048921	0.395132	5.073977	3.9E-07	5.9E-05
Gm5084	742.7829	2.0103837	0.623775	3.222932	0.00127	0.04465
Plod2	427.9721	2.0460628	0.478241	4.27831	1.9E-05	0.0017
Tm4sf1	4402.061	2.0709189	0.342605	6.044629	1.5E-09	4.7E-07
Lurap1l	513.678	2.0741328	0.478597	4.333777	1.5E-05	0.00139
Tle6	557.7789	2.1007753	0.653817	3.213095	0.00131	0.04575
Has1	2047.367	2.119133	0.62612	3.38455	0.00071	0.0288
Fabp5	4729.789	2.1395922	0.312842	6.839208	8E-12	4.2E-09
Htra1	2987.268	2.1424958	0.594945	3.601167	0.00032	0.01594
Ret	5183.56	2.1475545	0.533849	4.022779	5.8E-05	0.00396
Sdpr	715.061	2.159246	0.581301	3.714509	0.0002	0.0115
Nlrp10	1684.166	2.1620706	0.411759	5.250811	1.5E-07	2.8E-05
Mfap2	624.6505	2.1718427	0.575299	3.775153	0.00016	0.00925
Gprc5b	402.2502	2.1950723	0.610047	3.598202	0.00032	0.01607
Cyp27b1	521.3184	2.2060802	0.680323	3.242697	0.00118	0.04234
Prickle1	1448.606	2.2068363	0.562115	3.925951	8.6E-05	0.00561
Lrrc75b	1870.812	2.2072803	0.43268	5.101415	3.4E-07	5.2E-05

Gsr	1218.288	2.2095264	0.534151	4.136518	3.5E-05	0.00277
Oaf	404.8924	2.2314772	0.639041	3.491914	0.00048	0.0221
Cdca2	247.2369	2.24681	0.639931	3.511019	0.00045	0.02103
Tgfbr3	1480.798	2.251955	0.554756	4.059361	4.9E-05	0.00352
Slc23a3	215.1686	2.2923523	0.629855	3.639494	0.00027	0.01439
Defb6	641.2023	2.3016475	0.441165	5.217201	1.8E-07	3.2E-05
Mmp2	2640.201	2.3122982	0.431343	5.360694	8.3E-08	1.7E-05
Lcn2	294.609	2.3291361	0.60602	3.843329	0.00012	0.00746
Muc15	357.1881	2.3362428	0.507444	4.603941	4.1E-06	0.00045
Slc6a4	394.8646	2.3527802	0.566393	4.153971	3.3E-05	0.0026
Pcsk5	442.8549	2.3567076	0.592012	3.980846	6.9E-05	0.00458
Fndc1	2036.843	2.4378766	0.499267	4.882916	1E-06	0.00013
Agap2	1394.877	2.4538527	0.628843	3.902172	9.5E-05	0.00604
Lingo1	216.1692	2.4693371	0.720949	3.425121	0.00061	0.02582
Cntn2	622.2801	2.4711949	0.605555	4.080876	4.5E-05	0.00332
Srgap1	246.4638	2.4786672	0.649488	3.816342	0.00014	0.00815
Adcy7	299.1454	2.5014378	0.685827	3.64733	0.00026	0.01411
Pxdn	8016.725	2.5036682	0.40827	6.132389	8.7E-10	3.1E-07
Nav2	1427.445	2.5061663	0.52981	4.730315	2.2E-06	0.00026
Apobec1	647.2889	2.5176196	0.593858	4.239431	2.2E-05	0.00196
Krt71	289.2771	2.5234181	0.543948	4.639083	3.5E-06	0.00038
Lamb1	12160.72	2.5708298	0.422707	6.081825	1.2E-09	3.9E-07
Arhgdib	334.2218	2.5732374	0.633194	4.0639	4.8E-05	0.00349
Itih5	1302.457	2.5758259	0.720797	3.573582	0.00035	0.01742
Efemp1	1256.413	2.5976474	0.813332	3.193835	0.0014	0.04814
Nfe2l3	397.0077	2.6095579	0.641618	4.067152	4.8E-05	0.00346
Col14a1	553.8772	2.620816	0.431076	6.079708	1.2E-09	3.9E-07
Gsap	345.8162	2.6233294	0.530417	4.945786	7.6E-07	0.0001
Aadac	294.826	2.658754	0.542442	4.901455	9.5E-07	0.00012
Anxa3	390.0088	2.684678	0.647599	4.145586	3.4E-05	0.00267
Krt8	1060.034	2.6948373	0.710727	3.791661	0.00015	0.00883
S100b	170.3186	2.7668224	0.780168	3.546443	0.00039	0.01894
Ntn4	3357.003	2.7972039	0.560301	4.992325	6E-07	8.5E-05
Slc27a6	816.2614	2.8168567	0.684752	4.113688	3.9E-05	0.00297
Medag	639.9648	2.8394395	0.850565	3.338296	0.00084	0.03221
Abi3bp	3274.735	2.8644799	0.638905	4.483423	7.3E-06	0.00075
Fhod3	2805.533	2.8652762	0.548676	5.222164	1.8E-07	3.1E-05
Ntrk2	1772.842	2.9093573	0.386884	7.519983	5.5E-14	3.4E-11
Casp1	1704.742	2.918963	0.614764	4.748101	2.1E-06	0.00024
Prss12	273.1774	2.9233875	0.761297	3.840011	0.00012	0.00753
Serpine1	17185.52	2.9328513	0.511341	5.735604	9.7E-09	2.7E-06
Parm1	282.0105	2.9430319	0.732067	4.020168	5.8E-05	0.00399
Syn3	656.0739	2.9480516	0.7052	4.180448	2.9E-05	0.00241

Trib2	178.7135	3.0067295	0.792739	3.792838	0.00015	0.00882
Gm11127	724.0717	3.082834	0.481826	6.398235	1.6E-10	6.6E-08
Ggt1	1183.231	3.0859507	0.609281	5.064902	4.1E-07	6E-05
Phactr1	770.587	3.2025079	0.847941	3.776804	0.00016	0.00922
Ccdc80	594.9083	3.2359625	0.632167	5.118842	3.1E-07	4.8E-05
Adamts3	1623.724	3.2435454	0.719658	4.507067	6.6E-06	0.00068
Atp12a	2578.284	3.302205	0.698231	4.729386	2.3E-06	0.00026
Slc4a4	655.5906	3.3240012	0.808668	4.110466	3.9E-05	0.003
Gjb6	1536.956	3.3956372	0.318714	10.65418	1.7E-26	6.1E-23
Bhlhe41	699.0447	3.3958706	0.690529	4.917779	8.8E-07	0.00012
Rassf4	1195.654	3.4068058	0.538224	6.329721	2.5E-10	9.5E-08
Fa2h	432.2929	3.4242465	0.993238	3.447558	0.00057	0.02479
Gxylt2	261.7476	3.4300502	1.001099	3.426285	0.00061	0.02582
Gjb2	7927.883	3.4574419	0.372384	9.284623	1.6E-20	3E-17
Plekhb1	111.466	3.5588361	0.959686	3.708332	0.00021	0.0117
Slc7a2	875.7288	3.5710358	0.517585	6.899424	5.2E-12	2.9E-09
Loxl2	753.8905	3.5991768	0.766732	4.694176	2.7E-06	0.0003
Slc1a3	1371.21	3.6543894	0.638035	5.727569	1E-08	2.7E-06
Cyp2f2	208.5847	3.728089	0.798884	4.666622	3.1E-06	0.00034
Basp1	1149.452	3.7577673	0.573464	6.552756	5.6E-11	2.6E-08
Dnah7b	1405.422	3.7749377	0.638272	5.914307	3.3E-09	9.6E-07
Astn2	102.4907	3.8623032	0.953294	4.051534	5.1E-05	0.00362
H2-K2	126.0851	3.8826802	0.926321	4.191504	2.8E-05	0.00232
Elovl3	122.9013	4.1553975	1.094133	3.797891	0.00015	0.00871
Dio3	179.9053	4.2356637	0.786213	5.387425	7.1E-08	1.5E-05
Csf3	254.8649	4.2549723	1.292418	3.292256	0.00099	0.03719
Ttyh1	175.981	4.3223984	1.247108	3.465936	0.00053	0.02361
H2-Q5	305.5866	4.3561608	1.012316	4.303162	1.7E-05	0.00156
Ptch2	149.6794	4.4115404	1.130081	3.903738	9.5E-05	0.00604
Akap5	99.22547	4.4415238	1.217367	3.648467	0.00026	0.01409
Fam71f2	178.1635	4.5153375	1.284086	3.516381	0.00044	0.02067
Kcnf1	279.5481	4.5340764	0.916855	4.945251	7.6E-07	0.0001
Olfr1033	64.46381	4.7254128	1.436638	3.289217	0.001	0.0375
Svopl	53.70934	4.7935727	1.423892	3.366529	0.00076	0.03034
Frmd7	86.26299	5.1567171	1.423635	3.622218	0.00029	0.01503
Adamts8	70.56919	5.3286664	1.590195	3.350952	0.00081	0.03146
Fgf21	144.4554	5.4942716	1.088281	5.048577	4.5E-07	6.5E-05
Ripply3	39.04847	7.4440453	2.177318	3.418906	0.00063	0.02626
Col2a1	85.4901	7.5206412	1.631384	4.609976	4E-06	0.00044
Sash3	23.54847	8.1520861	2.49159	3.27184	0.00107	0.03949
4930486F22Rik	28.04323	8.4049242	2.386065	3.522504	0.00043	0.02027
Qrfp	28.11938	8.4061597	2.479781	3.38988	0.0007	0.02832
Rasgrf1	30.348	8.5182991	2.305401	3.694932	0.00022	0.01223

Acox2	35.16928	8.7315868	2.235451	3.905963	9.4E-05	0.00602
Gal3st3	35.57177	8.7453739	2.336961	3.742199	0.00018	0.01047
Hist1h1b	38.33772	8.8536133	2.241674	3.949554	7.8E-05	0.00518
Strc	38.51045	8.8598921	2.304637	3.844376	0.00012	0.00746
Fgf2	57.16112	9.4303363	1.986702	4.74673	2.1E-06	0.00024
Meox1	80.47816	9.9235246	2.000412	4.960741	7E-07	9.8E-05

Supplementary Table 5. Downregulated genes in aged and cKO HF-SCs

	old_bulk	padj	foxc1_cko	padj	nfatc1_cko	padj
Hhip	-3.6140927	1.241E-19	-3.708738	6.96E-06	-5.713482	2.8E-12
Peg3	-2.6224108	2.67E-27	-1.4132455	0.006809	-2.743177	4.6E-14
Nptx1	-2.124405	0.0001875	-4.3419455	5.19E-07		
Scn5a	-1.923414	0.0014635	-4.5275339	3.4E-05		
Cyp26b1	-1.8946503	2.206E-08			-1.693062	0.00151
Cpa4	-1.8525351	2.747E-05	-2.838357	8.58E-10		
Spon2	-1.7548325	5.405E-05			-1.314024	0.0032
Ramp1	-1.6833759	2.786E-07	-2.1931359	0.016981		
Atoh8	-1.6666011	0.0291312	-3.349125	1.57E-08		
Chst13	-1.5367287	0.009769	-7.9541083	0.000974		
Fam46c	-1.4563943	0.0042245	-3.3268853	3.32E-08		
Cnksr2	-1.3931642	0.0135938			-5.235216	0.02201
Ltbp1	-1.3770614	2.132E-13	-2.0927453	0.001051	-1.917246	0.00227
Col4a3	-1.3527163	0.000178	-3.6659537	0.000129		
Sorbs2	-1.3417046	0.0001129			-3.022694	5.3E-18
Atp6v0e2	-1.3309015	0.0060358	-2.9266496	0.001285	-1.525594	0.04948
Pcolce2	-1.3119549	0.0101155	-2.9872526	0.003513	-6.512199	1.8E-08
Col4a4	-1.2854189	0.0003128	-3.436445	2.89E-06	-4.607017	1.5E-05
Ngef	-1.2780774	8.816E-05	-4.259039	1.02E-11	-1.847602	0.0314
Fgf18	-1.2135163	0.0009229	-3.5203002	0.000132		
Cacna2d2	-1.2003271	0.0445837	-3.0435782	1.43E-08		
Krt80	-1.1797824	0.0001588	-2.8023975	6.21E-06	-1.598348	2E-05
Ogdhl	-1.1712494	0.0001382	-2.8315252	0.003102		
Rnf208	-1.1063727	0.0015167	-1.9824538	1.44E-05	-0.912643	0.02223
Pi15	-1.1010056	5.267E-06			-1.642699	0.04324
Nog	-1.0957449	0.0159015	-3.3441901	2.18E-06		
Ctgf	-1.0953981	1.016E-06			-3.505159	5.9E-16
Kcnk10	-1.0857014	0.0261378			-9.713626	4.7E-05
Atp2a3	-1.0773715	0.0155778	-7.0101189	2.82E-05	-3.867246	1.5E-35
Chat	-1.068343	2.952E-08	-4.421112	3.65E-11	-5.542728	3.1E-14
Kcnma1	-1.0443917	0.0007289			-4.345984	0.03178
Itgb6	-1.032291	8.598E-08	-1.5566642	0.023129		
Bcl2	-0.9570747	3.411E-05			-1.321144	8.8E-05
Antxr1	-0.9051461	0.0459221	-2.4122489	9.23E-05	-1.915691	0.00013
Myh14	-0.8823168	0.0010108	-2.0109416	1.13E-08		
Ccdc88c	-0.8682823	0.0078804	-3.8240617	5.65E-15		
Igdcc4	-0.8330836	0.000509			-1.362902	0.00031
Kif21a	-0.7978368	0.0080721			-0.880848	0.02122
Pmp22	-0.7945333	0.0278976			-1.035504	0.01502
Gfra1	-0.7876568	0.0088347	-4.4833011	1.73E-14		
Hspb8	-0.7807813	0.0099385	-2.0904839	0.000206	-0.946863	0.02511
Ppap2b	-0.7203017	0.0135938			-1.421894	0.00254
Cd34	-0.6460393	0.0023511			-1.524107	2.8E-05

Duox1	-0.6270249	0.0292797	-2.1578751	1.09E-08	-1.295426	0.00194
Dab2	-0.6268207	0.0197611			-4.821079	8.2E-08
Tle4	-0.6150786	0.0353213	-1.6393636	0.012611		
Vwa2	-0.5719791	0.0326916	-2.7549622	2.07E-11	-3.575422	3.7E-17

Supplementary Table 6. Downregulated genes in dKO HF-SCs (scRNA-seq)

	p_val	avg_logFC	pct.1	pct.2	log2_FC
Hspa1b	1.76E-86	-1.700212	0.978	0.782	-2.452887355
Cyr61	5.19E-44	-1.543313	0.89	0.609	-2.226530009
Hspa1a	4.85E-56	-1.320203	0.986	0.824	-1.904650804
Krt24	1.72E-47	-1.265225	0.394	0	-1.825333261
Calml3	6.11E-73	-1.202131	0.781	0.26	-1.734307986
Sfrp1	1.19E-66	-1.13089	0.799	0.316	-1.631528857
Dmkn	1.72E-52	-1.12596	0.943	0.801	-1.62441724
Ctgf	1.38E-29	-1.09769	0.571	0.206	-1.583631263
Cd34	8.51E-62	-1.06769	0.677	0.166	-1.540350688
Pi15	5.38E-45	-1.044567	0.455	0.047	-1.506991158
Serpinb11	9.17E-39	-1.015819	0.335	0.002	-1.465517329
Grem1	7.29E-48	-0.959695	0.516	0.077	-1.384546501
Krt6a	3.02E-24	-0.940258	0.878	0.745	-1.356506148
Aqp3	2.17E-38	-0.880698	0.931	0.792	-1.270578987
Pthlh	6.73E-10	-0.859903	0.339	0.173	-1.240577261
Postn	1.99E-28	-0.834549	0.957	0.927	-1.203999774
Wfdc3	7.40E-50	-0.821069	0.557	0.096	-1.184552538
Ank	3.65E-34	-0.797435	0.451	0.101	-1.150455338
Cox7b	6.85E-90	-0.793141	0.99	0.911	-1.14426053
Sbsn	2.31E-30	-0.788728	0.963	0.911	-1.137894035
Igfbp3	3.02E-27	-0.769297	0.423	0.105	-1.109860844
Tgm5	2.03E-40	-0.763216	0.616	0.222	-1.101087707
S100a4	1.88E-23	-0.754476	0.839	0.595	-1.088478158
Cited2	3.41E-25	-0.728501	0.819	0.562	-1.05100444
Hspb1	9.32E-37	-0.702648	0.998	1	-1.013706348
Sema3e	8.61E-54	-0.694401	0.48	0.03	-1.001808259
Fst	0.000313	-0.689998	0.754	0.768	-0.995457384
Ubc	9.73E-41	-0.687631	0.998	0.988	-0.992041881
Emp1	8.01E-25	-0.681802	0.959	0.871	-0.983631759
Dnajb1	1.28E-31	-0.680876	0.986	0.944	-0.982295732
Rcan1	2.64E-19	-0.673008	0.526	0.26	-0.970945312
Klf4	4.63E-29	-0.65709	0.988	0.96	-0.947980192
Ptn	3.68E-24	-0.648467	0.925	0.876	-0.935540004
Cxcl14	1.59E-40	-0.645571	0.998	0.974	-0.931362665
Hsp90aa1	1.72E-37	-0.628956	0.996	0.988	-0.907392162
Ddx3y	1.26E-82	-0.627103	0.612	0	-0.904719019
Myc	4.84E-27	-0.603389	0.831	0.625	-0.870506578
Ptgs2	6.30E-06	-0.598993	0.219	0.112	-0.864164776
Ifrd1	1.25E-18	-0.59167	0.963	0.937	-0.853599311
Lhx2	2.62E-37	-0.586133	0.854	0.55	-0.845611075
Nfkbiz	1.41E-25	-0.579953	0.886	0.71	-0.836695246
Cadm1	7.09E-37	-0.573209	0.795	0.468	-0.826965571
Bmp2	4.23E-16	-0.569823	0.551	0.316	-0.822080516

Hspa8	4.88E-42	-0.565717	0.996	1	-0.816157527
Fbln1	4.67E-31	-0.560201	0.488	0.141	-0.808199529
Id1	5.28E-17	-0.553789	0.941	0.792	-0.798948066
Krtdap	0.035332	-0.551071	0.413	0.496	-0.795027991
Prlr	5.34E-36	-0.548053	0.669	0.276	-0.790673222
Id3	4.76E-21	-0.540936	0.976	0.897	-0.780405829
Gas1	4.51E-21	-0.537238	0.892	0.721	-0.775069969
Col6a1	3.07E-38	-0.535323	0.427	0.052	-0.772308435
Hspb8	4.83E-21	-0.530056	0.774	0.562	-0.764708948
Tfap2b	1.24E-33	-0.524859	0.699	0.335	-0.757211195
Gsto1	3.37E-24	-0.524339	0.726	0.489	-0.756461903
Nudt4	2.17E-19	-0.51896	0.659	0.436	-0.748700822
Krtap17-1	5.21E-06	-0.516153	0.163	0.068	-0.744650857
Anxa8	1.90E-26	-0.511435	0.835	0.56	-0.73784515
Uba52	2.14E-50	-0.506433	0.969	0.857	-0.730628043
Hsph1	2.13E-12	-0.501754	0.612	0.429	-0.723878544
Tle4	2.35E-36	-0.493217	0.652	0.269	-0.711562423
Efnb2	7.25E-21	-0.486416	0.614	0.328	-0.701749692
Kcnk2	1.44E-24	-0.485432	0.575	0.251	-0.700330164
Fam46c	8.28E-27	-0.479854	0.39	0.091	-0.69228327
Rnd3	2.21E-23	-0.478288	0.73	0.45	-0.6900244
Plxna2	1.01E-20	-0.476991	0.443	0.18	-0.688152745
Bdnf	2.17E-14	-0.466236	0.232	0.056	-0.672635979
Clstn1	8.71E-37	-0.465083	0.854	0.567	-0.6709733
Eif2s3y	2.62E-71	-0.46499	0.547	0	-0.670839106
mt-Atp8	6.96E-38	-0.462531	0.813	0.459	-0.667291634
Gm11808	4.51E-40	-0.460394	0.947	0.82	-0.664207817
Zfp703	1.03E-11	-0.459787	0.785	0.646	-0.663332742
Nt5e	2.38E-38	-0.455768	0.451	0.068	-0.657534346
Zfp36l2	7.03E-14	-0.45492	0.963	0.911	-0.656310933
Tob1	2.26E-19	-0.448194	0.876	0.749	-0.646607312
Tgfbi	3.11E-28	-0.445214	0.957	0.857	-0.642307691
Gm26825	1.38E-14	-0.437636	0.659	0.417	-0.631375585
Crim1	2.03E-23	-0.437374	0.783	0.548	-0.630997154
Tubb4b	9.42E-10	-0.435541	0.939	0.904	-0.628352444
Mat2a	4.39E-15	-0.433209	0.801	0.595	-0.624987976
Adh7	8.60E-19	-0.428269	0.606	0.342	-0.617861129
Gfra1	1.23E-33	-0.425618	0.372	0.042	-0.614036872
Tns1	5.45E-28	-0.425055	0.703	0.382	-0.61322483
Avpi1	8.93E-13	-0.424857	0.774	0.604	-0.612938628
Smarca2	4.37E-19	-0.424554	0.622	0.379	-0.612502063
Trib1	1.56E-12	-0.422142	0.734	0.576	-0.609022328
Kif21a	3.82E-16	-0.417508	0.587	0.382	-0.602336129
Ppp2r3a	1.26E-23	-0.412209	0.754	0.492	-0.594691399
Fos	1.10E-09	-0.402514	0.986	0.958	-0.580704539

Fosb	9.68E-17	-0.397524	0.984	0.953	-0.573505255
Sgms2	2.31E-16	-0.395379	0.427	0.183	-0.570411537
Iffo2	4.50E-10	-0.394813	0.843	0.749	-0.569594949
Cd44	5.52E-12	-0.391649	0.86	0.766	-0.565029457
Egfl6	1.84E-28	-0.391064	0.445	0.117	-0.564185425
Palmd	4.37E-16	-0.38799	0.935	0.867	-0.5597518
AC160336.	6.13E-14	-0.386126	0.565	0.309	-0.557061654
Rps28	2.19E-69	-0.384667	0.998	1	-0.554957634
Nfib	9.63E-29	-0.379794	0.986	0.974	-0.547926758
Anxa1	2.87E-11	-0.37972	0.913	0.829	-0.547820821
Txn1	4.49E-13	-0.379076	0.961	0.911	-0.54689051
Lgals3	1.17E-09	-0.378605	0.935	0.871	-0.546211876
Tnfrsf11b	7.02E-22	-0.3751	0.346	0.082	-0.541154505
Macf1	5.27E-20	-0.374662	0.929	0.841	-0.540522801
Ecm1	1.69E-14	-0.373702	0.732	0.525	-0.53913748
Vwa2	1.17E-30	-0.373517	0.356	0.047	-0.538871237
Gsn	1.94E-11	-0.372446	0.957	0.941	-0.537325305
Dusp1	5.42E-09	-0.371183	0.978	0.946	-0.535504196
Pdlim3	2.70E-24	-0.371096	0.323	0.054	-0.535378614
Enah	6.51E-12	-0.370056	0.856	0.766	-0.533878161
Serpinb8	7.99E-19	-0.369855	0.598	0.333	-0.533587279
Zfp36l1	2.21E-13	-0.368008	0.99	0.979	-0.530923162
Ier3	1.02E-10	-0.367171	0.994	0.965	-0.529715184
Eppk1	7.15E-21	-0.366924	0.431	0.162	-0.529359281
Hopx	3.66E-16	-0.366774	0.758	0.511	-0.529142837
Trabd2b	3.27E-21	-0.363502	0.616	0.321	-0.524422694
Dsp	1.17E-16	-0.36206	0.98	0.97	-0.522342773
Adrb2	1.03E-10	-0.35856	0.413	0.22	-0.517293147
H2-T23	1.68E-20	-0.355943	0.78	0.525	-0.513517434
Dnaja4	6.34E-11	-0.355133	0.746	0.574	-0.512349146
Myh14	2.45E-29	-0.35449	0.48	0.138	-0.51142077
Zfp36	3.97E-13	-0.352569	0.99	0.948	-0.508649631
Prnp	5.27E-17	-0.348716	0.687	0.443	-0.503090789
Actg1	1.84E-06	-0.347592	0.996	1	-0.501468777
Dsg3	5.71E-15	-0.347391	0.644	0.407	-0.501178657
Krt15	3.91E-17	-0.343947	0.994	0.993	-0.496211189
Col5a2	7.60E-22	-0.343194	0.443	0.162	-0.495124283
Shisa2	2.54E-11	-0.341804	0.762	0.574	-0.49311877
Foxc1	8.73E-33	-0.340864	0.364	0.042	-0.491762857
Cd47	7.17E-15	-0.340545	0.843	0.698	-0.491303016
Moxd1	4.04E-17	-0.339515	0.776	0.532	-0.489817137
Sfn	1.17E-12	-0.339447	1	1	-0.489718015
Tenm2	5.32E-15	-0.337592	0.833	0.67	-0.487042279
Rpl35	9.29E-37	-0.335842	0.996	0.993	-0.48451719
Sptbn1	7.49E-13	-0.33357	0.809	0.67	-0.481239989

Smad7	2.04E-10	-0.331908	0.748	0.637	-0.478842166
Hist1h2bc	0.241024	-0.3309	0.409	0.37	-0.477387631
Sox9	1.87E-07	-0.329926	0.974	0.965	-0.475982663
Baiap2	3.16E-13	-0.329414	0.506	0.286	-0.475244022
Dnajb4	2.08E-14	-0.329136	0.612	0.37	-0.474842179
Camk4	9.88E-29	-0.329088	0.309	0.028	-0.474772974
Lamc2	2.63E-13	-0.3284	0.717	0.506	-0.473781601
Jund	3.95E-20	-0.328141	1	1	-0.473407295
Slc29a1	4.17E-19	-0.328075	0.648	0.372	-0.473312485
Npnt	9.93E-13	-0.327843	0.494	0.276	-0.472977733
Gm26669	6.35E-16	-0.326336	0.593	0.342	-0.470803195
Col8a2	1.09E-21	-0.325962	0.518	0.208	-0.470264234
Trim59	5.03E-11	-0.325768	0.577	0.377	-0.4699845
Pdzk1ip1	4.89E-15	-0.325009	0.531	0.288	-0.46888864
Foxp1	7.46E-11	-0.323686	0.817	0.726	-0.466979673
Col17a1	6.74E-21	-0.320326	0.994	0.981	-0.462133021
Bok	1.04E-08	-0.317836	0.697	0.562	-0.458539724
Atf3	5.63E-11	-0.316838	0.978	0.934	-0.457101059
Steap4	8.27E-10	-0.316345	0.415	0.237	-0.456389063
Adgrg6	4.32E-15	-0.315762	0.634	0.419	-0.45554805
Dst	2.27E-14	-0.314081	0.963	0.897	-0.453122937
Fosl1	0.000225	-0.31287	0.789	0.728	-0.451375448
Tns4	9.81E-08	-0.312364	0.734	0.621	-0.450646008
Tpm1	2.47E-05	-0.312312	0.87	0.808	-0.450571189
Rps29	6.34E-53	-0.311764	1	1	-0.449779709
Nog	5.15E-22	-0.309227	0.278	0.042	-0.446120202
Lrrfip1	1.84E-12	-0.307109	0.789	0.635	-0.443065052
Plpp1	1.22E-29	-0.305501	0.339	0.04	-0.440744497
Clasrp	4.71E-15	-0.30399	0.746	0.529	-0.438564306
Hmox1	0.747697	-0.299504	0.476	0.48	-0.4320935
S100a6	4.14E-12	-0.296766	1	0.995	-0.428142396
Arid5b	9.86E-08	-0.295707	0.911	0.869	-0.426614874
Magt1	4.67E-16	-0.293872	0.591	0.351	-0.423968397
Cdkn1a	1.51E-11	-0.293426	0.862	0.763	-0.423324742
Plpp3	1.01E-15	-0.292261	0.406	0.169	-0.42164332
Prss23	0.001284	-0.291791	0.535	0.487	-0.420964941
Lmna	3.00E-11	-0.291246	0.994	0.998	-0.42017849
Jup	6.21E-15	-0.291234	0.957	0.951	-0.42016225
Pls3	2.88E-12	-0.28894	0.736	0.581	-0.416852014
Crlf1	1.24E-26	-0.288609	0.268	0.016	-0.416375153
Ptpn13	1.02E-08	-0.287225	0.644	0.52	-0.414378239
Fcgbp	0.002318	-0.28691	0.589	0.511	-0.413923122
Il31ra	3.05E-35	-0.284698	0.313	0.005	-0.410731917
Fam171b	8.18E-29	-0.280217	0.268	0.007	-0.404267075
Sdc4	4.76E-11	-0.278634	0.994	0.988	-0.401983562

Gadd45g	0.000209	-0.277332	0.467	0.344	-0.400105521
Mast4	2.74E-07	-0.274747	0.825	0.754	-0.396376386
Mcl1	4.64E-13	-0.27452	0.913	0.859	-0.396049166
Tuba1c	4.41E-09	-0.272128	0.911	0.855	-0.392597726
Zyx	1.02E-09	-0.272086	0.701	0.536	-0.392537684
Neat1	4.98E-10	-0.271009	0.984	0.988	-0.390983816
Fam25c	3.56E-07	-0.268556	0.543	0.396	-0.387444441
Tsc22d4	4.10E-10	-0.267798	0.766	0.642	-0.386350549
Pdzrn4	1.04E-11	-0.267789	0.522	0.326	-0.38633815
Skp1a	2.39E-05	-0.267372	0.846	0.817	-0.385736243
Urah	3.27E-07	-0.261578	0.953	0.927	-0.377377722
Dkk3	2.02E-11	-0.261482	0.594	0.375	-0.377239505
Rnf121	1.20E-10	-0.259424	0.654	0.461	-0.374269127
Ubb	2.03E-15	-0.259129	1	1	-0.373843556
mt-Nd4l	1.12E-14	-0.258389	0.955	0.911	-0.372776304
Dapk2	3.82E-13	-0.256063	0.677	0.45	-0.369420501
Capns2	4.95E-12	-0.255506	0.665	0.438	-0.36861713
Rpl38	6.73E-35	-0.253223	0.996	1	-0.365323597
Tacc2	6.91E-11	-0.252466	0.789	0.614	-0.364231618
Itgb6	8.01E-19	-0.252008	0.289	0.066	-0.363570046

Supplementary Table 7. Differentially Expressed Genes in induced Foxc1/Nfatc1 dKO HF-SCs.

	baseMean	log2FoldCh	lfcSE	stat	pvalue	padj
Sema4f	21.28085	-7.867891	2.006719	-3.920774	8.83E-05	0.006364158
Grik1	18.46464	-7.663221	2.069763	-3.702464	0.000213516	0.012413465
Tchhl1	18.24783	-7.646115	2.073702	-3.687181	0.000226752	0.012787666
Piezo2	17.1902	-7.560095	2.121618	-3.563362	0.000366135	0.018072087
Slc26a7	14.55661	-7.319923	2.250431	-3.252675	0.00114324	0.040520276
Kcna6	14.0142	-7.265233	2.232458	-3.254365	0.001136462	0.040377353
C1qb	13.76242	-7.239081	2.243341	-3.22692	0.001251304	0.043249357
Unc5c	24.71047	-6.620746	1.898061	-3.488162	0.000486353	0.021963072
Ptgir	23.84464	-5.576297	1.732233	-3.219137	0.001285769	0.043982282
Fam69c	34.79497	-5.072865	1.339859	-3.786119	0.000153018	0.009659855
Best2	58.07939	-4.846777	1.082349	-4.478017	7.53E-06	0.000852438
St6galna	50.98951	-4.838069	1.086423	-4.453208	8.46E-06	0.000942677
Nov	28.67455	-4.782911	1.441352	-3.31835	0.000905508	0.034505479
Lbp	76.27105	-4.27604	0.862711	-4.956512	7.18E-07	0.000124196
Atp2a3	620.8607	-4.079253	0.440415	-9.262284	2.00E-20	4.20E-17
Slc22a22	49.437	-3.989772	1.071158	-3.724726	0.000195528	0.01160676
Kcnma1	185.6813	-3.902873	0.534384	-7.303496	2.80E-13	1.79E-10
Wdfy4	102.9032	-3.729359	0.723121	-5.15731	2.51E-07	5.11E-05
Krt24	6645.218	-3.682812	0.318024	-11.58029	5.19E-31	7.63E-27
Kcne1	51.0482	-3.37905	0.961867	-3.513011	0.000443059	0.020429337
Chat	607.031	-3.359495	0.407515	-8.243853	1.67E-16	2.04E-13
Serpinb1	2686.789	-3.268924	0.317014	-10.31162	6.24E-25	3.06E-21
Serpinb1	1432.842	-3.250397	0.345057	-9.419891	4.52E-21	1.11E-17
Clip3	64.65161	-3.116931	0.804623	-3.873777	0.000107161	0.00723045
Lef1	65.91808	-3.030643	0.795836	-3.808124	0.000140025	0.008994025
Col4a3	78.38096	-2.980394	0.81799	-3.643559	0.000268894	0.014419832
Serpina3	247.0018	-2.806239	0.529435	-5.300443	1.16E-07	2.79E-05
Hhip	117.6333	-2.720934	0.709959	-3.832524	0.000126835	0.008328663
Lrguk	98.32976	-2.672511	0.687948	-3.884759	0.000102432	0.007079943
Foxc1	1867.52	-2.669469	0.272676	-9.789894	1.24E-22	4.58E-19
Tgm5	3857.118	-2.652004	0.350556	-7.565142	3.87E-14	3.00E-11
Upb1	536.0516	-2.583753	0.376258	-6.866969	6.56E-12	3.53E-09
Npas2	806.0826	-2.461465	0.425655	-5.782776	7.35E-09	2.40E-06
Sphkap	104.079	-2.447551	0.681484	-3.591504	0.000328775	0.016561479
Slc38a3	147.678	-2.403822	0.664206	-3.619089	0.000295642	0.015258227
Il31ra	3529.906	-2.381837	0.330671	-7.203031	5.89E-13	3.61E-10
Abca4	143.2542	-2.380357	0.558236	-4.264072	2.01E-05	0.001870495
Lmcd1	392.2634	-2.358578	0.450317	-5.237593	1.63E-07	3.74E-05
Ntf3	216.7182	-2.353757	0.49316	-4.772806	1.82E-06	0.000264582
Camk4	1741.687	-2.346223	0.318157	-7.374423	1.65E-13	1.10E-10
Mrgprf	961.466	-2.344963	0.310939	-7.541565	4.64E-14	3.42E-11
Bdnf	563.5718	-2.335819	0.385247	-6.063172	1.33E-09	5.03E-07

Apod	131.8148	-2.33264	0.632621	-3.687261	0.000226681	0.012787666
Mmp3	156.3183	-2.270676	0.556846	-4.077747	4.55E-05	0.003682117
Nt5e	7877.348	-2.256665	0.245944	-9.175527	4.49E-20	8.26E-17
Crlf1	2641.737	-2.237789	0.293339	-7.628682	2.37E-14	1.94E-11
Strip2	269.6535	-2.15766	0.476268	-4.530347	5.89E-06	0.000709113
Mme	420.4417	-2.151189	0.405657	-5.30297	1.14E-07	2.79E-05
Nkd1	542.4247	-2.115654	0.399927	-5.290101	1.22E-07	2.90E-05
Col6a1	9056.172	-2.107573	0.24437	-8.624527	6.44E-18	9.47E-15
4732456I	977.7922	-2.085335	0.351047	-5.940335	2.84E-09	9.96E-07
Gfra1	6388.538	-2.083111	0.239524	-8.696873	3.41E-18	5.58E-15
Serpinb3	328.8451	-2.059186	0.417932	-4.927083	8.35E-07	0.000139512
Fgl2	198.7413	-2.017348	0.595615	-3.387	0.000706613	0.029113649
Nptx1	1182.101	-1.985705	0.31673	-6.269398	3.62E-10	1.52E-07
Hid1	269.8016	-1.981236	0.46147	-4.293315	1.76E-05	0.00170312
Ramp3	737.2915	-1.977319	0.380255	-5.199984	1.99E-07	4.38E-05
Myh11	258.096	-1.932574	0.583463	-3.312249	0.000925491	0.035085163
Fam171b	1019.622	-1.896185	0.316816	-5.985132	2.16E-09	7.95E-07
Cdh13	1261.149	-1.895339	0.276154	-6.863328	6.73E-12	3.53E-09
Adcy1	7108.643	-1.89458	0.243295	-7.787157	6.85E-15	6.72E-12
Nrep	2117.409	-1.889626	0.375185	-5.036518	4.74E-07	8.94E-05
Vwa2	6544.915	-1.888504	0.243907	-7.742728	9.73E-15	8.42E-12
Slc39a8	1439.033	-1.884306	0.345936	-5.446979	5.12E-08	1.45E-05
Sncg	255.6989	-1.882083	0.438701	-4.290123	1.79E-05	0.001705612
Sema3e	4022.601	-1.866838	0.346593	-5.386253	7.19E-08	1.96E-05
Ednra	1075.9	-1.859943	0.333645	-5.574609	2.48E-08	7.60E-06
Cd207	374.0272	-1.858619	0.533902	-3.481196	0.00049918	0.022317431
Cd34	22222.51	-1.849512	0.238159	-7.765864	8.11E-15	7.45E-12
Col8a2	2960.181	-1.838818	0.270244	-6.804288	1.02E-11	5.15E-09
Rcan1	18853.13	-1.82833	0.278673	-6.560837	5.35E-11	2.46E-08
Me3	312.3131	-1.809737	0.417408	-4.335651	1.45E-05	0.00144436
Ogdhl	422.1508	-1.796258	0.389761	-4.608613	4.05E-06	0.000509617
Fstl1	4082.525	-1.788953	0.263427	-6.79109	1.11E-11	5.46E-09
Atp6v0e2	219.6895	-1.775324	0.469597	-3.78053	0.000156495	0.009795255
Plb1	306.7781	-1.771714	0.407611	-4.346581	1.38E-05	0.001393083
Gdpd1	221.3785	-1.763757	0.471942	-3.737231	0.000186058	0.011124889
Hpgd	934.2382	-1.74843	0.411744	-4.246398	2.17E-05	0.001960312
Car6	378.3351	-1.739561	0.435711	-3.992468	6.54E-05	0.004983461
Cgref1	739.5325	-1.730246	0.397798	-4.349554	1.36E-05	0.001383806
Nog	709.885	-1.70802	0.386072	-4.424101	9.68E-06	0.001063051
Tmem108	629.9532	-1.698376	0.338265	-5.020848	5.14E-07	9.46E-05
Unc13b	641.9012	-1.687252	0.347085	-4.861201	1.17E-06	0.000186542
Ank	14858.7	-1.675981	0.249842	-6.708174	1.97E-11	9.35E-09
Trnp1	959.7794	-1.635981	0.330415	-4.951295	7.37E-07	0.000126089
S100a4	8209.481	-1.607553	0.253818	-6.33348	2.40E-10	1.04E-07
Krt75	1213.285	-1.588036	0.314692	-5.046316	4.50E-07	8.63E-05

Lmo7	2928.085	-1.578193	0.282191	-5.592643	2.24E-08	7.00E-06
C1s1	272.9788	-1.572264	0.472437	-3.327984	0.000874769	0.033771586
Akt3	231.2349	-1.55458	0.455274	-3.414606	0.000638744	0.02715402
Hmox1	25054.82	-1.548349	0.365753	-4.233316	2.30E-05	0.002052761
Ccdc3	6425.853	-1.474902	0.268207	-5.499124	3.82E-08	1.12E-05
Fbxo2	632.7495	-1.470663	0.327019	-4.49718	6.89E-06	0.000796218
Spats2l	773.7126	-1.458992	0.313292	-4.656968	3.21E-06	0.00042144
Fst	47272.76	-1.405144	0.239596	-5.864639	4.50E-09	1.50E-06
Aff3	1392.089	-1.401521	0.377306	-3.714545	0.00020357	0.011929527
Peg10	354.739	-1.391147	0.408731	-3.40358	0.00066509	0.027988132
Cacna1c	2082.96	-1.370802	0.39043	-3.511002	0.00044642	0.020519993
Sgms2	9190.944	-1.364361	0.281321	-4.849833	1.24E-06	0.000195433
Sema7a	353.751	-1.346951	0.391378	-3.441559	0.000578373	0.024948056
Grip1	1113.874	-1.330785	0.302935	-4.392971	1.12E-05	0.001174747
Fam46b	2297.283	-1.319649	0.328011	-4.023182	5.74E-05	0.004444985
Enpp2	312.9323	-1.316233	0.408004	-3.226028	0.00125521	0.043249357
Col6a2	2761.398	-1.309186	0.277375	-4.719916	2.36E-06	0.000326624
Pknox2	359.1328	-1.304172	0.398024	-3.276612	0.001050607	0.038441235
Foxn2	4835.915	-1.299407	0.319742	-4.063916	4.83E-05	0.003857614
Dab2	1145.307	-1.279891	0.308504	-4.1487	3.34E-05	0.002859441
Nrcam	534.0529	-1.273845	0.342247	-3.722	0.000197651	0.011640613
Ccnf	588.7429	-1.268733	0.357195	-3.551935	0.000382409	0.018518594
Egfl6	2193.775	-1.260787	0.267201	-4.71849	2.38E-06	0.000326624
Krt80	10727.77	-1.260212	0.243959	-5.165677	2.40E-07	5.03E-05
Grem1	4020.187	-1.26016	0.334083	-3.772001	0.000161944	0.010008534
Fmn1	981.2812	-1.256675	0.293185	-4.28629	1.82E-05	0.001724099
Pdlim3	2755.292	-1.256528	0.284234	-4.420751	9.84E-06	0.00107167
Smad9	471.6208	-1.243774	0.369531	-3.365818	0.000763171	0.030839229
Cgnl1	3321.41	-1.223457	0.251355	-4.86744	1.13E-06	0.000182737
Bmp2	5009.117	-1.22148	0.247076	-4.943749	7.66E-07	0.000129565
Ppap2a	2026.581	-1.219848	0.254601	-4.791214	1.66E-06	0.000246302
Arhgap44	4047.838	-1.210263	0.258833	-4.675845	2.93E-06	0.000391454
Fam83d	881.0094	-1.199655	0.312115	-3.843633	0.000121226	0.008032047
Hoxb9	1806.541	-1.192602	0.286027	-4.169551	3.05E-05	0.00262526
Anxa8	48391.88	-1.180186	0.218357	-5.404841	6.49E-08	1.80E-05
Klhl21	6995.42	-1.179877	0.285417	-4.133871	3.57E-05	0.003032812
Tmem184	789.4083	-1.176427	0.319063	-3.687132	0.000226796	0.012787666
Gt(ROSA	6302.404	-1.165531	0.345356	-3.374868	0.00073851	0.030021068
Mt2	71326.58	-1.15008	0.245456	-4.685477	2.79E-06	0.000376913
Tnfrsf21	1038.718	-1.148953	0.294082	-3.906911	9.35E-05	0.006707569
Mt1	83906.33	-1.144405	0.220469	-5.190771	2.09E-07	4.46E-05
Mitf	1764.466	-1.143399	0.280198	-4.080688	4.49E-05	0.003669284
Crispld1	612.0789	-1.143297	0.347657	-3.288573	0.001006967	0.037402713
Pdzk1ip1	4757.001	-1.140573	0.247072	-4.616367	3.91E-06	0.000495181
Nudt4	17624.17	-1.138672	0.239651	-4.751384	2.02E-06	0.000283014

Ankrd35	2217.09	-1.127752	0.34822	-3.238617	0.001201107	0.041865119
Gadd45g	2869.742	-1.117754	0.287163	-3.8924	9.93E-05	0.006940842
Fam25c	3080.427	-1.116683	0.272119	-4.10366	4.07E-05	0.003360463
Ccdc88c	4190.424	-1.116527	0.330702	-3.376234	0.000734854	0.030021068
Adh7	5658.16	-1.110683	0.338523	-3.280967	0.001034517	0.038041769
Ube2q2	7911.492	-1.109088	0.238657	-4.647196	3.36E-06	0.00043037
Map3k6	2121.575	-1.10054	0.292536	-3.762071	0.000168512	0.010242334
Fam213a	892.4302	-1.085621	0.328446	-3.305327	0.000948657	0.03577898
Lipg	3803.585	-1.082598	0.319491	-3.388511	0.000702733	0.029035091
Igdcc4	2191.427	-1.079904	0.253269	-4.263862	2.01E-05	0.001870495
Cdkn1a	46367.71	-1.079627	0.240138	-4.495864	6.93E-06	0.000796218
Ano1	778.2772	-1.079307	0.339824	-3.176078	0.001492808	0.048794903
Fam46c	4572.453	-1.078844	0.295304	-3.653334	0.000258857	0.014101951
Ablim1	3838.757	-1.075104	0.261665	-4.108704	3.98E-05	0.003306494
Krt16	52635.1	-1.068653	0.329938	-3.238955	0.001199683	0.041865119
Postn	108508.1	-1.060028	0.22232	-4.768034	1.86E-06	0.000266626
Bach2	1138.567	-1.053688	0.32977	-3.195226	0.001397216	0.046626045
Ahcyl2	13389.26	-1.052536	0.262238	-4.013663	5.98E-05	0.004579991
Prnp	14349.13	-1.050772	0.247752	-4.241218	2.22E-05	0.001993873
Grwd1	2115.189	-1.046731	0.327607	-3.195079	0.001397925	0.046626045
Krt6b	2307.85	-1.043934	0.269135	-3.87885	0.000104951	0.007153684
Sh3rf1	11987.35	-1.040072	0.307722	-3.37991	0.000725096	0.02979173
Igfbp6	882.3715	-1.034807	0.314615	-3.289119	0.001005014	0.037402713
Ctgf	12940.96	-1.020781	0.278773	-3.6617	0.000250547	0.013802596
Dock8	1028.597	-1.018142	0.315675	-3.225287	0.001258462	0.043249357
Tcp11l2	4689.611	-1.01756	0.285347	-3.56605	0.000362402	0.01800867
Mafk	24656.21	-1.010994	0.231191	-4.372977	1.23E-05	0.001269567
Dmkn	92487.03	-1.004676	0.219219	-4.582982	4.58E-06	0.000566594
Fcgbp	19682.91	-0.996502	0.281463	-3.540435	0.000399468	0.019201879
Pmp22	2964.638	-0.996172	0.273637	-3.640483	0.000272127	0.014419832
Kif21a	12816.18	-0.990464	0.281104	-3.52348	0.000425918	0.019951704
Pi15	28234.92	-0.984042	0.225606	-4.361775	1.29E-05	0.0013178
Clic3	1875.695	-0.978866	0.260098	-3.763456	0.000167581	0.010228013
Krt6a	225755.1	-0.976555	0.229503	-4.255086	2.09E-05	0.001921077
Bmp6	2424.241	-0.970034	0.278112	-3.487931	0.000486774	0.021963072
Kctd1	3122.943	-0.966764	0.242997	-3.9785	6.94E-05	0.005204551
Rab8b	9098.517	-0.964272	0.26447	-3.646047	0.000266306	0.014419832
Calml3	18267.52	-0.96342	0.237523	-4.056118	4.99E-05	0.003945726
D1Ertd62	1214.12	-0.960754	0.284689	-3.374745	0.000738842	0.030021068
Serpinb8	10137.45	-0.957346	0.298552	-3.206625	0.001343017	0.045308355
Pard6b	3236.261	-0.953767	0.287309	-3.319659	0.000901276	0.034505479
Nt5dc2	4118.035	-0.947732	0.278481	-3.403216	0.000665976	0.027988132
Nrip3	1172.738	-0.939199	0.279252	-3.363269	0.000770253	0.031040145
Fam188a	5127.966	-0.937329	0.253931	-3.691279	0.00022313	0.012787666
Hspb8	29116.3	-0.932022	0.233951	-3.98384	6.78E-05	0.005115006

Sipa1l2	1481.853	-0.921988	0.288645	-3.194194	0.001402217	0.046663372
E130012	2734.33	-0.912303	0.263528	-3.461878	0.00053642	0.023623369
Slc35e4	5191.124	-0.910269	0.233165	-3.903964	9.46E-05	0.006724215
Rhbdl3	2258.481	-0.907684	0.25043	-3.624497	0.000289525	0.014995137
Ehd4	6912.204	-0.903698	0.260508	-3.468979	0.000522441	0.023153761
Myh14	29569.55	-0.898098	0.251972	-3.564273	0.000364866	0.018070057
Hagh	4777.185	-0.890306	0.233723	-3.809241	0.000139394	0.008992744
Dedd2	5786.451	-0.882596	0.255404	-3.455682	0.000548903	0.024100948
Hspa8	189941.1	-0.873913	0.232951	-3.751488	0.000175788	0.010597003
Skp1a	13611.36	-0.869903	0.249801	-3.48239	0.000496959	0.02228587
Igfbp3	27958.43	-0.868313	0.259599	-3.344824	0.000823349	0.032509236
Aqp3	135512	-0.865105	0.229077	-3.776476	0.000159063	0.009913805
Tmem45a	5862.447	-0.859048	0.249311	-3.445694	0.000569595	0.024714367
Prss23	12633.45	-0.853687	0.235978	-3.617654	0.000297286	0.015287374
Npnt	15874.71	-0.848032	0.245933	-3.448217	0.000564301	0.024557109
Bok	19712.2	-0.844212	0.232791	-3.626475	0.000287317	0.014986338
Ppp2r3a	10762.56	-0.83705	0.226149	-3.701317	0.000214483	0.01242062
Dmd	3392.359	-0.832766	0.259571	-3.208243	0.001335484	0.045240635
Slc29a1	9150.366	-0.827436	0.227237	-3.641285	0.000271281	0.014419832
Slain2	7420.938	-0.826191	0.239278	-3.452853	0.000554692	0.024282633
Ptn	25650.39	-0.826189	0.232055	-3.560313	0.000370413	0.01816137
Tuba4a	18548.59	-0.818053	0.230766	-3.544953	0.000392683	0.01893761
Sat1	7395.777	-0.817654	0.231562	-3.531045	0.000413921	0.019591748
Cadm1	7836.324	-0.81696	0.232412	-3.515129	0.00043954	0.020429337
Lamb3	31961.14	-0.816835	0.233745	-3.494551	0.00047486	0.021618133
Ppp1r2	7244.264	-0.80807	0.242934	-3.32629	0.000880105	0.033800149
Ndrg1	107117.7	-0.805286	0.247392	-3.255102	0.001133517	0.040377353
Cyp4b1	7731.152	-0.797842	0.249933	-3.192221	0.00141183	0.046666541
Wsb2	9366.01	-0.792873	0.244019	-3.249226	0.001157196	0.040916339
Avpi1	17169.54	-0.786029	0.234443	-3.352747	0.000800137	0.031894893
Lgals3	52651.74	-0.759171	0.23272	-3.262168	0.001105636	0.039665349
Cdv3	18847.02	-0.757132	0.231978	-3.26381	0.001099249	0.03960536
Bnc1	8523.907	0.724284	0.228146	3.174648	0.001500183	0.048927247
Pde4b	13772.38	0.749323	0.230809	3.2465	0.001168333	0.041112456
Man2a1	7705.221	0.781087	0.245627	3.179972	0.001472893	0.048358903
Atp1b3	21977.29	0.788279	0.223191	3.531853	0.000412659	0.019591748
Lbh	9901.38	0.795851	0.23796	3.344473	0.000824389	0.032509236
Insig2	9663.679	0.809676	0.247935	3.26568	0.001092015	0.03946548
Dsg2	3394.02	0.815545	0.25011	3.260749	0.001111185	0.039767448
Rnps1	3116.389	0.82373	0.251842	3.270826	0.001072339	0.039139035
Irf3	3736.75	0.823834	0.248868	3.310323	0.000931885	0.035236763
Adamts1	2764.009	0.826166	0.247574	3.33704	0.000846758	0.033045839
Echdc2	2802.373	0.828056	0.251424	3.29346	0.000989625	0.037127435
Slc27a1	7459.482	0.832778	0.252909	3.292791	0.000991983	0.037127435
Farp1	5902.292	0.833601	0.239821	3.475928	0.000509088	0.022691449

Angptl2	3318.64	0.837022	0.263406	3.177687	0.001484552	0.048633118
Epm2aip	5089.585	0.837358	0.251063	3.335252	0.00085222	0.033162186
Panx1	3113.919	0.838039	0.251138	3.336966	0.000846984	0.033045839
Smox	7117.162	0.869193	0.270507	3.213201	0.001312642	0.044733389
Tle2	3606.235	0.877288	0.271956	3.225842	0.001256025	0.043249357
Fbln2	3774.932	0.881568	0.259608	3.395764	0.000684374	0.028546578
Rassf9	1261.874	0.894403	0.280152	3.192564	0.001410159	0.046666541
Arhgef19	6485.199	0.911053	0.268695	3.390656	0.000697256	0.028889974
Akap11	6665.069	0.91128	0.278107	3.276721	0.001050202	0.038441235
Scarb2	5828.904	0.917893	0.235385	3.899539	9.64E-05	0.006815347
Smoc2	2346.501	0.922008	0.253226	3.641043	0.000271536	0.014419832
Ttc14	2223.988	0.926161	0.26699	3.468893	0.000522609	0.023153761
Celsr1	15524.08	0.928921	0.249593	3.721748	0.000197848	0.011640613
Tsc22d1	8586.803	0.93341	0.261413	3.570633	0.00035612	0.01781691
Ccl2	3416.24	0.933734	0.274993	3.395479	0.000685087	0.028546578
Irf2bpl	3496.228	0.941305	0.293033	3.212282	0.001316851	0.044733389
Fads1	3409.968	0.944588	0.294474	3.207716	0.001337934	0.045240635
Dusp10	8211.506	0.949583	0.229991	4.128793	3.65E-05	0.00308274
Hilpda	3457.969	0.950973	0.264106	3.600726	0.00031733	0.016095195
Slc4a3	1725.204	0.965384	0.261852	3.686748	0.000227138	0.012787666
Il22ra1	2163.125	0.973694	0.264971	3.674717	0.000238113	0.01326669
Sugp2	1452	0.97635	0.273187	3.573922	0.000351673	0.017654468
St3gal4	1863.809	0.981389	0.261532	3.752466	0.000175103	0.010597003
4632428I	2717.561	0.998543	0.299181	3.33759	0.000845084	0.033045839
Tppp3	23332.13	0.999358	0.286646	3.486389	0.000489588	0.022022499
St5	3578.546	1.003182	0.258723	3.877442	0.000105561	0.00715526
Anln	1682.57	1.003501	0.293026	3.424611	0.00061568	0.02640243
P2rx7	977.0898	1.007373	0.308699	3.263289	0.001101271	0.03960536
9430015(	748.333	1.008698	0.313223	3.220382	0.0012802	0.043893849
Lrig1	9151.006	1.009381	0.237443	4.251041	2.13E-05	0.001943958
Mbd1	3039.571	1.010371	0.266398	3.792712	0.000149011	0.009488304
Stard5	4011.039	1.010717	0.275772	3.665044	0.000247296	0.013726346
Rassf5	1263.348	1.0151	0.287121	3.535446	0.000407088	0.019504402
Nrip1	6707.109	1.018453	0.266339	3.823902	0.000131356	0.00854918
Gja1	116079.9	1.028667	0.265215	3.878619	0.000105051	0.007153684
Ddit4	3190.59	1.032008	0.290124	3.557124	0.000374938	0.018322123
Fam193b	5891.619	1.03316	0.279523	3.696146	0.000218897	0.012626486
Epgn	10895.62	1.033941	0.230603	4.483646	7.34E-06	0.000836686
Hcar2	3674.898	1.037579	0.290815	3.567839	0.000359937	0.017946822
D3Ertd25	1140.846	1.038854	0.30975	3.35385	0.000796955	0.031854386
Wipi1	901.1665	1.046433	0.3062	3.417481	0.000632034	0.02694665
Ect2	1080.829	1.051769	0.306031	3.436808	0.000588612	0.025315479
Xdh	10205.55	1.057267	0.227169	4.6541	3.25E-06	0.000423565
Apbb3	933.493	1.061183	0.326765	3.247546	0.00116405	0.041059979
Ptprv	4446.16	1.07034	0.270862	3.951609	7.76E-05	0.005680712

Cxcl12	15344.32	1.072524	0.271137	3.955658	7.63E-05	0.005613269
Nek6	1467.929	1.073056	0.291114	3.686033	0.000227777	0.012787666
Mocs1	611.3627	1.080857	0.329191	3.28337	0.001025739	0.037908541
Neat1	72394.85	1.083113	0.306758	3.530842	0.000414238	0.019591748
Fzd8	689.4298	1.086215	0.342874	3.16797	0.001535071	0.049954335
Arhgap31	1181.668	1.086617	0.320431	3.391108	0.000696106	0.028889974
Ucp2	109061	1.088171	0.288403	3.773092	0.000161237	0.010006895
Tia1	1461.617	1.091897	0.295913	3.689923	0.000224322	0.012787666
Sepp1	12300.14	1.099688	0.290171	3.789795	0.000150772	0.009559046
Abi3bp	2284.624	1.10405	0.303867	3.633332	0.000279784	0.014697675
Cdca8	555.4619	1.10787	0.347215	3.190729	0.001419143	0.046803089
Rgs11	676.7579	1.108427	0.335643	3.302399	0.000958616	0.036062113
Cenpa	918.2764	1.112914	0.31499	3.533179	0.000410594	0.019591748
Bgn	19917.41	1.113903	0.232255	4.796044	1.62E-06	0.000242893
Slc43a2	973.196	1.115303	0.349268	3.193254	0.00140679	0.046666541
Cd276	586.592	1.118061	0.339913	3.289257	0.001004523	0.037402713
Leng8	8913.622	1.124999	0.278073	4.045692	5.22E-05	0.004081661
Pdlim4	1329.185	1.125555	0.277322	4.058653	4.94E-05	0.003924244
Fabp5	5743.973	1.126841	0.233237	4.831319	1.36E-06	0.000210001
Sema6a	1200.267	1.12765	0.311832	3.61621	0.000298948	0.015287374
Lif	1928.153	1.130286	0.323437	3.494614	0.000474747	0.021618133
Racgap1	761.6415	1.133059	0.346867	3.266552	0.001088658	0.039454118
Lrrc8c	700.6179	1.135282	0.342317	3.316461	0.000911654	0.034649926
Spaca6	944.9868	1.138512	0.351271	3.241122	0.001190603	0.041796148
Vsnl1	1920.372	1.147929	0.352703	3.254665	0.001135264	0.040377353
Ncapd2	1376.707	1.158416	0.316223	3.663289	0.000248997	0.013768783
Pnisr	3764.447	1.189405	0.274429	4.334111	1.46E-05	0.001444741
Heg1	5485.2	1.191846	0.252875	4.713183	2.44E-06	0.000332148
Igsf9	3084.341	1.194977	0.250661	4.767306	1.87E-06	0.000266626
Lacc1	405.6613	1.196913	0.372595	3.212366	0.001316464	0.044733389
Dbn1	1844.035	1.202579	0.330244	3.641482	0.000271073	0.014419832
Mcam	2989.636	1.203224	0.315663	3.811738	0.000137993	0.0089416
Tgfbr3	1060.854	1.208659	0.309486	3.905381	9.41E-05	0.006717373
Arrdc3	3457.179	1.212956	0.294037	4.125184	3.70E-05	0.003113586
Cxcl1	4153.015	1.217045	0.309908	3.927113	8.60E-05	0.006229336
Cep85l	386.4767	1.218396	0.377231	3.229839	0.0012386	0.043069886
Syde1	740.9782	1.220022	0.361175	3.377921	0.00073036	0.029924396
9330133	645.5384	1.225345	0.336636	3.639966	0.000272674	0.014419832
Agap2	727.5151	1.228665	0.329886	3.72451	0.000195695	0.01160676
Kif11	631.4823	1.232742	0.384553	3.205644	0.001347604	0.045359046
Pmaip1	3093.849	1.238789	0.285456	4.33968	1.43E-05	0.001427775
Ankrd6	750.8649	1.240035	0.308689	4.017098	5.89E-05	0.004537392
Speg	468.2388	1.242199	0.371506	3.343688	0.000826728	0.032514275
Sytl2	1837.884	1.259212	0.291745	4.31614	1.59E-05	0.00155701
Nppc	8603.031	1.264152	0.354896	3.562031	0.000367997	0.018103249

Itga2b	1062.444	1.266262	0.37729	3.356206	0.000790196	0.03167027
Abcd1	395.8266	1.269369	0.381334	3.328761	0.000872332	0.033766145
9430076(	396.6804	1.278846	0.399706	3.199467	0.001376817	0.046131222
Gjb2	3671.759	1.281869	0.31124	4.118582	3.81E-05	0.003185924
Tmtc4	2288.067	1.281982	0.26559	4.826926	1.39E-06	0.000212448
Casp1	1106.491	1.286932	0.289739	4.4417	8.93E-06	0.000987062
Pm20d1	2167.134	1.288944	0.324666	3.970065	7.19E-05	0.005337801
Pla2g7	739.1266	1.290148	0.363247	3.551711	0.000382735	0.018518594
Gnmt	1119.917	1.292656	0.332769	3.884539	0.000102524	0.007079943
Tk1	609.1414	1.306353	0.349296	3.739958	0.000184051	0.011049828
Snai3	803.4846	1.30981	0.324181	4.040361	5.34E-05	0.00415346
Gsr	551.7913	1.312182	0.371905	3.528276	0.000418275	0.019656263
Accs	658.1957	1.314046	0.379257	3.46479	0.000530645	0.023439199
Adamts2	939.405	1.317897	0.300145	4.390866	1.13E-05	0.001177766
Nckap5l	5902.152	1.31834	0.299355	4.403939	1.06E-05	0.001124896
Mdfic	820.2986	1.31869	0.375335	3.513365	0.00044247	0.020429337
Plk2	21965.3	1.319093	0.250955	5.256286	1.47E-07	3.43E-05
Timp1	547.1363	1.325769	0.346143	3.830117	0.000128082	0.008373172
Sorcs2	1002.652	1.339987	0.310798	4.311446	1.62E-05	0.001579904
Irx4	5215.235	1.341934	0.269861	4.972691	6.60E-07	0.000117661
Slco2b1	468.7598	1.355264	0.370735	3.655614	0.000256567	0.014081516
Bhlhe41	353.8277	1.358622	0.393686	3.451031	0.000558449	0.02437457
Ctsc	1789.925	1.372004	0.26381	5.200735	1.99E-07	4.38E-05
Serpine1	8136.363	1.382821	0.258995	5.339181	9.34E-08	2.41E-05
Gm1045	363.6751	1.388843	0.417449	3.326977	0.000877937	0.033800149
Spag5	391.8716	1.389289	0.396167	3.506825	0.000453487	0.020779855
Slc7a8	12704.44	1.396618	0.259979	5.372037	7.79E-08	2.08E-05
Cep55	269.8076	1.39681	0.431088	3.240195	0.001194479	0.041832345
Mybl2	415.3748	1.397483	0.379804	3.679488	0.000233703	0.013070462
Scd2	3260.79	1.401255	0.262045	5.347374	8.92E-08	2.34E-05
Aspm	354.3285	1.401611	0.398959	3.513175	0.000442785	0.020429337
Kif20a	364.9236	1.410006	0.391838	3.598439	0.000320133	0.016181593
2810474(	6335.333	1.41416	0.284446	4.971626	6.64E-07	0.000117661
Ivl	2179.127	1.420886	0.388895	3.653654	0.000258534	0.014101951
Cnn3	1615.719	1.423766	0.282168	5.045814	4.52E-07	8.63E-05
Lgals9	1204.179	1.425171	0.335453	4.248503	2.15E-05	0.001953968
Col16a1	17875.2	1.428181	0.240268	5.944117	2.78E-09	9.96E-07
Slc16a6	641.9601	1.43141	0.323915	4.419098	9.91E-06	0.001071957
Mki67	3156.687	1.440764	0.326649	4.410736	1.03E-05	0.001106073
Slc27a6	748.041	1.444187	0.406589	3.551958	0.000382376	0.018518594
Htra1	3420.336	1.451665	0.290743	4.992953	5.95E-07	0.00010798
Atp12a	2259.099	1.462967	0.323977	4.515648	6.31E-06	0.000748775
Ube2c	723.4533	1.472092	0.349637	4.210343	2.55E-05	0.00224584
Tmem98	310.6455	1.4738	0.428221	3.441681	0.000578111	0.024948056
2810029(	708.3266	1.481722	0.406914	3.641361	0.000271201	0.014419832

Ntn4	2021.638	1.4946	0.396866	3.76601	0.000165877	0.010166203
Procr	3031.048	1.516339	0.301218	5.034025	4.80E-07	8.94E-05
Aurkb	366.172	1.523677	0.471891	3.228879	0.001242766	0.043112836
Inhbb	3252.036	1.528085	0.321192	4.757548	1.96E-06	0.000277149
Timp3	27061.59	1.528771	0.279666	5.466424	4.59E-08	1.32E-05
Etv4	364.8169	1.530459	0.40586	3.770903	0.000162658	0.010010608
Lamb1	4767.611	1.536758	0.278203	5.523884	3.32E-08	9.95E-06
Tmem17	325.8254	1.536874	0.451328	3.405225	0.000661096	0.027942699
Kif15	270.6387	1.537595	0.459183	3.348542	0.00081238	0.032208355
Adgrb2	734.4324	1.540036	0.340048	4.528878	5.93E-06	0.000709113
St6gal1	411.2129	1.541354	0.376163	4.097574	4.18E-05	0.003430756
Steap2	245.0046	1.546188	0.460613	3.356808	0.000788479	0.03167027
Bub1b	458.0381	1.546484	0.380131	4.068293	4.74E-05	0.00380656
Slc6a2	946.8075	1.546815	0.387767	3.989034	6.63E-05	0.005030082
Slc25a42	779.9906	1.551333	0.400989	3.868766	0.000109387	0.007346943
Ncald	331.2067	1.569174	0.397656	3.946062	7.94E-05	0.005785079
Tnf	269.4179	1.577126	0.436166	3.615884	0.000299324	0.015287374
Zfp626	310.0142	1.583964	0.435254	3.639173	0.000273515	0.014419832
Pbk	284.1425	1.585631	0.436762	3.630426	0.000282954	0.014811259
Hsf4	281.3687	1.58701	0.47624	3.332373	0.000861089	0.033418869
Fhod3	636.6354	1.60117	0.470919	3.4001	0.000673612	0.028228382
Ppp1r3b	2583.486	1.601355	0.311241	5.145069	2.67E-07	5.32E-05
Apobec1	369.8659	1.606289	0.469206	3.423419	0.000618386	0.026441389
Slc40a1	791.9193	1.606754	0.479472	3.351089	0.000804945	0.031999836
Cxcr4	938.7637	1.607328	0.323867	4.962925	6.94E-07	0.000121593
Pxdn	2151.247	1.607484	0.30951	5.19364	2.06E-07	4.46E-05
Cdk1	486.2688	1.607837	0.383607	4.191367	2.77E-05	0.002413308
Col12a1	18322.4	1.612817	0.233931	6.894424	5.41E-12	3.06E-09
1810011	5322.954	1.620787	0.311223	5.207802	1.91E-07	4.32E-05
Krt42	730.2969	1.63197	0.318954	5.11663	3.11E-07	6.10E-05
Mcm3	649.4803	1.634224	0.335006	4.878188	1.07E-06	0.000174979
Gprc5b	612.149	1.649759	0.340379	4.846835	1.25E-06	0.000196297
Tril	789.9401	1.654596	0.42949	3.852463	0.000116936	0.007801915
Ccna2	464.6553	1.663541	0.427464	3.891647	9.96E-05	0.006940842
Plcl1	1233.166	1.66417	0.361417	4.604576	4.13E-06	0.000515197
Lurap1l	588.2292	1.670846	0.390325	4.280656	1.86E-05	0.001757003
D17H6S5	1238.735	1.684329	0.277383	6.072223	1.26E-09	4.88E-07
Wnt9a	551.4129	1.695651	0.485331	3.493804	0.00047619	0.021618133
Kifc1	239.8027	1.710156	0.520325	3.28671	0.001013652	0.037556172
Prkcq	413.9937	1.717609	0.442683	3.880002	0.000104456	0.007153684
Slc2a4	481.6992	1.719662	0.421764	4.077307	4.56E-05	0.003682117
Adcy7	471.0506	1.721578	0.360086	4.781024	1.74E-06	0.000256531
Mettl20	229.9378	1.746469	0.549117	3.180504	0.001470193	0.048358903
Cenpf	580.5765	1.750766	0.35747	4.897658	9.70E-07	0.000160288
Ccnb2	511.9217	1.755393	0.41249	4.255602	2.08E-05	0.001921077

Cdca3	576.0446	1.757946	0.385829	4.556283	5.21E-06	0.000638208
Dlgap5	224.1437	1.761545	0.536755	3.28184	0.001031321	0.038019303
Lcn2	423.1079	1.764394	0.367727	4.798108	1.60E-06	0.000242883
Angptl4	15382.59	1.768411	0.278493	6.349938	2.15E-10	9.60E-08
1110004I	1857.891	1.773919	0.286383	6.194229	5.86E-10	2.33E-07
Slpi	1461.395	1.775967	0.390531	4.547567	5.43E-06	0.000659714
Gabre	315.3278	1.802497	0.409058	4.406459	1.05E-05	0.001119952
Prss12	311.0091	1.834963	0.462792	3.964984	7.34E-05	0.005425386
Nceh1	423.4488	1.842802	0.40851	4.511033	6.45E-06	0.000759134
Stbd1	2716.491	1.843341	0.31141	5.919335	3.23E-09	1.11E-06
Slitrk6	143.7335	1.851147	0.557766	3.318857	0.000903867	0.034505479
Prr11	197.5451	1.886165	0.523753	3.601251	0.00031669	0.016095195
Mmp2	5535.802	1.897835	0.368156	5.154974	2.54E-07	5.11E-05
Birc5	372.3033	1.902456	0.42215	4.506591	6.59E-06	0.000769041
Igfals	184.3169	1.902749	0.582467	3.266709	0.001088056	0.039454118
Pappa	2286.252	1.909302	0.25841	7.388658	1.48E-13	1.04E-10
Cmah	8415.315	1.909681	0.359971	5.3051	1.13E-07	2.79E-05
C630043	302.0032	1.917053	0.516439	3.71206	0.000205579	0.01199945
Car12	10979.52	1.9262	0.227926	8.450994	2.89E-17	3.86E-14
Atp6v1b1	229.8854	2.041754	0.467523	4.367175	1.26E-05	0.00129464
Adamts3	569.2552	2.06603	0.36488	5.662219	1.49E-08	4.78E-06
Hs3st3a1	260.0873	2.083864	0.547935	3.803122	0.000142884	0.009137753
Clec2e	356.8107	2.180109	0.520028	4.192289	2.76E-05	0.002413308
Skint8	154.0899	2.256131	0.579262	3.89484	9.83E-05	0.006915587
Itih5	1669.294	2.259423	0.283188	7.978536	1.48E-15	1.56E-12
Anxa3	357.0898	2.263102	0.426089	5.311333	1.09E-07	2.76E-05
Stac2	116.6447	2.279491	0.697848	3.266458	0.001089018	0.039454118
B3gnt7	127.7083	2.307252	0.721008	3.200039	0.001374089	0.046131222
Pdgfc	128.6959	2.376593	0.655665	3.624706	0.000289291	0.014995137
C2cd4b	649.0807	2.425159	0.520062	4.663213	3.11E-06	0.000412529
Has2os	126.6803	2.437724	0.583953	4.174519	2.99E-05	0.002583736
Eid2	86.4587	2.438443	0.715058	3.410132	0.000649314	0.027523801
Slfn10-ps	171.3463	2.444958	0.636364	3.842076	0.000121998	0.008046932
Vtcn1	146.0819	2.463152	0.63947	3.851864	0.000117222	0.007801915
Aldh1a2	669.1885	2.495944	0.359506	6.9427	3.85E-12	2.26E-09
Bub1	201.585	2.613069	0.561997	4.649611	3.33E-06	0.000429093
Rps2	31052.62	2.614468	0.248749	10.51046	7.73E-26	5.69E-22
Rpl29	14863.02	2.660611	0.275718	9.649768	4.93E-22	1.45E-18
Dact2	111.3129	2.716128	0.670554	4.050575	5.11E-05	0.004018776
Ccdc8	70.37951	2.818614	0.800606	3.520598	0.000430575	0.02010578
Cntn2	316.0202	2.983177	0.477677	6.245177	4.23E-10	1.73E-07
Krt73	76.58111	3.265522	0.86309	3.783522	0.000154625	0.009719545
Dok1	49.98582	3.423794	0.970045	3.529521	0.000416312	0.019626705
Pcp4	210.1026	3.512763	0.681113	5.157388	2.50E-07	5.11E-05
Gm8615	137.3922	3.521051	0.885297	3.977253	6.97E-05	0.005205349

Vnn1	70.23769	4.923132	1.101711	4.468625	7.87E-06	0.000883934
Kcnf1	196.4471	5.49855	0.670807	8.196912	2.47E-16	2.79E-13
Hist1h3d	15.20979	7.370305	2.186989	3.37007	0.00075149	0.030450874
Pamr1	26.60769	8.177583	1.905355	4.291895	1.77E-05	0.00170312
Srd5a2	32.46583	8.46499	2.009768	4.211925	2.53E-05	0.002243602

Supplementary Table 8. Downregulated genes in old vs young IFE (scRNA-seq)

	p_val	avg_logFC	pct.1	pct.2
Gm8797	1.16E-141	1.594763805	0.976	0.202
Uba52	1.60E-123	0.917702386	0.994	0.987
Ybx3	1.59E-119	0.89864149	0.998	0.955
H2-Q7	9.78E-101	0.961893978	0.992	0.919
Nme2	6.80E-85	0.723684266	0.87	0.336
Rps27rt	8.58E-83	0.60240791	0.99	0.967
Gm12840	2.53E-70	1.376839019	0.77	0.23
Cd9	1.12E-63	0.362813659	1	1
H2-K1	1.85E-62	0.461741278	0.998	1
AY036118	1.57E-59	0.993174903	0.876	0.533
Wdr89	1.79E-56	0.513080074	0.939	0.78
Rpl10-ps3	1.57E-54	0.52329615	0.929	0.765
Skint11	9.71E-54	0.395540035	0.461	0
Rab21	1.11E-49	0.512849211	0.789	0.402
S100a11	2.54E-45	0.443689193	0.998	1
Slco3a1	2.61E-45	0.563840143	0.931	0.768
Rnaset2a	6.20E-45	0.47285744	0.827	0.53
Ppp1r14b	1.85E-44	0.430168996	0.982	0.972
Gm42418	1.03E-42	0.605207021	1	0.997
Zfp593	1.14E-41	0.569991013	0.872	0.702
Cdk2ap1	1.40E-40	0.433385819	0.772	0.462
Gm2000	2.09E-40	0.427335266	0.898	0.654
H2-Q6	1.38E-39	0.574198824	0.801	0.462
Itm2b	3.37E-39	0.352900344	1	1
Crip2	8.51E-38	0.536089156	0.959	0.851
Gm11808	1.97E-37	0.339307322	0.99	0.987
Slc6a4	1.43E-34	0.453304113	0.602	0.22
Cxcl14	1.83E-34	0.56907436	0.988	0.955
Gm10076	2.82E-34	0.296485466	0.539	0.174
H2-T23	5.47E-33	0.481055804	0.888	0.682
Rap2b	6.59E-33	0.756941297	0.841	0.644
Erh	9.68E-33	0.373217099	0.785	0.54
Prdx1	4.00E-32	0.319625646	0.992	0.995
Srsf5	6.94E-32	0.456708793	0.927	0.841
Sem1	7.63E-32	0.283827878	0.994	0.99
Ifitm3	2.65E-31	0.551430187	0.986	0.975
Ptp4a2	9.53E-31	0.398799333	0.984	0.947
Cst6	2.62E-30	0.309653593	0.661	0.303
Tppp3	5.48E-30	0.674275998	0.772	0.46
Ifi27	2.57E-29	0.483348213	0.927	0.848
Pkib	2.83E-29	0.430102943	0.5	0.146
Rps27l	7.72E-29	0.297477714	0.982	0.965
Chchd2	1.83E-28	0.2705652	0.992	0.997

H2-Q4	4.59E-28	0.412107463	0.888	0.742
Vmp1	3.11E-27	0.55374465	0.819	0.662
Tpm3	5.13E-27	0.367840271	0.959	0.912
Apoe	5.39E-27	0.38987036	1	1
Malat1	1.22E-26	0.293667161	1	1
Ppp2cb	1.64E-25	0.252794567	0.472	0.162
Akt1	3.03E-25	0.318383183	0.693	0.404
Cst3	1.36E-24	0.334742394	0.992	0.995
1810037I17R	4.01E-24	0.335309877	0.976	0.942
Mbd2	2.37E-23	0.320321556	0.787	0.576
Rnd3	6.99E-23	0.402425494	0.884	0.816
Tagln2	8.54E-23	0.290611212	0.994	0.987
Pdcd10	1.72E-22	0.339195636	0.864	0.74
Celf4	2.51E-22	0.361601592	0.472	0.189
Pdia3	2.64E-22	0.324804818	0.974	0.937
Hmgn1	1.12E-21	0.258733828	0.988	0.99
Cebpb	2.32E-21	0.507371197	0.852	0.71
Psmb8	5.84E-21	0.379921678	0.907	0.828
Cox6a1	6.44E-21	0.269978637	0.957	0.896
Ly6a	8.05E-21	0.510910655	0.961	0.932
Usmg5	8.99E-21	0.270088454	0.941	0.924
Pnn	3.82E-20	0.351570428	0.833	0.737
Tuba1a	4.18E-20	0.435934424	0.699	0.462
Son	1.31E-19	0.2752514	0.967	0.932
Arid4b	1.87E-19	0.350881043	0.886	0.79
Arpc1a	2.51E-19	0.281515424	0.831	0.664
Tuba1c	2.53E-19	0.484896099	0.937	0.881
Psme2	5.60E-19	0.372324798	0.898	0.803
Bag5	8.49E-19	0.286166209	0.709	0.53
Atxn7l3b	1.23E-18	0.304146561	0.744	0.543
Psme1	1.51E-18	0.314622256	0.915	0.841
Prss23	1.74E-18	0.500205357	0.892	0.816
Gramd3	1.84E-18	0.347774825	0.715	0.497
Serpinb5	1.86E-18	0.351236832	0.984	0.997
Ssr2	2.51E-18	0.261007207	0.811	0.684
Snu13	2.60E-18	0.306760989	0.955	0.914
Hsp90b1	3.12E-18	0.339078619	0.937	0.864
H2-T22	1.19E-17	0.322314865	0.817	0.634
Srpk2	1.22E-17	0.270841012	0.904	0.808
Sema3c	1.64E-17	0.353112347	0.947	0.919
Atp5g1	1.88E-17	0.252695528	0.951	0.927
Hnrnpa3	1.94E-17	0.250554502	0.967	0.955
Atp6v0b	1.99E-17	0.26011271	0.921	0.874
Odc1	2.57E-17	0.436285413	0.76	0.563
Gm15987	5.51E-17	0.306353527	0.742	0.528

Kif5b	1.32E-16	0.255422522	0.959	0.924
Uap1	1.53E-16	0.495502191	0.85	0.79
Ldha	2.17E-16	0.345866344	0.963	0.944
Ifi27l2a	2.72E-16	0.610543638	0.323	0.106
Nme1	5.07E-16	0.268691444	0.904	0.836
Hopx	5.29E-16	0.354492032	0.902	0.783
Adrb2	1.16E-15	0.461502392	0.858	0.793
Eif1a	1.31E-15	0.298722353	0.911	0.846
Mt1	1.34E-15	0.462511541	1	1
Eif2s2	1.37E-15	0.307084343	0.988	0.987
Calr	2.16E-15	0.258802152	0.984	0.98
Tapbp	4.26E-15	0.307019739	0.762	0.654
Prpf4b	4.61E-15	0.283813385	0.805	0.687
S100a16	1.55E-14	0.319711283	0.945	0.929
Fam162a	2.38E-14	0.36668912	0.88	0.823
Ran	4.46E-14	0.255311909	0.972	0.955
Arhgap5	5.69E-14	0.263405496	0.919	0.874
Prnp	5.93E-14	0.277443623	0.955	0.919
Ranbp1	8.47E-14	0.252573712	0.898	0.846
Tubb4b	8.77E-14	0.354646745	0.953	0.957
Reep3	9.45E-14	0.262729695	0.886	0.818
Bst2	9.64E-14	0.333949953	0.27	0.083
Rtn4	1.39E-13	0.253484513	0.984	0.985
Akirin1	1.48E-13	0.292420521	0.852	0.71
Cmip	1.56E-13	0.272140404	0.671	0.5
Pdia6	3.78E-13	0.254418746	0.921	0.884
Ndufa4l2	4.07E-13	0.41418756	0.937	0.934
Krt16	6.55E-13	0.627361253	0.774	0.616
Taf1d	9.91E-13	0.309155016	0.868	0.801
Uck2	1.13E-12	0.297412342	0.636	0.447
Dbi	1.19E-12	0.322597019	0.878	0.798
Clec2d	1.95E-12	0.28848705	0.573	0.371
Herc4	6.51E-12	0.286709252	0.799	0.71
Sprr1a	6.51E-12	0.570595793	0.492	0.278
Neat1	1.30E-11	0.296887982	0.986	0.992
Urah	1.64E-11	0.260350425	0.976	0.97
Arid5b	2.66E-11	0.323043357	0.947	0.896
Anxa1	2.95E-11	0.33675673	0.996	0.995
Ch25h	3.81E-11	0.866513726	0.321	0.146
Gsn	4.63E-11	0.354396088	0.927	0.917
Wnt4	5.91E-11	0.299018359	0.774	0.621
Krt77	2.16E-10	0.532804906	0.528	0.348
Higd1a	3.37E-10	0.339302492	0.939	0.917
Irf6	5.86E-10	0.281692314	0.97	0.952
Cldn1	1.01E-09	0.329884745	0.917	0.904

Clca3a2	1.39E-09	0.359229861	0.945	0.937
Tpm1	2.04E-09	0.408026233	0.884	0.891
Map2k3	3.19E-09	0.255193101	0.909	0.879
Clic4	4.84E-09	0.342276458	0.864	0.811
Gbp2	5.55E-09	0.344330257	0.157	0.038
Tsc22d2	5.79E-09	0.323592301	0.909	0.871
Tnfrsf12a	7.64E-09	0.261205865	0.945	0.947
Pyy	9.51E-09	0.687515196	0.104	0.01
Tmem158	2.30E-08	0.299687094	0.5	0.371
Fam46a	3.30E-08	0.475663634	0.671	0.561
Cd44	3.90E-08	0.257346712	0.949	0.912
Fgfbp1	4.66E-08	0.519128987	0.841	0.869
Sgms2	5.04E-08	0.267577367	0.559	0.424
Tcim	6.43E-08	0.309769842	0.817	0.745
Krt17	1.25E-07	0.575262681	0.85	0.843
Epha4	1.39E-07	0.360623223	0.646	0.563
Avpi1	1.55E-07	0.276235774	0.965	0.947
Cdc42ep3	7.87E-07	0.278836354	0.38	0.245
Nop58	1.08E-06	0.282257384	0.827	0.828
Dll1	3.18E-06	0.262287256	0.557	0.442
Ggct	3.80E-06	0.272556588	0.652	0.545
Kdm6b	1.85E-05	0.283312966	0.866	0.806
Chit1	2.05E-05	0.257819127	0.827	0.793
Stfa3	2.14E-05	0.470009815	0.163	0.071
Pxdc1	3.56E-05	0.305632755	0.856	0.836
Csrp2	4.62E-05	0.279507477	0.299	0.207
Igfbp3	0.000195522	0.41075792	0.671	0.634
Ccdc71l	0.000718411	0.300470903	0.244	0.164
Plk2	0.001776048	0.405369302	0.632	0.591
Crip1	0.00325101	0.376553631	0.675	0.652
Tslp	0.004697875	0.562473771	0.439	0.391

Supplementary Table 9. Upregulated genes in old vs young IFE (scRNA-seq)

	p_val	avg_logFC	pct.1	pct.2
Gm10260	1.64E-133	-0.7665215	0	0.831
Gm11361	9.91E-81	-0.4810412	0.089	0.707
Rps28	1.19E-80	-0.3702665	1	1
Eef1a1	7.86E-74	-0.3144413	1	1
Rpl27-ps3	1.46E-73	-0.5024362	0.165	0.74
Eef2	2.07E-73	-0.465881	1	1
Rpl6	5.03E-73	-0.3434546	1	1
Rpl29	1.17E-66	-0.3793354	0.996	1
Rpl3	1.70E-66	-0.3661894	1	1
Rpl10a	1.08E-62	-0.3184493	1	1
Rpl13a	3.61E-60	-0.427989	0.996	1
Clca3a1	8.83E-57	-0.4494037	0.142	0.654
Dusp1	3.94E-56	-1.0033487	0.923	0.99
Postn	1.47E-55	-0.6603096	0.126	0.639
Hs3st1	6.25E-55	-0.9152165	0.014	0.439
Rpl32	2.33E-52	-0.2785354	1	1
Rpl36	1.43E-50	-0.2789352	1	1
Rpl38	2.76E-50	-0.2634797	1	1
Gm9493	3.01E-47	-0.2930814	0.073	0.5
Hspa8	1.92E-45	-0.4338986	0.996	1
Tpm3-rs7	1.09E-40	-0.3671531	0.207	0.611
Rpl36a	1.25E-40	-0.273353	1	1
Cox7b	1.31E-40	-0.618192	0.949	0.98
Naca	9.60E-40	-0.2551517	1	1
Gpha2	1.79E-36	-0.5309247	0.287	0.672
Npm1	3.81E-36	-0.318815	0.994	1
Alad	5.59E-34	-0.4172387	0.238	0.616
Lmo1	2.88E-32	-0.367885	0.435	0.778
Ctsh	4.77E-32	-0.379274	0.494	0.803
Hspa1a	8.86E-31	-0.5436902	0.709	0.917
Klf10	1.48E-30	-0.430372	0.268	0.634
Timp3	2.05E-30	-0.578841	0.419	0.76
Tgfbi	4.11E-30	-0.3603408	0.982	0.992
Hspa1b	2.57E-29	-0.4199679	0.638	0.904
Rbm3	8.35E-29	-0.3882066	0.941	0.997
Cap1	4.96E-28	-0.3480953	0.785	0.957
Eif4b	2.75E-27	-0.3254029	0.9	0.98
Pnrc1	1.52E-24	-0.3882616	0.961	0.987
Ovol1	1.55E-24	-0.6187528	0.65	0.854
Scd1	2.57E-24	-0.2764778	0.366	0.687
Eif3e	2.88E-24	-0.2573053	0.97	0.997
Hes1	5.15E-24	-0.4225149	0.114	0.407
Dapl1	4.12E-23	-0.4692954	0.734	0.912

Rtraf	7.79E-23	-0.2723952	0.921	0.977
Ier3	2.16E-22	-0.6717188	0.927	0.955
AC160336.1	2.62E-22	-0.3062292	0.114	0.391
Efemp1	6.43E-21	-0.3206424	0.315	0.609
Egr3	8.76E-20	-0.3900793	0.394	0.644
Atp5g2	1.02E-19	-0.251457	0.984	0.997
Il33	2.18E-19	-0.3126459	0.528	0.798
Zfp36	9.41E-19	-0.6081068	0.854	0.952
Sh3d21	2.12E-18	-0.2676046	0.453	0.73
Impdh2	3.07E-18	-0.2807776	0.86	0.962
Angptl4	4.14E-18	-0.292239	0.132	0.384
Rhob	4.37E-18	-0.4947055	0.427	0.677
Hspb1	6.09E-18	-0.4374137	0.992	1
Tkt	1.03E-17	-0.3221841	0.789	0.912
Ubb	4.14E-17	-0.2852134	0.998	0.997
Ctsl	1.41E-16	-0.2813438	0.707	0.891
Spry1	1.47E-16	-0.3059258	0.114	0.341
Sertad1	4.45E-16	-0.2578034	0.488	0.727
Id1	1.10E-15	-0.3949527	0.183	0.442
Fos	1.17E-15	-0.7823209	0.752	0.912
Arc	1.48E-14	-0.3192522	0.108	0.316
Plet1	1.88E-14	-0.7293577	0.892	0.927
Tiparp	2.17E-14	-0.4146769	0.876	0.914
Fosb	8.40E-14	-0.4950202	0.776	0.934
Id3	9.17E-13	-0.4494732	0.856	0.952
Ppp1r14c	1.32E-12	-0.2745118	0.707	0.813
Atf3	1.73E-12	-0.2810738	0.898	0.97
Nfe2l2	1.28E-11	-0.2504912	0.766	0.909
Egr1	1.31E-11	-0.6521876	0.758	0.876
Sgk1	3.29E-11	-0.2790268	0.301	0.528
Zfp36l2	3.47E-11	-0.4713481	0.675	0.806
Epgn	4.65E-11	-0.7396737	0.689	0.801
Junb	8.89E-11	-0.4437181	0.982	0.99
Btg2	9.45E-11	-0.5243164	0.86	0.932
Dnajb1	1.20E-10	-0.3091573	0.935	0.98
Bhlhe40	1.80E-09	-0.3220195	0.86	0.902
Nr4a1	5.61E-09	-0.3190655	0.821	0.902
Klf4	1.14E-08	-0.4020144	0.904	0.949
Zfp36l1	2.05E-08	-0.2913857	0.835	0.924
Gm20186	7.12E-08	-0.464888	0.504	0.652
Jun	8.48E-08	-0.506705	0.978	0.97
Tob1	8.86E-08	-0.2802126	0.671	0.793
Jund	3.92E-07	-0.4237152	0.974	0.992
Tsc22d1	5.64E-07	-0.3133148	0.585	0.705
Icam1	8.39E-07	-0.4404532	0.758	0.848

Ndrg1	1.27E-06	-0.2949804	0.823	0.866
Cldn4	1.72E-06	-0.4278062	0.337	0.487
Socs3	1.76E-06	-0.4626391	0.451	0.596
Gem	2.55E-06	-0.2702745	0.457	0.588
Ier2	3.93E-06	-0.4388085	0.809	0.879
Txnip	7.10E-06	-0.3061672	0.256	0.396
Cxcl1	0.00012851	-0.2786531	0.124	0.215
Sat1	0.00030592	-0.273691	0.941	0.957